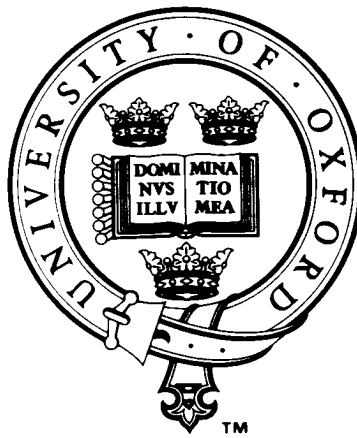


Signal Processing Methods

for

Heart Rate Variability



Gari D. Clifford
St. Cross College

Supervised by Prof. L. Tarassenko
Michaelmas Term, 2002

This thesis is submitted to the Department of Engineering Science,
University of Oxford, in fulfilment of the requirements for the degree of
Doctor of Philosophy. This thesis is entirely my own work,
and except where otherwise stated, describes my own research.

Signal Processing Methods For Heart Rate Variability Analysis

Gari D. Clifford

St Cross College

Doctor of Philosophy

Michaelmas term 2002

Heart rate variability (HRV), the changes in the beat-to-beat heart rate calculated from the electrocardiogram (ECG), is a key indicator of an individual's cardiovascular condition. Assessment of HRV has been shown to aid clinical diagnosis and intervention strategies. However, the variety of HRV estimation methods and contradictory reports in this field indicate that there is a need for a more rigorous investigation of these methods as aids to clinical evaluation. This thesis investigates the development of appropriate HRV signal processing techniques in the context of pilot studies in two fields of potential application, sleep and head-up tilting (HUT).

A novel method for characterising normality in the ECG using both timing information and morphological characteristics is presented. A neural network, used to learn the beat-to-beat variations in ECG waveform morphology, is shown to provide a highly sensitive technique for identifying normal beats.

Fast Fourier Transform (FFT) based frequency-domain HRV techniques, which require re-sampling of the inherently unevenly sampled heart beat time-series (RR tachogram) to produce an evenly sampled time series, are then explored using a new method for producing an artificial RR tachogram. Re-sampling is shown to produce a significant error in the estimation of an (entirely specified) artificial RR tachogram. The Lomb periodogram, a method which requires no re-sampling and is applicable to the unevenly sampled nature of the signal is investigated. Experiments demonstrate that the Lomb periodogram is superior to the FFT for evaluating HRV measured by the $\frac{LF}{HF}$ -ratio, a ratio of the low to high frequency power in the RR tachogram within a specified band (0.04–0.4Hz). The effect of adding artificial ectopic beats in the RR tachogram is then considered and it is shown that ectopic beats significantly alter the spectrum and therefore must be removed or replaced. Replacing ectopic beats by phantom beats is compared to the case of ectopic-realted RR interval removal for the FFT and Lomb methods for varying levels of ectopy. The Lomb periodogram is shown to provide a significantly better estimate of the $\frac{LF}{HF}$ -ratio under these conditions and is a robust method for measuring the $\frac{LF}{HF}$ -ratio in the presence of (a possibly unknown number of) ectopic beats or artefacts.

The Lomb periodogram and FFT-based techniques are applied to a database of sleep apnoeic and normal subjects. A new method of assessing HRV during sleep is proposed to minimise the confounding effects on HRV of changes due to changing mental activity. Estimation of $\frac{LF}{HF}$ -ratio using the Lomb technique is shown to separate these two patient groups more effectively than with FFT-based techniques. Results are also presented for the application of these methods to controlled (HUT) studies on subjects with syncope, an autonomic nervous system problem, which indicate that the techniques developed in this thesis may provide a method for differentiating between sub-classes of syncope.

Acknowledgements

Firstly I would like to thank the SPANN research group; Lionel Tarassenko for support, guidance, freedom and a wonderful working environment, Neil for unending tolerance, support and suggestions, Patrick for diversionary research and a wealth of mathematics, Mayela for saving my plants from neglect and a thousand helpful computing hints, Dileepan, Tim, Simukai Paul and Stephen for many insightful discussions, Rich and Sunay for the jokes and evening ‘research’, Laura for advice and banter, Al ‘n’ Al for sustenance, Nick for taking the coffee club on and all the others for helping me along. I’d also like to thank Professors Noble and Murray for their helpful comments.

Roy Jackson, Adam Fullerton, and Alex Niarac saved me from my hardware nightmares, for that I am in their debt.

On the clinical side I’d like to thank Janet for support and emails, James Price for an invaluable medical perspective and all the clinical team at the JRH and RI.

On the funding side of things I’d like to thank Oxford Instruments (in particular James Pardey for lifts, cold mornings, papers, databases, and relieving me of my car stereo) as well as Oxford BioSignals Ltd. and all the crew there for tools, data, and the funding to make it all possible.

Not only is it an honour to work in such a wonderful place, it’s a privilege to live here too. So many people have enriched my life here I am surely blessed to have met you all. Please forgive me if I’ve forgotten to thank you... the list is too long!

Finally, and most of all I’d like to thank my family for being so supportive and patient, David and Jo for long nights of wit and music (without whom I would have surely become a mad hermit) and most of all to Rachel, for supporting me in the final push and making everything worth it.

Thankyou!

Contents

1	Introduction	1
1.1	Overview	1
1.2	Identifying the problem	2
1.3	Physiology of the human heart	2
1.3.1	ECG waveform generation and recording	4
1.3.2	Lead configurations	5
1.3.3	Heart disease	7
1.4	Abnormalities in the ECG - <i>ectopic</i> beats	7
1.5	The physiology of beat-to-beat heart rate control and HRV	8
1.5.1	The autonomic nervous system and the sympathovagal balance	9
1.5.2	Reflexes controlling heart rate and its variability	13
1.5.3	Factors influencing heart rate and its variability	14
1.5.4	HR and HRV correlation	19
1.6	Quantifying HRV	19
1.6.1	HRV metrics from the RR tachogram	19
1.6.2	Selected time domain measures of HRV	20
1.6.3	Scale-independent measures of HRV	21
1.6.4	Components in the frequency domain	24
1.7	The cardiovascular respiratory system - parameters and models	29
1.7.1	Baroreflex sensitivity	29
1.7.2	The connection between HR, HRV, BP and respiration - a possible mechanism .	30
1.7.3	The DeBoer model	31
1.7.4	Data-driven models	34
1.8	The clinical utility of Heart Rate Variability	34
1.8.1	ATRAMI trials	35
1.8.2	Standardisation and clinical community recommendations	35
1.8.3	Standard terminology	36
1.8.4	Measurement standards	37
1.8.5	Physiological and pathophysiological correlates	38
1.8.6	Commercial manufacturers	39
1.8.7	Appropriate clinical applications	39
1.8.8	Future research areas	41
1.9	The problem of HRV measurement and repeatability	42
1.10	Overview of thesis	43
2	QRS detection	46
2.1	Introduction	46
2.2	QRS detection algorithms - overview	47
2.2.1	Available data — the MIT-BIH database	49

2.3	The Hamilton and Tompkins QRS detector	52
2.3.1	Detection of QRS complexes: Implementation of the Hamilton and Tompkins method.	54
2.3.2	Comparison of performance on MIT normal data	59
2.3.3	Discussion of results	61
2.4	Conclusion.	65
3	Abnormal Beat Detection in the ECG	66
3.1	Introduction	66
3.2	Pre-processing	67
3.2.1	Ectopic rejection	67
3.2.2	Artefact rejection	68
3.2.3	Robust methods	69
3.3	Using morphological information to identify normal QRS complexes	70
3.3.1	Template matching for the detection of ectopic beats	70
3.3.2	Neural Network for ECG analysis	75
3.3.3	The multi-layered perceptron	76
3.3.4	Auto-associative networks	78
3.3.5	Structure of auto-associative network for QRS reproduction.	79
3.3.6	Principal Component Analysis for architecture definition	82
3.3.7	Training the auto-associative network	82
3.3.8	QRS classification	86
3.3.9	Pruning the training set	90
3.3.10	Size of training set and training time.	90
3.3.11	VEB detection performance.	91
3.3.12	Initialisation with PCA	93
3.3.13	Conclusions	96
3.4	Using timing information to identify artefact and abnormal beats	97
3.4.1	Distribution of artefacts and ectopic beats	98
3.4.2	Data fusion algorithms	100
3.4.3	Summary	101
4	HRV experiments using spectral techniques	102
4.1	Overview	102
4.1.1	The RR tachogram - an unevenly sampled time series	102
4.1.2	FFT methods compared to AR methods	103
4.1.3	Re-sampling to enable spectral estimation	104
4.1.4	PSD estimation without re-sampling - the Lomb periodogram	105
4.2	From FFTs to the Lomb method - PSD estimation	105
4.2.1	The Discrete Fourier Transform	106
4.2.2	Generalising the DFT - PSD estimation via the Lomb periodogram	107
4.3	Practical considerations	111
4.3.1	Window size	111
4.3.2	Sampling frequency	112
4.3.3	Pre-processing	112
4.3.4	Performance metrics	112
4.4	Generating artificial data	113
4.4.1	A simple model	113
4.4.2	Spectral estimation of artificial RR time series	116

4.4.3	Frequency variation	117
4.4.4	Frequency resolution	119
4.5	Comparison of spectral estimation methods using artificial data	120
4.5.1	Comparison of even and uneven sampling for a single sinusoid	121
4.5.2	Comparison of even and uneven sampling for LF and HF components	124
4.5.3	Comparison of even and uneven sampling with frequency variation	128
4.6	Performance of algorithms on artificial data when coping with ectopy	130
4.6.1	Previous Work	131
4.6.2	Artificial ectopy	132
4.6.3	Beat replacement and removal: a comparison	134
4.6.4	Metric performance when removing or replacing ectopic beats	134
4.6.5	Discussion	135
4.7	Conclusions	136
5	HRV analysis during sleep	138
5.1	Introduction	138
5.2	Physiological control and variation	139
5.2.1	The autonomic nervous system	139
5.2.2	Circadian rhythms	140
5.3	Changes in HRV with activity	142
5.4	HRV and sleep	143
5.4.1	The physiology and classification of sleep	143
5.4.2	HRV changes with sleep state	145
5.4.3	Sleep disruption; pain, drugs and noise	147
5.5	Summary	147
5.6	Methods for analysing HRV during sleep	148
5.6.1	The MIT polysomnographic database	148
5.6.2	Preprocessing and artefact rejection	149
5.7	Mathematical analysis of HRV during sleep	151
5.7.1	Mathematical analysis	151
5.7.2	Results on normal subjects	153
5.7.3	Results on sleep apnoeic subjects	157
5.7.4	Comparison of PSD estimations methods for separating patients groups using REM and SWS	162
5.8	Conclusions	163
6	HRV: Applicability in controlled studies - Head-up tilts	166
6.1	Introduction	166
6.2	Syncope: Classification	167
6.2.1	Neurally mediated syncope	168
6.2.2	Orthostatic Hypotension	170
6.2.3	Cardiac arrhythmia/structural heart disease	170
6.2.4	Cerebrovascular (steal syndromes)	171
6.2.5	Controversial classifications	171
6.3	Syncope: Tests and Diagnosis	171
6.3.1	Head Upright Tilt Table Testing	171
6.4	HRV in the context of HUT and syncope	172
6.5	HUT data analysis	174
6.5.1	Methodology	174

6.5.2	Clinical protocol	174
6.5.3	Description of patients	175
6.5.4	Signal Analysis	182
6.6	Conclusions	184
7	Summary, conclusions and future work	185
7.1	Summary and key conclusions	185
7.2	Future work	187
7.2.1	Signal processing	187
7.2.2	Clinical studies	188
A	The MIT-BIH database	190
A.1	Appendix: The Annotation Definitions	190
B	Mathematical derivations	192
B.1	Appendix: Derivation of error back-propagation	192
B.2	Appendix: Karhunen-Loéve Transformation	194
C	Normal Values of Standard Measures of HRV	196
D	Cubic Spline Interpolation	197
E	A Simple Illustration of the Lomb Periodogram	199

List of Figures

1.1	Source nodes of electrical stimulation within the heart.	3
1.2	One second of a typical ECG waveform for one heart beat. The vertical axis represents the mV fluctuations scaled to ± 1 over the whole record. The horizontal (time) axis shows the sample number (with a sampling rate of 256 Hz, there are 256 samples in one second).	4
1.3	Electrical vectors for the standard ECG lead configurations.	5
1.4	10 of the standard electrode positions for 12-lead ECG recording.	6
1.5	A Ventricular Ectopic Beat in the middle of a set of normal beats (3 rd beat from the left) for subject 109 of the MIT-BIH database.	8
1.6	Instantaneous or beat-to-beat heart rate, HR_i ,(lower trace) and RR interval (middle trace) for a 1 minute segment of ECG (upper trace).	9
1.7	Organisation of the autonomic nervous system. The sympathetic system (left) is stimulated by stressful situations, increases HR, cardiac output, blood flow to the muscles and inhibits digestive activity. Stimulation of the parasympathetic branch of the ANS (right) leads to increased digestive activity, and depresses BP, HR, cardiac output. Taken from [70].	11
1.8	Chronotropic RR interval (--) and HR_i (->-) responses to graded efferent vagal stimulation (from Malik [105]). Note that the increase in RR interval is proportional to the increase in vagal stimulatory frequency.	12
1.9	Two minutes of ECG, HR_i , RR interval and respiration (from upper to lower trace respectively) from a healthy subject exhibiting RSA. Compressions and rarefactions can clearly be seen in the occurrence of the R-peaks (tall spikes in the ECG). This is reflected in the cyclical changes in the HR and RR interval (2 nd and 3 rd traces). Note that the lower trace represents volume changes in the chest; as the subject inhales the trace rises and the HR (2 nd trace) rises, and when the subject exhales the lower trace falls and the HR drops. From 120 to 180 seconds the subject is breathing at almost 4 respirations per minute (rpm). From 180 to 220 seconds the subject was instructed to breathe at about 7 rpm	15
1.10	BP and HR profile in a normal subject over a 24-hour period. On the horizontal axis, a time of 16 means 4pm and a time of 28 means 4am. Taken from [186].	18
1.11	Typical FFT of RR intervals over 24hrs. (Taken from [184]). Note that the Meyer waves are masked by the power spectral dominance of the VLF and ULF contributions	25

1.12	AR spectral analysis (model order 12, 10 minute window) of an RR tachogram in a healthy subject at rest and during 90° head-up tilt. At rest, two major components of similar power are detectable at low frequencies (LF) and high frequencies (HF). During tilt, the LF component becomes dominant, but as total variance is reduced, the absolute power of LF appears unchanged compared with that at rest. Normalisation leads to predominant LF and smaller HF components, which express the alteration of spectral components due to tilt. The pie charts show the relative contributions from each band together with the absolute power of the two components represented by the area. Taken from Malik <i>et al.</i> , 1996 [184].	26
1.13	PSD (linear axes) of RR intervals for figure 1.6. Note the peaks at < 0.04 Hz, 0.1 Hz (probably due to BP fluctuations) and one around 0.27 Hz - a modulation of the RR tachogram due to respiration. From observation of figure 1.6 it can be seen that the subject was indeed breathing at about 16 breaths per minute, or 0.27 Hz.	27
1.14	Schematic diagram of the cardiovascular system according to DeBoer [64]. Dashed line indicates slow sympathetic control.	32
2.1	Five stage filter sequence of Pan and Tompkin's QRS detector.	54
2.2	5.5 seconds of MIT-BIH ECG data sampled at a frequency of 128Hz, at each stage of data processing. The processing delays in each digital filter have been compensated for.	55
2.3	Low pass filter frequency and phase response (dB/Hz and deg/Hz).	58
2.4	High pass filter frequency and phase response (dB/Hz and deg/Hz).	58
2.5	The time-averaged waveform for two consecutive QRS complexes. The upper threshold is set at 90% of the peak amplitude of each packet. The point where this intersects the time-averaged waveform defines the region in the original data in which the algorithm scans back to locate a peak.	59
2.6	Incorrectly labelled file 114 by algorithm due to noise.	62
2.7	File 114 correctly labelled by clinicians.	62
2.8	Low amplitude QRS complexes (in lead II, the upper channel) missed in file 114.	63
2.9	Artefacts in file 203	63
2.10	File 228 scored by the clinicians	64
2.11	Missed QRS complexes in file 228 due to high energy VEBs.	64
3.1	Flow of logic for beat classification. If a beat, detected by a conventional QRS detector, has a template correlation value greater than C_{min} or an MLP reconstruction error greater than $RMSE_{min}$, it is classified as abnormal. Otherwise the beat is labelled as a VEB.	72
3.2	From top down: Original ECG waveform, $RMSE$ and C for a 12 second segment of file 109 of the MIT-BIH database. Note the third QRS complex - a VEB - in the original ECG has a small $RMSE$. The dashed lines are the thresholds $RMSE_{min}$ and C_{min}	73
3.3	The basic neuron	76
3.4	Schematic of a 5-3-2 multi-layer perceptron. Bias units and weights are omitted for clarity.	77
3.5	Layout of a D - J - D auto-associative neural network.	79
3.6	A typical ECG waveform sampled at 256Hz.	81
3.7	A typical ECG waveform down-sampled to 64Hz.	81
3.8	Size-ranked set of eigenvectors for a training set.	82
3.9	Mean Square Error during training at the end of each training epoch for file 109. The horizontal axis is the number of epochs.	84
3.10	Ratio of the variance in the input patterns to that in the output patterns at each epoch for MIT-BIH file 109. The horizontal axis is the number of iterations through the data set (epochs).	85

3.11	The average QRS complex in file 109 over all of the training set. Note that this vector represents a one second time interval since the signal has been down-sampled to 64Hz.	85
3.12	A normal QRS complex (above) in file 109 and its reconstruction (below). Note that the R-peak is not central when presented to the neural network.	87
3.13	A normal QRS complex (above) in file 109 and its reconstruction (below) when presented to the neural network centred on the R-peak.	88
3.14	Distribution of percentage change in RR interval for normal to normal intervals (N_n on the upper plot) and normal to abnormal intervals (N_e lower plot) for all 19 subjects in the MIT-Physionet NSRDB.	98
3.15	Distribution of percentage change in RR interval for sinus to sinus intervals (upper plot), sinus to non-sinus intervals (middle plot) and sinus to artefacts (lower plot) for all 19 subjects in the Physionet NSRDB.	99
3.16	Percentage of N-N beat pairs remaining (*), N-E (+) and N-A (Δ) removed for $3\% < \lambda \leq 25\%$ for all 19 subjects in the NSRDB	100
4.1	Section of (artificial) RR tachogram. The ‘idealised’ signal (—•—) is a perfect sinusoid. The physiologically realistic RR tachogram is indicated by a series of stars (*). The cubic spline re-sampled signal is represented by —+— and the linearly re-sampled signal by —▷—.	104
4.2	Real RR intervals (▷) with a (7Hz) cubic spline re-sampling overlaid.	113
4.3	PSD of figure 4.2 - a real RR tachogram.	114
4.4	Artificial RR time series generated from equation 4.25 with a sampling rate of 1000 Hz (top figure, A). Figure B shows the physiologically plausible RR intervals extracted from the time series in figure A. Figure C shows these RR intervals with 7Hz linear re-sampling. Figure D shows the RR intervals with 7Hz cubic spline re-sampling.	115
4.5	Periodograms of equation (4.25) for even sampling ($HR_o = 60$, $\frac{\omega_l}{2\pi} = 0.095$, $\frac{\omega_h}{2\pi} = 0.275$, $A_h = 2.5$, $\phi = 0$, $A_l = 2$, $t = 300$) computed using: A) FFT with $f = 1000\text{Hz}$, B) FFT with $f = 7\text{Hz}$ and C) Lomb periodogram with $f = 7\text{Hz}$	116
4.6	Periodograms of physiologically realistic data derived from equation (4.25). a) Lomb method of 300 individual beats in a 5 minute interval. b) 7 Hz linear re-sampling with FFT. c) 7 Hz cubic spline re-sampling with FFT.	117
4.7	Sample-quantised frequency distribution with associated RR tachogram.	118
4.8	PSD of RR tachogram with a Gaussian ($\sigma = 3$) spread of frequencies generated by equations 4.26.	119
4.9	PSDs of evenly sampled (7Hz) artificial RR tachogram with a single component: $A_h \sin(2\pi(0.275)t)$, derived from the Welch FFT (upper) and Lomb (lower) methods.	122
4.10	PSDs of unevenly sampled artificial RR tachogram with a single component: $A_h \sin(2\pi(0.275)t)$, derived from the FFT with linear re-sampling (upper), FFT with cubic spline re-sampling (middle) and Lomb (lower) methods.	123
4.11	PSDs of evenly sampled artificial RR tachogram with a two sinusoidal components: $A_l \sin(2\pi(0.095)t) + A_h \sin(2\pi(0.275)t)$, derived from Welch’s FFT (upper) and Lomb method (lower).	124
4.12	PSDs of unevenly sampled artificial RR tachogram (with two sinusoidal components: $A_l \sin(2\pi(0.095)t) + A_h \sin(2\pi(0.275)t)$) derived from the FFT with linear re-sampling (upper), FFT with cubic spline re-sampling (middle) and Lomb (lower) methods.	126
4.13	PSDs of a Gaussian ($\sigma = 3$) frequency modulated evenly sampled artificial RR tachogram (with two sinusoidal components: $A_l \sin(2\pi f_l t) + A_h \sin(2\pi f_h t)$) derived from the FFT (upper) and Lomb (lower) methods.	127

4.14 PSDs of a $\sigma = 3$ frequency modulated unevenly sampled artificial RR tachogram (with two sinusoidal components: $A_l \sin(2\pi f_l t) + A_h \sin(2\pi f_h t)$) derived from the FFT with linear re-sampling (upper), FFT with cubic spline re-sampling (middle) and Lomb (lower) methods.	129
4.15 Sinus beats occurring at times t_0 , t_1 , t_3 and t_4 , and an ectopic beat occurring at t_2 . The ectopic beat occurs earlier than would be expected for a sinus rhythm beat and shortens the first associated RR interval (RR_{t+1}) and lengthens the second (RR_{t+2}). To avoid introducing high frequency components at this point, a phantom beat can be placed at t'_2 half way between t_1 and t_3 so that RR_{t+1} and RR_{t+2} become RR'_{t+1} and RR'_{t+2} , both equal to $\frac{t_3 - t_1}{2}$	130
4.16 RR intervals from data in figure 4.15. Sinus beats occurring at times t_0 , t_1 , t_3 and t_4 , and an ectopic beat occurring at t_2 . The ectopic beat occurs earlier than would be expected for a sinus rhythm beat and shortens the first associated RR interval (RR_{t+1}) and lengthens the second (RR_{t+2}). To avoid introducing high frequency components at this point, a phantom beat placed at t'_2 , half way between t_1 and t_3 changes RR_{t+1} and RR_{t+2} to RR'_{t+1} (indicated by a red *) and RR'_{t+2} (indicated by a red +). Both these new intervals have the same value.	131
4.17 <i>Realistic</i> RR tachogram (+) evenly re-sampled with linear interpolation (— · —). An ectopic beat is chosen to occur at about 55 seconds. Application of equation 4.28 moves the corresponding RR interval downwards and to the left. The following RR interval occurs at the same time as before, but has a much larger magnitude since the previous RR intervals occurred prematurely and thus its location in time has moved. Note that the line of magenta dots which forms a straight line through this segment (54 to 57 seconds) corresponds to the 7Hz re-sampled (linearly interpolated) RR tachogram after these two points are removed (see section 4.6.4).	132
4.18 Re-sampled data (magenta dots) from original RR intervals (+) using the four methods detailed in the text; (i) Ectopic RR interval removal followed by 7Hz linear resampling; (ii) Ectopic beat replacement followed by 7Hz linear re-sampling; (iii) Ectopic RR interval removal followed by 7Hz cubic spline re-sampling; (iv) Ectopic RR interval removal with no re-sampling.	134
4.19 $\frac{LF}{HF}$ -ratio LF/HF-ratio estimates for methods i (*), ii (o), iii (▷) and iv (+) when dealing with differing numbers of ectopic beats in a five-minute RR tachogram with an actual $\frac{LF}{HF}$ -ratio of 0.64. Each point is an average of 1000 randomly seeded runs.	135
5.1 The regions of the brain that control rapid eye movement (REM) sleep (dotted), non-REM sleep (striated), wakefulness (black) and the respiratory-cardiovascular system (nuclei in the hypothalamus). See sections 5.2.1 and 5.4.1 for details. Adapted from [165]. .	139
5.2 The propensity for a normal subject to fall asleep over the 24 hour clock (adapted from [165]).	140
5.3 A typical sleep-wake plot (taken from [165]) showing the stages of sleep for a healthy young adult (top). Note that stage 1 is labelled ‘drowsy’ and stages 3 and 4 have been merged and labelled SWS (slow wave sleep). Within about 45 minutes of the young adult falling asleep, a deep phase of sleep occurs. This is interrupted after about an hour by a less deep phase of sleep leading to REM sleep. As the night progresses, the periods of deep sleep become progressively shorter and more shallow, whereas REM sleep becomes more prominent. The lower graph demonstrates how elderly patients tend to suffer from a significantly more fragmented sleep pattern than young healthy adults.	144

5.4	5 minute PSDs of RR intervals, according to sleep states: awake (W), stage 2 (St2), slow-wave sleep (SWS), and rapid eye movement sleep (REM). $\frac{LF}{HF}$ -ratio is also indicated for each physiological state. Taken from Otzenberger <i>et al.</i> [213].	146
5.5	Two different expert sleep scores are plotted in blue and magenta for patient 02-01 from the OBS polysomnographic database. The horizontal time axis is in 30 second epochs. 1 represents wakefulness, 0 REM sleep and -1, -2, -3 and -4 indicate sleep states 1 to 4 respectively. Movement artefact is assigned a value of 2. Note the close correspondence between expert scores (86% agreement.)	150
5.6	6 minutes of HR_i data with a 5 minutes sliding window marked along the time axis. PSD calculations are made on each of these windows, which overlap by 270 seconds.	152
5.7	$\frac{LF}{HF}$ -ratio estimates (a-c) and sleep scores (d) during 7.2 hours of sleep for a normal healthy human male (subject OBS-02-02). $\frac{LF}{HF}$ -ratio is estimated using the three methods; (a) Lomb periodogram, (b) FFT after cubic spline interpolation and (c) FFT after linear interpolation. Note the FFT methods produce estimates with a higher variance. The lower graph (the corresponding hypnogram) is plotted for two expert scorers (one in blue and one in magenta). Note the high degree of agreement between scorers.	153
5.8	$\frac{LF}{HF}$ -ratio estimates for normal healthy humans (OBS Polysomnographic database 02). Each patient's average $\frac{LF}{HF}$ -ratio is given for REM sleep (*), NREM sleep (+) and SWS sleep (>) for each of the three spectral estimation methods (see text for details).	156
5.9	Expert scored hypnogram (lower trace) and $\frac{LF}{HF}$ -ratio estimates (upper plots) for a non-apnoeic and non-noisy section of data for patient 03 of the MIT polysomnographic database using the three methods; Lomb periodogram (blue), FFT after cubic spline interpolation (green) and FFT after linear interpolation (red).	159
5.10	Expert scored hypnogram (lower trace) and $\frac{LF}{HF}$ -ratio estimates (upper plots) for a non-apnoeic and non-noisy section of data for patient 04 of the MIT polysomnographic database using the three methods; Lomb periodogram (blue), FFT after cubic spline interpolation (green) and FFT after linear interpolation (red).	159
5.11	Expert scored hypnogram (lower trace) and $\frac{LF}{HF}$ -ratio estimates (upper plots) for a non-apnoeic and non-noisy section of data for patient 41 of the MIT polysomnographic database using the three methods; Lomb periodogram (blue), FFT after cubic spline interpolation (green) and FFT after linear interpolation (red).	160
5.12	Expert scored hypnogram (lower trace) and $\frac{LF}{HF}$ -ratio estimates (upper plots) for a non-apnoeic and non-noisy section of data for patient 48 of the MIT polysomnographic database using the three methods; Lomb periodogram (blue), FFT after cubic spline interpolation (green) and FFT after linear interpolation (red).	160
5.13	$\frac{LF}{HF}$ -ratio estimates for sleep apnoeic subjects (MIT Polysomnographic database). Each patient's average $\frac{LF}{HF}$ -ratio is given for REM sleep (*), NREM sleep (+) and SWS sleep (>) for each of the three spectral estimation methods (see text for details).	161
5.14	$\frac{LF}{HF}$ -ratio estimates for normal subjects (x) and patients suffering from sleep apnoea () in REM sleep for each of the three spectral estimation methods being tested; the Lomb periodogram, the FFT after cubic spline interpolation (FFT_{cub}) and FFT after linear interpolation (FFT_{lin}). Note that better patient group separation is achieved by $\frac{LF}{HF}$ -ratio estimates using the Lomb periodogram.	163
5.15	$\frac{LF}{HF}$ -ratio estimates for normal subjects (x) and patients suffering from sleep apnoea () in NREM sleep for each of the three spectral estimation methods being tested; the Lomb periodogram, the FFT after cubic spline interpolation (FFT_{cub}) and FFT after linear interpolation (FFT_{lin}). Note that no spectral estimation method gives better separation between patient groups in NREM sleep.	164

5.16	$\frac{LF}{HF}$ -ratio estimates for normal subjects (\times) and patients suffering from sleep apnoea ([\square]) in deep sleep (SWS) for each of the three spectral estimation methods being tested; the Lomb periodogram, the FFT after cubic spline interpolation (FFT_{cub}) and FFT after linear interpolation (FFT_{lin}). Note that better patient group separation is achieved by $\frac{LF}{HF}$ -ratio estimates using the Lomb periodogram.	165
6.1	Proposed mechanisms for various types of neurally mediated syncope. Taken from [28].	168
6.2	RR and HRV data for subject A1 during HUT. From top to bottom; beat-to-beat RR interval, $\frac{LF}{HF}$ -ratio over 5 minute windows with 240 second overlap, standard deviation of the same windows. The time marker represents the front of the 5 minute window. Note also that each plot appears in pairs, one with an optimal scaling to observe the changes, and one with the same scaling as each of the other patient plots. The left vertical line represents the time of the initial tilt to 70° and the right line represents the return to the supine position.	176
6.3	RR and HRV data for subject A2 during HUT. From top to bottom; beat-to-beat RR interval, $\frac{LF}{HF}$ -ratio over 5 minute windows with 240 second overlap, standard deviation of the same windows. The time marker represents the front of the 5 minute window. Note also that each plot appears in pairs, one with an optimal scaling to observe the changes, and one with the same scaling as each of the other patient plots. The left vertical line represents the time of the initial tilt to 70° and the right line represents the return to the supine position.	177
6.4	RR and HRV data for subject B1 during HUT. From top to bottom; beat-to-beat RR interval, $\frac{LF}{HF}$ -ratio over 5 minute windows with 240 second overlap, standard deviation of the same windows. The time marker represents the front of the 5 minute window. Note also that each plot appears in pairs, one with an optimal scaling to observe the changes, and one with the same scaling as each of the other patient plots. The left vertical line represents the time of the initial tilt to 70° and the right line represents the return to the supine position.	178
6.5	RR and HRV data for subject B2 during HUT. From top to bottom; beat-to-beat RR interval, $\frac{LF}{HF}$ -ratio over 5 minute windows with 240 second overlap, standard deviation of the same windows. The time marker represents the front of the 5 minute window. Note also that each plot appears in pairs, one with an optimal scaling to observe the changes, and one with the same scaling as each of the other patient plots. The left vertical line represents the time of the initial tilt to 70° . Note that the recording was terminated before the return to supine position.	179
6.6	RR and HRV data for subject C1 during HUT. From top to bottom; beat-to-beat RR interval, $\frac{LF}{HF}$ -ratio over 5 minute windows with 240 second overlap, standard deviation of the same windows. The time marker represents the front of the 5 minute window. Note also that each plot appears in pairs, one with an optimal scaling to observe the changes, and one with the same scaling as each of the other patient plots. The left vertical line represents the time of the initial tilt to 70° and the right line represents the return to the supine position.	180
6.7	RR and HRV data for subject C2 during HUT. From top to bottom; beat-to-beat RR interval, $\frac{LF}{HF}$ -ratio over 5 minute windows with 240 second overlap, standard deviation of the same windows. The time marker represents the front of the 5 minute window. Note also that each plot appears in pairs, one with an optimal scaling to observe the changes, and one with the same scaling as each of the other patient plots. The left vertical line represents the time of the initial tilt to 70° . Note that the recording was terminated before the return to supine position.	181

- E.1 Comparison of calculating the periodogram from the DFT of evenly sampled data (left) and using the Lomb periodogram on unevenly sampled data (right). See text for explanation. 200

List of Tables

2.1	Standard output of MIT files.	51
2.2	Filter properties used for coefficient generation with MATLAB5.	57
2.3	Standard output of MIT files.	60
3.1	Performance of Hamilton and Tompkins/Correlation combination algorithm on patient 109 for classifying beat morphologies for different values of C_{min}	74
3.2	Performance of Hamilton and Tompkins/ $RMSE$ combination algorithm on patient 109 for classifying beat morphologies for different values of $RMSE_{min}$	74
3.3	Reciprocal Mean Square Error ($RMSE$) between (downsampled, energy normalised) MLP input and output patterns (QRS complex candidates) for subject 109 of the MIT-BIT arrhythmia database. Column one presents values for each ectopic beat, column two for each normal beat following the corresponding ectopic beat in column one, and column three details the $RMSE$ for the <i>next but one</i> normal beat, following the ectopic beat in column one. See text for details.	89
3.4	Performance of Hamilton and Tompkins/auto-associative network combination algorithm for different numbers of training patterns.	91
3.5	Performance of Hamilton and Tompkins/auto-associative network combination algorithm for different sizes of temporal window (in seconds) used to segment the P-QRS-T complexes during training. 1700 training patterns were used for each case.	93
4.1	Mean estimates of the $\frac{LF}{HF}$ -ratio and the variance $\sigma_{\frac{LF}{HF}}^2$ over 1000 runs using the Lomb method for differing mean heart rates.	120
4.2	Total power (P_T), peak power (P_{peak}), frequency of peak (f_{peak}), 3dB bandwidth (Δf_{3dB}), fraction of power in a $\pm 0.01Hz$ band centred on the peak ($\frac{P_p}{P_T}$) and amplitude of the first side-lobe (P_{sl}) for figure 4.9; even sampling, single HF frequency. Note that Δf_{3dB} , $\frac{P_p}{P_T}$ and P_{sl} represent the ‘gold standard’ (see text).	122
4.3	Total power (P_T), peak power (P_{peak}), frequency of peak (f_{peak}), 3dB bandwidth (Δf_{3dB}), fraction of power in a $\pm 0.01Hz$ band centred on the peak ($\frac{P_p}{P_T}$) and amplitude of the first side-lobe (P_{sl}) for figure 4.10; uneven sampling, single HF frequency.	123
4.4	Total power (P_T), peak power (P_{peak}), frequency of peak (f_{peak}), 3dB bandwidth, (Δf_{3dB}) fraction of power in a $\pm 0.01Hz$ band centred on the peak ($\frac{P_p}{P_T}$) and amplitude of the first side-lobe (P_{sl}) for figure 4.11 (even sampling, LF and HF sinusoids).	125
4.5	Standard frequency metrics from the results presented in figure 4.11 (even sampling, LF and HF sinusoids). $\frac{A_l}{A_h}(\exp)$ is the experimentally measured ratio of the two peak amplitudes in the low and high frequency regions.	125
4.6	Total power (P_T), peak power (P_{peak}), frequency of peak (f_{peak}), 3dB bandwidth (Δf_{3dB}), fraction of power in a $\pm 0.01Hz$ band centred on the peak ($\frac{P_p}{P_T}$) and amplitude of the first side-lobe (P_{sl}) for figure 4.12.	126

4.7	Standard frequency metrics from the results presented in figure 4.12 (uneven sampling, LF and HF sinusoids)	126
4.8	Total power (P_T), peak power (P_{peak}), frequency of peak (f_{peak}), 3dB bandwidth, (Δf_{3dB}) and the fraction of power in a $\pm 0.01Hz$ band centred on the peak ($\frac{P_p}{P_T}$) for figure 4.13.	128
4.9	Standard frequency metrics from the results presented in figure 4.13 (even sampling, LF and HF sinusoids).	128
4.10	Total power (P_T), peak power (P_{peak}), frequency of peak (f_{peak}), 3dB bandwidth (Δf_{3dB}) and fraction of power in a $\pm 0.01Hz$ section centred on the peak ($\frac{P_p}{P_T}$).	128
4.11	Standard frequency metrics from the results presented in figure 4.14 (uneven sampling, LF and HF sinusoids)	129
4.12	Standard frequency metrics for differing magnitudes of ectopy (γ).	133
4.13	Standard frequency metrics for $\gamma = 0.8$ and two ectopic beats.	133
5.1	Activity dependent changes of the $\frac{LF}{HF}$ -ratio for conscious normal patients (with ± 1 standard deviation). Taken from results of [31].	142
5.2	$\frac{LF}{HF}$ -ratios during Wakefulness, NREM and REM sleep. N/A = not available, Norm = normal, Post-MI = a few days after myocardial infarction, † indicates a non-cardiac related problem. Taken from [213, 184, 275, 166].	146
5.3	The labelling scheme for the polysomnographic database. Each sleep stage or apnoea annotation applies to a thirty-second segment.	149
5.4	Patients and sections chosen from the MIT polysomnographic database with little or no noise and apnoeic episodes.	151
5.5	Mean $\frac{LF}{HF}$ -ratio (\bar{x}) and S.D. (σ) for each of the three PSD estimation methods for normal subjects in REM sleep, NREM sleep and SWS.	155
5.6	Results of significance of F-test, K-S test and unequal t-test between $\frac{LF}{HF}$ -ratio variances, distribution and means in REM and NREM sleep for normal subjects. Significance is denoted with an asterisk (*) for $P < 10^{-4}$, or as $P < 0.0005$, $P < 0.005$, $P < 0.01$, $P < 0.05$. NS denotes not significant. Note that in general, only the Lomb method gives significantly different variances in NREM and REM sleep. Although there is a high probability that the $\frac{LF}{HF}$ values in REM sleep have a different distribution to those in NREM sleep for each spectral estimation technique, only the Lomb periodogram gives significantly different mean $\frac{LF}{HF}$ -ratios for all subjects.	155
5.7	Results of significance of F-test, K-S test and unequal t-test between $\frac{LF}{HF}$ -ratio variances, distribution and means in SWS and REM sleep for normal subjects. Significance is denoted with an asterisk (*) for $P < 10^{-4}$, or as $P < 0.0005$, $P < 0.005$, $P < 0.01$, $P < 0.05$. NS denotes not significant. Note that in general, all three spectral estimation methods give significantly different variances, means and distributions between SWS and REM sleep. Although the variance in SWS is significantly lower for subject 02, no significant differences in the mean $\frac{LF}{HF}$ -ratio values calculated by each of the three PSD methods exists. However, in the case of the Lomb periodogram only, the K-S test indicates that the distribution of $\frac{LF}{HF}$ -ratio values is significantly different between SWS and REM sleep.	156
5.8	Mean $\frac{LF}{HF}$ -ratio (\bar{x}) and variance for each of the three PSD estimation methods in REM sleep, NREM sleep and SWS for sleep apnoeic subjects. N/A indicates not applicable; in the segment of data analysed the subject did not experience this category of sleep.	161

5.9	Results of significance of F-test, K-S test and unequal t-test between $\frac{LF}{HF}$ -ratio variances, distribution and means in NREM and REM sleep for sleep apnoeic subjects who experienced all three sleep categories (REM, NREM and SWS). Significance is denoted with an asterisk (*) for $P < 10^{-4}$, or as $P < 0.005$, $P < 0.01$, $P < 0.05$. NS denotes not significant. Note that in general, only the Lomb method gives more significantly different variances between NREM and REM sleep. Although there is a high probability that the $\frac{LF}{HF}$ values in REM sleep have a different distribution to those in NREM sleep for each spectral estimation technique, all PSD estimation methods lead to the conclusion that no significant difference exists between the mean $\frac{LF}{HF}$ -ratios calculated in NREM and REM sleep.	162
5.10	Results of significance of F-test, K-S test and unequal t-test between $\frac{LF}{HF}$ -ratio variances, distribution and means in SWS and REM sleep for sleep apnoeic subjects who experienced all three sleep categories (REM, NREM and SWS). Significance is denoted with an asterisk (*) for $P < 10^{-4}$, or as $P < 0.005$, $P < 0.01$, $P < 0.05$. Note that there exist significantly different variances, distributions and means of the $\frac{LF}{HF}$ -ratio between SWS and REM sleep.	162
5.11	Average $\frac{LF}{HF}$ -ratio estimates for subjects tested in the OBS polysomnographic normal database 02 (*), normals in the current literature ([213, 275]), the MIT polysomnographic (sleep apnoeic) database (**) and a post-MI population (taken from [252]). N/A indicates the results are not available from current literature. $\frac{LF}{HF}$ -ratios quoted from this study are means over all subjects in the group using Lomb periodogram-derived estimates. ‡ indicates that no variance calculations were given in the paper	164
A.1	Beat annotation codes.	190
A.2	Non-beat annotation codes.	191
C.1	Nominal 24-hour HRV metric values for normal subjects (mean values \pm one standard deviation). Taken from [184]).	196

Glossary of clinical terms

In the interest of clarity and since the nature of this thesis is cross-disciplinary yet highly specific, a glossary of clinical terms, technical abbreviations and explanations of contextual descriptors are provided.

- Adventiita – Membranous structure, usually morbid, covering but not belonging to an organ.
- Afferent Nerves – Carry impulses to the muscle/gland/organ.
- Angiotensin – A powerful vasoconstricting polypeptide which stimulates the production of aldosterone and vasopressin and results in an increase in blood pressure (more fully angiotensin II); angiotensin I, the inactive precursor of this, which is formed in the liver by the action of renin on a plasma protein (angiotensinogen), and is converted in the lungs to angiotensin II by a second enzyme.
- Aortic stenosis – progressive narrowing of the aortic valve resulting in the obstructed passage of blood from the left ventricle into the aorta. Chronic stenosis can lead to left ventricular enlargement and congestive heart failure.
- Arrhythmia – Any variation from the normal (sinus) rhythm of the heart beat, including premature beats, heart block, atrial fibrillation and atrial flutter.
- Artefact (Sometimes Artifact) – a product or effect that is not present in the natural state (of an organism, etc.) but occurs during or as a result of investigation or is brought about by some extraneous agency such as electrode movement.
- Atrial myxoma – a very rare primary cardiac tumour, composed of connective tissue, located in the left or right atrium.
- Autonomic Nervous System (ANS) – The system of nerves of the glands and of the involuntary muscle that regulates key functions including the activity of the cardiac muscle, smooth muscles (e.g., of the gut), and glands. In 1940 R. S. Woodworth defined the autonomic nerves to be those

that run to the heart, blood vessels, lungs, stomach, intestines, and other viscera. These nerves are composed of extra-slender nerve fibres, which grow out from cells in the brain stem and cord. The ANS comprises the sympathetic nervous system (which accelerates the heart rate, constricts blood vessels, and raises blood pressure) plus the parasympathetic nervous system (which slows the heart rate, increases intestinal and gland activity, and relaxes sphincter muscles).

- Autonomic Neuropathy – A disease of the autonomic nervous system.
- Baroreflex – A reflex whereby the heart speeds up and beats more forcefully when BP falls.
- Blood Pressure (BP) – The pressure that must be applied to an artery in order to stop the pulse in the vessel beyond the point of pressure. It is generally assumed to be equivalent to the systolic pressure to which the blood is subjected by the force of the heart and the elasticity of the vessels, but also depends upon thickness and hardness of vessel wall, and of volume of blood thrown out of the heart at each beat. BP is greatest at each heart beat (systolic blood pressure - SBP) and lowest between beats (diastolic blood pressure DBP). Mean arterial (blood) pressure (MAP) is taken to be $DBP + \frac{SBP-DBP}{3}$.
- Bradycardia – A slowness of the beating of the heart (to less than 60 bpm).
- Carotid Sinus Massage (CSM) – firmly massaging the right carotid artery for 5-10 seconds at the anterior margin of the sternocleo-mastoid muscle at the level of the cricoid cartilage.
- Cardiac Output – $HR \times$ stroke volume.
- Cardiomyopathy – A weakness of the heart muscle, often leading to heart failure. Can be caused by a number of underlying disorders including coronary artery disease, valvular heart disease, viral infection, diabetes, alcohol abuse, or connective tissue disorders. Sometimes no specific cause can be identified, in which case the cardiomyopathy is referred to as *idiopathic*.
- Cardiothoracic ratio – The ratio of the maximal transverse diameter of the cardiac silhouette to the distance between the internal margins of the ribs at the level of the right hemidiaphragm.
- Cataplexy – A sudden loss of muscle tone that may be induced by severe mental shock or as an additional feature of narcolepsy.
- Cerebral perfusion – Quantity of blood flow to the cerebrum or the brain.
- Central Nervous System – Pertaining to the brain, cranial nerves and spinal cord. It does not include muscles or peripheral nerves.
- Chronotropic – Affecting (increasing) the rate of contraction.

- Circadian – Designating physiological activity which occurs approximately every twenty-four hours, or the rhythm of such activity.
- Coronary Artery Disease (CAD) – is a chronic disease in which there is a atherosclerosis (hardening) of the arteries on the surface of the heart. It is also referred to as coronary heart disease (CHD).
- Coronary Heart Disease (CHD) – See Coronary Artery Disease.
- Diastole – The time, in between ventricular contractions (systole), at which ventricular filling occurs.
- Diastolic Blood Pressure – The pressure exerted on the walls of the arteries when the heart is in the relaxation phase (diastole). Considered abnormally elevated if consistently over 90 mmHg.
- Efferent Nerve – Carry impulses away from the muscle/gland/organ
- Ejection Fraction - a measure of the function of the left ventricle, also called left ventricular ejection fraction (LVEF). The ejection fraction is the percentage of blood ejected from the left ventricle with each heart beat. An LVEF of 50% indicates that the left ventricle ejects half its volume each time it contracts. A normal ejection fraction is 50% or higher. A reduced ejection fraction can indicate that cardiomyopathy is present.
- Embolism – The plugging of a small blood vessel by material which has been carried through larger vessels by the blood stream.
- Endocrine System – The system of glands that release their secretions (hormones) directly into the circulatory system.
- Entrainment – To adjust such that synchronisation occurs.
- Fibrillation – A small, local, involuntary contraction of muscle, invisible under the skin, resulting from spontaneous activation of single muscle cells or muscle fibres.
- Heart Beat – A full cycle depolarisation and repolarisation of the cardiac muscle. Each heart beat is followed by a period of rest where ventricular filling occurs.
- Heart Rate (HR) – The number of heart beats per minute (bpm)
- Hemorrhage – An escape of blood from the blood-vessels; a flux of blood, either external or internal, due to rupture of a vessel; bleeding, esp. when profuse or dangerous.
- Humoral – Of or belonging to, consisting of, or containing, any of the humours or fluids of the body; Contained in or involving the blood or other body fluid; involving or consisting of a chemical agent, esp. one present in the blood (such as hormones or ions).

- Hypertension – Persistently high arterial blood pressure. Hypertension may have no known cause (essential or idiopathic hypertension) or be associated with other primary diseases (secondary hypertension).
- Hypertrophic cardiomyopathy – enlargement of the ventricular septum can result in ventricular outflow obstruction (subaortic stenosis) and eventual cardiomyopathy (disease of the cardiac muscle mass).
- Hypoglycaemia – An abnormally diminished concentration of glucose in the blood. This occurs when a person with diabetes has injected too much insulin, eaten too little food, or has exercised without extra food. Taking small amounts of sugar, sweet juice, or food with sugar will usually help the person feel better within 10-15 minutes. Symptoms of hypoglycaemia include nausea, sweating, weakness, faintness, confusion hallucinations, headache, cold sweat, piloerection, hypothermia, irritability, bizarre behaviour and fainting. Prolonged hypoglycaemia can result in complete loss of consciousness, convulsions, coma and brain damage.
- Hypovolemia – Decreases in venous return of the blood to the heart.
- Innervate – To supply (some organ or part) with nerve-force, or with nerves.
- Inotropic – Affecting the strength of contraction.
- Intoxication – A disorder resulting from absorption of the waste products of metabolism, decomposed matter from the intestine, or the products of dead and infected tissue as in gangrene.
- Ipsilateral – Belonging to or occurring on the same side of the body; connecting two parts on the same side.
- Left Ventricular Ejection Fraction (LVEF) – see Ejection Fraction
- Narcolepsy – A disorder of sleep associated with excessive daytime sleepiness, involuntary daytime sleep episodes, disturbed nocturnal sleep and cataplexy.
- Neurohumoral – Nervous plus hormonal stimuli
- Norepinephrine – or noradrenaline; a precursor of adrenaline whose main function is to mediate the impulses in the sympathetic nervous system. Increased levels are associated with stress and it is often referred to as the 'fight or flight hormone'.
- Noise – a collective term for: fluctuations or disturbances which are not part of a wanted signal or which interfere with its intelligibility or usefulness such as muscle activity (for ECG analysis) and ectopic beats (for HRV analysis).

- Orthostatic hypotension – A drop in blood pressure that is precipitated by changes in body position.
May be related to hydration status, drug side effect or be caused by a dysfunction in the autonomic nervous systems ability to maintain blood pressure with positional changes (for example autonomic neuropathy secondary to diabetes).
- Myelin – The medullary (inner) sheath of nerve-fibres.
- Mycroneurography – A technique for measuring electrical signals from human peripheral nerves using a microelectrode.
- Myocardial Infarction (MI) – A blockage in the normal electrical conduction paths of the heart that cause the muscle contraction, often leading to permanent damage to the heart muscle.
- Parasympathetic system – Part of the autonomic nervous system which is connected with the brain and spinal cord through certain nerve centres in the mid-brain, medulla, and lower end of the cord, including the vagus (see below). Its action is usually antagonistic to that of the sympathetic system in that it inhibits the action of the heart and stimulates the intestine.
- Paroxysm – The fit, attack, or exacerbation, of a disease that occurs at intervals, or has decided remissions or intermissions.
- Paroxysmal – Recurring in paroxysms, spasms or seizures.
- Peripheral Resistance – The resistance to blood flow at the peripheral blood vessels.
- Psychogenic syncope – Fainting spells related to anxiety, panic or major depression.
- Renin – the enzyme (or catalyst) that produces angiotensin
- Reninangiotensin System – Part of the renal (kidney) regulatory sysstem; very important in BP regulation.
- R-on-T ventricular (premature) beat – A potentially dangerous condition is induced when a premature ventricular contraction occurs during the T-wave of the preceding QRS-T complex. R-on-T phenomenon can induce ventricular tachycardia or ventricular fibrillation.
- Sinus pause – A spontaneous interruption in the regular sinus rhythm, the pause lasting for a period that is not an exact multiple of the sinus cycle.
- Splanchnic – Situated in, connected with, the viscera or intestines.
- Steal syndrome – stenosis or obstruction of artery near its origin
- Stenosis – Narrowing or stricture of a duct or canal.
- Subclavian artery – Artery extending under the clavicle.

- Sympathetic system – Part of the autonomic nervous system consisting of ganglia united by an irregular network of nerve fibres. The major part of the sympathetic system consists of two ganglionated cords that run through the neck, chest and abdomen, lying close in front of the spine. Its action is usually antagonistic to that of the parasympathetic system in that it stimulates the action of the heart and inhibits the intestine.
- Syncope – A temporary suspension of consciousness due to generalised cerebral ischaemia, a faint or swoon.
- Systole – The time at which ventricular contraction occurs; a contraction of the heart that alternates with the diastole occupying, respectively.
- Systolic Blood Pressure (SBP) – The pressure exerted on the walls of the arteries during the contraction phase of the heart. Considered abnormally elevated if consistently over 150 mmHg. Systolic blood pressure varies with age, sex, size and relative condition.
- Tachycardia – The excessive rapidity in the action of the heart, the term is usually applied to a heart rate above 100 per minute and may be qualified as atrial, junctional (nodal) or ventricular and as paroxysmal.
- Tonically – Of resting tone (baseline)
- Vagal Nerve (Vagus or Pneumogastric) – The 10th cranial nerve and part of the parasympathetic nervous system formed by numerous filaments from the respiratory tract.
- Vagus – See Vagal Nerve.
- Valsalva – an attempt is made to exhale air while the nostrils and mouth, or the glottis, are closed, so as to increase pressure in the middle ear and the chest.
- Vasovagal syncope – A transient vascular and neurogenic reaction marked by pallor, nausea, sweating, bradycardia, and rapid fall in arterial blood pressure which, when below a critical level, results in loss of consciousness and characteristic electroencephalographic changes. It is most often evoked by emotional stress associated with fear or pain. It is also called vasovagal attack and gowers' syndrome.
- Viscera – The soft contents of the principal cavities of the body; esp. the internal organs of the trunk; the entrails or bowels together with the heart, liver, lungs, etc.

Taken from [61], [109] and [204].

Abbreviations and units

ACE	Angiotensin-Converting Enzyme
AEB	Atrial Ectopic Beat
AF	Atrial Fibrillation
AR	Autoregressive
BP	Blood Pressure
bpm	Beats per minute
CA	Cardiac Arrest
CAD	Coronary Artery Disease
CHF	Congestive Heart Failure
CNS	Central Nervous System
CSM	Carotid Sinus Massage
dB	Decibels
ECG	Electrocardiogram
EEG	Electroencephalogram
EF	Ejection Fraction
FDA	Federal Drug Administration (USA)
FFT	Fast Fourier Transform
HCM	Hypertrophic Cardiomyopathy
HF	High Frequency
HR	Heart Rate
HR _I	Instantaneous HR ($= \frac{60}{RR}$)
HRV	Heart Rate Variability
Hz	Hertz

ICA	Independent Component Analysis
IV	Intravenous - injected into the vein
LDL	Low Density Lipoprotein (cholesterol)
LF	Low Frequency
MI	Myocardial Infarction
mm/Hg	Millimetres of Mercury (as a measure of pressure)
ms	Milliseconds
MVP	mitral valve prolapse
NN	Normal-to-normal beats (excluding ectopics).
NYHA	New York Heart Association classification
PCA	Principal Component Analysis
QRS	Central part of heart beat morphology
RR	Beat-to-beat (R-peak to R-peak).
rpm	Respirations Per Minute
s	Seconds
SCD	Sudden Cardiac Death
SD	Standard Deviation
SVT	Supraventricular Tachycardia
VEB	Ventricular Ectopic Beat
VF	Ventricular Fibrillation
VLF	Very Low Frequency
VT	Ventricular Tachycardia
ULF	Ultra Low Frequency

Dedicated to the memory of Joe Ensor (1915-2001),
farmer, grandfather, and friend
... and to the rest of my family.

Chapter 1

Introduction

1.1 Overview

Over the last 20 years there has been a widespread interest in the study of variations in the beat-to-beat timing of the heart, known as heart rate variability (HRV). In certain circumstances, the evaluation of HRV has been shown to provide an indication of cardiovascular health [181]. However, often contradictory results have left clinical researchers sceptical about the efficacy of HRV assessment and there exists no clear consensus on how to estimate HRV in clinical practice.

This thesis explores techniques for signal processing of HRV from motivation to application, in an attempt to develop robust methods for HRV analysis. This study considers signal extraction, the errors introduced at each stage of the processing, the cardiovascular interpretation of the metrics being estimated and methods for minimising the number of free parameters in clinical situations.

This chapter introduces the main characteristics of the electrocardiogram (ECG), a record of the biopotentials associated with the contractions of the heart muscle. A description of some of the common types of signals that can be derived from the ECG is also presented, together with the motivation behind the analysis of these signals. A detailed description of how the different branches of the human central nervous system (CNS) and respiratory cardiovascular (RCV) system interact to produce beat-to-beat variability in the human heart rate is then given.

1.2 Identifying the problem

The heart is composed of muscle tissue that contracts and relaxes in a coordinated manner when an electrical stimulus is applied. The heart's function is to pump blood around the body, through the arterial system to enable the transport of vital nutrients and oxygen. Like all other muscles, the heart receives its oxygen and nutrients from arteries, which are the coronary arteries in this case. A blockage of these vessels often leads to a heart attack (the cessation of the beating of the heart). In fact, coronary heart disease has been shown to be the leading cause of death in developed countries [192]. Myocardial Infarction¹ (MI), heart failure, angina, and sudden death can all occur from the blockages which occur in the coronary arteries. Following an MI, the conventional treatment is to inject a 'clot-busting' de-coagulation agent, in order to remove the blockage. However, often the heart has already suffered much damage and muscle-tissue loss, leading to an increased likelihood of re-infarction [181].

Since the cardiovascular system is controlled by the CNS, a deterioration in this control mechanism also leads to cardiac-related problems. The rest of this chapter details how the CNS controls cardiac activity and how this is measured to assess the functionality of this control.

1.3 Physiology of the human heart

The human heart is controlled by a series of electrical discharges from specific localised nodes within the myocardium (cardiac muscle). These discharges propagate through the cardiac muscle and stimulate contractions in a co-ordinated manner in order to pump deoxygenated blood via the lungs (for oxygenation) and back into the vascular system. The physical action of the heart is therefore induced by a local periodic electrical stimulation. As a result of the latter, a change in potential of the order of 1mV can be measured during the cardiac cycle between two surface electrodes attached to the patient's upper torso (usually either side of the heart). This signal is known as the electrocardiogram (ECG).

In a normal heart, each beat begins with the stimulation of the sinoatrial (SA) node, high up in the right atrium (see figure 1.1) which causes depolarisation of the cardiac muscle in this locality. This stimulation is both regular and spontaneous and is the source of the primary pacemaker within the heart with an intrinsic frequency of 100 to 120 beats per minute (bpm). Note that the resulting heart rate is

¹A blockage in the normal electrical conduction paths of the heart that cause the muscle contraction, often leading to permanent damage to the heart muscle.

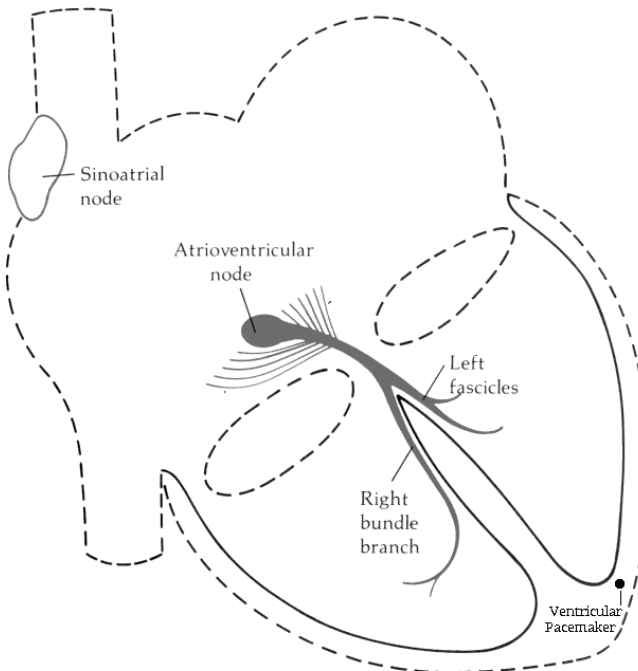


Figure 1.1: Source nodes of electrical stimulation within the heart.

often lower than this because of the complex set of chemical exchanges that occur between the initial stimulation and the subsequent depolarisation of the surrounding cardiac tissue. The impulse spreads from the SA node to depolarize the atria (the upper two cavities). The electrical signal then reaches the atrioventricular (AV) node, located in the right atrium. Normally, an impulse can only reach the ventricles via the AV node since the rest of the myocardium is separated from the ventricles by a non-conducting fibrous ring.

As the AV node is activated it momentarily delays conduction to the rest of the heart and so acts as a safety mechanism by preventing rapid atrial impulses from spreading to the ventricles at the same rate. If the AV node fails to receive impulses it will take over as the cardiac pacemaker (at a much lower frequency of 40 to 60 bpm). The SA node will inhibit this pacemaking whenever its impulses reach the AV node.

Once the impulse has passed the AV node, it enters the bundle of His. This conducting network spreads out into the inter-ventricular septum and divides into left and right bundle branches. As the impulse moves through this region and into the posterior and anterior fascicles it stimulates depolarisation of the ventricles. There is a ventricular pacemaker² (with a beat frequency of 15 to 40 bpm) which takes over as the main pacemaker if the AV node fails.

After the depolarisation of the ventricles, a transient period follows where no further ionic current

²Strictly speaking it is not localised; all the cells have an innate rhythmicity.

can be flow through the myocardium. This is known as the refractory period and lasts at least 200ms. There is then a recharging (repolarisation) of the ventricular myocardium to its resting electrical potential and the heart is then ready to repeat the cycle.

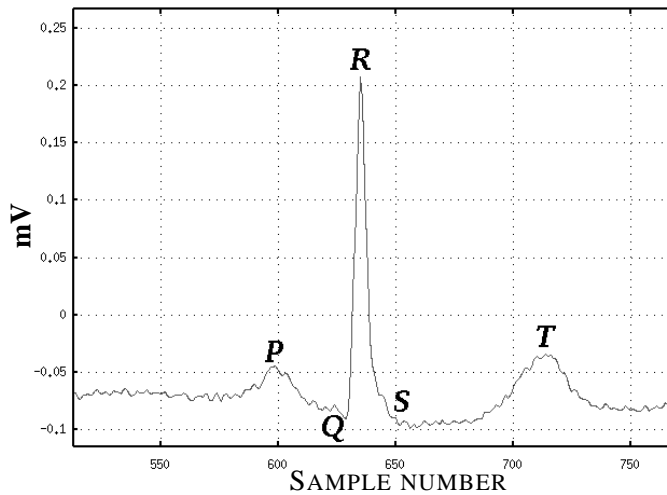


Figure 1.2: One second of a typical ECG waveform for one heart beat. The vertical axis represents the mV fluctuations scaled to ± 1 over the whole record. The horizontal (time) axis shows the sample number (with a sampling rate of 256 Hz, there are 256 samples in one second).

1.3.1 ECG waveform generation and recording

A typical ECG waveform comprises of an initial P-wave, followed by the main ‘QRS’ complex and then a trailing T-wave (see figure 1.2). These waves are defined as follows:

- **P-wave** – The low voltage fluctuation caused by the depolarisation of the atria prior to contraction.
The atria contain very little muscle and thus the voltage change is quite small.
- **QRS complex** – The largest-amplitude portion of the ECG caused by the ventricular depolarisation. The time during which ventricular contraction occurs is referred to as the *systole*. Although atrial repolarisation occurs simultaneously, it is not seen due to the low amplitude of the signal generated by this process.
- **T-wave** – Caused by ventricular repolarisation.

The time between ventricular contractions, during which ventricular filling occurs, is referred to as the *diastole*. Although the R-peak is often the largest amplitude component, the morphology of a healthy ECG can vary greatly from patient to patient with the P- or T-waves sometimes dominating or merging

with the QRS complex. Swapping the two electrodes over gives an inverted signal with the R-peak being the lowest (or most negative) part of the signal. The time averaged heart rate (HR_{60}) is usually calculated by counting the number of beats in a 60 second time period. The instantaneous heart rate, HR_i , is $\frac{60}{RR}$ where RR is the time between successive R-peaks (an RR interval). HR_{60} can vary between 30 and 220 beats per minute (bpm) and although the instantaneous heart rate can be as high as 300 bpm, this is not sustainable for more than a few beats without serious problems manifesting themselves.

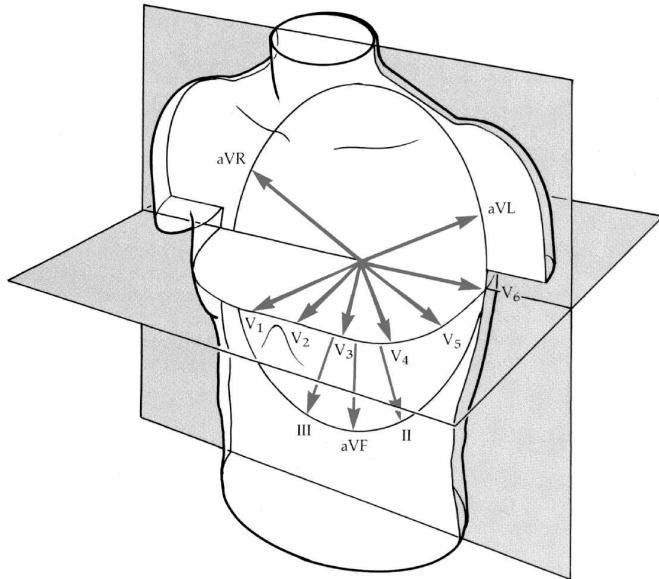


Figure 1.3: Electrical vectors for the standard ECG lead configurations.

1.3.2 Lead configurations

The choice of location on the thorax for the electrodes used to record the ECG is dictated by the type of clinical information required. Since the voltage difference between a pair of electrodes (known as a lead) is only representative of the variations along one axis from the heart (see figure 1.3), there is no three-dimensional activity information in single lead measurements. However, there are standard lead configurations for acquiring 3-D information about the electrical activity of the heart [121]. Figure 1.4 shows many of the standard positions for 12-lead ECG recordings and figure 1.3 shows the standard vectors that are visualised by these leads. For example, lead II represents the electrical activity vector from the centre point (close to the heart) to the left leg. Lead V5 represents the vector from electrode

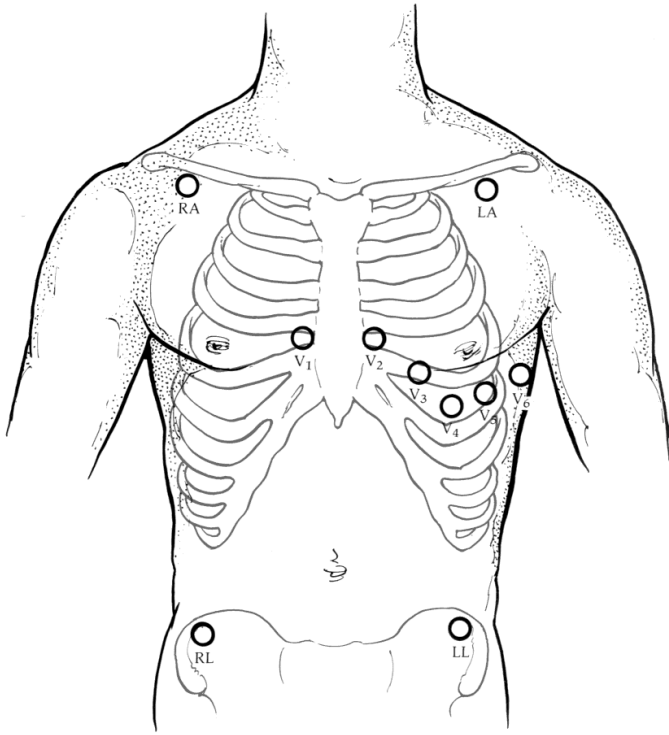


Figure 1.4: 10 of the standard electrode positions for 12-lead ECG recording.

position V₅ (as in figure 1.4) to the heart. The potential must be measured with respect to some common ground and this is often taken to be the right leg.

When a serious heart problem is suspected, (such as following a suspected MI) a clinician will usually order a full (12-lead) ECG recording to be made. This gives a detailed picture of a patient's cardiac activity, and any possible problems, such as QT-syndrome (significant changes in the time between the Q and T points on each cycle) and ST-elevation (a significant rise in the point of inflection between the S and T points) [86, 134, 179]. However, since visual inspection is often used to evaluate these features, and this can be done on only a few cycles of the ECG, the recording is short (typically 10 seconds long). Routine analysis of the ECG does not normally involve such a high number of vectors being recorded. Even in an intensive therapy unit (ITU), when data from many lead configurations is available, only one or two leads are routinely monitored. Typically, leads II and V₅ are chosen since they offer the most useful information in the context of medical diagnosis [121]. Note that these two lead configurations are the two channels of ECG data in the standard MIT-BIH database (see chapter 2). The analysis in this thesis concerns data taken over the course of hours, where it is unusual to record ECG data from more than these two channels.

1.3.3 Heart disease

Heart disease patients can be broadly classed as either myopathies or ischemics. Myopathies usually experience a slow degeneration of the heart over years or months, manifesting as inflammation of the cardiac muscle. In contrast, myocardial ischemia (a lack of oxygen to cardiac muscles) is often caused by a rapid build up (over hours) of plaque or other blood flow-impeding particles and leads to muscle damage. The latter will usually manifest itself as a morphological change on particular sections of the ECG [134, 179].

In both cases, the onset of potentially fatal arrhythmias often resulting in MI can be preceded by two main changes: a higher than normal incidence of ectopic beats, and a reduction in the short term variations of the instantaneous heart rate [181].

1.4 Abnormalities in the ECG - *ectopic beats*

Most human beings exhibit a normal cardiac (sinus) rhythm composed of very similar beats occurring at regular (but slightly varying) intervals. Beats which occur prematurely in the cycle, often with a different morphology, are known as ectopic beats³. Recent research has shown that an increased number of these beats can be indicative of poor recovery after a traumatic event or denote the onset of potentially fatal arrhythmias⁴ [113, 181, 184, 282]. Although the electrical impulses around the heart originate from the SA node (see figure 1.1) and propagate to the ventricles (see section 1.3), signal block can occur at many different regions along this route [121]. As previously mentioned, the heart has a number of subsidiary pacemakers located in the AV junction (or node) and the ventricular myocardium.

If the AV junction fails to receive impulses, as a result of sinoatrial (SA) arrest or block, it will take over as the cardiac pacemaker. If the AV junctional pacemaker fails or its impulses are blocked then a ventricular pacemaker will take over and the resulting QRS complexes will be broadened. These are known as escape rhythms and their morphologies vary significantly from normal beats.

If the R-peak of the beat occurs earlier than expected then it is known as an ectopic beat, such as the third peak in figure 1.5. (Definitions vary, but a typical value is around 20% earlier than the previous beat [138].) Although non-sinus beats can arise from any region of the heart an ectopic beat is usually classified as atrial, AV junctional or ventricular. A ventricular ectopic beat (VEB) is characterised by a

³From the Greek meaning ‘out of place’; also known as extrasystoles or premature beats.

⁴Any variation from the normal (sinus) rhythm of the heart beat, including premature beats, heart block, atrial fibrillation and atrial flutter.

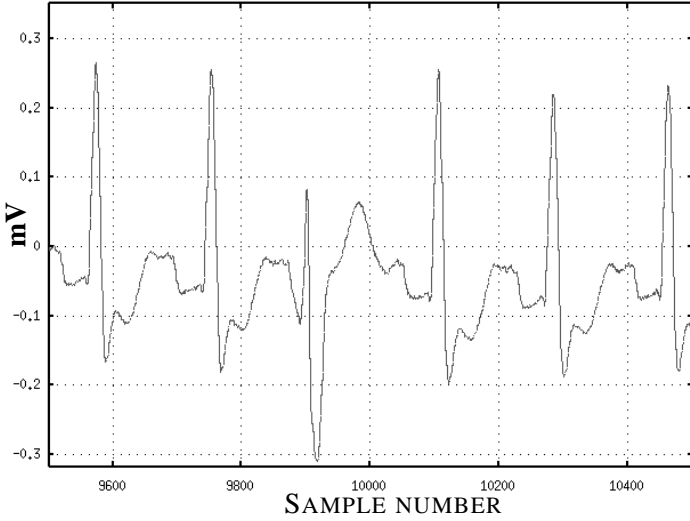


Figure 1.5: A Ventricular Ectopic Beat in the middle of a set of normal beats (3rd beat from the left) for subject 109 of the MIT-BIH database.

broad QRS complex. Occasionally a VEB is followed by an inverted P-wave, but there may be a full compensatory pause before the next normal beat instead. VEBs can also occur at the same time as the T-wave of the preceding beat (R on T ectopics) and may trigger ventricular arrhythmias. VEB identification is an important step in detecting the onset of such fatal arrhythmias.

In the mid 1980's the literature surrounding the utility of ectopic beats as an independent measure of increased risk of MI or sudden death was highly contradictory and no clear conclusion could be drawn at that time [96, 147, 177, 228] even during stress tests [217]. However, by the mid 1990's a large body of research had accumulated to indicate that an increased frequency of ectopic beats (particularly ventricular) is an independent marker associated with a statistically significant increase in risk of cardiovascular disease [12, 261, 280, 282].

1.5 The physiology of beat-to-beat heart rate control and HRV

A subject's baseline heart rate (usually the beat-to-beat HR averaged over 60 seconds HR_{60}) varies on an intra-patient basis (depending upon activity) and on an inter-patient basis (depending on their cardiovascular fitness). However, the instantaneous RR interval or beat-to-beat heart rate (HR_i) also varies around the mean (HR_{60}). Figure 1.6 illustrates how HR_i typically varies for a normal subject at rest over approximately 60 seconds. Note that the average heart rate is about 72 bpm, although there appears to be a trend from this mean to around 80 bpm and then down to about 70 bpm over this 60

second segment. This phenomenon of the heart rate rising and falling on different time scales is known as Heart Rate Variability (HRV). Although the irregularity of the beat-to-beat intervals of a human heart was first noted in the early 1600's [181], its physiological importance was not appreciated until 1965 when Hon and Lee [119] noted that fetal distress was preceded by changes in the pattern of beat-to-beat intervals before any significant change in the baseline heart rate. Since then many different indices and techniques have been proposed and tested on a great variety patient groups with varying degrees of success [181]. Before an overview of the most promising HRV analysis techniques is presented, a detailed description of the regulators of HR and HRV is required.

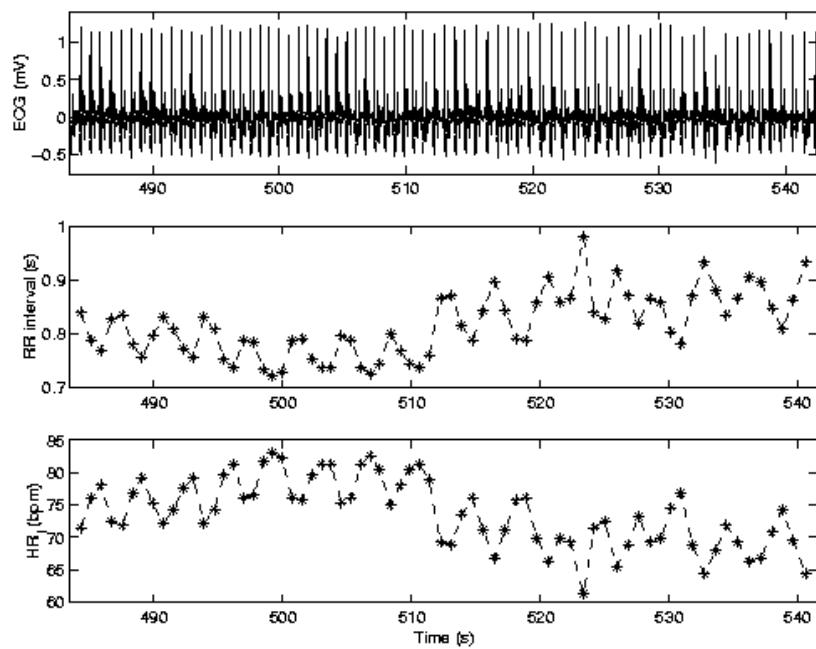


Figure 1.6: Instantaneous or beat-to-beat heart rate, HR_i , (lower trace) and RR interval (middle trace) for a 1 minute segment of ECG (upper trace).

1.5.1 The autonomic nervous system and the sympathovagal balance

The brain, via the CNS, regulates two motor systems, the voluntary motor system (muscular control of the limbs, body and head) and the involuntary motor system or autonomic nervous system (ANS). The ANS regulates the internal organs, including the heart, digestive tract, lungs, bladder and blood vessels. (It should be noted, however, that it is possible to exert voluntary control over internal organs, e.g. by deliberately overbreathing.)

The ANS is divided into two opposing branches, the sympathetic and the parasympathetic nervous systems, which exert opposing effects on most organs. The parasympathetic nervous system can be thought of as the ‘rest and digest’ mechanism and causes HR and blood pressure (BP) to drop (as well as the pupils to constrict) and the digestive system activity to increase. The sympathetic nervous system is rapidly activated in physically or mentally stressful situations and is therefore sometimes referred to as the ‘fight or flight’ response. It causes increases in HR, cardiac output⁵, blood flow to the muscles, pupil dilation and a decrease in digestive system activity. Animals lacking a healthy sympathetic nervous system find it difficult to deal with physical and mental stress. The complicated interaction between the sympathetic and parasympathetic branches of the ANS and the overall effect that they have on the auto-regulation of the cardiovascular system and the *autonomic tone*, has become known as the *sympathovagal balance*.

In the sympathetic system (the left side of figure 1.7) the spinal cord neurons innervate an adjacent series of ganglia. Neurons from these ganglia innervate the internal organs. In the parasympathetic system (right side of figure 1.7), motor neurons from the brain stem innervate ganglia found in the internal organs themselves which in turn innervate the organ in which they are found. The parasympathetic axons from the brain stem extend to the internal organs in various cranial nerves, particularly the vagal nerve (vagus). This nerve, which fans out over a significant portion of the interior lung wall lining is the dominant path for parasympathetic stimulation. For this reason, parasympathetic action is often referred to as vagal nerve activity.

The sympathetic and parasympathetic nervous system ganglia are not simply relay stations and their internal synaptic interactions are not well understood. However, it is well established [70] that the neurons of the parasympathetic ganglia release acetylcholine at their terminals whereas norepinephrine (or *noradrenalin*) is released from the terminals of the sympathetic ganglia. Internal organ regulation is consequently achieved by administering chemical blockers of these agents and norepinephrine is therefore currently used as the clinical standard for measuring the level of sympathetic nerve traffic to the human heart.

Note that the stimulatory frequencies of the branches of the nervous system are much higher than the resultant frequency of the cardiac cycle (HR_i). The vagal and sympathetic stimulations do not have a direct effect on the sinoatrial node but change the sensitivity of this region of the heart (in a competing fashion). When the varying levels of stimulation cross a certain threshold, the sinoatrial node

⁵The volume of blood ejected from the right ventricle (stroke volume) times HR.

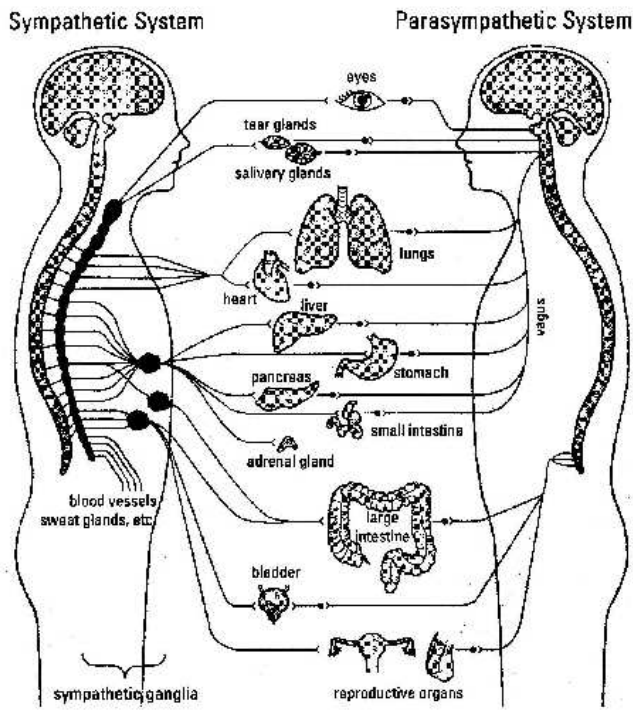


Figure 1.7: Organisation of the autonomic nervous system. The sympathetic system (left) is stimulated by stressful situations, increases HR, cardiac output, blood flow to the muscles and inhibits digestive activity. Stimulation of the parasympathetic branch of the ANS (right) leads to increased digestive activity, and depresses BP, HR, cardiac output. Taken from [70].

is activated. Heart cells have two types of neuromodulatory receptors, one for acetylcholine and one for norepinephrine corresponding to the parasympathetic and sympathetic nervous systems respectively. Their receptors in turn interact with inhibitory or excitatory proteins which through a series of chemical exchanges, decrease or increase the calcium (Ca^{2+}) in the heart cell membrane and inhibits or stimulates HR and the strength of contraction [170].

The heart's intrinsic pacemaker (the sinoatrial node) causes a HR of around 100 to 120 bpm in the absence of any neurohumoral (nervous and hormonal) influence. However, for a healthy heart with no conduction block, the variation of the heart rate is a manifestation of both the (antagonistic) effects of the parasympathetic and the sympathetic nerves through changes in acetylcholine and norepinephrine levels, and a resting healthy human is likely to have a heart rate of around 70 to 80 bpm. During rest both autonomic divisions (the sympathetic and parasympathetic) are thought to be tonically active (i.e. they

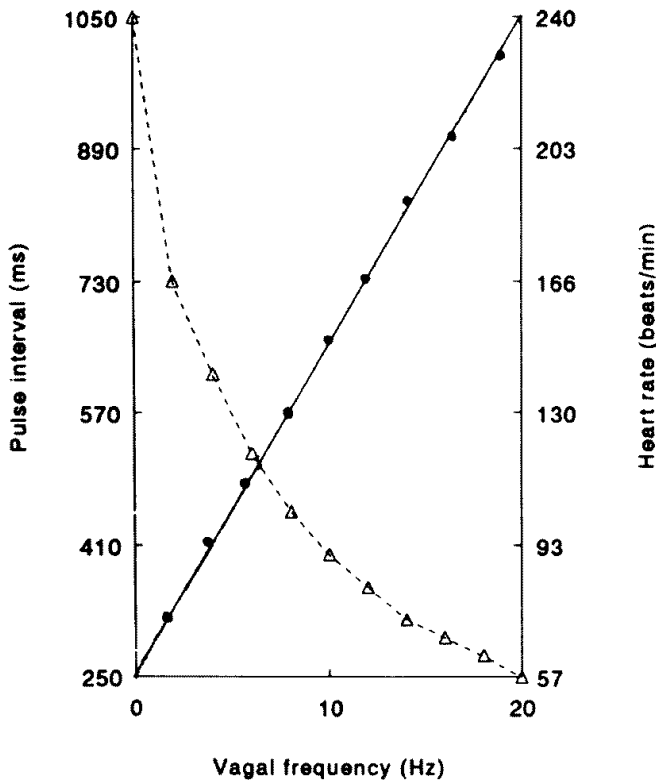


Figure 1.8: Chronotropic RR interval (--) and HR_i (->) responses to graded efferent vagal stimulation (from Malik [105]). Note that the increase in RR interval is proportional to the increase in vagal stimulatory frequency.

have a minimum baseline activity) with the parasympathetic (vagal) effects achieving dominance [170]. Each set of motor neurons that form these two nerve divisions interact in a highly complex manner and the modulation of HR cannot simply be interpreted as a linear sum of two opposing effects: a tachycardic response (i.e. increase in HR) from the sympathetic branch of the ANS and a bradycardic response (a slowing of the HR) from the parasympathetic branch, since they act over different time scales. The parasympathetic response is almost immediate (with only a 400ms latency period) and short lasting, whereas following the onset of sympathetic stimulation there is a delay of up to 5 seconds followed by a steady increase in HR for the next 20 to 30 seconds [105]. Sympathetic activity augmentation is the body's principal method for increasing the HR above the intrinsic level generated by the sinoatrial node to the maximum possible (from about 110 to 200 bpm).

Furthermore, while increased frequency of vagal nerve stimulation tends to slow the beat-to-beat

heart rate, HR_i , (see figure 1.8) and increased frequency of signalling in the sympathetic nerves tends to increase HR_i , at stimulatory frequencies close to that of the sinoatrial node, the cardiac pacemaker can synchronise with the vagal impulses and small increases in vagal frequency may actually cause the HR_i to increase instead. i.e. an increase in the frequency of vagal stimulation can cause an almost immediate increase in heart rate, the opposite of the normal response.

1.5.2 Reflexes controlling heart rate and its variability

The vagal and sympathetic centres are simultaneously stimulated by many different receptors in the cardiovascular and central nervous systems. These receptors, in general, have either a tachycardic or bradycardic effect on the heart rate. The following summary of HR-modulating response mechanisms is taken from Hainsworth *et al.* [105]:

Bradycardic Reflexes

- **Baroreceptors** are situated in the adventitia⁶ of some arteries and cause increases in vagal and decreases in sympathetic activity. Increases in blood pressure will stretch these vessels and cause a rapid increase in baroreceptor discharge frequency. However, this frequency then rapidly falls to a moderate (but still elevated) level. The receptors quickly reset to change their operating range if a change in pressure continues although chronic resetting can occur over a period of many months. These receptors modulate HR on a beat-to-beat basis through parasympathetic stimulation and over a much longer period through sympathetic nerve stimulation.
- **Carotid chemoreceptors** – Stimulation by noradrenalin leads to slowing HR and increases in the rate and depth of respiration. The direct effect on HR changes may be masked by the effect of respiration (which also modifies the HR - see below).
- **Coronary chemoreflex** – A slowing of the HR, mainly stimulated by increases in ventricular pressure - thought to be present only in MI patients.
- **Lung hyperinflation** – Abnormally large increases in lung volume may stimulate certain pulmonary nerves which innervate the bronchi and lungs and may be stimulated during hyperinflation of the lungs.

⁶Membranous structure covering the organ.

- **Indirect RCV changes** – Pulmonary congestion, embolisms or intra-venous (IV) injections of CNS depressants will also cause a bradycardic response.

Tachycardic Reflexes

- **Metabaroreceptors** – Situated in the muscle and stimulated by metabolites produced during exercise. Unlike the baroreceptors they do not respond to stretching or pressure.
- **Atrial receptors** – Stimulated mainly by stretching from increases in atrial volume with a frequency proportional to the atrial pressure.
- **Aortic chemoreceptors** – Stimulation leads to an increase in HR and in the rate and depth of respiration.
- **Muscle receptors** – Effort in the muscle groups associated with the cardiovascular system will innervate the heart through stimulation of receptors sited in particular muscles.
- **Lung inflation (moderate pressures)** – stimulates airway stretch receptors attached to the myelinated nerves.
- **Baroreflex** – Receptors in the arterial and vascular systems sense changes in tension through being stretched by the pressure changes. A decrease in tension (from a drop in BP for example) causes the heart to beat more often and more forcefully while a BP increase produces a bradycardic response.

1.5.3 Factors influencing heart rate and its variability

Apart from the autonomic regulation of the heart via the sympathetic and parasympathetic motor neurones, the average heart rate and the variation of the RR interval (and hence instantaneous heart rate, HR_i) are controlled by a variety of other factors.

Intra-patient factors

The following is a list of known changes that can occur for most humans from either internal stimuli or exogenous interventions.

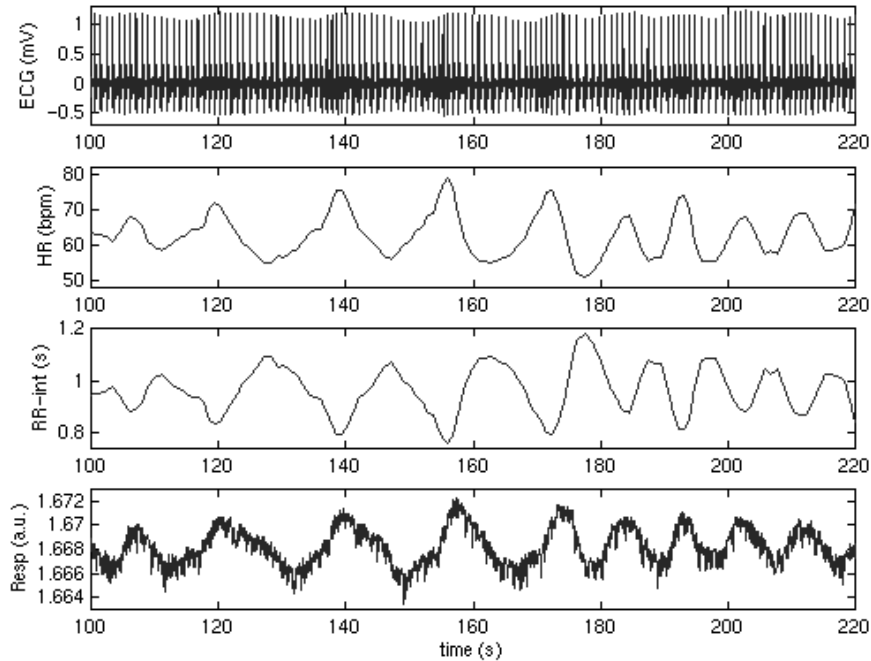


Figure 1.9: Two minutes of ECG, HR_i , RR interval and respiration (from upper to lower trace respectively) from a healthy subject exhibiting RSA. Compressions and rarefactions can clearly be seen in the occurrence of the R-peaks (tall spikes in the ECG). This is reflected in the cyclical changes in the HR and RR interval (2^{nd} and 3^{rd} traces). Note that the lower trace represents volume changes in the chest; as the subject inhales the trace rises and the HR (2^{nd} trace) rises, and when the subject exhales the lower trace falls and the HR drops. From 120 to 180 seconds the subject is breathing at almost 4 respirations per minute (rpm). From 180 to 220 seconds the subject was instructed to breathe at about 7 rpm

- Respiratory Sinus Arrhythmia (RSA) – this phenomenon, initially documented by Hales in 1733 [7], is the acceleration or HR_i on inspiration, and its deceleration on expiration. The magnitude of the effect is highly variable (or non-existent in some older or infirm subjects) and tends to be larger the slower and deeper the breathing is [181]. Figure 1.9 illustrates this phenomenon whereby the QRS complexes are bunched more closely when the respiration trace is moving upwards indicating inspiration. (Here the respiration signal is derived from impedance pneumography; a 22 kHz signal is passed between two ECG electrodes and as air moves in and out of the thorax, the capacitance and hence electrical impedance of the upper body (between these electrodes) changes. The sinusoidal-like variations in electrical impedance at this frequency are therefore representative of the inhalations and exhalations of the subject.) In this case the breathing is deliberately controlled, at about 4 respirations per minute (rpm) initially and then at 7 rpm. Note that the beat-to-beat heart

rate changes synchronously with the (noisy) respiration trace.

RSA is mainly mediated through changes in efferent vagal activity and its magnitude is claimed to provide an index of the level of vagal activity to the heart [161]. RSA is partly influenced by the physical action of the lungs and the cardiac filling volume from the variations in intra-thoracic pressure. However, RSA can be observed in the absence of breathing and therefore the mechanism is partly due to a CNS effect [181]. Furthermore, changes in HR similar to those caused by RSA have also been observed in denervated hearts⁷ and this is thought to be related to increased stretching of the sinus node caused by inspiratory increases in venous return [255]. A more detailed explanation of this will be presented in section 1.7.2.

- Cardiac Output (stroke volume × HR) changes – At rest, changes in HR between about 80 and 150 bpm have little effect on cardiac output because the increase in HR is compensated for by the decrease in stroke volume. Below about 50 bpm stroke volume tends to be fixed and so output falls with HR.
- Valsalva Manœuvre – A respiratory procedure which is thought to provide a rough guide to the integrity of the autonomic neural pathways involved [181]. The subject takes a deep breath followed by a maximal expiratory effort against a closed glottis. This generates an intra-thoracic pressure of around 100 mmHg which is transmitted to the intra-thoracic and abdominal blood vessels. Initially, pulmonary arterial pressure increases but venous return from outside this region is impaired so the cardiac output falls and BP decreases. The resulting baroreceptor activity causes a rising HR and vascular resistance together with the restoration of mean arterial pressure. On removal of the obstruction, venous return is initially enhanced causing a marked overshoot of BP and baroreflex-mediated bradycardia. Patients suffering from autonomic neuropathy show a sustained fall in pressure during the procedure with little or no compensatory tachycardia or a following BP overshoot and bradycardia.
- Decreases in Venous Return – A decrease in the amount of blood returning to the heart can be caused by haemorrhage and postural stress (causing blood pooling). Cardiac filling pressures are consequently reduced (hypovolemia) and the intra-vascular volume moves towards the peripheral veins. This normally causes a HR increase in the short term.

⁷Those physically disconnected from the CNS by a medical procedure.

- The Baroreflex and the vasovagal reaction – The Baroreflex uses arterial and vascular mechanical stretch receptors to adjust the HR if the BP changes. When venous return decreases, BP remains constant or slightly increases while vascular resistance and HR increase. However, despite these increases in vascular resistance and HR this is not enough to compensate for the falling BP from a decreased return in blood volume. Finally if the venous return is too low there may be an abrupt fall in BP and loss of consciousness accompanied by a decrease in vascular resistance and HR. This is known as the vasovagal reaction.
- Exercise – This immediately induces an increase in HR through a CNS mediated vagal withdrawal. Metabaroreceptors within the muscle also become stimulated to increase HR further through increased sympathetic activity which vasoconstricts the non-exercising muscles and splanchnic (soft internal organ) circulation. Receptors involved in lung inflation and possibly baroreceptor inhibition also contribute to the process. Less fit, aged or extremely youthful hearts have a lower HR maximum and a higher resting HR. Training increases the amount of cardiac muscle and stroke volume to produce a higher maximum and lower resting HR.
- Thermoregulation – Peripheral and core body temperature are controlled by both internal and external factors. This may affect peripheral resistance, the resistance to blood flow in the peripheral blood vessels.
- Embolisms – When a small blood vessel is obstructed by fragments of material carried by the blood flow the result is often a tachycardic response as well as the destruction of the organ (in whole or part) that is supplied by this vessel.
- Intra-venous (IV) injections – Stimulatory or inhibitory chemicals can be intra-venously injected to increase or reduce HR.
- Circadian Rhythms – These are defined to be variations in biological activity that appear to have a natural cycle of between 23 and 27 hours, but are often locked into the 24-hour day-night cycle [165] (due to light exposure). The most prominent 24-hour physiological variation in humans is that of the fall in blood pressure and HR for a normal subject while asleep (see figure 1.10). The factors which affect this variation include the health of a patient's ANS, circulating and local hormones, level of patient awareness and the strength of the heart itself [186]. A more in-depth description of these complicated changes will be presented in chapter 5.

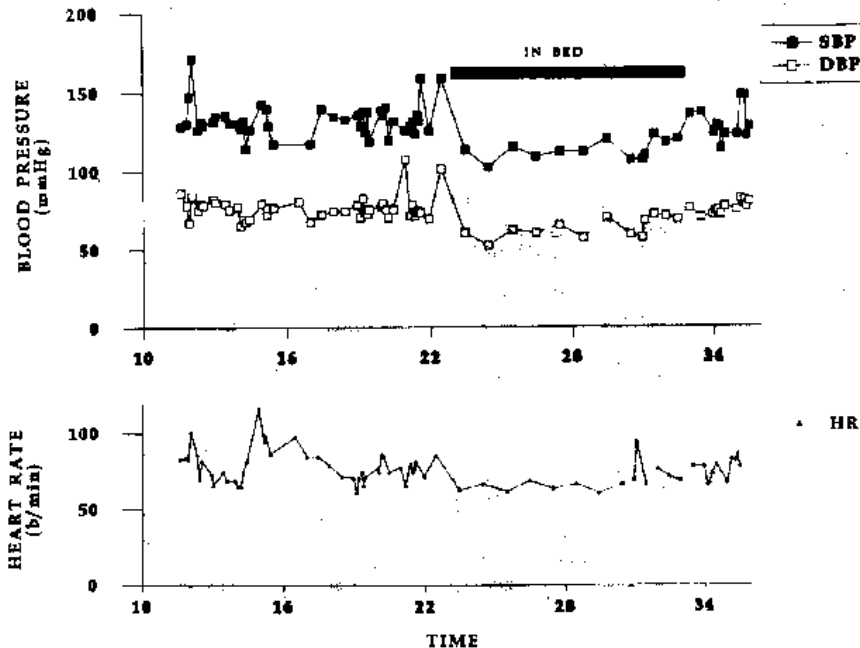


Figure 1.10: BP and HR profile in a normal subject over a 24-hour period. On the horizontal axis, a time of 16 means 4pm and a time of 28 means 4am. Taken from [186].

Inter-patient factors

Although it is possible to expect certain differences in baseline (resting) HR and HRV depending on the type of patient, there are multiple factors that contribute to these differences. It is therefore difficult to categorise or assess patients without using demographic data. The major factors that lead to inter-patient differences in HR and HRV (independently of the intra-patient factors presented above) are:

- Genetics and family history – Although family history can be an important risk factor for cardiovascular disease [21], relatively little is known about the nature of specific genetic risk factors. Research into this area is beginning to grow and some researchers [146] are attempting to identify and characterize genes responsible for inherited disorders in the hope that this information will also provide some insight into common forms of cardiovascular disease.
- Sex – The depression of HRV with age tends to be more marked in males and post-menopausal women, supporting the idea that oestrogen provides some form of protection against coronary heart disease [254]. Furthermore, Barrett-Conner *et al.* [21] found that a positive family history of heart attacks was only independently predictive of death in men and not (pre-menopausal) women.
- Age – HRV is lower in the old and very young although this may be masked by the subject's sex and overall level of fitness [254].

- Medical condition and level of fitness – High cholesterol levels tend to be associated with lower HRV [254].

Furthermore, Blood Pressure Variation (BPV) which affects the overall HRV is known to depend on body mass index, mean BP and BRS, which are known to have a significantly lower within patient population variance than inter-group variance [163].

1.5.4 HR and HRV correlation

Coumel *et al.* [59] stress that the strong correlation between HR and HRV should not be interpreted as the fact that HRV is simply a complex way to measure HR. Although they point out that HR is probably the best index of the sympathovagal balance, they emphasise that a loss of correlation between HRV and other physiological parameters should be looked for as a sign of deterioration in the patient's state (such as the haemodynamic state if the correlates are HR and HRV). Furthermore, since HRV tends to be a function of the baseline HR they suggest that it could be advantageous to normalise the HRV using the HR but do not suggest a scheme other than the fact that it should not be linear.

1.6 Quantifying HRV

Short term and long term variations in HR are known to have different physiological origins and the magnitude of these variations has been shown to be indicative of the autonomic state of a patient [181]. Over the last 20 years, much effort has been put into quantifying these variations with a view to making clinically useful assessments of patient welfare [184]. This section provides an overview of the metrics (and their relevance to autonomic function) which have been found to be the most useful.

1.6.1 HRV metrics from the RR tachogram

HRV metrics are calculated from an analysis of the RR tachogram; the time series of RR intervals. It is important to note that this is an unusual time series in that both axes are time intervals, one being related to the other. Furthermore, since the variability in HR occurs on a beat-to-beat basis, the time series is inherently *unevenly* spaced along the horizontal axis. Figure 1.6 illustrates this concept; each star indicates the location of a beat in time (along the horizontal axis). The horizontal distance between each point (time stamp) is different for each adjacent pair, with the difference recorded on the vertical

axis. The fact that the RR tachogram is inherently unevenly sampled leads to complications and errors in metrics that utilise interpolation, as will be demonstrated in chapter 4.

There are many ways of assessing HRV and a comprehensive list of metrics investigated since the 1960's are detailed by Malik *et al.* [184]. They can be broken down into three basic categories:

- those that measure the statistical properties of the data (often referred to as geometrical indices as they attempt to categorise the shape of a histogram of RR intervals),
- those that evaluate statistics in the time domain,
- and thirdly, frequency domain metrics.

Note that these are all linear techniques. Some nonlinear techniques have been proposed, but there is as yet no clear consensus on the applicability or accuracy of such techniques [184].

1.6.2 Selected time domain measures of HRV

Geometric indices

HRV indices that are generally referred to as geometric (in contrast to time-series methods) attempt to quantify the shape of the histogram of the RR tachogram. According to Malik [182] there are three basic approaches:

1. some measurement of the geometrical form of the histogram is made (e.g. the baseline width or the height of the sample density) and the HRV measure is derived from this number or,
2. the geometrical pattern is approximated by a mathematically defined shape and the HRV measures are derived from the shape parameters, or
3. the general pattern of the geometrical form is classified into one of several predefined categories and the HRV metric is derived on a category specific basis.

The following list of indices is recommended by the Task Force of the European Society of Cardiology and the North American Society of Pacing Electrophysiology, [184], the accepted standard for HRV measurement practice:

- HRV triangular index (or HRV index) – Total number of all NN (normal-to-normal)⁸ divided by the maximal height of the histogram of all NN intervals measured on a discrete scale with bins of $\frac{1}{f_s}$ seconds, where f_s is the sample rate of the ECG recording.
- TINN – (ms) Triangular Interpolation of the histogram of the NN intervals. This is calculated by approximating the NN interval distribution to an isosceles triangle and measuring the width of the unequal side (the base).
- Differential index – (ms) Difference between the widths of the histogram of differences between adjacent NN intervals ($\text{hist}[\delta\text{NN}(t)]$) measured at selected heights (e.g., at the levels of 10^3 and 10^4 samples).
- Logarithmic index – Coefficient, κ of the negative exponential curve $Ae^{-\kappa d}$, which is the best approximation of the histogram of absolute differences between adjacent NN intervals where $d=|\delta\text{NN}(t)|$ and A is an arbitrary scaling factor. Estimation of κ is usually done by fitting to the log of the distribution. The higher the value of κ , the tighter the distribution and the lower the overall variability.

These methods tend to be relatively insensitive to outliers and are therefore considered to be robust to artefacts and computational errors in the RR tachogram derivation. However, they are sampling frequency and recording length dependent. Furthermore, they do not deal well with multi-modal distributions (often caused by sudden shifts in the baseline HR), concentrating on the dominant peak in the histogram and underestimating the overall HRV. For this reason they tend to be used only on very stable patients with little change in baseline HR over well-defined periods (usually 24 hrs).

1.6.3 Scale-independent measures of HRV

Various detrending techniques have been proposed to remove baseline shifts, but usually a scale must be chosen over which the detrending is performed and the HRV is over-estimated at this scale. Recently, scale-invariant techniques have also been proposed [15, 16, 17, 29, 268] to allow a measure of the fractal behaviour of the RR tachogram. These methods include:

- The Fano Factor [268]: the variance of the number of events in a specified counting time T divided by the mean number of events in that counting time. It is a measure of correlation over different

⁸intervals formed from the RR tachogram by excluding non-sinus beats.

time scales T . This measure is sometimes called the index of dispersion of counts.

- Wavelet variance estimation or Wavelet-Transform Standard Deviation [130] is given by $\sigma_{wav}(m) = E[|\mathbf{W}(m)|^2]^{\frac{1}{2}}$ where $\mathbf{W}(m)$ is the wavelet transform calculated over a set of m scales in integer powers of 2 (in the case of the dyadic wavelet).
- The Allan factor [268]: the ratio of Allan variance to twice the mean for a given segment. The Allan Variance, $\sigma_A^2 = \frac{1}{2} < (\Delta RR)^2 >$, is the expectation of the first difference of an RR time series (ΔRR). Since the Allan factor functions as a derivative, this variance converges for most of the commonly encountered kinds of noise, whereas the classical variance does not always converge to a finite value and therefore the Allan factor has the additional effect of mitigating against nonstationarities.
- Detrended Fluctuation Analysis (DFA) [15]: An integrated RR interval time series, is divided into boxes of equal length, n . In each box of length n , a least squares line (or polynomial curve) is fit to the data. The local trend is then removed from the box (detrending). The root-mean-square fluctuation of this integrated and detrended time series is denoted by $F(n)$. $F(n)$ is calculated over all applicable time scales (box sizes), between some reasonable minimum and maximum length. Typically, $F(n)$ will increase with box size n . A linear relationship on a $\log[F(n)]$ to $\log[n]$ plot indicates the presence of power law (fractal) scaling and under such conditions, the fluctuations can be characterized by a scaling exponent, the slope of this plot.

However, Teich *et al.* [268] demonstrated explicit links between these methods and power spectral density and it has been shown that all these measures could be expressed in terms of the power spectral density of the signal. In fact, in the case of stationary or quasi-stationary data, the above methods have been shown to give the same results as power spectral density methods. Furthermore, Heneghan *et al.* [112] have shown that there is a one-to-one correspondence between measures such as the DFA slope ($\frac{\log[F(n)]}{\log[n]}$) and the PSD measured over the same time scales. The analysis in this thesis is therefore confined to linear PSD estimation techniques and the results can be relevant to scale-invariant techniques.

Statistical indices

Statistical HRV indices are calculated on a beat-to-beat basis and are based on Euclidean root-mean-square (rms) metrics. They are therefore, sensitive to outliers and more suited to hand-edited data (which is usually short term due to the labour-intensive nature of such work). Time series indices are generally broken down into two broad categories [154]:

1. Variables directly derived from the beat-to-beat intervals, such as the mean HR and the standard deviation (SD) for the entire record.
2. Variables based on the differences between adjacent cycles, such as the proportion of differences between adjacent cycles that exceed an arbitrary limit.

The following indices are recommended by the Task Force of the European Society of Cardiology and the North American Society of Pacing Electrophysiology, [184]:

- SDNN (ms) – Standard deviation of all NN intervals (also known as SDRR) usually over 24 hours.
- SDANN (ms) – Standard deviation of the averages of NN intervals in all 5-minute segments of the entire (24-hour) recording.
- RMSSD (ms) – The square root of the mean of the sum of the squares of differences between adjacent NN intervals.
- SDNN index (ms) – Mean of the standard deviations of all NN intervals for all 5-minute segments of the entire (24-hour) recording.
- SDSD (ms) – Standard deviation of differences between adjacent NN intervals.
- NN50 (count) – Number of pairs of adjacent NN intervals differing by more than 50 ms in the entire recording; three variants are possible - counting all such NN intervals pairs, counting only pairs in which the first interval is longer, and counting only pairs in which the second interval is longer.
- pNN50 (%) – Percentage of adjacent NN differing by more than 50ms over an entire 24-hour ECG recording.

Many variations of these indices have been investigated with varying degrees of success. For instance, Griffin and Moorman [98] recently showed that neonatal sepsis is associated with a reduced baseline HR variability coupled with short-lived decelerations of HR and consequently the mean and SD of such distributions are often similar to those calculated from the ECG of normal (healthy) neonates. However, Griffin and Moorman found that the observed decelerations significantly altered the third moment of the distribution of one hour RR interval segments. Therefore, measuring this *skewness* allowed the differentiation between septic neonates and normal neonates up to 24hrs before diagnosis of sepsis in the degenerating group. It should be noted however, that the robustness of higher order moments in the context of HRV has yet to be demonstrated.

1.6.4 Components in the frequency domain

Heart rate changes occur on a wide range of time scales; millisecond sympathetic changes stimulated by exercise cause an immediate increase in HR resulting in a lower long term baseline HR and increased HRV over a period of weeks and months. Similarly, a sudden increase in blood pressure (due to an embolism for example) will lead to a sudden semi-permanent increase in HR. However, over many months the baroreceptors will reset their operating range to cause a drop in baseline HR and BP. In order to better understand the contributing factors to HRV and the time scales over which they affect the heart it is useful to consider the RR time series (or tachogram) in the frequency domain.

Components in the long term

Power spectral analysis was first introduced into HRV analysis in 1981 by Akselrod *et al.* [6]. Since then many authors have applied a variety of power spectral estimation techniques. In order to facilitate inter-study comparisons, the frequency spectrum of an RR interval tachogram has been split (by definition) into four frequency bands:

- ULF - Ultra Low Frequency – $0.0001\text{Hz} \geq \text{ULF} < 0.003\text{Hz}$
- VLF - Very Low Frequency – $0.003\text{Hz} \geq \text{VLF} < 0.04\text{Hz}$
- LF - Low Frequency – $0.04\text{Hz} \geq \text{LF} < 0.15\text{Hz}$
- HF - High Frequency – $0.15\text{Hz} \geq \text{HF} < 0.4\text{Hz}$

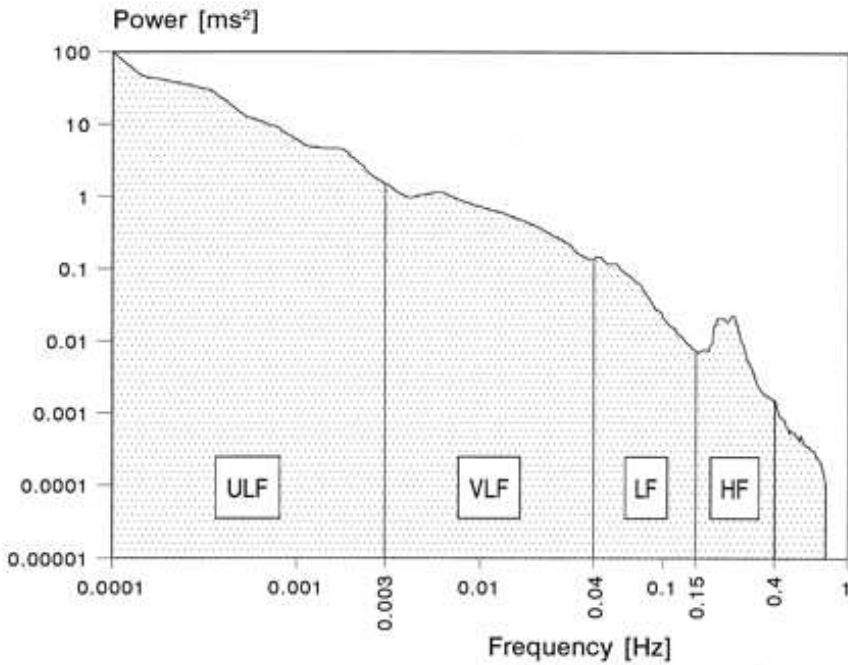


Figure 1.11: Typical FFT of RR intervals over 24hrs. (Taken from [184]). Note that the Meyer waves are masked by the power spectral dominance of the VLF and ULF contributions

Figure 1.11 shows a typical 24-hour PSD with the above bands marked (using logarithmic scales on both axes). Over such a period, frequencies below 0.04 Hz (VLF and ULF) become dominant.

The motivation for splitting the spectrum into these frequency bands lies in the belief that the distinct biological regulatory mechanisms that contribute to HRV act at frequencies that are confined (approximately) within these bands. Fluctuations below 0.04 Hz in the VLF and ULF bands are thought to be due to long-term regulatory mechanisms such as the thermoregulatory system, the reninangiotensin system (related to blood pressure and other chemical regulatory factors) and other humoral factors [46]. In 1998 Taylor *et al.*[267] showed that the VLF fluctuations appear to depend primarily on the parasympathetic outflow. In 1999 Serrador *et al.* [247] demonstrated that the ULF band appears to be dominated by contributions from physical activity and that HRV in this band tends to increase during exercise. They therefore assert that any study that assesses HRV using data (even partially) from this frequency band should always include an indication of physical activity patterns.

Components in the short term

It is generally accepted in the clinical community that the HF band is a measure of the parasympathetic outflow [46]. However, the physiological interpretation of the LF band is more controversial and although

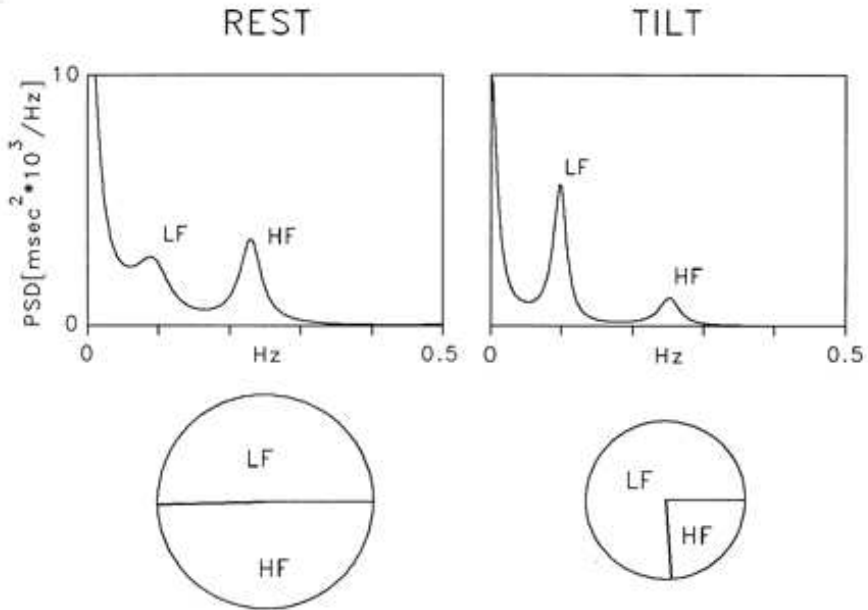


Figure 1.12: AR spectral analysis (model order 12, 10 minute window) of an RR tachogram in a healthy subject at rest and during 90° head-up tilt. At rest, two major components of similar power are detectable at low frequencies (LF) and high frequencies (HF). During tilt, the LF component becomes dominant, but as total variance is reduced, the absolute power of LF appears unchanged compared with that at rest. Normalisation leads to predominant LF and smaller HF components, which express the alteration of spectral components due to tilt. The pie charts show the relative contributions from each band together with the absolute power of the two components represented by the area. Taken from Malik *et al.*, 1996 [184].

sympathetic and parasympathetic mechanisms can operate at these frequencies many authors ascribe fluctuations in the LF band to sympathetic activation only [74].

Consider figure 1.12 where auto-regressive (AR) analysis has been used to generate the power spectral density (PSD) of a 10 minute RR tachogram. We are only interested in the region below 0.4 Hz since the respiratory modulation frequency is the highest component of the HRV signal and this is rarely above 20 rpm (about 0.33 Hz). Two distinctive peaks are usually observed in the PSD, the lower frequency (around 0.1 Hz) being referred to as *Meyer waves*⁹ and the higher frequency component (around 0.25 Hz) being attributed to respiration effects. Figure 1.13 is the PSD of the HR from figure 1.6 derived using Fourier techniques¹⁰. Note the spectral peaks at 0.27 Hz (due to RSA; which corresponds to the recorded rate of respiration of 16 breaths per minute) and at 0.1 Hz (the Meyer waves). There is also a

⁹Often attributed to blood pressure variations.

¹⁰Method to be described in detail in chapter 4.

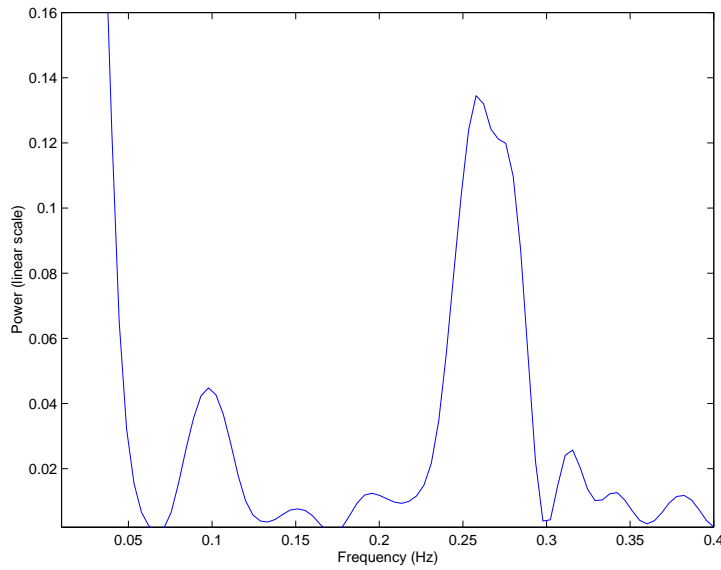


Figure 1.13: PSD (linear axes) of RR intervals for figure 1.6. Note the peaks at < 0.04 Hz, 0.1 Hz (probably due to BP fluctuations) and one around 0.27 Hz - a modulation of the RR tachogram due to respiration. From observation of figure 1.6 it can be seen that the subject was indeed breathing at about 16 breaths per minute, or 0.27 Hz.

significant VLF contribution below 0.04 Hz.

The $\frac{LF}{HF}$ -ratio and sympathovagal balance

Rhythms within the HF band, synchronous with the respiration rate, are due to the intra-thoracic pressure changes and mechanical variations caused by the action of breathing. The manifestation of the respiration rhythms on the RR tachogram is known as Respiratory Sinus Arrhythmia (RSA) as can clearly be seen in figure 1.12. This higher frequency peak (above 0.15 Hz) is mediated almost exclusively by fluctuations of the vagal-cardiac nerve activity [74] and is generally accepted as a marker of parasympathetic activity [116]. The 0.1 Hz peak corresponding to the most dominant of the Meyer waves is mostly mediated by fluctuations of sympathetic nerve activity. Although sympathetic and parasympathetic mechanisms are involved in the LF band, an increase in LF power has always been observed as a consequence of sympathetic activation such as rest-tilt manoeuvres, mental stress, haemorrhage, and coronary occlusion [46]. An increase in LF power is therefore accepted as a marker of sympathetic activation by many authors [137].

Since physiological interventions produce reciprocal changes of sympathetic and vagal outflows¹¹ it has been suggested [7, 74, 163] that the balance between these opposing neural regulatory mechanisms can be quantified by the ratio of the power in the LF to the power in the HF band ($\frac{LF}{HF}$) which is then taken as a measure of the sympathovagal balance. Although this metric is generally thought to quantify the relative contributions of the two branches of the CNS, this idea remains a topic of much debate amongst clinicians. However, there is a consensus that this is a useful model for clinical applications [153].

For instance, clinical studies [252, 273] have presented evidence that the $\frac{LF}{HF}$ -ratio is the best indicator of post-MI mortality up to one year from discharge, although Valkama *et al.* [273] show that only changes in the HF band are relevant for assessment of post-MI convalescence. However, there are two problems with the use of the sympathovagal balance for studying cardiac problem related patients. First, their norepinephrine levels may not change or they may decrease (rather than the usual increase for healthy subjects) when sitting upright, thus confusing any averages taken over an extended period. Second, these patients may have unusually high levels of muscle sympathetic nerve activity and norepinephrine levels with low SD of RR intervals and a low $\frac{LF}{HF}$ -ratio [74]. The measure must therefore be considered on a patient specific basis. In fact sympathovagal balance is only considered to be useful in patients with less advanced stages of heart failure, with little guidance as to which exact criteria identify such patients [74].

Eckberg points out that normalised 0.1 Hz RR interval spectral power changes bear no significant relation to baseline levels or baroreflex-mediated changes to sympathetic nerve activity (as measured by changes in myocardial norepinephrine) [74]. Furthermore, although there is a quantitative relation between respiratory frequency RR interval (HF) spectral power and vagal-cardiac nerve activity, moderate changes of this activity away from the baseline do not alter this HF power. Conversely, large changes of HF RR interval spectral power provoked by respiratory changes may not reflect changes of vagal-cardiac activity. Therefore any analysis must take into account the respiratory changes that occur during the period under analysis.

It has therefore been suggested that power in the HF band is too problematical to measure in most circumstances and that frequency domain measures should concentrate on the lower end of the spectrum. Signorini *et al.* [250] claim that only the contributions below 0.1 Hz help define the differences between pathological and non-pathological conditions. These results have been corroborated by the work of Teich *et al.* [268] in a study to determine which HRV indices proved the most able to differentiate between pathological cases. They found that the indices which were best able to differentiate between

¹¹Over a limited range of arterial pressure; however, some physiological interventions provoke parallel changes [74].

pathological and normal clinical states all relied on a variability calculation equivalent to computing the PSD in the LF range. However, it is clear that the power in the HF band does carry information about the beat-to-beat variability of the heart and its ability to function in a healthy manner. For example, La Rovere *et al.* [164] and McClements [187] have shown that the HF as well as the LF metrics may be useful in long term prediction post-MI. Furthermore, the wealth of clinical studies that have presented evidence for the $\frac{\text{LF}}{\text{HF}}$ -ratio being an excellent indicator of recovery [184, 252] and even the HF band alone [273], illustrates that it would be unwise to discount the HF metric completely at this stage.

The majority of the literature in the field of HRV analysis has demonstrated that frequency domain metrics, rather than time series or geometric metrics, are the most useful indices for assessing patient welfare and differentiating between patient groups [184]. This thesis will therefore concentrate on frequency domain metrics. Furthermore, the origin of long term HRV metrics is unclear and estimates of them may be influenced by factors as diverse as local conditions (e.g. temperature) [181] and quality of sleep [57]. However, short term metrics have been shown to be capable of assessing neurological activity [181, 184] and therefore may have a clinical interpretation as well as be more amenable to controlled experimentation. The scope of this thesis is thus further narrowed to include studies on only the short term (LF and HF) HRV metrics.

1.7 The cardiovascular respiratory system - parameters and models

In order to gain an understanding of when an analysis of HRV may offer useful clinical information, it is necessary to analyse the interactions between the heart and the rest of the respiratory cardiovascular system.

1.7.1 Baroreflex sensitivity

The baroreflex causes the heart to speed up and beat more forcefully when the BP falls. Since vasoconstriction then alters the BP and rate of flow, the speed of the baroreflex therefore determines the peripheral resistance. The empirical investigation of the sensitivity of the baroreceptor control of the heart rate gives rise to the concept of Baroreflex Sensitivity (BRS) which is usually calculated from a measurement of the instantaneous heart rate-arterial pressure response to an intra-venous injection of phenylephrine [161]. The baroreflex gain is therefore defined to be the change in RR interval per change in systolic arterial pressure.

It has been shown [161] that BRS and HRV may be loosely correlated and that BRS may prove a better indicator for the onset of fatal arrhythmias. In a recent paper Kim *et al.* [153] used a method they called complex demodulation, separating the signal into a series of band-pass filtered signals of varying length in order to maximise the resolution. They defined BRS to be the instantaneous amplitude of complex-demodulated oscillations in the RR interval divided by the instantaneous amplitude of complex-demodulated oscillations in systolic blood pressure. They claim that this technique was equivalent to power spectral analysis of the RR tachogram.

La Rovere *et al.* [164] state the need for care in the use of BRS since it is not static after myocardial infarction and sometimes improves shortly after the event. Furthermore, they pointed out that it also varies with activity and emotional state, although not necessarily in the same manner as HRV varies with these states. Despite such complications they found that the values of BRS studied in the first month after myocardial infarction remain predictive of outcome during the next one to two years.

1.7.2 The connection between HR, HRV, BP and respiration - a possible mechanism

There is no simple connection between HR, HRV and BP although some measures of HR and HRV are often (inversely) correlated. That is, stimuli that increase HR often depress the variability of the HR in the short term. Conversely, activities that cause a drop in the average HR can lead to an increase in short term HRV. Although the strength of this correlation can change over time and from individual to individual [212], it is useful to consider the cardiovascular system from a static perspective in order to gain an insight into the relationship between the cardiovascular parameters.

The cardiovascular system is a pressure controlled system and therefore factors that influence changes in BP will also cause fluctuations in HR. In resting humans, beat-to-beat fluctuations in BP and HR are mainly due to respiratory influences and to the slower Meyer waves [64]. Sleight and Casadei [255] emphasise that there is much evidence to support the idea that beat-to-beat HR variations are a manifestation of a CNS oscillator which becomes entrained to the respiratory rate as a result of afferent input from bronchopulmonary receptors.

It is generally agreed [255] however, that coupling of HR, respiration and the cardiac cycle (the flow of blood around the body with its consequent pressures) can be broadly explained as follows: inspiration lowers intra-thoracic pressure and enhances filling of the right heart from extrathoracic veins. Right ventricular stroke volume therefore increases and a consequent rise in the effective pressure of the rest

of the (lesser) circulation is observed. The rise in effective pressure in the pulmonary veins leads to an increased filling of the left heart and hence to an increased left ventricular stroke volume.

The resistance and hydraulic capacitances of the lesser circulation create a lag between inspiration and right ventricular output increase and between the rise of effective pulmonary venous pressure and left ventricular filling. A consequence of this is that stroke volume modulation will decrease with increasing respiratory rate (for a given respiratory depth). Furthermore, the phase lag of the stroke volume change with respect to the corresponding respiratory oscillation will increase for higher rates. In reality, at moderately rapid respiratory rates, the BP and stroke volume fall throughout most of the inspiration. Therefore the fall in arterial pressure with inspiration is due to the preceding expiration. Furthermore, the strength of this relationship increases as the patient moves from a supine to upright position (see figure 1.12).

During expiration, the longer pulse (or RR) interval buffers any change in diastolic pressure caused by the resultant increase in stroke volume, so diastolic pressure changes may correlate poorly with reflex changes. This supports the notion that respiration drives BP changes, which in turn drive the RR (HR_i) changes. Diastolic BP changes with respiration are quite small since the inspiratory tachycardia tends to reduce any inspiratory fall in diastolic pressure (as there is less time for the diastolic pressure to drop).

This observation was first explained by DeBoer in 1987 [64] and although there have been other mathematical models proposed since then (such as the Baselli Model [24] and the Saul Model [238]), most experimental evidence is thought to support DeBoer's model [255]. For a more detailed survey of the last 50 years of cardiovascular respiratory modelling the reader is referred to Batzel *et al.* [26].

1.7.3 The DeBoer model

DeBoer's model [64] first published in 1987, explains how the BP affects both RR interval length and peripheral (capillary) resistance through baroreceptors and the CNS. Note that no slow regulatory mechanisms (< 0.05 Hz) are included in the model. Figure 1.14 shows how the cardiac output is determined by the current value of respiration and the previous RR interval. The new BP value is set by this value of cardiac output and the peripheral resistance. The new BP value then sets the new value for the RR interval. Therefore the model assumes that respiration first affects BP which in turn affects the RR interval. The LF peak in HR at 0.1 Hz observed in steady-state conditions for humans is explained as a resonance phenomenon due to the delay in the sympathetic control loop of the baroreflex: the reflex sympathetic

neural outflow cannot follow beat-to-beat changes in the BP as sensed by the baroreceptors.

The respiratory signal that drives the HF (RSA) variations in the model is assumed to be unaffected by the other system parameters. DeBoer chose the respiratory signal to be a simple sinusoid, although other authors [281] have used more complicated signals. DeBoer's model was the first to allow for the discrete (beat-to-beat) nature of the heart beat. (All previous models had used continuous differential equations to model the system). The model consists of a set of difference equations involving systolic blood pressure (S^{bp}), diastolic pressure (D^{bp}), pulse pressure ($P = S^{bp} - D^{bp}$), peripheral resistance (R), RR interval (I) and an arterial time constant ($T = RC$), with C as the arterial compliance. The equations are then based upon four distinct mechanisms:

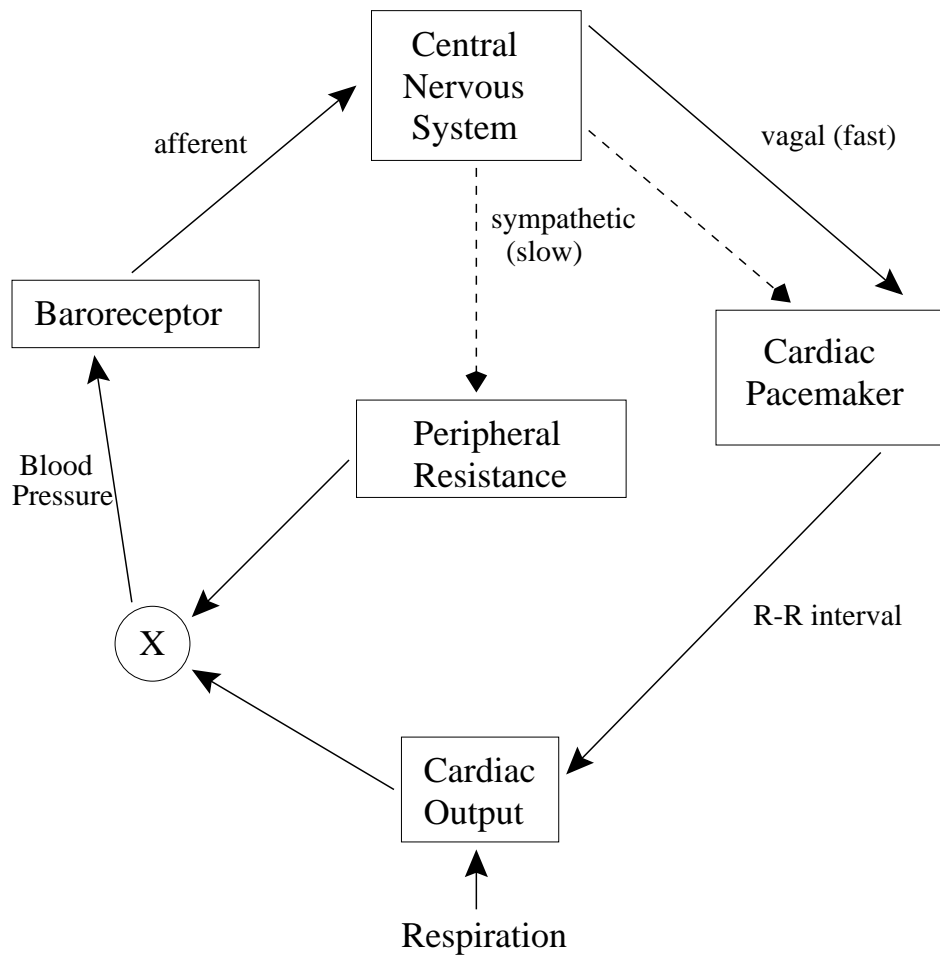


Figure 1.14: Schematic diagram of the cardiovascular system according to DeBoer [64]. Dashed line indicates slow sympathetic control.

1. Control of the HR and peripheral resistance by the baroreflex - The current RR interval value is a linear (weighted) combination of the last 7 systolic blood pressure values ($a_0 S_n^{bp} \dots a_6 S_{n-6}^{bp}$). The current systolic value S_n^{bp} , represents the vagal effect weighted by coefficient a_0 (fast with short delays), whereas $S_{n-2}^{bp} \dots S_{n-6}^{bp}$ represent sympathetic contributions (slower with longer delays). The previous systolic value, S_{n-1}^{bp} , does not contribute ($a_1 = 0$) because its vagal effect has already died out and the sympathetic effect is not yet effective.
2. Windkessel properties of the systemic arterial tree - This represents the sympathetic action of the baroreflex on the peripheral resistance. Basically the Windkessel equation ($D_n^{bp} = c_3 \cdot S_{n-1}^{bp} \times \exp\left(\frac{-I_{n-1}}{T_{n-1}}\right)$) describes the diastolic pressure decay, governed by the ratio of the previous RR interval to the previous arterial time constant. The time constant of the decay T_n and thus (assuming a constant arterial compliance C) R_n , the current value of the peripheral resistance depends on a weighted sum of the last 6 values of S^{bp} .
3. Contractile properties of the myocardium - The influence of the length of the previous interval on the strength of the ventricular contraction is given by $P_n = \gamma I_{n-1} + c_2$ where γ and c_2 are physiology-dependent constants. A longer pulse interval ($I_{n-1} > I_{n-2}$) therefore tends to increase the next pulse pressure¹², P_n , a phenomenon motivated by the increased filling of the ventricles after a long interval, leading to a more forceful contraction (Starling's law) and by the restitution properties of the myocardium (which also leads to an increased strength of contraction after a longer interval).
4. Mechanical effects of respiration on BP - Respiration is simulated by a disturbing P_n with a sinusoidal variation in I . Without this addition, the equations themselves do not imply any fluctuations in BP or HR but lead to stable values for the different variables.

DeBoer uses linearisation around operating points¹³ (normal human values for S^{bp} , D^{bp} , I and T) to facilitate analysis of the model. He found that with the addition of a simulated respiratory signal there is a good correspondence between the power spectra of real and simulated data. He also pointed out the need to perform cross-spectral analysis between the RR tachogram and the S^{bp} and respiration signals. Pitzalis *et al.* [223] performed such an analysis supporting DeBoer's model and showed that the respiratory rate modulates the inter-relationship between the RR interval and S^{bp} variabilities: the higher the rate

¹²if $\gamma > 0$

¹³A good approximation when the subject is at rest

of respiration, the smaller the gain and the smaller the phase difference between the two. They also provided evidence¹⁴ suggesting that the sympathetic drive is not involved in this process. Sleigh *et al.* [255] also present much evidence to support the DeBoer model.

It is known that in some pathological cases (or in the elderly) the coupling between respiration and RR interval can be greatly diminished or completely absent. Some authors [212] have gone further to show that in such cases there may be a reversal of the direction of flow of information, so that the RR interval affects (and leads) the respiration.

1.7.4 Data-driven models

In 1999 Cao and Mees [41] developed a data-driven model for analysing nonlinear interactions between HR, respiration and blood oxygen concentration in the cardiovascular system. They found that it is possible to construct a model which enables reasonably close prediction of the next time step in one signal from a combination of 11 or fewer previous values extracted from the other two signals only. This therefore provides further evidence that BP, respiration and the intrinsic HR are the three main interacting factors in the cardiorespiratory cycle since no other signal is required to provide accurate predictions. However, it should be noted that this analysis was performed on only one subject who was a sleep apnoeic and for which the correlations between the signals would be abnormal (see chapter 5 for a more detailed description).

1.8 The clinical utility of Heart Rate Variability

HRV is probably a less straightforward measure of autonomic system activity than plasma catecholamine concentration, baroreflex sensitivity measured by response to phenylephrine response, or sympathetic activity as measured through microneurography¹⁵. However, there exists a consensus [181] that HRV does give a useful quantification of ANS activity.

Recently Nolan *et al.* [207] have pointed out that chronic heart failure (CHF) is associated with autonomic dysfunction, which can be quantified by measuring HRV. They showed that a reduction in HRV identifies patients at high risk of death and that HRV is a better predictor of death due to progressive heart failure than other conventional clinical measurements, such as elevated BP, the cardiothoracic ratio¹⁶, left

¹⁴The same response is found after β -adrenoceptor blockade.

¹⁵A technique for measuring electrical signals from human peripheral nerves using a tungsten microelectrode

¹⁶The ratio of the maximal transverse diameter of the cardiac silhouette to the distance between the internal margins of the

ventricular end-diastolic diameter and the presence of non-sustained ventricular tachycardia. Their results show that high-risk subgroups can be identified by HRV and elected as candidates for additional therapy.

1.8.1 ATRAMI trials

In 1998 the ATRAMI (Autonomic Tone and Reflexes After Myocardial Infarction) trial [164] results were published. The trial was intended to assign dichotomy limits for positive/negative outcome post-MI and other cardiac dysfunction, establishing the sensitivity, specificity and predictive accuracy of abnormal HRV for the prediction of subsequent events. The ATRAMI study provides clinical evidence that after myocardial infarction the analysis of vagal reflexes (measured by the HF metric) has significant prognostic value independently of left ventricular ejection fraction¹⁷ (LVEF) and of ventricular arrhythmias and that it significantly adds to the prognostic value of heart-rate variability. This is consistent with earlier work of McClements *et al.* [187] and indicates that the HF as well as the LF metrics may be useful in risk-stratification.

1.8.2 Standardisation and clinical community recommendations

In Malik's 1995 book on HRV, Kennedy *et al.* [148] suggest that definite standards for the following characteristics are required:

1. Acceptable ECG recording noise (including baseline wander, electrical artefact etc)
2. Identification of ectopic beats
3. Determination of stationarity and measurement artefact
4. Sampling rates
5. Recommended filter procedures to be used in spectral frequency identification and analysis
6. Optimal short and long term segments of data for time and frequency analysis
7. Guidelines applicable to PSD estimation
8. Stratification based on patient group types - age, ailment, gender

ribs at the level of the right hemidiaphragm.

¹⁷LVEF - the fraction of blood volume in the left ventricle, ejected from this chamber each beat

This led, in 1996, to the European Society of Cardiology and the North American Society of Pacing Electrophysiology forming a task force to produce a document entitled *Heart Rate Variability: Standards of Measurement, Physiological Interpretation, and Clinical Use*, [184]. They were charged with five main tasks;

1. to standardise nomenclature and develop definitions of terms,
2. to specify standard methods of measurement,
3. to define physiological and pathophysiological correlates,
4. to describe currently appropriate clinical applications and
5. to identify areas for future research.

This thesis endeavours to use their standard notation and follow the guidelines whenever possible. However, where there is room for improvement it has been made clear in the text and the opportunity has been taken.

They addressed five main issues in their report [184] and their recommendations are detailed in the following six subsections (1.8.3 to 1.8.8).

1.8.3 Standard terminology

When using time-domain indices, it was recommended that at least two of the following four measures are used¹⁸: SDNN and HRV triangular index for an estimate of overall (long term) HRV, SDANN for an estimate of the long-term components of HRV and RMSSD. The choice should be specific to the type of medical condition being considered and the type of data that it is possible to collect. Furthermore it is inappropriate to compare time domain measures, especially for long term recordings that are derived from ECGs of different time lengths.

For frequency domain measures the Task Force recommended that the number of samples used for the calculation, the size and type of spectral window used and the method of calculating the power in respect of the window is reported to allow inter-study comparisons. Furthermore, when using parametric methods, the type of model, the number of samples, the central frequency for each component and the model order should be quoted. Reporting statistics to test the reliability of the model (such as the

¹⁸as defined above

prediction error whiteness test for goodness of the fit and the optimal order test to check the suitability of the model order used) is also important.

1.8.4 Measurement standards

For long duration recordings (usually in the time domain) the Task Force recommends at least 18 hours for long term HRV analysis. However, Haaksma *et al.* [104] performed an in-depth study of the influence of different time segments on HRV and found that at least 20 hours of data were required for time domain variables or total power¹⁹ in frequency analysis.

The Task Force recommends avoiding the use of frequencies below LF in the PSD for HRV assessments as the major constituent of VLF is the nonharmonic component which is strongly affected by algorithms for baseline or trend removal. The Task Force also recommends that if the LF and HF are normalised by TP (the total power less the VLF and ULF contributions) then both the values for the absolute and normalised calculations should be recorded.

Furthermore, it should be noted that components of HRV provide a measure of the degree of autonomic modulation rather than the level of autonomic tone: the averages of the modulations do not represent an average level of tone. There is therefore a great deal of inter-patient variation. Typical values and their spread over typical patient populations can be found in Appendix C.

Other significant recommendations include:

- ECG sampling rates between 250 Hz and 500 Hz,
- Careful checks to ensure baseline or trend removal does not affect the frequencies of interest,
- Use of an accepted and accurate *fiducial*²⁰ point detector to identify a stable and noise-independent beat location,
- Use of appropriate interpolation techniques, especially in the presence of artefact or ectopy,
- Careful thought as to whether the artefact and ectopic rejection criteria cause a bias in analysing the data that is not discarded,
- Reporting the relative number and relative duration of RR intervals that were omitted and interpolated,

¹⁹calculated between 0.0001 Hz and 0.4 Hz

²⁰consistent reference point on each beat on the ECG

- Reporting the type of interpolation algorithm and frequency of resampling,
- Frequency domain methods to be preferred to time domain methods for short term recordings. The recording should be at least 10 times the lower frequency bound of the investigated component, but no longer (to ensure stability of the signal)²¹,
- Short term HRV assessment to be carried out on 5-minute segments,
- 24-hour indices recommended to assess intervention therapies,
- Environmental variables to be controlled as much as possible during long-term ECG recordings (nature of physical activity as well as mental and emotional state),
- Consideration of whether it is appropriate to compare HRV across patient groups *and*
- Simple automatic editors of RR sequences (such as static timing thresholds) not to be used since they are known to have undesirable effects leading to potentially serious errors.

Sampling rates

In the same year that Malik *et al.* published the recommendations, Abboud and Barnea [2] showed that a sampling frequency of 128 Hz is sufficient, in patients with normal HRV levels, to give a large enough signal to noise ratio in the RR tachogram. However, for patients with significantly lower levels (such as heart transplant patients) they found that a sampling rate of at least 1000 Hz is required.

1.8.5 Physiological and pathophysiological correlates

HRV analysis may permit inferences on the state and function of

1. the central oscillators,
2. the sympathetic and vagal efferent activity,
3. humoral factors, and
4. the sinus node.

²¹A minimum of one minute to assess the HF component and two minutes for the LF component.

Frequency domain methods are more easily interpreted in terms of physiological regulatory mechanisms and the HF band is considered a good marker of efferent vagal activity. The interpretation of the LF component²² as a marker of sympathetic modulation is more controversial. However, the ULF and VLF components account for 95% of the power in the PSD and their physiological correlates are still unknown.

1.8.6 Commercial manufacturers

Commercial companies rarely disclose the methods they employ for assessing HRV, although studies have been carried out on particular systems [195]. Information available in the public domain has been collated by clinicians [181] and a detailed overview of the use of different indices by commercial manufacturers and their products can be found in Kennedy *et al.* [148]. This 1995 report highlights the fact that most of the frequency and time domain parameters listed above are included in almost all commercial devices. In general all the standard HRV parameters are calculated, allowing the user to choose their preferred methods as well as setting relevant parameters (such as the size and type of window for calculating PSDs). Artefact and ectopic rejection criteria tend to follow Malik *et al.* [184] as closely as possible. For example, Reynolds Medical use a simple timing criterion for ectopic rejection and a high frequency noise threshold to reject artefactual segments.

1.8.7 Appropriate clinical applications

HRV assessment is considered by the task force on HRV Standards ([184]) as useful in the following clinical conditions:

- Assessment of risk after acute MI - Depressed HRV is a powerful predictor of mortality and of arrhythmic complications. The predictive value of HRV is independent of other factors established for post-infarction risk stratification (such as depressed LVEF and increased ventricular ectopic activity) [184, 282].
- Prediction of mortality - For prediction of all-cause mortality, HRV is similar to that of left ventricular ejection fraction [184, 208].
- Prediction of arrhythmic events - HRV is superior to left ventricular ejection fraction in predicting arrhythmic events such as sudden cardiac death or ventricular tachycardia [184, 208]

²²particularly when expressed in normalised units

- Assessment of Myocardial Dysfunction - Most patients with a very advanced phase of the disease and a drastic reduction in HRV show little or no LF component, despite clinical signs of sympathetic activation. Therefore, in conditions characterised by a marked and unopposed persistent sympathetic excitation, the sinus node seems greatly to diminish its responsiveness to neural inputs.
- Assessment of outcome after cardiac transplantation: post-operative HRV is highly depressed [257], [77], [14]. In 1995 Bernardi *et al.* [30] conducted a large study to measure HRV in response to carotid baroreceptor stimulation in 26 heart transplant recipients at 2 to 63 months after transplantation and found no evidence for return of parasympathetic control of heart rate during this period.
- Assessment of Diabetic Neuropathy - A reduction in the time domain parameters of HRV not only carries a negative prognostic value but also precedes the clinical expression of autonomic neuropathy.
- Tetraplegia²³ patients represent a unique clinical model to evaluate the contribution of supraspinal mechanisms in determining the sympathetic activity responsible for LF oscillations of HRV since spinal sympathetic neurons are deprived of modulatory control and in particular of baroreflex supraspinal inhibitory inputs.

In 1996 Malik *et al.* [184] produced a summary of selected studies investigating the clinical value of HRV in cardiological diseases other than those reported above. They also point out that there are several well reported intervention strategies that lead to changes in a patient's HRV, namely,

- β -blockade: β -blockers cause modest increases in HRV, although they prevent the normal rise in the LF component observed in the morning hours. In conscious post-MI dogs, β -blockers do not modify HRV. Importantly, β -blockade increases HRV in the animals destined to be at low risk for lethal arrhythmias post-MI.
- Anti-arrhythmic drugs: These tend to decrease HRV.
- Scopolamine: Low dose muscarinic receptor blockers markedly increase HRV indicating an increase in vagal activity. However, the efficacy during long term treatment with this drug is not

²³Patients with chronic complete high cervical spinal cord lesions that have intact efferent vagal and sympathetic neural pathways directed to the sinus node.

known.

- Thrombolysis: HRV is higher 90 minutes after thrombolysis in patients with patency of the infarct related artery²⁴. The difference is not evident on a 24 hour assessment.
- Exercise Training: Exercise training over a reasonable period of time significantly increases HRV and regular exercise is thought to modify the autonomic balance. Exercise can also accelerate the recovery of the physiological sympathovagal interaction, as shown in post-MI patients.

1.8.8 Future research areas

The Task Force recommends the following areas for HRV assessment:

1. Physiological phenomena - investigating the change in HRV during the sleep cycle.
2. Physical training - Assessment of the autonomic nervous system to athletic training and rehabilitative exercise programmes after various disease states, prolonged bed rest and space flight.
3. Pharmacological responses - Considerably more research is required to understand the effects and clinical relevance of altered vagal tone and adrenergic tone on total HRV power and its various components in health and disease.
4. Risk stratification - Prospective studies are needed to evaluate the sensitivity, specificity and predictive accuracy of combined testing (with other factors such as ST-segment variability).
5. Fetal and neonatal HRV studies - for risk stratification and insight into autonomic maturation in the developing fetus.
6. Disease mechanisms - The role of the autonomic nervous system in essential hypertension is an important area of investigation. Furthermore, several autonomic disorders including Parkinson's disease, multiple sclerosis, Guillain- Barre syndrome and orthostatic hypotension of the Shy-Drager type are associated with altered autonomic dysfunction and therefore changes in HRV may be an early manifestation of the condition and be useful in quantifying the rate of the disease progression and the efficacy of therapeutic interventions. This approach may also be useful in evaluating secondary autonomic neurological disorders that accompany diabetes mellitus, alcoholism, and spinal cord injuries.

²⁴Those whose artery remains open.

Malik *et al.* [184] suggest that additional population based studies involving the full age spectrum for both sexes need to be performed. Furthermore, recent research [38, 131] has shown that guidelines need to be formulated which address the issues of how exercise, wakefulness and drug administration affect variability and how HRV can be meaningfully quantified in the light of this.

This thesis addresses the first and last points (1 and 6) above. In chapter 5, the changes in HRV and the ANS (as measured by the $\frac{LF}{HF}$ -ratio) are investigated during the sleep cycle. Chapter 6 presents $\frac{LF}{HF}$ -ratio changes over the course of controlled experiments on orthostatic hypotensives to investigate the reaction of the ANS to postural changes in such patients.

1.9 The problem of HRV measurement and repeatability

Although commercial systems for HRV measurement and assessment are available, no existing techniques are considered to be accurate or meaningful enough by clinicians to provide robust measures of patient welfare and outcome prediction [181]. The following points highlight the main reasons for this:

1. In 1993 the FDA stopped approving HRV monitors because they felt there was no consensus on the usefulness or applicability of HRV measures [3]. Furthermore there was a lack of methods or studies to attest to the accuracy and validity of the methodologies of the commercial manufacturers.
2. Pre-processing methods for the RR time series tend to be arbitrary and *ad hoc*. Data is selected based on its usefulness for the study and lack of artefact. Therefore the techniques are rarely transferable to other studies.
3. Long term HRV metrics include beat-to-beat variations as well as definite shifts in the overall heart rate. A shift into tachycardia or bradycardia will lead to a rise in the contribution to the HRV measure employed, yet the intrinsic variability may be quite low. Detrending techniques are often employed to remove such shifts, yet these changes are part of the overall HRV.
4. The non-linear and nonstationary nature of HRV - This leads to abrupt changes in the signal so that HRV metrics are highly susceptible to outliers and artefacts. The complex variation of the RR intervals are due to many interacting stimuli on many different time scales with different magnitudes. It is difficult to choose the window over which to assess HRV and an appropriate weighting for each scale (or contribution). For example, is a small change in the parasympathetic control more relevant than a slightly larger change in the sympathetic control?

5. Drugs are continually administered to an ITU patient and dominate the changes in HRV, seriously affecting the clinical utility of such measures.
6. The problem of inter-patient comparability - Due to significant inter-patient variation within similar groups it is difficult to ascribe definite values of HRV metrics to delineate pathology from normal behaviour.

1.10 Overview of thesis

This introductory chapter highlights the main problems that remain in HRV analysis. In a large proportion of the literature concerning HRV metrics, the data is pre-processed by hand, with experts performing artefact rejection and noise removal. Furthermore, many publications are contradictory in asserting which HRV methods produce useful results. This is sometimes due to the manner in which the data is selected or pre-processed. Malik [181] states that there is a need for a fully automatic method of HRV measurement (from the raw data) which is robust and will provide clinically useful results on recordings which possess a typical level of noise and artefact. Furthermore, Malik suggests that the perceived need for visual verification and manual correction of long term records has discouraged the assessment of HRV in routine clinical practice and has confined HRV investigations to academic research.

The objectives of this thesis are therefore to (respectively) address each of the six problems detailed in section 1.9 as follows:

1. Chapter 4 introduces an artificial RR interval generator which provides a method of testing the accuracy of HRV estimation methods.
2. Chapter 3 presents methods for automatically removing artefact and ectopic beats from the ECG based upon beat morphology and timing with known confidence levels, allowing the derivation of an RR tachogram with a known level of missing data. Chapter 4 presents a method for the optimal estimation²⁵ of the power in the RR tachogram and results on artificial and real data are presented to evaluate the performance of these new algorithms in comparison to standard methods. These methods are patient type and ECG database independent .
3. To avoid the complications involved in assessing long term HRV introduced through the highly nonstationary nature of the RR tachogram, only short term periods are analysed, where the data

²⁵In the least squares sense

can be considered to be stationary or quasi-stationary.

4. In particular, nonstationarity is reduced by evaluating HRV within sleep states (chapter 5) and during controlled head-up tilt experiments (chapter 6). The equivalence between PSD estimation techniques and non-stationary techniques (see section 1.6.3) for such data, allows the results of this thesis to apply not only to linear PSD-based HRV indices, but to a wider group of scale-independent indices.
5. The issue of drug administration is addressed by limiting the analysis of real data within the thesis (in chapters 5 and 6) to patient groups with either no or highly similar medication regiments.
6. Chapter 5 addresses the issue of inter-patient comparability by presenting a detailed overview of the functioning of the ANS in response to the external and internal stimuli that can have a significant effect on HRV variations. An analysis is then proposed which allows an improved method for minimising within-group HRV variations. An age and sex matched normal test group is compared to an obstructive sleep apnoeic group to demonstrate the improved ability of this method for minimising within-group variation, and increasing between-group separation in terms of the $\frac{LF}{HF}$ -ratio.

This thesis therefore investigates signal processing methods for deriving a clinically useful HRV metric in the context of these six issues. Early chapters concentrate on a robust scheme for extracting an accurate, artefact-free, beat-to-beat heart rate time series (or RR tachogram) using first morphology and then timing information from the ECG. A generic method of identifying ectopic beats and estimating HRV metrics in the noisy conditions of real clinical situations is then produced. Results of HRV signal analysis are presented with both an empirical and physiological justification for concentrating on one particular branch of HRV research (frequency domain evaluation).

Chapter 2 presents a detailed description of a robust algorithm for locating peaks in the ECG (for calculating beat-to-beat timing intervals) and its performance on a standard database. Chapter 3 investigates different methods for removing abnormal beats from the ECG that have been shown to affect frequency-domain estimation of HRV. Chapter 4 gives an overview of frequency-domain metrics and, using artificially generated data for which the frequency components are known exactly, reports on a comparison between the various techniques for HRV analysis. Results are then presented to test the hypothesis that the removal of abnormal beat-to-beat timings from the heart rate time series is essential for

accurate HRV metric estimation.

Chapter 5 describes results of frequency-domain HRV analysis on various patient groups. In particular, the activity-dependence of this type of evaluation is highlighted. A new type of analysis is proposed, involving sleep stage specific recordings, and results are presented to demonstrate its effectiveness in separating normal from unhealthy patients.

Chapter 6 demonstrates the performance of the algorithms developed in this thesis to assess cardiovascular changes in patients taking part in a strictly-controlled physiological test. The sensitivity of the subjects to external factors is examined and a resultant future research plan is proposed in the final chapter.

Chapter 2

QRS detection

2.1 Introduction

The RR tachogram is formed from a series of beat-to-beat timing intervals. Therefore, in order to derive a meaningful RR tachogram, a salient point on the ECG waveform, which can be found consistently on each beat, must be identified. Since the R-peak is the easiest feature to identify, most beat detection algorithms are written to locate this point. The accuracy of the location in time of each peak, and hence the accuracy of the value of each inter-beat interval that comprises the RR tachogram, is therefore dependent on the sampling rate at which the ECG is digitised. As was highlighted in chapter 1, although the current ANSI standards [13] require a sampling frequency of at least 250Hz, subjects with extremely low variability in the RR tachogram may require digitisation rates of 500 to 1000Hz [2] to allow a high enough signal-to-noise ratio and differentiate between the subtle differences in HRV between certain patient populations. However, for the artificial data and the types of patients analysed in this thesis, sampling rates of 128Hz and 256Hz are sufficient [2].

Furthermore, since beats other than normal (sinus rhythm) beats are generated from outside the normal conduction mechanisms they are not considered to be representative of autonomic control mechanisms that manifest the observed variability in the RR tachogram [181]. The beat-to-beat intervals that do not correspond to the time differences between two sinus beats must therefore be excluded from the RR tachogram. This is discussed in more detail, together with methods for identifying and removing abnormal (non-sinus) beats from the RR tachogram in chapter 3. This chapter provides an overview of the most popular and effective QRS detectors together with a detailed analysis of an implementation of the best known technique.

2.2 QRS detection algorithms - overview

In 1990 Friesen *et al.* [85], published a comparison of the noise sensitivity of the most robust automatic QRS detection algorithms available at the time. The following nine algorithms were chosen:

Algorithms based upon amplitude and first derivative:

- Moriet-Mahoudeaux's [200] method based upon thresholded peak detection between restricted windows defined by thresholded derivatives,
- Fraden and Neuman's scheme [82] similar to [200] but with rectification and clipping of the signal,
- Gustafson's ([102]) algorithm based upon analysis of consecutive derivatives and thresholding.

Algorithms based on first derivatives only:

- Menrad's algorithm ([193]), which locates QRS complexes by thresholding the time-derivative within specific windows,
- The method of Holdinger ([117]), which is similar to that of Menrad ([193]) but involves several consecutive derivatives. Algorithms based on first and second derivatives:
- Balda's method ([19]), which uses a thresholding scheme for both the first and second derivatives over a specified time window,
- Ahlstrom and Tompkins' algorithm ([5]), which uses a similar method to Balda ([19]) with the addition of rectification and smoothing.

Algorithms based upon digital filters:

- Engelese and Zeelenberg's method ([76]), whereby the signal is differentiated and low pass filtered to locate amplitudes over a certain threshold. This defines regions within which alternate threshold crossings are sought. These are then categorised as being either baseline shifts or QRS complexes.
- Okada's technique ([211]), which involves smoothing with a 3 point moving average filter, followed by low pass filtering, squaring and then thresholding to locate the QRS complex.

The test data in Friesen *et al.*'s paper [85] was a time series of idealised QRS complexes corrupted by the following noise and artefacts:

1. Power line interference. — $50\text{Hz} \pm 0.2\text{Hz}$ mains noise (60Hz in US data) with an amplitude of up to 50% of full scale deflection (FSD), the peak-to-peak ECG amplitude.

2. Electrode pop or contact noise. — Loss of contact between the electrode and the skin manifesting as sharp changes with saturation at FSD levels for periods of around 1 second on the ECG (usually due to an electrode being nearly or completely pulled off).
3. Patient–Electrode Motion Artefacts. — Movement of the electrode away from the contact area on the skin, leading to variations in the impedance between the electrode and skin causing potential variations in the ECG and usually manifesting themselves as rapid (but continuous) baseline jumps or complete saturation for up to 0.5 seconds.
4. Electromyographic (EMG) noise. — Electrical activity due to muscle contractions lasting around 50ms between DC and 10000 Hz with an average amplitude of 10% of the FSD on the ECG.
5. Baseline drift. — Usually from respiration with an amplitude of around 15% FSD at a frequency of 0.15 to 0.3Hz.
6. Data collecting device noise. — Artefacts generated by the signal processing hardware, such as signal saturation.
7. Electrosurgical noise. — Noise generated by other medical equipment present in the patient care environment at frequencies between 100kHz and 1MHz for between 1 and 10 seconds.

Engelese and Zeelenberg's algorithm [76] performed best for the various combinations of noise, in part due to its powerline notch filter. If the same filter is added to any of the other algorithms, Engelese and Zeelenberg's algorithm is no better than the others. The results of Friesen *et al.* [85] suggest that algorithms based on amplitude and slope are most immune to EMG noise (one of the largest noise contributions). However these algorithms are sensitive to baseline fluctuations. If these can be corrected by high pass filtering or other filtering methods then they offer the best system for QRS detection. A detailed study of an algorithm which incorporates these features (the method of Hamilton and Tompkins [107]) is presented later in this chapter.

It should be noted that the Hamilton and Tompkins algorithm, like all of the non-pattern matching algorithms, is essentially a peak energy-amplitude detection algorithm which almost completely ignores the detailed morphology of the ECG.

2.2.1 Available data — the MIT-BIH database

Over recent years, advances in hardware technology have made possible the acquisition of large databases of multi-channel ECGs such as the Harvard and Massachusetts Institute of Technology Division of Health Science and Technology's MIT-BIH arrhythmia database [194]. This comprises hundreds of two-channel ECGs recorded from patients who suffer from various known heart conditions, as well as examples of healthy ECGs. The two leads of ECG used in the MIT-BIH database are lead I (which gives a morphology similar to lead V5) and lead II (see figures 1.3 and 1.4 in chapter 1). These records have been annotated by clinicians and thus can be used to develop diagnostic software.

Tools, available from MIT's web site¹, enable the programmer or researcher to call libraries that read and compare the clinician-annotated files (for each patient) with any test algorithm he or she chooses. The database and libraries of comparative tests conform to the relevant American National Standards Institute (ANSI) guidelines [13] developed by the Association for the Advancement of Medical Instrumentation (AAMI) [1]. The MIT-BIH database is usually quoted as the ECG data source when results of detection algorithms are presented in the literature and all the associated analysis libraries are in ANSI C. This therefore makes it an ideal database on which to test and evaluate any new developments.

Another source of ECG data, used in later chapters of this thesis, was recorded using a multi-parameter patient monitoring system developed in the Department of Engineering Science in Oxford University, known as the "Software Monitor" [266]. Only three electrodes are used to record the ECG in the Software Monitor, one at V5 (the electrode position close to the cardiac apex, defined as 5th intercostal space, anterior axillary line), one at RA (right arm) and one at LL (left leg) - see figure 1.3. This gives the following three possible ECG signals:

- V5—RA : Approximately equivalent to the clinical definition of channel V5.
- RA—LL : Equivalent to the clinical definition of channel II.
- LL—V5 : Unspecified in clinical literature.

The data collected using the Software Monitor is referred to as the SMP (Software Monitor Project) database. The first channel of this database is therefore equivalent to the first channel of the MIT-BIH database. Unless otherwise stated, single lead data in this thesis will be lead I from the MIT-BIH database.

¹<http://ecg.mit.edu>

Each patient record in the MIT-BIH database, labelled 100-124 and 200-234, consists of 30 minutes of ECG's sampled at 360Hz with 16 bit accuracy and labelled by experts. For the purposes of this study the ECG records have been down-sampled using the MIT tools² to the same frequency and resolution (256Hz, 12 bit) as the ECG data recorded by the *Software Monitor*. The MIT tools account for any changes caused by the down-sampling (such as aliasing, and annotation timing differences) and generate header files to allow synchronisation of the labels with the new data files. The clinicians' annotations consist of the following labels for each beat (a full list of which can be found in Appendix A):

- N — Normal; any beat that does not fall into the S, V, F or Q categories. This category also includes Bundle Branch Block Beats (BBBB) which give a widened QRS complex and can be indicative of myocardial infarction³. However, the broadening is very hard to detect.
- V — Ventricular Ectopic Beat (VEB); ventricular premature beat, an (R-on-T)⁴ ventricular premature beat, or a ventricular escape beat.
- F — Fusion Beat; a fusion of a ventricular and a normal beat.
- Q — Paced Beat; a fusion of a paced (artificially induced) and a normal beat or a beat that cannot be classified.
- S — Supraventricular Ectopic Beat (SVEB); an atrial or nodal (junctional) premature or escape beat, or an aberrant atrial premature beat.

The latter two types of beats are excluded from the analysis described in this report. There are additional labels which are of interest:

- U — marks the centre of unreadable data segments, beginning 150ms after the last beat label and 150ms before the next,
- X — a pseudo-beat label generated during a segment marked as unreadable,
- [and] — rhythm labels marking the onset and cessation of ventricular fibrillation or flutter (VF) respectively.

²The *xform* executable.

³A blockage in the normal conduction paths of the heart that leads to permanent damage to the heart muscle.

⁴A potentially dangerous condition is induced when a premature ventricular contraction occurs during the T-wave of the preceding QRS-T complex. R-on-T phenomenon can induce ventricular tachycardia or ventricular fibrillation.

Note that beat labels are never paired with rhythm labels and beat labelling is discontinued between these labels. Incorporation of the MIT libraries into an algorithm that a user wishes to test enables the generation of a test annotation file of time stamped event labels in a comparable format to the clinician annotation files. When the MIT tools are run on these files a beat by beat comparison is performed, and an output file is created that compares the time scoring of events. Two events are held to be simultaneous (by the ANSI standards [1]) if they occur within $\pm 150ms$ of each other. Thus, in order to perform beat by beat comparisons a pseudo-beat label ‘O’ is generated any time the test algorithm labels a point in the data as a beat and there is no clinician scored label within $150ms$. Table 2.1 is a typical file generated by these tools⁵ for scoring the results from the QRS detector to be described in chapter 3.3.1 being applied to three different records (patients 100, 101 and 103).

Record	Nn'	Vn'	Fn'	On'	Nv'	Vv'	Fv'	Ov'	No'	Vo'	Fo'	Q Se	Q+P
100	1901	1	0	0	0	0	0	0	0	0	0	100.00	100.00
101	1521	0	1	4	0	0	0	0	0	0	1	99.93	99.74
103	1725	0	0	1	0	0	0	0	4	0	0	99.77	99.94

Table 2.1: Standard output of MIT files.

Columns 2 to 12 refer to the beat by beat scoring with a capitalised label denoting the actual event (as labelled by the clinicians) and the lower case letter denoting the labelling provided by the algorithm under test. Nn', Vn' and Fn' are thus, respectively, the number of normals, VEBs and fusion beats that the test algorithm labelled as normals. On' is the number of normal pseudo-beats that the algorithm generated (a ‘normal’ label being generated when there was no beat there). Nv' and Vv' are, respectively, the numbers of normals and VEBs that have been labelled as VEBs. Fv' is the number of fusion beats labelled as VEBs and Ov' the number of pseudo VEB labels (a VEB label being generated by the algorithm when no beat at all occurred in the original)⁶. No', Vo' and Fo' are the number of pseudo-beats generated in the test annotation file for the cases when there was a normal, VEB or fusion beat in the original data but the algorithm failed to detect such a beat.

The scoring thus records the number of false positives (FP; beats identified by the algorithm when the clinician has not scored one), false negatives (FN; beats missed by the algorithm when the clinician has scored one) or true positives (TP; both annotations agree on the time of the event). These are thus defined as⁷ $TP = Nn' + Vn' + Fn'$, $FN = No' + Vo' + Fo'$ and $FP = On'$. The final two columns in

⁵the executable ‘xbx’ in particular

⁶Note that these latter four columns are zero in this example since this algorithm was only designed to identify normal beats

⁷Beat type classification is detailed in the output file but incorrect classification (such as labelling a VEB as a normal) does

table 2.1 are QSe , the sensitivity of the algorithm or the number of True Positives (TP) as a percentage of the total that really exist and $Q + P$, the Positive Predictivity, or the number of TP's as a percentage of the number detected by the algorithm. These two parameters are therefore calculated as follows:

$$QSe = \frac{TP}{TP + FN} = \frac{Nn' + Vn' + Fn'}{Nn' + Vn' + Fn' + No' + Vo' + Fo'} \quad (2.1)$$

$$Q + P = \frac{TP}{TP + FP} = \frac{Nn' + Vn' + Fn'}{Nn' + Vn' + Fn' + On'} \quad (2.2)$$

From table 2.1 one can see that patient 100's heart beat 1902 times over the 30 minute period (an average heart rate of 63.4 beats per minute (bpm)). All the beats were classified as normals by the algorithm (non zero entries in the 2nd, 3rd and 4th columns), although one of these beats was actually a VEB. For this record, the QSe and Q + P are therefore both 100% for the algorithm under test.

The algorithm labelled patient 101's ECG as containing 1522 normals, all of which were normals except one fusion beat. However, four normals were detected by the algorithm when there were no actual beats there. Thus, the Sensitivity is $\frac{1521+1}{1521+1+4} = 0.9974$ or 99.74%. Furthermore, one fusion beat was missed since a pseudo-beat was generated from the MIT annotation file ($Fo' = 1$). Thus the Positive Predictivity is reduced to $\frac{1521+1}{1521+1+1} = 0.9993$ or 99.93%. Patient 103 has a total of 1729 beats, all of which were normal, but 4 of which were missed by the algorithm. Only one beat was labelled as a normal and did not actually occur. It is important to note that the ANSI standards ([13]) allow 5 minutes of adjustment and adaptation for any algorithm being tested and therefore the first five minutes of data are not included in the results generated by the MIT tools.

2.3 The Hamilton and Tompkins QRS detector

Hamilton and Tompkins developed a robust algorithm for the detection of QRS complexes in single channel ECG data and reported the performance of the algorithm on the MIT-BIH database in their 1986 paper ([107]).

The method consists of two stages;

1. Pre-processing of time-series ECG data involving both linear and non-linear filtering and

not affect the statistics; they are based on how many QRS complexes are detected regardless of their classification.

- Post-processing decision rules that operate on this output to identify relevant sections within the ECG for detailed analysis in order to extract the R-peak which is referred to as the fiducial point ([215]). It is this point that corresponds to the clinicians' labelling in the annotation files.

This first stage is broken down into four separate distinct filtering procedures:

- 5-15Hz Band Pass Filtering** — A low pass filter to remove high-frequency noise (such as 50Hz mains interference) is followed by high-pass filtering to remove low frequency components due to breathing (at around 1Hz or below).
- Slope Information Extraction** — Differentiating the signal emphasises the changes from the baseline.
- Squaring** — This emphasises the higher frequencies (where the R-peak is to be found) and ensures that all the data is positive for the final stage of filtering;
- Time Averaging** — Integrating the squared signal within a moving window gives a measure of how the energy is distributed in the ECG and aids fiducial point localisation.

After preprocessing the following set of heuristics and rules are applied:

- A peak (of the time averaged waveform) is located within a segment of the time averaged waveform. The segment is defined by noting points where the time averaged waveform exceeds and then falls below a threshold, which is a fraction of the median-value of the last 10 fiducial points.
- The fiducial point is then found by a scan-back procedure, searching back through the band-pass filtered data for a peak between the points found in the above step.
- If the time integrated packet is significantly longer than usual (probably due to dominant P or T waves) then the length of the window of interest is set to between 150ms and 250ms.
- Refractory Blanking:** As a result of the properties of cardiac tissues, there is a minimum time required to repolarise. A new peak cannot therefore be detected until at least 200ms have elapsed since the last peak detection within the time averaged signal. If a positive detection occurs within this time frame either the previous or current beat must be false. The algorithm assumes the latter.
- If a peak is not detected within a certain fraction (slightly greater than unity) of the current average RR interval then a secondary search through the band-filtered data is conducted with lower thresholds on the median filter.

Using this method Hamilton and Tompkins quote a sensitivity of 99.69% and a positive predictivity of 99.77% over all of the non-paced records within the MIT-BIH database. A description of the implementation of this algorithm used for the work in this thesis now follows with results obtained on the same database originally used by Hamilton and Tompkins.

2.3.1 Detection of QRS complexes: Implementation of the Hamilton and Tompkins method.

The basic algorithm introduced in 2.3 forms the basis of the implementation described in this section.

Figure 2.1 illustrates the various stages of the pre-processor. The sampled input signal $x(n)$ is scaled to ± 1.0 ; $b(n)$ is the sampled signal after band-pass filtering, $d(n)$ after differentiation, $s(n)$ after squaring and $y(n)$ the final output signal after time averaging.

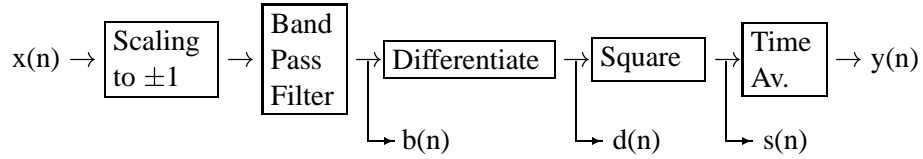


Figure 2.1: Five stage filter sequence of Pan and Tompkin's QRS detector.

A series of heuristics applied to the time-averaged signal then determines in which regions of the ECG waveform, peak detection should take place.

Figure 2.2 shows the output for each of the above stages for three subjects in the MIT-BIH database, with the original ECG data, (scaled to ± 1.0) at the top. In order to compare the implementation of this algorithm with the original results of Hamilton and Tompkins, the MIT-BIH data has been down-sampled to 128Hz. Each window in figure 2.2 therefore represents 5.5 seconds of data. Each stage introduces a delay (except for the point squaring), with a cumulative delay of 40 samples which has been corrected for in the plots shown.

Note that the algorithms were originally developed in 1985 when the standard sampling rate for ECGs was 128Hz. The plots shown in figure 2.2 are for an implementation of Hamilton and Tompkins original algorithms. Modifications of the original algorithm for today's ANSI standard ([13]) will be described later in this chapter.

Band-pass filtering is achieved by cascading a low-pass filter and high-pass filter, the output of which is plotted on the second row of figure 2.2. In the original algorithm the following difference equations

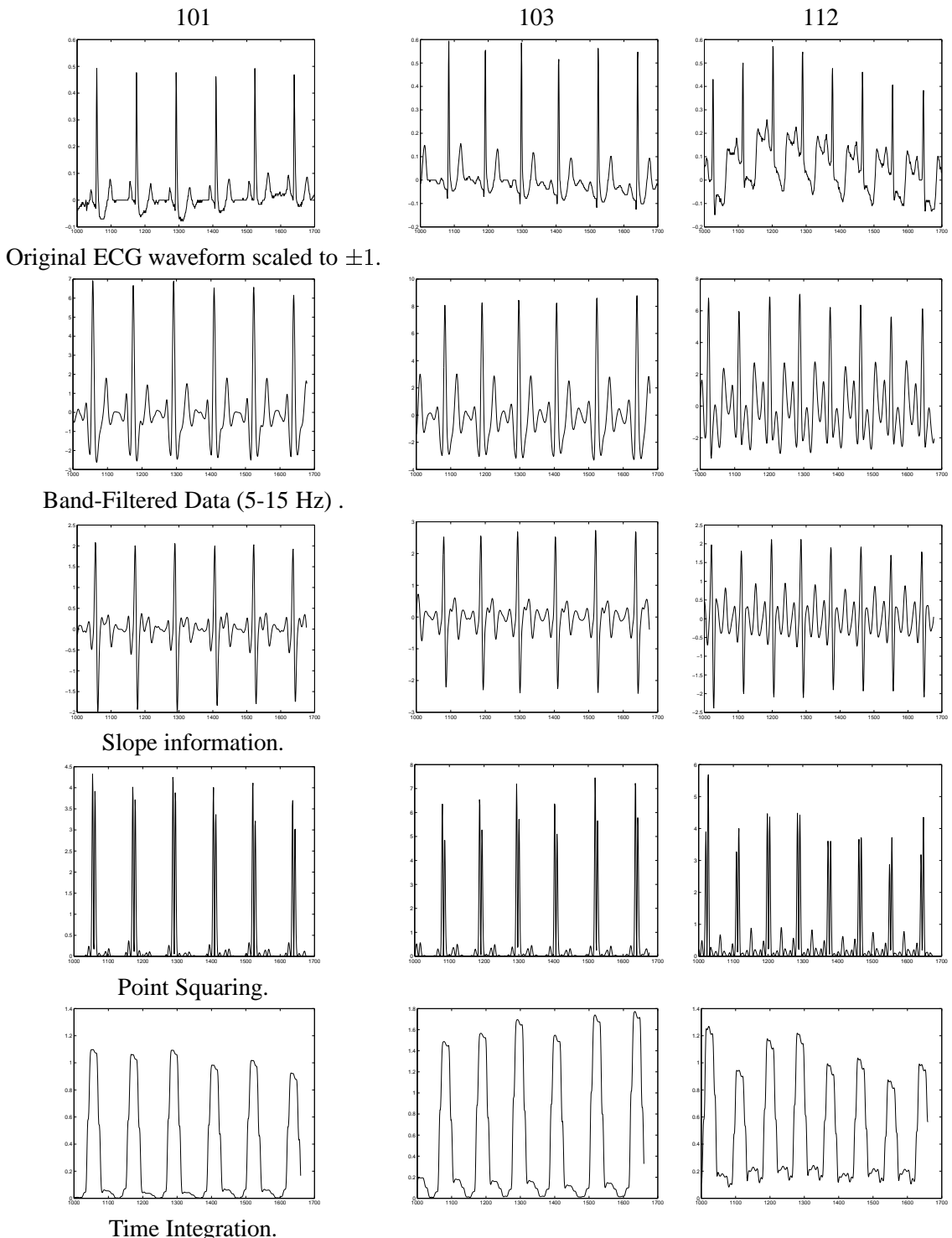


Figure 2.2: 5.5 seconds of MIT-BIH ECG data sampled at a frequency of 128Hz, at each stage of data processing. The processing delays in each digital filter have been compensated for.

represent the equations for the low and high pass filters respectively ⁸:

$$\begin{aligned} l(nT) &= 2l(nT - T) - l(nT - 2T) + x(nT) - 2x(nT - 6T) + x(nT - 12T) \\ b(nT) &= b(nT - T) - \left(\frac{l(nT)}{32}\right) + l(nT - 16T) - l(nT - 17T) + \frac{l(nT - 32T)}{32} \end{aligned} \quad (2.3)$$

where n is the current sample number, T the sample rate, $x(n)$ the original (scaled) data, $l(n)$ the low-pass filtered data and $b(n)$ the subsequent high-pass (and thus band-filtered) data. The low pass filter introduces a delay of 6 samples, whilst the 32 point window of the high pass filter adds a further 16-sample delay. Both filters are IIR filters and thus have a non-linear phase response which introduces shape distortion. However, since the function of the processing is simply to locate high-energy regions in the original ECG waveform, this should not affect the ability of the algorithm to locate the fiducial points.

The third row of figure 2.2 demonstrates how differentiation of the signal emphasises the higher frequency components such as the R wave. The 4-point difference equation introduces a further 2-sample delay;

$$d(nT) = \frac{1}{8} (2b(nT) + b(nT - T) - b(nT - 3T) - 2b(nT - 4T)) \quad (2.4)$$

where $d(nT)$ is the output of the filter at the n^{th} sample

The effect of point squaring ($s(nT) = (d(nT))^2$) can clearly be seen on the fourth row of figure 2.2. Note that the baseline has a very low value and the peaks are now localised within the region of the QRS complex. The positive values are time-averaged over a 32 point window ($y(nT) = \frac{1}{32} \sum_{n=1}^{32} s(nT)$) in order to indicate the most likely regions for the QRS complex. This step contributes a further 16 sample delay to the overall 40 sample delay.

However, since the ECG in the Software Monitor is sampled at 256Hz (in line with the 1999 ANSI standards), changes in the implementation of the algorithm were necessary. Furthermore, given the increase in power and performance of processors since 1986 an FIR band-pass filter design has been introduced, involving floating-point calculations and many more sample delays. The choice of an FIR filter rather than an IIR filter is motivated by the high levels of noise encountered in much of the data analysed in later chapters. The peak-detection algorithm is therefore modified to perform the peak search back through the band-pass filtered data rather than the original ECG waveform. A linear phase response

⁸Integer coefficients are used as integer multiplication was required to achieve real-time processing when the algorithm was originally designed.

is therefore required to ensure the accuracy in locating the time-stamp of the R-peak. Matlab5 has been used to calculate the coefficients of the low-pass and high-pass filters specified by the criteria given in table 2.2. The linear-phase FIR filter is designed using the Parks-McClellan algorithm ([230]) based on the Remez exchange algorithm and Chebyshev approximation theory to obtain a filter with an optimal fit between the desired and actual frequency responses. This is achieved by minimising the maximum error between the desired frequency response and the actual frequency response. Filters designed by this method exhibit an equiripple behaviour in their frequency response in both the pass and stop bands.

Filter Type	f1 (Hz)	f2 (Hz)	Rs (dB)	Rp (bB)	fs (Hz)	Order
High Pass	0.00128	1.28	48	2.096	256	312
Low Pass	35	45	48.25	1.925	256	37

Table 2.2: Filter properties used for coefficient generation with MATLAB5.

Rs is the attenuation between frequencies f1 and f2 (the transition band), Rp is the ripple in the pass band, fs is the sampling frequency and the order is the number of coefficients required to meet the attenuation criteria. Figures 2.3 and 2.4 show the frequency and phase responses for the low-pass and high-pass filters respectively. Notice that they have a linear phase response over the range of interest (below 45Hz) and so the shape of the ECG waveform will not be distorted. There is now a cumulative band-pass filter delay of 175 samples (0.68s).

In the Hamilton and Tompkins algorithm (see section 2.3) the R peak is identified by searching for a maximum within a localised region of points whose amplitude is greater than a threshold set to be the median value of the last 10 R peaks. Tests of the median filter applied to the successive R peaks previously detected showed that the optimal number of peaks was five for this implementation. If a greater number of peaks was included, the median filter was not adaptive enough to track the fluctuations in the amplitude of the R peak.

The median filtering is implemented by saving the peak height of the last five time-integrated QRS packets (the last row on figure 2.2) and determining the median value. Then, when the time integrated data for a new beat crosses a threshold corresponding to a fraction, ϕ , of this value, a flag is triggered so that the algorithm then begins to search for the peak in the central region of this time averaged packet.

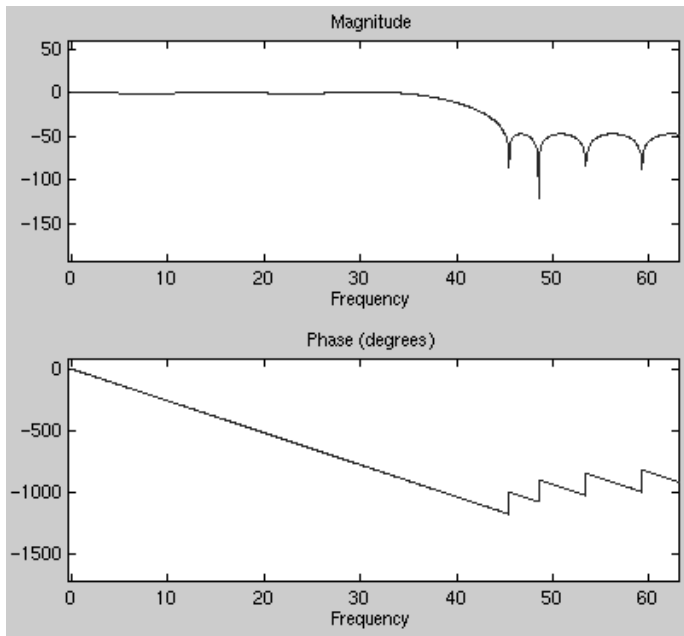


Figure 2.3: Low pass filter frequency and phase response (dB/Hz and deg/Hz).

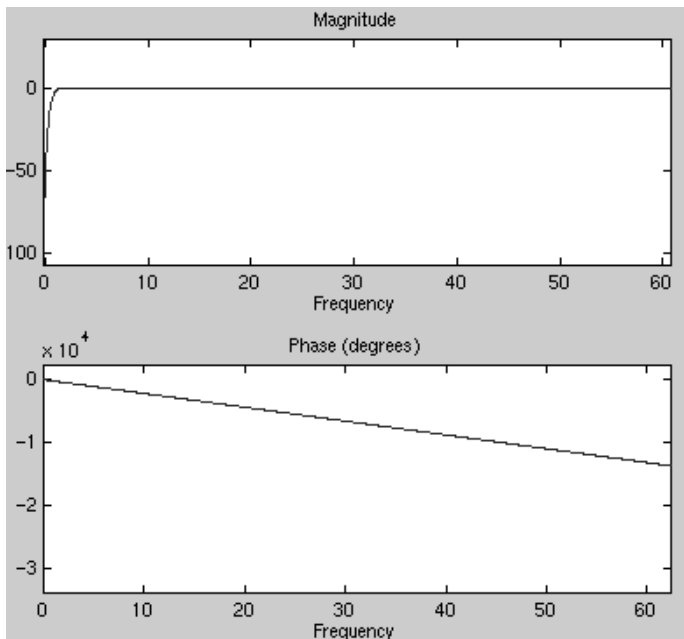


Figure 2.4: High pass filter frequency and phase response (dB/Hz and deg/Hz).

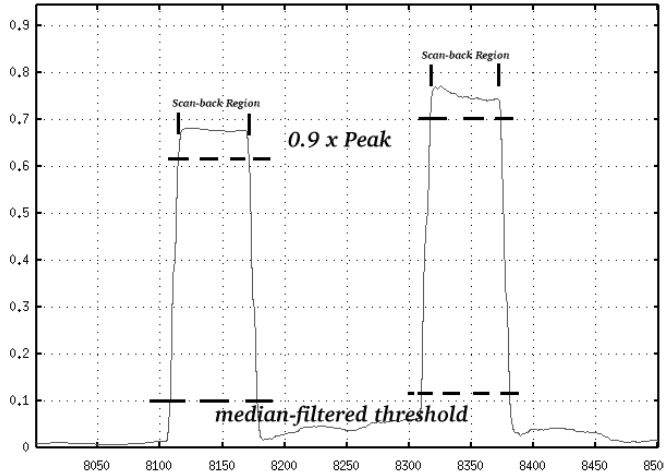


Figure 2.5: The time-averaged waveform for two consecutive QRS complexes. The upper threshold is set at 90% of the peak amplitude of each packet. The point where this intersects the time-averaged waveform defines the region in the original data in which the algorithm scans back to locate a peak.

The search is narrowed by defining a window between the point at which a fraction, ψ , of the *current* peak is crossed on the upslope and the point at which it is crossed on the downslope (see figure 2.5). This procedure is applied to each processed time-averaged energy packet and a search back procedure is then initiated to look for the peak value (i.e. the R-peak) in the original ECG waveform within the central window. Once found, this peak is labelled as the fiducial point. Values between 10% and 90% were investigated (in 10% increments) in order to find the optimal values of the thresholds ϕ and ψ . These were found to be $\phi = 0.2$ and $\psi = 0.9$.

2.3.2 Comparison of performance on MIT normal data

On further, more detailed analysis the algorithm was found to be particularly sensitive to the value of ϕ and when tested on all of the 44 non-paced⁹ lead II ECGs from the MIT-BIH database for different threshold values, an optimum was found for ϕ at 0.16. The optimum peak threshold, ψ , remained unchanged at 0.9. Experiments on threshold adjustment showed that the data recorded from subjects 114, 201, 203 and 228 cause the most problems. The other files were fairly robust to small changes in the value of ϕ .

The results for these values are presented in table 2.3.2, shown on the next page. The average over all the relevant recordings in the MIT-BIH database of $QSe = 99.33\%$ and $Q + P = 99.06\%$ compare well with the results reported in Hamilton and Tompkins' 1986 paper ($QSe = 99.69\%$ and $Q + P = 99.77\%$) on the same data.

⁹as pacemaker spikes will cause problems during peak detection.

Record	Nn'	Vn'	Fn'	On'	Nv'	Vv'	Fv'	Ov'	No'	Vo'	Fo'	Q Se	Q+P
100	1901	1	0	0	0	0	0	0	0	0	0	100.00	100.00
101	1521	0	1	4	0	0	0	0	0	0	1	99.93	99.74
103	1725	0	0	1	0	0	0	0	4	0	0	99.77	99.94
105	2117	29	4	133	0	0	0	0	4	0	1	99.77	94.17
106	1236	459	0	1	0	0	0	0	0	1	0	99.94	99.94
108	1461	13	2	257	0	0	0	0	4	0	0	99.73	85.17
109	2067	28	0	1	0	0	0	0	0	4	0	99.81	99.95
111	1774	1	0	3	0	0	0	0	1	0	0	99.94	99.83
112	2111	0	0	1	0	0	0	0	0	0	0	100.00	99.95
113	1506	0	0	0	0	0	0	0	0	0	0	100.00	100.00
114	1459	30	4	140	0	0	0	0	111	0	0	93.08	91.43
115	1637	0	0	0	0	0	0	0	0	0	0	100.00	100.00
116	1896	97	0	2	0	0	0	0	23	1	0	98.81	99.90
117	1284	0	0	1	0	0	0	0	0	0	0	100.00	99.92
118	1903	13	0	1	0	0	0	0	0	0	0	100.00	99.95
119	1297	364	0	1	0	0	0	0	0	0	0	100.00	99.94
121	1557	1	0	1	0	0	0	0	2	0	0	99.87	99.94
122	2054	0	0	2	0	0	0	0	0	0	0	100.00	99.90
123	1265	3	0	1	0	0	0	0	1	0	0	99.92	99.92
124	1315	36	5	1	0	0	0	0	0	11	0	99.20	99.93
200	1466	698	1	5	0	0	0	0	0	2	1	99.86	99.77
201	1265	198	2	1	0	0	0	0	56	0	0	96.32	99.93
202	1849	10	1	1	0	0	0	0	6	5	0	99.41	99.95
203	2083	369	2	61	0	0	0	0	20	4	3	98.91	97.57
205	2123	64	11	1	0	0	0	0	2	1	0	99.86	99.95
207	1482	109	0	6	0	0	0	0	1	0	0	99.94	99.62
208	1303	817	301	12	0	0	0	0	7	7	2	99.34	99.51
209	2515	1	0	7	0	0	0	0	2	0	0	99.92	99.72
210	2026	150	5	3	0	0	0	0	4	15	4	98.96	99.86
212	2285	0	0	1	0	0	0	0	0	0	0	100.00	99.96
213	2236	192	267	0	0	0	0	0	0	3	2	99.81	100.00
214	1663	212	3	3	0	0	0	0	0	0	0	100.00	99.84
215	2662	131	0	1	0	0	0	0	1	0	1	99.93	99.96
219	1722	51	0	1	0	0	0	0	0	0	0	100.00	99.94
220	1694	0	0	1	0	0	0	0	0	0	0	100.00	99.94
221	1704	309	0	1	0	0	0	0	0	7	0	99.65	99.95
222	2115	0	0	59	0	0	0	0	1	0	0	99.95	97.29
223	1736	447	8	1	0	0	0	0	0	8	0	99.64	99.95
228	1225	300	0	49	0	0	0	0	176	2	0	89.55	96.89
230	1858	1	0	1	0	0	0	0	0	0	0	100.00	99.95
231	1278	0	0	1	0	0	0	0	0	0	0	100.00	99.92
232	1485	0	0	5	0	0	0	0	0	0	0	100.00	99.66
233	1862	688	6	1	0	0	0	0	1	4	0	99.80	99.96
234	2288	0	0	1	0	0	0	0	0	3	0	99.87	99.96
Sum	77011	5822	623	774	0	0	0	0	427	78	15	99.33	99.06
Average													

Table 2.3: Standard output of MIT files.

2.3.3 Discussion of results

The MIT tool set includes a waveform browser which loads and displays the original file together with an annotation file (either the standard ‘attribute’ file scored by clinicians or user generated). The display format is channel 0 as the upper trace and channel 1 as the lower. The annotations (as defined earlier) that appear between the two channels refer to those scored by an analysis of channel 0.

The poor results from data file 114 can be explained by the presence of noise. In figure 2.7 one can observe that the clinicians have annotated a section of heavy noise correctly because the information in the second (lower) channel is also available to them. The algorithm, however, only analyses channel 0 (as with Hamilton and Tompkins original analysis) and identifies several peaks within a high energy region in the second half of the trace (figure 2.6). Figure 2.8 shows how low energy QRS complexes can be missed unless the median filter threshold is reduced but this, of course, would have the effect of increasing the number of false positives.

Figure 2.9 demonstrates how artefacts can seriously affect the ECG waveform and hence the ability to locate the QRS complex. The human eye can just make out where the complexes are on the upper artefactual trace although the clinicians again used the second channel to identify the fiducial points. The algorithm cannot do anything else but miss all the beats during the artefact at the end of the upper trace (marked with an ‘O’). Figure 2.10 is a section of file 228 scored by clinicians. Note that the VEBs (annotated as ‘V’) have a much larger amplitude and width (and hence time integrated energy) and thus increase the median-filtered average of the last five peaks. This has the effect that the algorithm misses the smaller amplitude QRS complexes (see figure 2.11).

The average performance over all the files of 99.33% sensitivity and 99.06% positive predictivity for this implementation of this algorithm is comparable to that of the original Hamilton and Tompkins algorithm. The slightly better results achieved by Hamilton and Tompkins are likely to be due to the utilisation of a scan back procedure in the case of a missing beat. However, an analysis of the beat-to-beat timing intervals is presented in the next chapter. The inclusion of such an heuristic in the algorithm may bias the results of the study.

The morphology of a heart beat can vary greatly depending on the patient and the detection hardware configuration. Often a normal beat for one patient can resemble an abnormal beat for another. The Hamilton and Tompkins algorithm [107] is essentially a peak energy-amplitude detection algorithm which almost completely ignores the detailed morphology of the ECG.

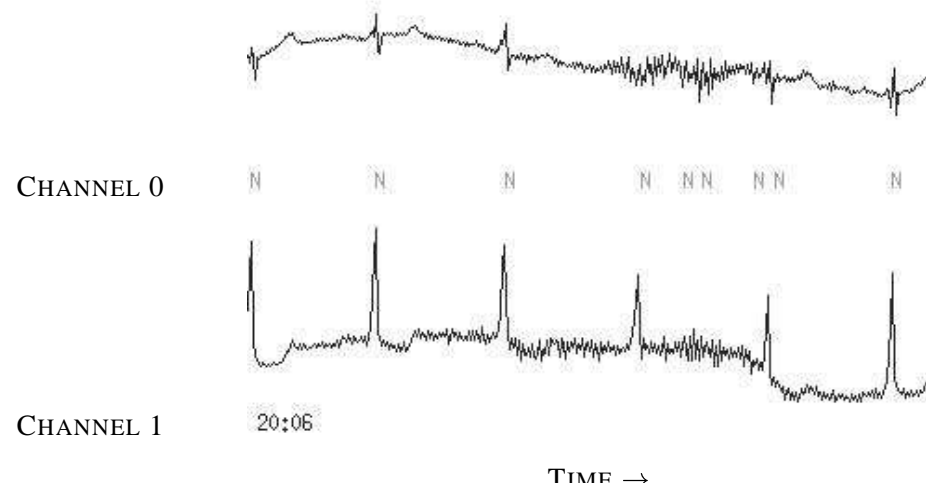


Figure 2.6: Incorrectly labelled file 114 by algorithm due to noise.

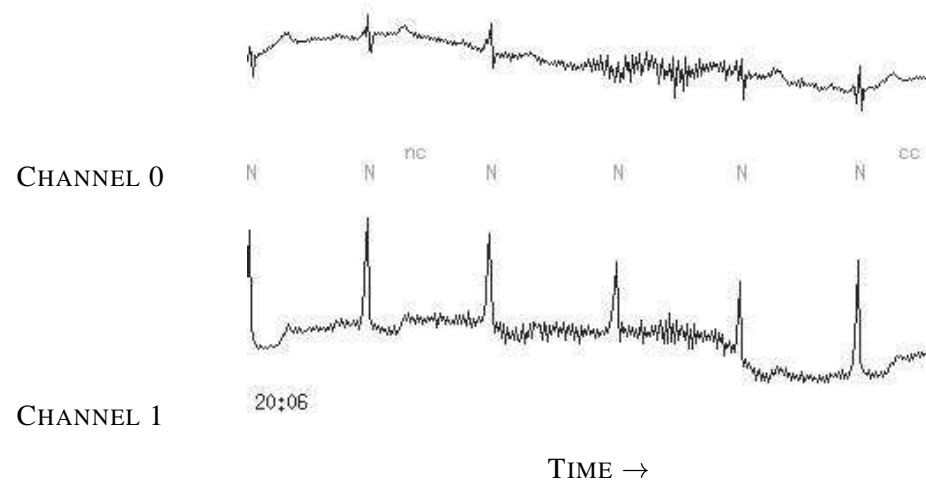


Figure 2.7: File 114 correctly labelled by clinicians.

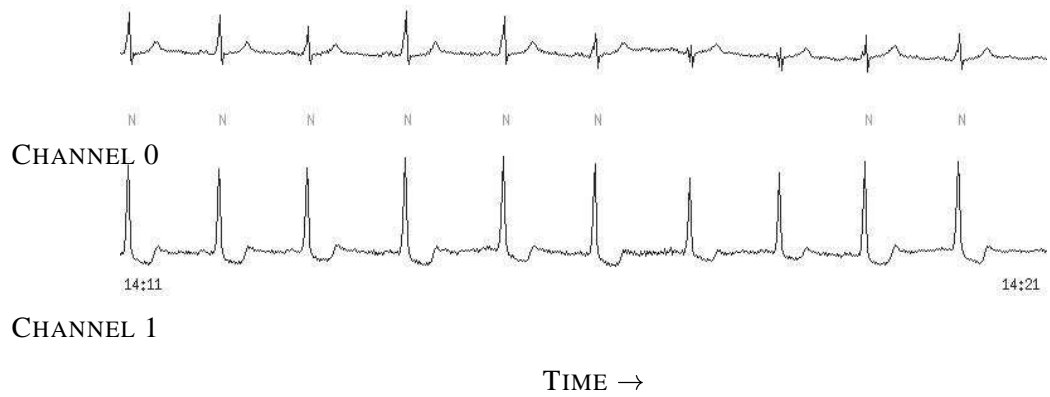


Figure 2.8: Low amplitude QRS complexes (in lead II, the upper channel) missed in file 114.

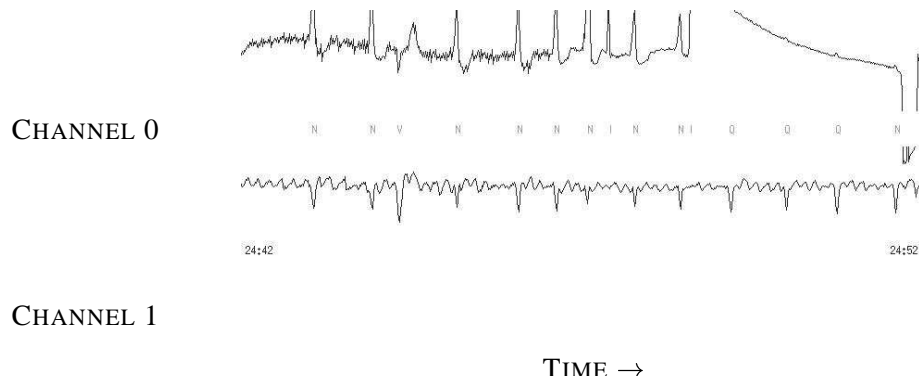


Figure 2.9: Artefacts in file 203

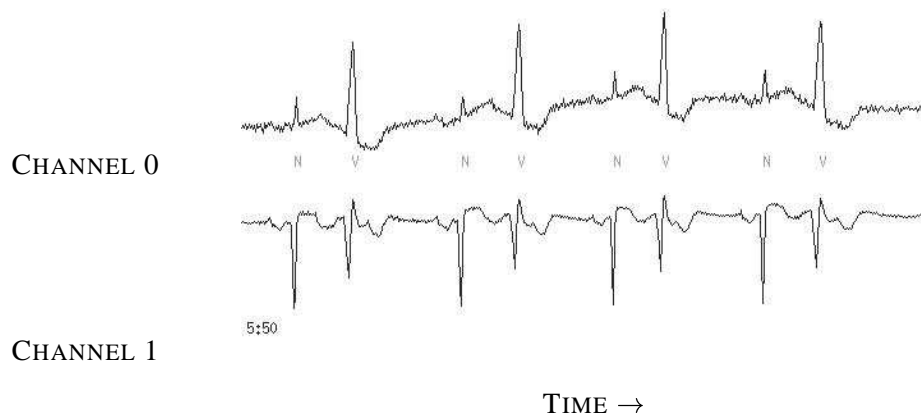


Figure 2.10: File 228 scored by the clinicians



Figure 2.11: Missed QRS complexes in file 228 due to high energy VEBs.

2.4 Conclusion.

Since beats other than normal (sinus rhythm) beats are generated from outside the normal conduction mechanisms they are not considered to be representative of autonomic control mechanisms that manifest the observed variability in the RR tachogram [181]. The beat-to-beat intervals that do not correspond to the time differences between two sinus beats must therefore be excluded from the RR tachogram.

Since the energy/amplitude detection algorithms described in this chapter are not able to distinguish between morphologies, they cannot be used for the exclusion of normal beats from the RR tachogram. Furthermore, the use of thresholds which cannot be pre-determined and are difficult to set on-line indicates that a more adaptive and patient specific approach is necessary. To date, all attempts to recognise ectopic beats have relied on heuristics or pattern matching which are not sensitive to an individual's ECG morphology [1, 85, 11]. Moreover they are based on necessarily unrepresentative and small populations [194] (due to the difficulty in collecting a necessarily large data base). Chapter 3 presents a set of possible solutions to these problems involving a generalisable procedure that can be trained *in-situ* on an individual.

Chapter 3

Abnormal Beat Detection in the ECG

3.1 Introduction

It is common practice to adjust the RR tachogram in order to remove the effect that abnormal (non-sinus, ectopic or aberrant) beats [138] would have on estimating HRV. While it is reasonable to attempt to remove artefacts in the ECG (such as spurious distortions of the signal such as muscle movement or electrode pop; see section 2.2), it is less obvious why the clinical community excludes ectopic beats from HRV analysis since ectopic beats, like sinus beats, are electro-physiological in origin.

There are two main arguments for the removal of ectopic beat related timings from the RR tachogram prior to the calculation of HRV metrics. Firstly, heart rate modulatory signals involving the brain and cardio-vascular system act upon the sinoatrial (SA) node in the heart, influencing the sinus rhythm. Assessments of autonomic function reflect the ability of this system to stimulate the SA node. Ectopic beats originate from secondary and tertiary pacemakers (see section 1.3) and this type of locally aberrant beat will temporarily disrupt normal neurocardiac modulation. Secondly, an ectopic beat will often appear late or early with respect to the timing of a sinus beat. This creates a sharp spike in the RR tachogram which is likely to add a significant power contribution to the power spectrum at an artefactual frequency. Many of the commonly used standard time-series HRV measures involve Euclidean distance computations and therefore just one outlier (such as an ectopic beat) can significantly alter the value of a metric.

Although bursts of sympathetic activity (significantly higher in amplitude and duration than similar bursts during sinus rhythm) have been observed to follow sporadic ectopic beats, it is generally believed that isolated ectopic beats do not cause any significant change in the HRV signal or its power spectrum

calculated once the ectopics beats have been removed [138]. Recent work on 'heart rate turbulence' [241] (the changes in the RR tachogram in the few seconds following an ectopic beat) has shown that ectopic beats can cause a measurable change in the RR interval, but the effect is short lived and is generally ignored for the purpose of HRV metric calculation over five minutes periods [181]. Since HRV analysis is thought only to be relevant to the timing variations in the sinus rhythm, and the presence of ectopic beats can cause errors in the calculation of HRV metrics a robust method for excluding non-sinus beats and artefacts from the RR tachogram is therefore needed.

For the purposes of preprocessing to remove abnormal beats, the ECG can be thought of as two separate components;

1. The P-QRS-T wave generated from the cycle of depolarisation and polarisation of the cardiac muscle *and*,
2. the inter-beat timing separation between each P-QRS-T beat

Both of these components have generally accepted clinical definitions of normality (see sections 3.2.1 and 3.3.1) and this chapter presents methods for analysing the timing and morphology with respect to these definitions to produce a *noise-free* RR tachogram. An algorithm based upon morphology is presented initially. The application of this algorithm results in the exclusion of a high percentage of non-sinus beats from the ECG-derived RR tachogram, without the need for heuristics (as with conventional template matching algorithms). An analysis of the distribution of timings for artefacts, non-sinus and sinus beats is then presented which allows optimal application-specific timing thresholds to be chosen.

3.2 Pre-processing

3.2.1 Ectopic rejection

In general, there are two accepted methods for dealing with the effect of ectopic beats on the RR tachogram [181]. If the ectopic or anomalous beats are very occasional, they are removed and interpolation can be used to add a beat where a sinus beat would have been expected to occur. This is usual in spectral frequency methods where interpolation and resampling are often used to facilitate the calculation of the power spectral density (PSD) using standard methods. Alternatively, if the incidence of ectopics is high within a given segment then it is preferable to eliminate from the analysis, the segments of the HRV signal that contain such a high occurrence. However, this may be very restrictive for some patients

and lead to a great deal of data being discarded. Molgaard *et al.* [195] demonstrate how certain time-series metrics (such as RMSSD - see section 1.6.3) are extremely sensitive to missed beats especially in patients with reduced HRV and therefore it is extremely important to consider whether the data in such cases should be used at all.

Although it is preferable to have an expert clinician selecting the beat classification [138], the processing of lengthy data segments and long term studies is very time consuming. Furthermore, a human expert cannot reliably assign exact markers to the QRS complex over long periods of time and may be more prone to mistakes than automated methods. Malik [183] states that there is a need for a fully automatic method of HRV measurement (from the original ECG) which is robust and will provide clinically useful results for typical recordings. Furthermore, he suggests that the perceived need for visual verification and manual correction of a long term ECG has discouraged the assessment of HRV in routine clinical practice and has confined HRV investigations to academic research.

Malik *et al.* [182] recommend that RR intervals of sinus rhythm should not differ by more than 20% whereas Kamath [138] suggests that each RR interval should not increase/decrease by more than 32.5/24.5% with respect to the previous interval. Malik also recommends that all 5 minute segments with fewer than 30 sinus beats should be rejected. Finally, it should be noted that the rejection criteria [138, 182] are either arbitrary or have been set through empirical testing on limited and disease-specific databases. There is no reason to consider them as definitive limits for general patient populations.

3.2.2 Artefact rejection

When considering the robustness of HRV analysis to RR interval error, Malik [183] suggests that sequences with fewer than 1000 sinus, or Normal-to-Normal (N-N), intervals should be rejected from a study. However, he also acknowledges that this is an arbitrary threshold. Many different exclusion criteria have been proposed by other authors [138, 147, 172, 181, 184], often with little justification. In many cases, where trials have been carried out to analyse the performance of algorithms using different RR interval exclusion criteria, the types of noise and artefacts that are excluded, and/or the database being used, are not specified. In many studies the investigator visually excludes sections of data that appear to be heavily artefactual.

For short term recordings, Kennedy [147] suggests that at least 80% of a 5 minute segment of data should contain acceptable N-N intervals. Kamath [138] suggests that regions with the presence of ectopic

beats or noise for more than 3 seconds should be removed from any analysis. In order to exclude sections of data that involve major distortion, some medical equipment manufacturers have looked at the power in the high frequency content of the ECG and set upper limits for rejection, although the exact thresholds (of power and frequency) that they use are often proprietary information and therefore difficult to ascertain.

Haaksma et. al. [104] have attempted to provide a more theoretical basis for rejecting artefacts and noise using Parseval's theorem. The power evaluated in the frequency domain should be equal to the power evaluated in the time domain. They postulate a *Parseval index* ($\frac{\sqrt{LF+HF}}{SDNN}$) which should be close to unity for any given segment with enough data points to be statistically significant. However, their rejection criterion for ignoring segments with a Parseval index that deviates by more than ± 1 from unity, is still arbitrary and no justification is given for this threshold.

3.2.3 Robust methods

In a comparison of geometric and time-series indices, Malik [183] found that the geometric indices are the most robust to errors introduced by automated HRV calculations of RR tachograms derived from long term ECG recordings. In particular the HRV (Triangular) index and TINN performed better than SDNN and SDANN metrics in noisy scenarios. However, the prevalence of studies reporting positive results involving the use of time-series, and more particularly spectral indices (which are thought to be even more sensitive to such errors) over geometric indices indicates that more robust methods for removing artefact and non-sinus beats from the RR tachogram are required for time-series analysis to be employed more universally.

Recently, blind source separation, or independent component analysis (ICA), has been used to separate biomedical signals into their (independent) components [22, 42, 135, 278, 283]. ICA involves taking multiple observations of a signal which is a mixture of several statistically independent signals and identifying the independent signal sources (usually by minimising or maximising a cost function such as mutual information or kurtosis). ICA is particularly advantageous where the signals that require separation overlap in the frequency domain, and for which traditional linear filtering techniques are therefore not useful. As long as there is no correlation, or entrainment between different signals, and the signal to noise ratio is high enough, then for N independently measured channels of input data, $N - 1$ sources (or components) can be resolved. Therefore, if there are at least three channels of ECG available, the ECG can be resolved into two separate signals. For example, foetal and maternal ECG waveforms have

similar frequency components and are difficult to record without cross-channel interference due to the proximity of the mother and foetus. Recently, Cardoso [42] successfully used ICA to separate out these two ECGs from observations of the mixed ECG signals from three electrodes. This works well because the assumption of signal source independence is valid.

The fact that independent signal sources are responsible for the generation of the ECG and many of the artefacts observed on the ECG suggests that ICA could also be used to remove artefacts from the ECG. Recently, Barros *et al.* [22] and others [110] have implemented ICA techniques to eliminate artefacts from the ECG such as electrode pop and muscle noise. However, ICA involves a non-linear transformation which will distort the ECG waveform to some extent and in some scenarios (such as diagnosis), this may be highly significant. Although other non-linear techniques [242, 250], have also been used to remove stationary non-correlated noise from ECGs, such methods have not been used to remove artefacts as yet.

3.3 Using morphological information to identify normal QRS complexes

Since the variations in morphology are highly patient-specific it is logical to consider an adaptive algorithm that learns a template of normality based on Euclidean distance metric comparisons. This involves creating an average of the last n artefact-free ECG waveforms (centred on the QRS complex) and then performing a statistical comparison between this average or template and the next section of the ECG waveform. Patient 109 in the MIT-BIH database was chosen to test this method since the file contains a significant proportion (2067 out of 2099) of normal QRS complexes with some inter-beat variation in morphology and a small number of abnormal morphologies (32 VEBs).

3.3.1 Template matching for the detection of ectopic beats

Recently Acar *et al.* [4] have developed an algorithm to remove ectopic beats for beat to beat HR measures based on timing considerations and template matching in a multiple-lead signal (using ectopic beats to form the templates). The differential of three ECG leads are added and thresholded to produce QRS complex candidates. The candidates are cross correlated with a pre-selected template with an acceptance threshold of 0.8. If the candidate fails then its energy is compared with the median of the last nine normal QRS complexes. Ectopic beat identification is based upon both timing and morphological considerations. Firstly, if the new RR interval deviates from the median of the last nine normal-to-normal

(N-N) intervals by more than 10% it is rejected. Malik *et al.* are quick to point out that this criterion is arbitrary and will not disqualify ectopic beats which happen to fall within the 10% timing window¹, although they claim that this misclassification will not affect HRV analysis. Secondly, the morphology of the QRS complex is investigated with arbitrary thresholds on the original and differentiated signal, including a check on a median-filtered template of the last nine P-waves².

Although Malik *et al.* [4] claim a specificity of 0.99, a SVEB (Supra-Ventricular Ectopic Beat³) sensitivity of 0.99 and a VEB sensitivity of 0.98 for this technique, the results are specific to one type of commercial ECG recorder and confined to a specific population group (69 healthy adult males) and may not be entirely representative of either the population as a whole or abnormal patient groups. The following sections explore methods which require fewer heuristics, fewer arbitrary thresholds, and no predefined morphological templates.

Matching Indices (MSE and Correlation)

Initially, two statistical comparisons will be considered, the mean square error (MSE) between the test ECG waveform and the template, and the correlation between the test ECG and the template. The waveforms are energy normalised to emphasise differences in shape rather than scale as two similar waveforms with significantly different baselines will have a large MSE between them. The mean is removed from each sample of the ECG waveform in the calculation of the correlation coefficient, C , [95] and the same procedure is applied for the calculation of the MSE. This is motivated by the need to minimise the effect of baseline wander. The correlation coefficient has been chosen since it is a standard technique in image processing to quantify the difference between two patterns. $C \ll 1$ represents a poor match while $C = 1$ represents a one-to-one correspondence between patterns.

If μ_n is the mean value of the n^{th} pattern with D samples then $\mu_n = \frac{1}{D} \sum_{i=1}^D (x_n^i)$ where x_n^i is the i^{th} element of the n^{th} pattern. Similarly, if the mean of the template is calculated from $\bar{\mu}_N = \frac{1}{DN} \sum_{j=1}^N \sum_{i=1}^D (x_j^i)$, where x_j^i is the i^{th} element of the j^{th} (energy scaled) pattern and N is the number of patterns used to calculate the template, $x_N = \frac{1}{N} \sum_{n=1}^N (x_n^i)$. Each pattern includes all of the heart beat from the P wave to the T wave (around one second for a heart rate of 60 bpm). The averaging process and the comparison between the template and the next (test) ECG waveform are performed with

¹Moreover, in this scenario the following compensatory pause will lead to the exclusion of a normal sinus beat as an ectopic beat.

²The P-waves are detected by assuming they are the peak of the waveform in a 200ms window before the R-peak.

³Originates from outside of the ventricles.

the R-peak of the QRS complex as the centre sample of the vector. By choosing D to be equal to 64, this corresponds to creating a vector with 32 points either side of the R-peak. Down-sampling from 256Hz to 64Hz, therefore sets the window of interest (for calculating C) to be one second wide (0.5s either side of the R-peak). N , the number of valid waveforms to be averaged to calculate the template, is set at 10 to allow a smoothing of the beat-to-beat variations common in the ECG [11, 121].

The MSE between the n^{th} pattern, x_n and the template, x_N , is given by

$$MSE = \sum_{i=1}^D \left((x_n^i - \mu_n) - (x_N^i - \bar{\mu}_N) \right)^2 \quad (3.1)$$

and the correlation coefficient, C , is given by ([95])

$$C = \sum_{i=1}^D (x_n^i - \mu_n) \times (x_N^i - \bar{\mu}_N) \quad (3.2)$$

The strategy for classifying a beat as a normal or a VEB is presented in figure 3.1. If the Hamilton and Tompkins algorithm (from chapter 2) detects a heart beat and then the correlation, C , is greater than the threshold C_{min} the beat is classified as a normal. However, if C is less than C_{min} , then the beat is classified as a VEB. The procedure is also repeated using the reciprocal MSE, ($RMSE = \frac{1}{MSE}$), instead of C and thresholding on $RMSE_{min}$ to compare the two quantities as exclusion methods.

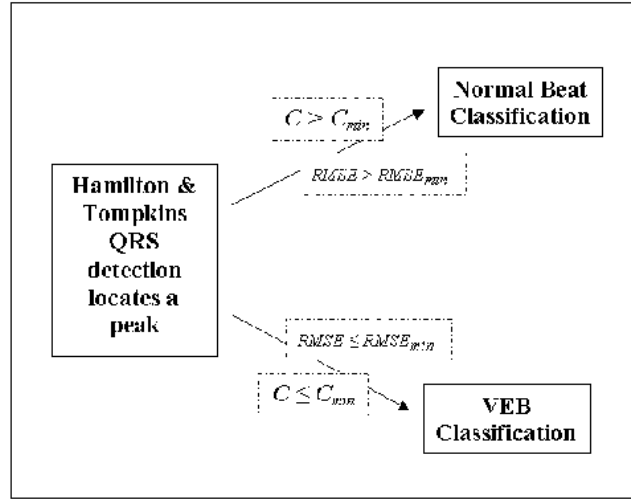


Figure 3.1: Flow of logic for beat classification. If a beat, detected by a conventional QRS detector, has a template correlation value greater than C_{min} or an MLP reconstruction error greater than $RMSE_{min}$, it is classified as abnormal. Otherwise the beat is labelled as a VEB.

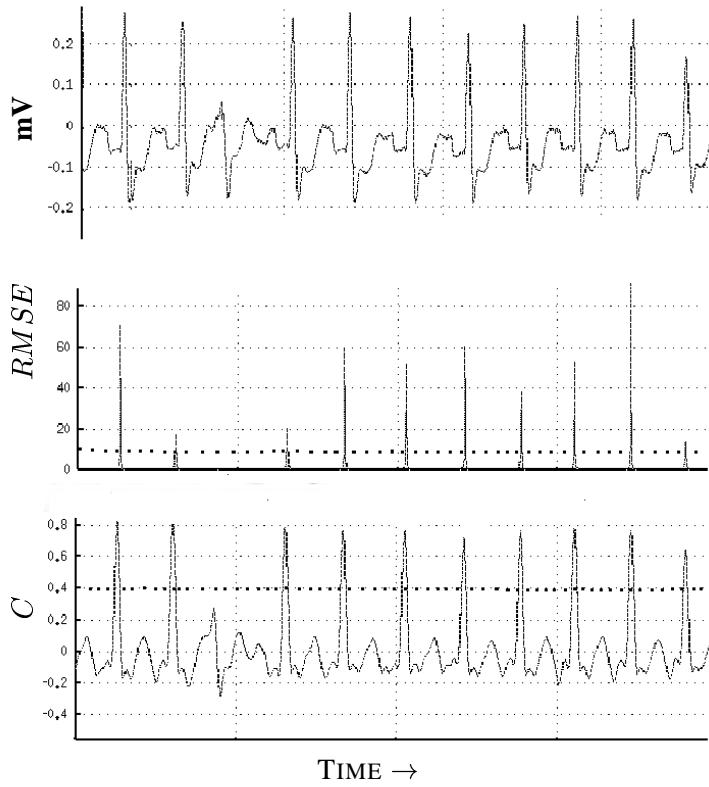


Figure 3.2: From top down: Original ECG waveform, $RMSE$ and C for a 12 second segment of file 109 of the MIT-BIH database. Note the third QRS complex - a VEB - in the original ECG has a small $RMSE$. The dashed lines are the thresholds $RMSE_{min}$ and C_{min} .

Results

The upper graph in figure 3.2 is a 12 second segment of the ECG waveform for subject 109 of the MIT-BIH database. The waveform under test is moved sample by sample, and equations 3.1 and 3.2 are computed using a template which is updated every time a valid QRS complex is detected. The middle plot shows the sample-by-sample computation of the $RMSE$. Note how the $RMSE$ varies greatly from one QRS complex to another whereas the correlation peaks (in the lower graph) have a more uniform distribution. The thresholds which distinguish ectopic from normal beats, $RMSE_{min}$ and C_{min} , are shown as dashed lines across the graphs.

Table 3.1 illustrates how increasing the correlation coefficient threshold C_{min} from 0.25 to 0.8 leads to a steadily increasing number of VEBs being correctly classified. However, this is also matched by an increase in the normals being misclassified by this system. A value of $C_{min} = 0.8$ allows the highest number of VEBs to be detected (28 out of 32, the maximum possible number, given that the Hamilton and Tompkins algorithm only detects 28 of the beats that are annotated as VEBs; see table 2.3.2 in section 2.3.2) but this leads to more than half of the normals being classified as VEBs.

C_{min}	N classed as N	N classed as VEB	VEB classed as VEB	VEB classed as N	artefact classed as VEB	Normals missed
0.80	840	1227	28	0	1	0
0.70	1929	138	27	0	1	0
0.60	2032	35	26	0	1	0
0.50	2058	9	26	0	1	0
0.40	2063	4	24	0	1	0
0.30	2065	3	8	0	1	0
0.25	2066	1	1	0	1	0

Table 3.1: Performance of Hamilton and Tompkins/Correlation combination algorithm on patient 109 for classifying beat morphologies for different values of C_{min}

$RMSE_{min}$	N classed as N	N classed as VEB	VEB classed as VEB	VEB classed as N	artefact classed as VEB	Normals missed
10.0	1981	86	28	0	1	0
2.0	2053	14	26	0	1	0
1.5	2056	11	26	0	1	0
1.0	2059	8	22	0	1	0
0.6	2061	6	14	0	1	0
0.5	2062	5	6	0	1	0

Table 3.2: Performance of Hamilton and Tompkins/ $RMSE$ combination algorithm on patient 109 for classifying beat morphologies for different values of $RMSE_{min}$

Table 3.2 presents the results for different reciprocal MSE thresholds, $RMS E_{min}$. As the threshold is increased the number of VEBs classified correctly increases. Note that the lowest classification error that can be achieved with this method is for a value of $RMS E_{min}$ of 10.0. All the possible VEBs are correctly classified (given the restrictions of the Hamilton and Tompkins algorithm) but at the cost of classifying 86 normals as VEBs. Therefore, a much improved classification performance is achieved using $RMS E$ rather than C .

Limitations of template matching

The use of thresholds which cannot be pre-determined or set on-line, together with the limited performance of template matching algorithms to distinguish normal beats from VEBs suggests that a more adaptive approach is necessary. Since artificial neural networks (ANNs) can be trained to learn and emphasise certain features of a pattern (as opposed to giving equal weighting to all parts of a given pattern as in the above statistical comparisons), they are an ideal choice for an adaptive method. The next section presents the basic theory of neural networks and a practical implementation of an ANN for the detection of VEBs.

3.3.2 Neural Network for ECG analysis

Background

Section 3.3.1 demonstrated that the use of simple statistical methods to identify abnormal morphologies in the ECG leads to either a high number of false negatives or false positives. Preliminary studies by Jabri *et al.* [132], and Hu *et al.* [125] have shown that the application of ANNs to ECG analysis enables different QRS morphologies to be classified more accurately than with conventional algorithms. Hu *et al.* [125] investigated a 6-3-1 multi-layer perceptron (MLP) for classifying 13 different morphologies found within the MIT-BIH database. They extracted 51 samples from each beat and reported results of 84.5% accuracy on a small subset of the MIT-BIH database (across several patients). Jabri *et al.* [132] extracted 21 features from the ECG time series and implemented a 21-5-3 MLP to classify segments of ECG into three types of arrhythmias. Classification accuracy on a database of 70 patients was found to be around 95%, but details of training and test sets are not given in the paper.

Before a description of how an MLP can be used to perform dimensionality reduction to encode the relevant features of a normal heart beat in sections 3.3.5 to 3.3.10, the MLP architecture and its learning

algorithm are introduced in section 3.3.3 and 3.3.4.

3.3.3 The multi-layered perceptron

This section describes relevant aspects of neural network theory. The error back-propagation algorithm is derived from first principles in order to lay the groundwork for training an auto-associative neural network.

The neuron

The basic unit of a neural network is the neuron. It can have many inputs and its output value, ϕ , is a function, f , of all these inputs. Figure 3.3 shows the basic architecture of a neuron with three inputs.

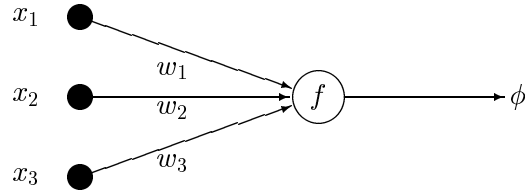


Figure 3.3: The basic neuron

For a linear unit, the function f , is the linear weighted sum of the inputs, sometimes known as the activation a , in which case the output is given by

$$\phi = a = \sum_i w_i x_i \quad (3.3)$$

For a non-linear unit, a non-linear function f , is applied to the linearly weighted sum of inputs. This function is usually the sigmoid function defined as

$$f_\sigma(a) = \frac{1}{1 + e^{-a}} \quad (3.4)$$

The output of a non-linear neuron is then given by

$$\phi = f_\sigma\left\{\left(\sum_i w_i x_i\right)\right\} \quad (3.5)$$

If the outputs of one layer of neurons are connected to the inputs of another layer, a neural network is formed.

Multi-layer networks

The standard MLP consists of three layers of nodes, the layers being interconnected via synaptic weights w_{ij} and w_{jk} as shown in Figure 3.4. The input units simply pass all of the input data, likewise the non-linear output units of the final layer receive data from each of the units in the hidden layer. Bias units (with a constant value of 1.0), connect directly via bias weights to each of the neurons in the hidden and output layers (although these have been omitted from the diagram for clarity).

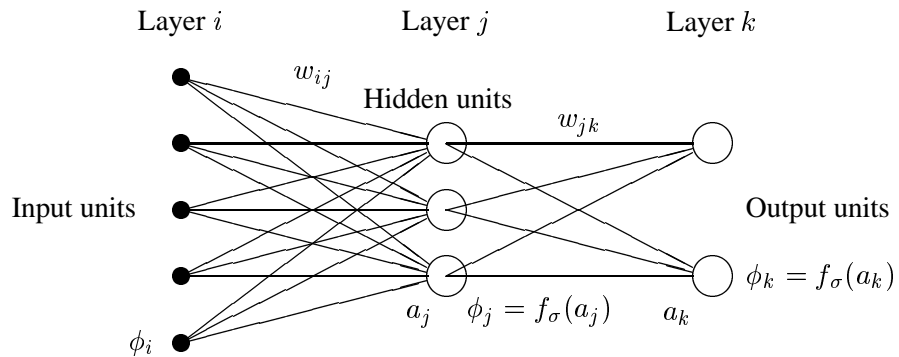


Figure 3.4: Schematic of a 5-3-2 multi-layer perceptron. Bias units and weights are omitted for clarity.

Learning algorithm

The input data used to train the network, now defined as ϕ_i for consistency of notation, is fed into the network and propagated through to give an output ϕ_k given by

$$\phi_k = f_\sigma \left(\sum_j w_{jk} f_\sigma \left(\sum_i w_{ij} \phi_i \right) \right) \quad (3.6)$$

During training, the target data or desired output, t_k , which is associated with the training data, is compared to the actual output ϕ_k . The weights, w_{jk} and w_{ij} , are then adjusted in order to minimise the difference between the propagated output and the target value. This error is defined over all training patterns, p , in the training set as

$$E = \frac{1}{2} \sum_p \sum_k (f_\sigma \left(\sum_j w_{jk} f_\sigma \left(\sum_i w_{ij} \phi_i^p \right) \right) - t_k^p)^2 \quad (3.7)$$

The squared error, E , can be minimised using the method of gradient descent [34]. This requires the gradient to be calculated with respect to each weight, w_{ij} and w_{jk} . The weight update equations for the hidden and output layers are given as follows:

$$w_{jk}^{(\tau+1)} = w_{jk}^{(\tau)} - \eta \frac{\partial E}{\partial w_{jk}} \quad (3.8)$$

$$w_{ij}^{(\tau+1)} = w_{ij}^{(\tau)} - \eta \frac{\partial E}{\partial w_{ij}} \quad (3.9)$$

The full derivation of the calculation of the partial derivatives, $\frac{\partial E}{\partial w_{ij}}$ and $\frac{\partial E}{\partial w_{jk}}$, is given in Appendix B.1. Using equations B.20 and B.12 we can write:

$$w_{jk}^{(\tau+1)} = w_{jk}^{(\tau)} - \eta \delta_k \phi_j \quad (3.10)$$

$$w_{ij}^{(\tau+1)} = w_{ij}^{(\tau)} - \eta \delta_j \phi_i \quad (3.11)$$

where η is the learning rate and δ_j and δ_k are given below:

$$\delta_k = (\phi_k - t_k) \phi_k (1 - \phi_k) \quad (3.12)$$

$$\delta_j = \sum_k \delta_k w_{jk} \phi_j (1 - \phi_j) \quad (3.13)$$

For the bias weights, the ϕ_i and ϕ_j in the above weight update equations are replaced by unity.

Training is an iterative process (repeated application of equations 3.10 and 3.11) but, if continued for too long, the network starts to fit the noise in the training set and that will have a negative effect on the performance of the trained network on test data. The decision on when to stop training is of vital importance and section 3.3.7 investigates this in more depth.

3.3.4 Auto-associative networks

Architecture

An auto-associative neural network performs dimensionality reduction from D to J dimensions ($D > J$) and then projects back up to D dimensions, as shown in figure 3.5.

The standard linear dimensionality reduction procedure is Principal Component Analysis (PCA) which is a form of unsupervised learning [34]. The full derivation given in Appendix B.2, shows that

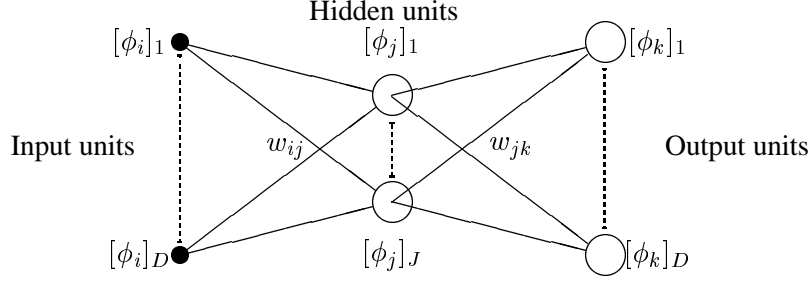


Figure 3.5: Layout of a D - J - D auto-associative neural network.

PCA is based on minimising a sum-of-squares error cost function. Bishop, [34], shows that PCA can be achieved by the use of an auto-associative MLP. He also shows that there is no need to use non-linear units in the hidden layer to perform the dimensionality reduction, since the solution for the non-linear network asymptotically approaches the global minimum of the cost function achieved by the linear network. Therefore only linear units will be used with the auto-associative networks described in the rest of this thesis. With an auto-associative network, no labelling of the training data is required because the target data is simply the input data.

Network with linear hidden layer and output units

Since $\phi_k = a_k$

$$\frac{\partial \phi_k}{\partial a_k} = 1 \quad (3.14)$$

the expression for δ_k reduces to

$$\delta_k = \frac{\partial E}{\partial a_k} = \frac{\partial E}{\partial \phi_k} \cdot \frac{\partial \phi_k}{\partial a_k} = (\phi_k - t_k) \quad (3.15)$$

Similarly for δ_j :

$$\delta_j = \frac{\partial E}{\partial a_j} = \frac{\partial E}{\partial a_k} \cdot \frac{\partial a_k}{\partial \phi_j} \cdot \frac{\partial \phi_j}{\partial a_j} = \sum_k \delta_k w_{jk} \quad (3.16)$$

3.3.5 Structure of auto-associative network for QRS reproduction.

This section describes the research carried out to investigate how a linear auto-associative neural network might be used to perform QRS detection of normal beats and rejection of ectopic beats. The aim is to train the auto-associative network to reconstruct a *normal* P-QRS-T waveform centred on its R-peak as faithfully as possible for the particular subject or patient being analysed. The number of output nodes

must therefore equal the number of input nodes (i.e. $i = k$). In order to identify if a segment of ECG contains a normal P-QRS-T waveform, a conventional QRS detector is used to locate candidate QRS complexes in the patient's ECG. The candidate is then presented to the input nodes of the trained MLP. If the input data is an ECG waveform (from the patient on which the network was trained) centred on its R-peak then the MLP will then reconstruct the QRS complex accurately. Otherwise the reconstruction will be poor since the mapping was learnt for R-peak centred P-QRS-T waveforms for that particular subject.

If a simple Euclidean distance measure (e.g. the MSE as in section 3.3.1) is used to compare the input and output patterns then it should be possible to differentiate normal from ectopic beats. Thus the following strategy is adopted: If a beat is identified by the Hamilton and Tompkins algorithm and $RMSE(\frac{1}{MSE})$ is used as the test criterion, a large $RMSE$ identifies the beat as normal. If the $RMSE$ is less than $RMSE_{min}$, then the beat is identified as an ectopic beat. The decision tree is the same as that shown in figure 3.1 except that this time the test criterion is $RMSE > RMSE_{min}$ where the MSE is the mean square error between the auto-associative network's reconstruction and the original pattern presented to the inputs.

Since the QRS complexes are easily located by their R-peak, a 0.5 second window either side of the R-peak is used in order to segment each heart beat. To reduce the input/output dimensionality for the auto-associative network and avoid learning irrelevant detail, the P-QRS-T waveform is down-sampled, while still preserving the main features. Figures 3.6 and 3.7 show how down-sampling to 64 Hz achieves this requirement. Further down-sampling would begin to affect relevant features of the ECG. A one-second window centred on the R-peak then corresponds to 64 nodes in both the input and output layers.

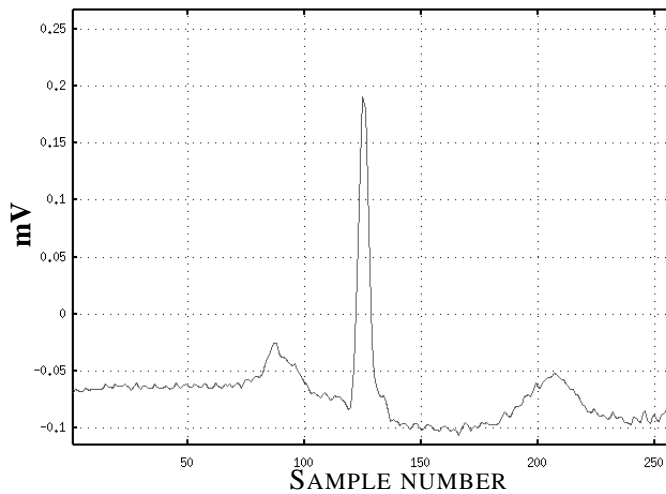


Figure 3.6: A typical ECG waveform sampled at 256Hz.

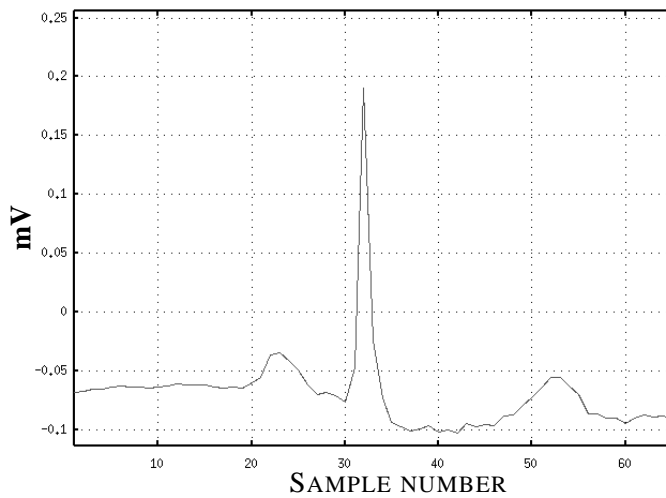


Figure 3.7: A typical ECG waveform down-sampled to 64Hz.

3.3.6 Principal Component Analysis for architecture definition

Simple analysis of typical P-QRS-T waves show that they are composed of approximately 10 major turning points. Although individual nodes in an MLP do not encode individual features, eight nodes in the hidden layer can be considered as a reasonable choice to provide enough data compression (4:1) to encode salient features without significant information loss [36].

An auto-associative MLP encodes the variance in the training set in the same manner as Principal Component Analysis, projecting the variance onto the same number of orthogonal axes as there are hidden units [34]. A more rigorous method for determining the number of hidden units is to perform PCA on the training set, rank the components in order of magnitude and identify the knee of the curve (see figure 3.8). In this case the knee appears to be at a value of 2, although it is arguable that a second knee occurs at 8. At this point any further components will add little to the information encoded by the principal components.

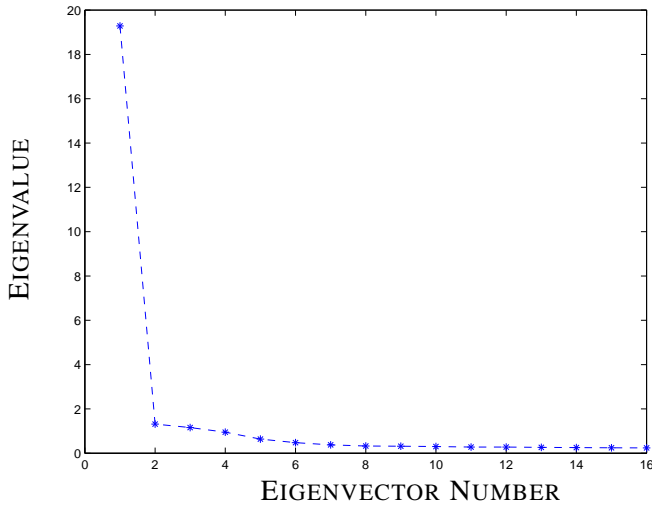


Figure 3.8: Size-ranked set of eigenvectors for a training set.

3.3.7 Training the auto-associative network

For any subject, the training set will consist of one-second windows of 64 points centred around the R-peak for each complex detected by the Hamilton and Tompkins algorithm (see section section 2.3). Patient 109 with 99.9% normals and 0.1% VEBs out of just over 2000 heart beats, (see table 2.3.2) is used as an illustration.

The weights are initialised with random values ± 0.01 and a learning rate of $\eta = 0.05$ is chosen. The neural network is trained by presenting each of the 2067 normals, (as detected by the Hamilton

and Tompkins algorithm) centred on the R-peak and then back propagating the errors. The mean square error between each input and output pattern summed over all patterns, is the error criterion used during learning, and is shown for each epoch⁴ in figure 3.9 for subject 109. It should be noted that the 28 VEBs and one artefact are not presented to the neural network for training, as it is important that the MLP only learns the morphology of normal beats. Given that the QRS detection algorithm cannot differentiate between normals and abnormal beats, a method for ensuring that only normal beats are included in the training set is required. This is discussed in more detail in section 3.3.9.

Now consider comparing the variance of the output patterns over one epoch to the variance of the input patterns over one epoch. The variance for each pattern is a measure of how different that pattern is from the mean pattern (the average across the entire training set). The variance of the d th dimension in a set of N D -dimensional vectors, $\phi^n = [\phi_1^n, \phi_2^n, \dots, \phi_D^n]^T$ where $n = 1, \dots, N$, is given by

$$\sigma_d^2 = \frac{1}{N-1} \sum_{n=1}^N (\phi_d^n - \mu_d)^2 \quad (3.17)$$

where the mean μ_d is given by

$$\mu_d = \frac{\sum_{n=1}^N \phi_d^n}{N} \quad (3.18)$$

The overall variance for one epoch (N training patterns) is given by

$$V = \sum_{d=1}^D v_d \quad (3.19)$$

A new parameter, the variance ratio, is now defined as follows

$$V_{ratio} = \frac{V_{out}}{V_{in}} \quad (3.20)$$

If it were possible to train an auto-associative neural network to reconstruct each input vector perfectly⁵, the variance at the input and output would be the same, and hence V_{ratio} would have a value of 1. The variance ratio is therefore a measure of how well the input vectors are reconstructed. By monitoring the variance ratio, V_{ratio} , during training, a decision to terminate training can be made based on the closeness of the variance ratio to unity.

During training the weights are updated (equations 3.10 and 3.11) every time a pattern is presented to

⁴An epoch is an iteration through the whole training set.

⁵which is not possible since $D > J$

the network. At the end of each epoch, the mean output pattern and the variance V_{out} are calculated. This procedure is repeated for as many epochs as is required to produce a plateau in the variance ratio. Figure 3.10 shows that, for patient 109, this occurs at 1600 epochs. Note the first minimum is reached around 100 epochs where the network has learned to produce the mean of the training set as the output pattern, regardless of the input pattern. At this point, *any* input pattern will be reconstructed as the average QRS complex across the training set. If the network is allowed to continue training it will learn the variance about that mean until, at the end of learning, the variance in the reconstructed (output) patterns approaches that in the input patterns ($V_{ratio} \approx 0.9$ at 1600 epochs). At this point, as much of the variance in the training set as possible has been learned.

This criterion for the termination of training is used in preference to the use of a validation set⁶ so that all the QRS complexes available can be assigned to the training set. Although this is not crucial in an off-line implementation, it becomes crucial when the amount of data is limited as in a real-time system. The ANSI guidelines [13] stipulate that only the first 5 minutes of data can be used for testing any ECG algorithm (after that it can only be scoring the data). At a heart rate of 60 beats per minute this is equivalent to 300 QRS complexes. It should be noted that the trained weights will be subject specific; a different patient will require a different MLP to be trained.

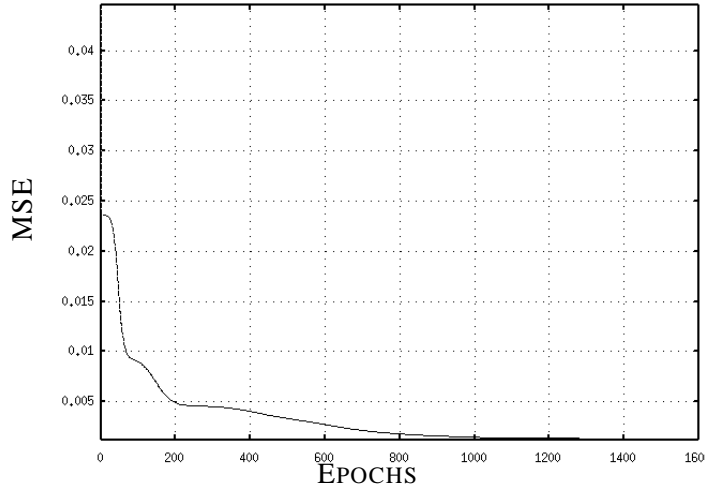


Figure 3.9: Mean Square Error during training at the end of each training epoch for file 109. The horizontal axis is the number of epochs.

⁶The standard method for ensuring over-training does occur.

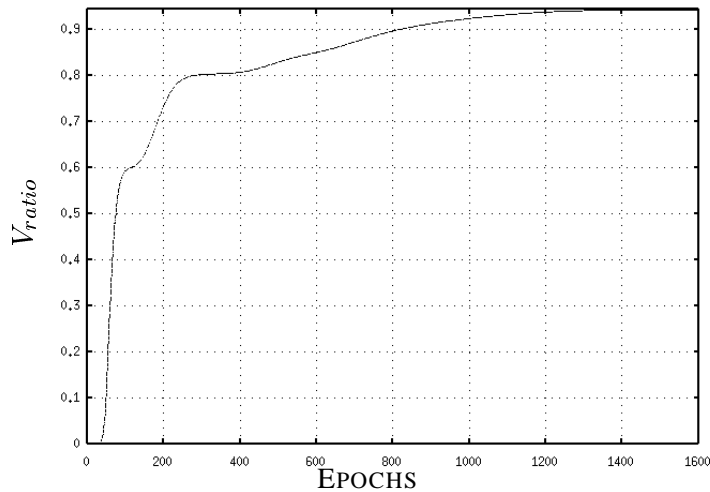


Figure 3.10: Ratio of the variance in the input patterns to that in the output patterns at each epoch for MIT-BIH file 109. The horizontal axis is the number of iterations through the data set (epochs).

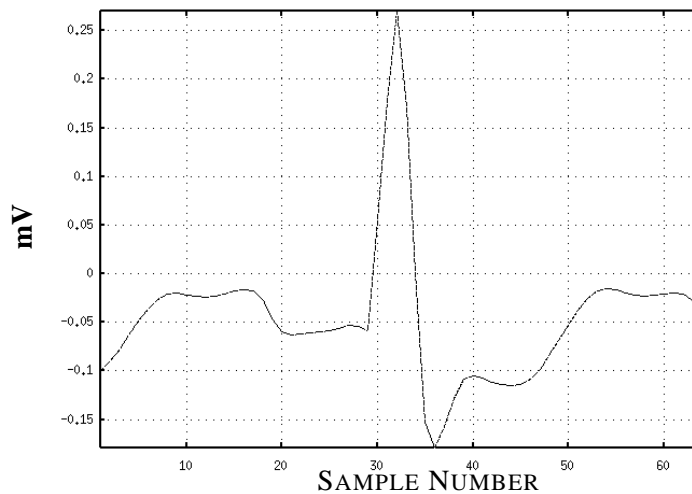


Figure 3.11: The average QRS complex in file 109 over all of the training set. Note that this vector represents a one second time interval since the signal has been down-sampled to 64Hz.

3.3.8 QRS classification

Once the auto-associative network has been trained, each QRS complex candidate ECG waveform (identified by the QRS detector) is presented to the 64 input nodes. In order to classify each QRS complex as normal or abnormal, the reconstructed data is energy normalised (as in section 3.3.1, to emphasise shape and not amplitude differences) and compared to an energy normalised version of the input pattern (figure 3.11) via a calculation of the $RMSE$ between the two patterns. The $RMSE$ acts as a sensitive measure of the ability of the MLP to reconstruct the pattern presented at the input nodes accurately. An accurate reconstruction is only possible if the input is an R-peak centred normal QRS complex for the patient on whose data the MLP was trained, and therefore an accurate R-peak detector is required.

Figure 3.12 shows the reconstruction of a non-centred QRS complex with a consequent high value of reconstruction MSE and thus a low $RMSE$. A ‘good fit’ to the normal template (encoded in the weights of the MLP) is only found when a normal beat is positioned with its QRS complex at the centre of the input window. Figure 3.13 shows the quality of match when the R-peak is centred on the mid-point of the 64-sample window.

Table 3.3 presents some of the results of $RMSE$ calculations for the QRS complexes in the ECG of subject 109 of the MIT-BIT arrhythmia database. The first column presents the $RMSE$ between each of the 32 (downsampled, energy normalised) ectopic beats and the corresponding (energy normalised) reconstructed output from the MLP. The second column presents the same calculation for each beat that directly follows each ectopic beat in column one, which all have a normal morphology. The third column presents the $RMSE$ for each beat following the beat analysed in column two. These also have a normal morphology. Note that the values in column three (for normal beats) are all significantly higher than in the first column, demonstrating that all ectopic beats (identified by the conventional QRS detector) can be classified as normal if an $RMSE$ threshold of 10 is chosen.

However, using this threshold, some QRS complexes with normal morphology are classed as abnormal. In particular, the QRS complexes that precede or follow ectopic beats have a slightly distorted P-wave, due to the broadening of the P-QRS-T complex itself. This effect is clearly observed in column two of table 3.3, which gives the $RMSE$ for each (normal) QRS complex that follows each ectopic. Note that these $RMSE$ values lie in between those for the normal and abnormal beats (columns one and three), demonstrating that beats which immediately follow ectopic beats exhibit small differences from a normal morphology. This illustrates the sensitivity of the auto-associative network to any deviation in

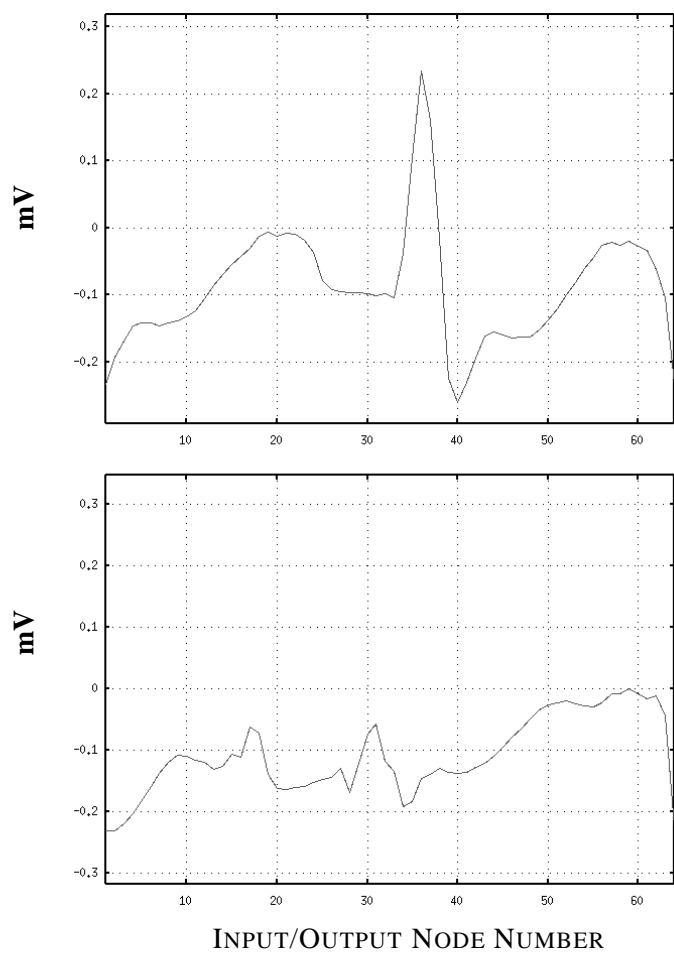


Figure 3.12: A normal QRS complex (above) in file 109 and its reconstruction (below). Note that the R-peak is not central when presented to the neural network.

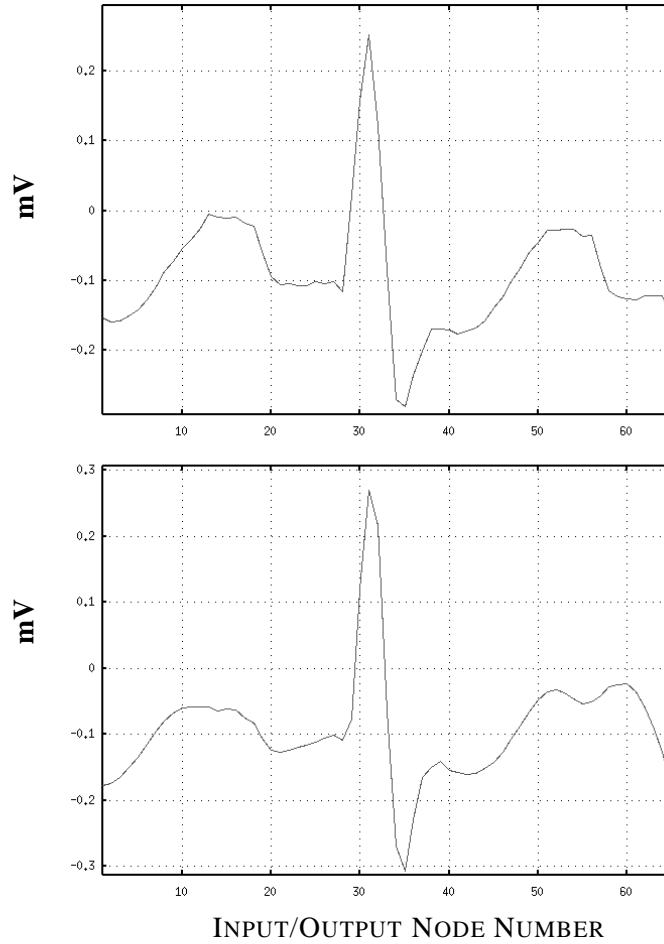


Figure 3.13: A normal QRS complex (above) in file 109 and its reconstruction (below) when presented to the neural network centred on the R-peak.

$RMSE$ of ectopic	$RMSE$ of following beat	$RMSE$ of following beat +1
3.54	10.91	328.57
3.41	8.36	213.98
3.31	18.61	221.47
7.70	26.51	313.42
1.09	21.70	216.32
6.19	55.08	204.37
2.19	13.31	171.80
3.15	18.42	117.39
7.08	16.23	130.28
2.98	12.67	175.62
3.29	9.70	182.26
2.99	15.69	114.23
2.12	24.52	159.65
3.41	10.50	157.03
3.34	13.67	201.31
2.82	15.21	147.34
3.41	13.78	126.96
4.86	12.49	316.33
3.79	18.43	246.09
3.88	14.93	193.32
3.76	15.72	251.44
3.76	12.60	162.40
1.75	12.48	232.20
2.70	30.13	201.57
2.52	22.28	305.28
4.11	12.11	243.12
5.86	19.07	353.41
3.79	13.38	181.41
3.81	14.21	86.90
3.68	17.02	51.73
6.47	19.46	72.51
4.73	15.66	65.85

Table 3.3: Reciprocal Mean Square Error ($RMSE$) between (downsampled, energy normalised) MLP input and output patterns (QRS complex candidates) for subject 109 of the MIT-BIT arrhythmia database. Column one presents values for each ectopic beat, column two for each normal beat following the corresponding ectopic beat in column one, and column three details the $RMSE$ for the *next but one* normal beat, following the ectopic beat in column one. See text for details.

the ECG from a normal morphology. In this example, the P-waves of the normal beats which follow ectopic beats are slightly deformed by the abnormal amplitude of the preceding ectopic beat. Although it is possible to minimise this effect by reducing the size of the temporal window used to segment each P-QRS-T complex, a large reduction in the width of the window may result in a reduced sensitivity to abnormality. Reducing the width of the P-QRS-T complex that is presented to the MLP leads to the exclusion of part of the P- and T-wave morphology, which would therefore not be encoded in the weights of the MLP. Ectopic beats exhibit differences in both P- and T-wave morphology from normality and therefore including them in the training pattern may lead to a higher sensitivity to abnormality for this method. Experiments to find the optimal size of temporal window are described in section 3.3.11.

3.3.9 Pruning the training set

The essential feature of using an auto-associative MLP to recognise normal beats is the encoding of normality within the MLP's weights. It is important to note that since the network uses a square error learning algorithm, the MLP is disproportionately sensitive to variations in the training vectors presented to the network during training. Therefore, in order to learn only normal morphologies, it is important to exclude abnormal vectors from the training set. Herein lies a problem; the MLP is trained to recognise normality, but a method for recognising normality is required in order to train the network in the first place.

One possible solution to this problem is to use a set of expert labelled normal beats for the training set. However, since the MLP requires retraining for each individual's ECG, the algorithm described in this chapter becomes redundant if the data has to be labelled in the first place. An automatic method of pruning the outliers from the training set is required. During identification of the R-peak centred beats using the conventional QRS detector, whenever a new QRS complex is sufficiently different from an average of the last 10 beats ($C < 0.7$) the new complex is removed from the training set.

3.3.10 Size of training set and training time.

The practical constraints in applying a neural network to the on-line detection of VEBs mean that the number of training patterns and the time during which the network can be trained are limited. As with the ANSI guidelines, the AAMI recommendations for testing and reporting performance results of ventricular arrhythmia detection ([1]) and [13]) state that any algorithm is allowed five minutes of adjustment

and training time. After this it must be correctly scoring fiducial points in the ECG waveform.

The implication of this, as already explained, is to restrict the training set to around 300 heart beats for an average patient with a resting mean heart rate of 60 beats per minute. Figure 3.10 however, shows that 1600 epochs are required to train the network such that the variance in the reconstructed patterns is maximised. In order to consider the effect of the size of training, the following data sets were assembled:

1. The ‘gold standard’ data set which includes every P-QRS-T pattern in the patient record (excluding the ‘outliers’ detected by the template matching algorithm with a threshold chosen to limit the number of patterns to 1700).
2. The first 1000 patterns (excluding the outliers).
3. The first 300 patterns (excluding the outliers).

The number of training epochs (as defined by the convergence of the variance ratio) rises from 1600 to 2000 for 1000 training patterns, but to 10000 for 300 training patterns. This is consistent with theoretical expectations, since the product of the number of training patterns with the number of training epochs should be of the same order of magnitude for any given data set [34, 263].

3.3.11 VEB detection performance.

no. training patterns	N identified as N	N identified as VEB	VEB identified as VEB	VEB identified as N	artefact identified as VEB
1700	2059	8	28	0	1
1000	2055	12	28	0	1
300	2052	15	28	0	1

Table 3.4: Performance of Hamilton and Tompkins/auto-associative network combination algorithm for different numbers of training patterns.

Table 3.4 presents the results from running the auto-associative network with pruned training sets of 1700, 1000 or 300 patterns attempting to detect ectopic beats over the entire ECG for subject 109, in conjunction with the Hamilton and Tompkins algorithm (as per figure 3.1).

As previously shown in table 2.3.2 the Hamilton and Tompkins algorithm identifies, for this record every single normal ($N_n=2067$), only one artefact ($O_n=1$) and 28 of the 32 VEBs ($V_n=28$, $V_o=4$). The combination of the MLP and Hamilton and Tompkins algorithms classifies 28 of the 32 VEBs as VEBs

(only 4 False Negatives —VEBs missed by the Hamilton and Tompkins algorithm) and in the worst case, with only 300 training patterns, classifies 15 normals and one artefact as VEBs (16 False Positives).

Varying the temporal window

As mentioned earlier in this chapter, the size of the temporal window used to segment the P-QRS-T morphology and form the training set, affects the amount of information concerning the varying morphology of normal beats encoded in the weights of the auto-associative MLP, and hence its ability to accurately reconstruct a normal beat at its output. The performance of the algorithm described above, for detecting normal beats is therefore studied for varying sizes of the temporal window and the results are presented in table 3.5. Note that reducing the window from one second to 0.5 seconds does not affect the ability of the algorithm to identify VEBs. This is because their morphology is sufficiently different from the training set of normals, and a low *RMSE* always results. However, as the window is reduced from 1s to 0.8s the number of normals identified as VEBs drops from 8 to 2, since the abnormalities that can often exist at the start of a P-wave or the end of a T-wave are now excluded from the analysis. An optimal performance is found for a temporal window of between 0.7 and 0.8 seconds. However, when the window is reduced below 0.7s the number of normals identified as VEBs increases, since the amount of information available concerning normality is reduced and the MLP becomes sensitive to small differences from normality in QRS complex width and height.

It can be seen that, when using the highly morphology-sensitive MLP, an error rate of less than 0.1% is achieved (2 out of 2067 beats misclassified) using a temporal window of between 0.7s and 0.8s. However, for heart rates as high as 120 bpm, a beat will occur on average once every 0.5s. In order to avoid the appearance of P- and T-waves of other beats in the window of a particular P-QRS-T complex, a window width of 0.5 seconds should be used. If the heart rate is known to exceed 120bpm in the data, then a shorter window may be necessary.

Previous work by Blanchet *et al.* [36] investigated ECG compression using PCA on the the first channel of 48 patients in the MIT-BIH database, using a one second window to segment the ECG. They showed that for normal beats, 3 components is generally sufficient to encode that relevant (clinical) features of normal beats. However, they found that abnormal beats require up to 14 components to retain detailed information, such as ST segment changes. For abnormality detection, 8 components is therefore a reasonable choice. Since the width of normal QRS complexes does not vary highly over a wide patient

population [121] and the results of Blanchet *et al.* [36] indicate that the number of principal components required to retain information concerning P-QRS-T complexes is also invariant across a wide population, there is no need to optimise the temporal window size across further subjects⁷.

window size (s)	N identified as N	N identified as VEB	VEB identified as VEB	VEB identified as N	artefact as VEB
1	2059	8	28	0	1
0.95	2061	6	28	0	1
0.9	2063	4	28	0	1
0.8	2065	2	28	0	1
0.775	2065	2	28	0	1
0.75	2065	2	28	0	1
0.725	2065	2	28	0	1
0.7	2065	2	28	0	1
0.6	2064	3	28	0	1
0.5	2063	4	28	0	1

Table 3.5: Performance of Hamilton and Tompkins/auto-associative network combination algorithm for different sizes of temporal window (in seconds) used to segment the P-QRS-T complexes during training. 1700 training patterns were used for each case.

3.3.12 Initialisation with PCA

If the MLP training set is restricted to 300 patterns, and 10000 epochs are required to trained the MLP weights, a training time of over 5 minutes is required using commercially available digital processors. A method for reducing the training time is therefore required. As stated in section 3.3.4, the two layer auto-associative MLP with linear hidden units and a sum-of-squares error function used in the previous section, learns the principal components for that data set. PCA can of course be performed and the weights can be calculated directly by computing a matrix pseudo-inverse [34], and this shall reduce ‘training time’ significantly. Consider equation 3.7 where the activation function is linear ($f_\sigma = 1$) for the input and hidden layers;

$$E = \frac{1}{2} \sum_{p=1}^N \sum_{j=1}^J \left(\sum_{i=0}^D \phi_i^p w_{ij} - t_j^p \right)^2 \quad (3.21)$$

⁷Sections 3.3.5 to 3.3.11 have been previously published by Clifford *et al.* in [54] and [265]

where J is the number of hidden units. If this expression is differentiated with respect to w_{ij} and the derivative is set to zero the usual equations for least-squares optimisation are given in the form

$$\sum_{p=1}^N \left(\sum_{i'=0}^D \phi_i^p w_{i'j} - t_j^p \right) \phi_i^p = 0 \quad (3.22)$$

which is written in matrix notation as

$$(\Phi^T \Phi) W^T = \Phi^T T \quad (3.23)$$

Φ has dimensions $N \times D$ with elements ϕ_i^p where N is the number of training patterns and D the number of input nodes to the network (i.e. 64 here). W has dimension $J \times D$ and elements w_{ij} and T has dimensions $N \times J$ and elements t_j^p . The matrix $(\Phi^T \Phi)$ is a square $J \times J$ matrix which may be inverted to obtain the solution

$$W^T = \Phi^\dagger T \quad (3.24)$$

where Φ^\dagger is the $(J \times N)$ pseudo-inverse of Φ and is given by

$$\Phi^\dagger = (\Phi^T \Phi)^{-1} \Phi^T \quad (3.25)$$

In practice $(\Phi^T \Phi)$ usually turns out to be near-singular and singular valued decomposition (SVD) is used to avoid problems caused by the accumulation of numerical roundoff errors. SVD automatically selects from a set of nearly degenerate solutions, the solution for which the length of the i^{th} weight vector is the shortest.

Consider N training patterns presented to the auto-associative MLP with i input and k output nodes ($i = k$) and $j \leq i$ hidden nodes. For the n^{th} ($n = 1 \dots N$) input vector x_i of the $i \times N$ ($N \geq i$) real input matrix, X , formed by the N (i -dimensional) training vectors, the hidden unit output values are

$$h_j = f(W_1 x_i + w_{1b}) \quad (3.26)$$

where W_1 is the input-to-hidden layer $i \times j$ weight matrix, w_{1b} is a rank- j vector of biases and f is an activation function. The output of the auto-associative MLP can then be written as

$$y_k = W_2 h_j + w_{2b} \quad (3.27)$$

where W_2 is the hidden-to-output layer $j \times k$ weight matrix and w_{2b} is a rank- k vector of biases. Now consider the singular value decomposition of X , given by [94] as $X_i = U_i S_i V_i^t$ where U is an $i \times i$ column-orthogonal matrix, S is an $i \times N$ diagonal matrix with positive or zero elements (the singular values) and V^t is the transpose of an $N \times N$ orthogonal matrix. The best rank- j approximation of X is given by [93] as $W_2 h_j = U_j S_j V_j^t$ where

$$h_j = T S_j V_j^t \quad \text{and} \quad (3.28)$$

$$W_2 = U_j T^{-1} \quad (3.29)$$

with T being an arbitrary non-singular $j \times j$ scaling matrix. U_j has $i \times j$ elements, S_j has $j \times j$ elements and V^t has $j \times N$ elements. It can be shown that [37]

$$W_1 = \alpha_1^{-1} T U_j^t \quad (3.30)$$

where W_1 are the input-to-hidden layer weights and α is derived from a power series expansion of the activation function, $f(x) \approx \alpha_0 + \alpha_1 x$ for small x . For a linear activation function, as in this application, $\alpha_0 = 0, \alpha_1 = 1$. The bias weights given in [37] reduce to

$$\begin{aligned} w_{1b} &= -\alpha_1^{-1} T U_j^t \mu_X = -U_j^t \mu_X, \\ w_{2b} &= \mu_X - \alpha_0 U_j T^{-1} = \mu_X \end{aligned} \quad (3.31)$$

where $\mu_X = \frac{1}{N} \sum_N x_i$, the average of the training (input) vectors and T is here set to be the $(j \times j)$ identity matrix since the output is unaffected by the scaling. Using equations (3.26) to (3.31)

$$\begin{aligned} y_k &= W_2 h_j + w_{2b} \\ &= U_j T^{-1} h_j + w_{2b} \\ &= U_j T^{-1} (W_1 x_i + w_{1b}) + w_{2b} \\ &= U_j T_1^{-1} T U_j^t x_i - U_j T^{-1} U_j^t \mu_X + \mu_X \end{aligned} \quad (3.32)$$

giving the output of the auto-associative MLP as

$$y_k = U_j U_j^t (X - \mu_X) + \mu_X. \quad (3.33)$$

Equations (3.29), (3.30) and (3.31) represent an analytical solution to determine the weights of the auto-associative MLP ‘in one pass’ with as few as $Ni^3 + 6Ni^2 + O(Ni)$ multiplications [39]. With $i = 64$ this compares favourably with the usual error back-propagation training algorithm which requires $gNi^2j + O(gNij) + O(gN(i+j))$ multiplications, where g is the number of iterations through the $N \times i$ training set. For a typical value of $N \approx 300$ QRS complexes (approximately 5 minutes of data), g is of the order 2×10^3 . For $N = 300$ the same accuracy was achieved using the SVD decomposition method as with the network trained with the error back-propagation algorithm (99.3% of the 2067 normal beats and 28 of the 32 ectopic beats correctly classified).

The AAMI allows only five minutes for ECG data collection and classifier training [1, 13]. Although the MLP allows effective identification of ectopic beats in the ECG in real time, the number of iterations required to train the network using the error back-propagation training algorithm is such that the AAMI guidelines cannot be adhered to with conventional desktop computational power. SVD, however, permits an initialisation of the weights in a single epoch which takes less than one second on most modern desktop computers. Once the ‘training’ is complete, the weights can then be updated using error back-propagation to adapt to any gradual morphological changes in the ECG waveform. (These changes could be due to a change in patient condition or due to a deterioration in electrode-contact impedance). Template matching could again be used to determine whether a new QRS complex was sufficiently novel to initiate retraining. The trained weights can be updated on-line with the error back propagation algorithm with $g'i^2j + O(g'ij) + O(g'(i+j))$ floating point operations where g' is the number of iterations to encode the change in variance in the training set due to a new QRS complex being added to the training set. (Typically $g' \approx 10$ [263]).

3.3.13 Conclusions

The auto-associative neural network has been shown to be highly sensitive to the set of ECG morphologies on which it is trained. Once this was recognised, it was possible to design a system which uses a QRS detector followed by an auto-associative MLP and proved to be an efficient VEB detector. However, given that the trained MLP also missed some normals, it could be that the criterion for rejecting

abnormal morphologies using template matching is so stringent as to exclude certain types of normals.

Training time is proportional to the number of nodes in the auto-associative network and it may be possible to decrease the number of hidden nodes without seriously affecting performance. Although PCA can be used to reduce the ‘training time’, on-line learning is required beyond the initial five-minute period to track long-term changes in ECG waveform morphology⁸.

3.4 Using timing information to identify artefact and abnormal beats

Even with sensitive morphology detection techniques, the morphology of an abnormal beat is sometimes sufficiently close to the beat-to-beat variations encountered in a normal sinus rhythm to allow the abnormal beat to be identified. However, an ectopic beat is defined to be of either abnormal morphology [181] or abnormal timing [138]; i.e it arrives earlier or later than would be normally expected for the beat-to-beat variations in RR interval in a sequence of normal beats. Therefore the timing of a beat in relation to the previous beat provides further information about beat type. The accepted limits for the n^{th} RR interval (RR_n) to be classed as normal are:

1. $\text{RR}_n < 0.8 \times \text{RR}_{av}^N$ where RR_{av}^N is the average sinus cycle length (according to Malik *et al.* [181])
or
2. $1.325 \times \text{RR}_{n-1} > \text{RR}_n > 0.755 \times \text{RR}_{n-1}$ (according to Kamath and Fallen [138]),

where RR_{n-1} is the last recorded interval (from a sinus beat pair). The first definition presents the task of having to calculate the average sinus cycle length (which requires the removal of the non-sinus RR intervals in the first place). The second method proposed by Kamath and Fallen, was derived from an analysis of an unspecified amount of data scored for beat type with a template matching technique.

In this section an analysis of the distribution of timings associated with sinus beats, abnormal beats and artefacts for normal subjects is presented. A method for identifying abnormal beats based on timing alone is proposed. All the data analysed in the rest of this chapter are taken from the MIT-Physionet Normal Sinus Rhythm Database (NSRDB) [194]. This comprises 19 normal (healthy) adult subjects of mixed sex and aged between 20 and 50 years with no known illnesses.

⁸This section has been previously published by Clifford *et al.* in [55]

3.4.1 Distribution of artefacts and ectopic beats

In the MIT-Physionet database, artefacts are defined to be disturbances in the ECG with beat-like morphology such that a conventional QRS detector would identify them as a beat. They are labelled as an ‘isolated QRS-like artefact’, or by ‘|’ in the Physionet annotations. Ectopic or abnormal beats are defined to be non-sinus rhythm beats and are labelled by L, R, A, a J, S, V, r, F, e, j, n, E, P, f, Q, or ?. Appendix A details the meaning of these annotations. These abnormal beats are usually labelled by experts from their knowledge of the associated abnormal morphology and timing .

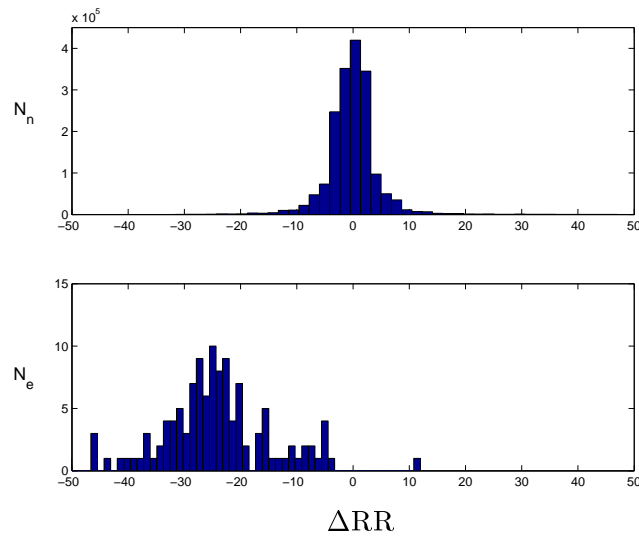


Figure 3.14: Distribution of percentage change in RR interval for normal to normal intervals (N_n on the upper plot) and normal to abnormal intervals (N_e lower plot) for all 19 subjects in the MIT-Physionet NSRDB.

This section uses the NSRDB to quantify the distribution of timings of normal to normal beats (N_n), normal to ectopic beats (N_e) and normal to artefact (N_A) in terms of percentage change from the previous $N-N$ interval. In effect, this quantifies the relative acceleration of the instantaneous heart rate, $\text{HR}_i (= 60\text{RR}_n)$. The percentage change in the n_{th} RR interval is calculated from

$$\Delta\text{RR}_n = 100 \times \frac{\text{RR}_n - \text{RR}_{n-1}}{\text{RR}_{n-1}}. \quad (3.34)$$

Figure 3.14 illustrates the distribution of ΔRR for $N-N$ intervals (N_n on the upper plot) and $N-E$ intervals (N_e lower plot) for all 19 subjects in the MIT-Physionet NSRDB. Note that the distributions are approximately Gaussian centred around zero for the $N-N$ distribution, and around -24% for the $N-E$ dis-

tribution. A negative percentage change indicates that the interval is shorter than the previous interval. An even-sided distribution, centred around zero, is therefore expected for N-N beats. However, ectopics usually arrive early, and therefore the distribution of N-E intervals is expected to be centred around a negative value. Note that in all the NSRDB subjects' ECGs, only one ectopic arrives late (illustrated by the positive valued datum for the distribution of N_e). Beat-to-beat intervals between normal beats and artefacts are however, always shorter than the previous beat because they occur in addition to the normal sequence of sinus beats. The distribution of ΔRR for N-A is therefore always negative. If the modulus

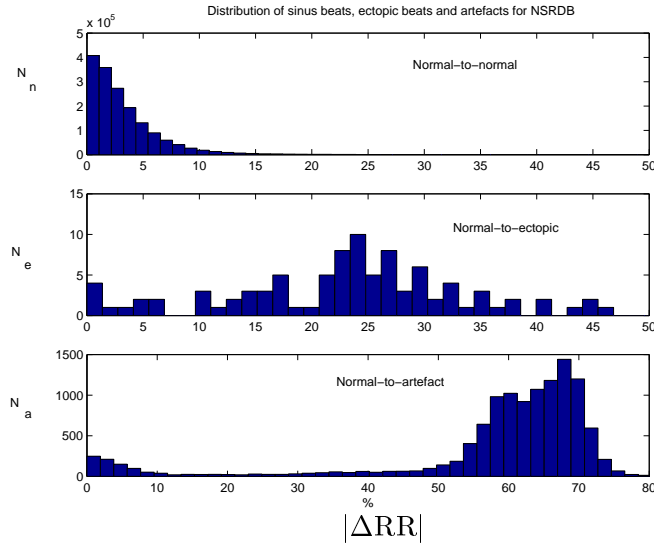


Figure 3.15: Distribution of percentage change in RR interval for sinus to sinus intervals (upper plot), sinus to non-sinus intervals (middle plot) and sinus to artefacts (lower plot) for all 19 subjects in the Physionet NSRDB.

of ΔRR is used as a criterion for labelling beats, then it can be seen from figure 3.15, which illustrates the distribution of $|\Delta RR|$ for all 3 beats pair categories (N-N, N-E and N-A), that there is only a relatively small overlap between the histograms for each beat pair category. This indicates that it might be possible to chose a threshold which maximises the removal of non-sinus beats (ectopic and artifacts).

Figure 3.16 illustrates the percentage of N-E and N-A intervals that are removed and the percentage of N-N intervals that remain when the exclusion criterion $|\Delta RR| > \lambda$, is set to values between 3% and 24%. Artefact removal is almost independent of the value of range (i.e. 92% of the artefacts are removed when $\lambda = 24\%$ and 97% of the artefacts are removed when $\lambda = 3\%$). From figure 3.16, it can be seen that an optimal value of λ for this data set (19 subjects with normal sinus rhythms) is 10%, in which case 96% of sinus beats are retained and 90% of ectopic beats are removed. If the distribution of the beat to

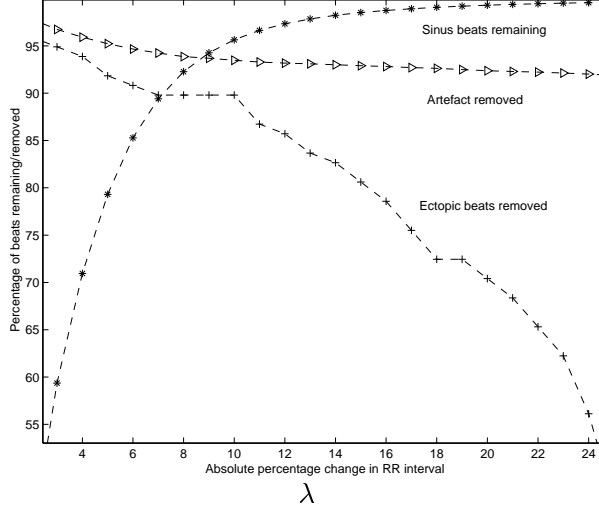


Figure 3.16: Percentage of N-N beat pairs remaining (*), N-E (+) and N-A (\triangle) removed for $3\% < \lambda \leq 25\%$ for all 19 subjects in the NSRDB

beat changes in RR intervals for normal beats, N_n , is plotted as a one sided distribution $|\Delta RR_n|$, (which is assumed to be Gaussian; see upper plot in figure 3.15) then the 2σ point is also at $\lambda = 10\%$ (see figure 3.16) and the 3σ point corresponds to the standard $\lambda = 20\%$ quoted by Malik *et al.* [181]. This latter threshold corresponds to removing only 71% of the ectopic beats on this group of patients and it would be more appropriate to use the value suggested above of $\lambda = 10\%$.

3.4.2 Data fusion algorithms

If timing and morphology are assumed to be two independent sources of information when attempting to identify abnormal beats, the two tests described in this chapter could be used on an *OR* basis to fuse the two sources of information. Thus, the n^{th} beat would be classified as normal if the *RMSE* was below 10 for an auto-associative MLP trained on that patient, *OR* the n^{th} and $(n + 1)^{\text{th}}$ RR intervals did not change by more than 10 percent. In chapter 4, spectral methods of assessing the RR tachogram are analysed and a threshold based on timing will be suggested which maximises the removal of non-sinus RR intervals, whilst retaining sufficient sinus RR intervals to analyse the segment of the RR tachogram under consideration. The success of this approach meant that there was no need to explore the application of the data fusion algorithm suggested here, especially as the overhead of training the MLP for each patient is not insignificant⁹.

⁹Section 3.4 has been previously published by Clifford *et al.* in [56]

3.4.3 Summary

About one third of normal, healthy men have one or more premature ventricular ectopic beat(s) per hour and 12% have up to 6 per hour with associated complex ventricular arrhythmias [138]. The incidence of ectopic beats in patients suffering from cardiac-related problems, such as Myocardial Infarction, is far higher [282]. The implementation of a robust automatic method for calculating RR intervals between only normal (sinus) beats for a large range of environmental and physiological conditions is therefore a pre-requisite for an accurate derivation of an RR tachogram. A threshold of $\lambda = 10\%$ for rejecting abnormal beats, based on timing has been proposed. In the next chapter a particular spectral estimation method for the RR tachogram is investigated. This requires a minimum number of beats for the analysis window, the non-valid beats (i.e. the ectopics and artefacts) being identified using the timing test investigated in this chapter.

Chapter 4

HRV experiments using spectral techniques

4.1 Overview

Chapter 1 reviewed the application of spectral techniques for heart rate variability analysis, especially in the context of the evaluation of cardiac-related problems [184]. This chapter provides a detailed analysis of frequency-based methods with reference to the type of data to which they are typically applied. The drawbacks and inaccuracies of these techniques are quantified and compared to an alternative method, the Lomb periodogram, that is specifically designed to calculate the power spectral density (PSD) of unevenly sampled signals [176].

4.1.1 The RR tachogram - an unevenly sampled time series

Since the RR tachogram is a representation of the beat-to-beat variability of each systole in the cardiac cycle with both axes representing the time between beats, it is inherently a discrete, uneven time series (otherwise there would be no *variability* in the heart rate). However, almost all of the published PSD estimation techniques described in the relevant literature require evenly sampled data. Pre-processing of the RR tachogram with re-sampling techniques (such as linear or cubic spline re-sampling) is usually the means of producing an evenly sampled time series. Re-sampling introduces an implicit assumption about the form of the underlying variation in the RR tachogram; for example, cubic spline techniques assume that the variation between beats can be modelled accurately by a cubic polynomial.

This chapter concentrates on the various re-sampling and spectral estimation methods that are in general use for HRV computation. Artificial RR interval data (for which the constituent frequency components are known) are used in order to determine whether current spectral estimation techniques introduce significant errors in the calculation of HRV metrics. The Lomb periodogram is evaluated as an alternative technique for HRV spectral estimation and its performance is reviewed with respect to the more traditional FFT based methods.

4.1.2 FFT methods compared to AR methods

The two most common methods for frequency-domain HRV metric estimation are auto-regressive (AR) spectral estimation and Fourier techniques [181]. The seminal report, *Heart Rate Variability: Standards of Measurement, Physiological Interpretation, and Clinical Use*, produced by the task force of the European Society of Cardiology and the North American Society of Pacing Electrophysiology [184], is unclear which spectral methods it considers more applicable to HRV frequency-domain analysis. They therefore recommend using both parametric and nonparametric assessments when evaluating frequency domain HRV measures. While the nonparametric methods have the advantage of algorithmic simplicity and rapidity, the parametric methods produce smoother spectral components that can be distinguished more easily, and if the model order is chosen correctly can allow an accurate estimation of the PSD over very short windows.

In 1989 Albrecht and Cohen [10] carried out experiments to compare the Fast Fourier Transforms (FFT) of linearly re-sampled RR tachograms with an autocorrelation method for constructing the PSD from only the original data points. They showed that for many typical RR tachograms, the PSD of the linearly re-sampled RR tachogram was more accurate than that of the autocorrelation method. This may be due to the fact, however, that attempts to estimate the autocorrelation function of unevenly sampled data all produce some loss of information [240].

However, more recent work by Clayton *et al.* [51] (in 1997) demonstrated that FFT and AR methods can provide a comparable measure of the LF and HF metrics on linearly re-sampled 5 minute HR segments across a patient population with a wide variety of ages and medical conditions (ranging from heart transplant patients who have the lowest HRV to normals who often exhibit the highest overall HRV). As both methods appear to give equivalent results, it is only necessary to concentrate on one and, in this thesis the FFT was chosen as there are far more results in the literature with which to compare re-

sults. Furthermore, in the even sampling limit, the Lomb and FFT methods are equivalent and a direct comparison can be made.

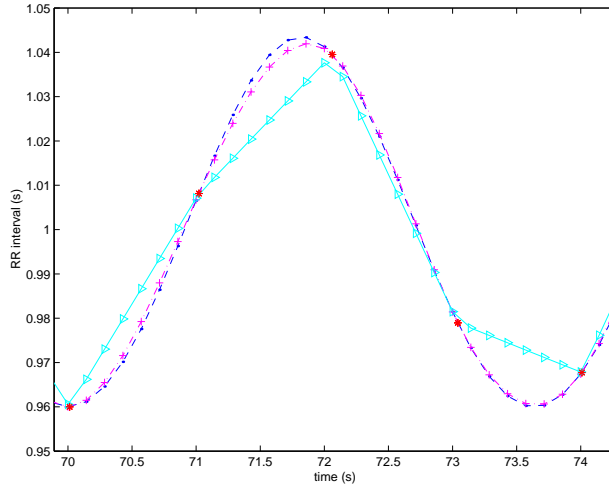


Figure 4.1: Section of (artificial) RR tachogram. The ‘idealised’ signal ($\text{---} \bullet \text{---}$) is a perfect sinusoid. The physiologically realistic RR tachogram is indicated by a series of stars (*). The cubic spline re-sampled signal is represented by $\text{---} + \text{---}$ and the linearly re-sampled signal by $\text{---} \triangleright \text{---}$.

4.1.3 Re-sampling to enable spectral estimation

In order to provide an evenly sampled time series prior to FFT analysis re-sampling is required. Previous studies have used linear or cubic spline interpolation to re-sample RR tachograms at frequencies between 1 Hz [114] and 10 Hz [181]. However, the distortion this causes is generally not appreciated when reporting results on HRV analysis. Figure 4.1 shows an example of how these commonly used re-sampling methods approximate the behaviour of a sinusoid. The underlying sinusoid we wish to model is marked by dots (---). Unevenly sampled points have been chosen along the sinusoid (marked by *) and re-sampling between these points has been performed at 7Hz. Linear re-sampling (marked by \triangleright) produces a poor approximation of the underlying sinusoid but the cubic spline re-sampling (marked by *) passes very closely through each point (*) on the sinusoid and generates a very close approximation of underlying signal.

The effect of local polynomial interpolation for re-sampling can be understood by considering the Taylor expansion ($f(a + h) \approx f(a) + hf'(a)$) of a sinusoid around a point t with a small error ϵ [122];

$$\sin(t + \epsilon) = \sin(t) + \epsilon \cos(t) + \dots \quad (4.1)$$

$$\begin{aligned}
&= t - \frac{t^3}{3!} + \frac{t^5}{5!} \dots + \epsilon - \epsilon \frac{t^2}{2!} + \epsilon \frac{t^4}{4!} \dots \\
&\approx \epsilon + t - \epsilon \frac{t^2}{2!} - \frac{t^3}{3!}
\end{aligned}$$

(to third order) - i.e. a cubic polynomial. It is therefore unsurprising that such a re-sampling method produces a close approximation of a sinusoid. It should be noted however, that the accuracy of this approximation will decrease if the underlying variability of the HR is not truly sinusoidal in nature. Appendix D presents a mathematical description of how cubic spline interpolation for re-sampling is calculated.

4.1.4 PSD estimation without re-sampling - the Lomb periodogram

In 1976, Lomb [176] described a method of deriving the PSD of an unevenly sampled signal. In the Lomb method, re-sampling to create an evenly-sampled time series is unnecessary and in the evaluation of the power spectrum the data are weighted on a point by point basis rather than on a per time interval basis as in the conventional FFT. This technique is described in detail in the following section (§4.2).

Several papers have presented results on HRV spectral estimation using the Lomb periodogram [43, 162, 198]. Laguna *et al.* [162] found that the Lomb method for estimating the PSD of unevenly sampled signals produces a better estimate of the PSD of an RR tachogram than re-sampling at 2Hz and using a conventional FFT. Moody [198] applied the Lomb method to an artificial HR time series and showed that AR, FFT (of cubic spline re-sampled RR tachograms) and Lomb methods are equivalent techniques for spectral estimation when the data contains no noise. Furthermore, he showed that when noise is added to a HR time series, the AR and FFT based methods introduce peaks in the spectral estimate at spurious frequencies and broaden the existing peaks. Results indicated that the Lomb method provides a spectral estimate closer to the original (no-noise) case.

However, no systematic experiments have been published to quantify the exact improvement in spectral estimation and frequency domain HRV metric calculations the Lomb method provides over evenly-sampled spectral estimation techniques for differing levels of noise or missing data.

4.2 From FFTs to the Lomb method - PSD estimation

The power spectral density $P_X(f)$ and the autocorrelation function $C_X(t)$ of a wide-sense stationary random process (such that the statistical characterisation of the process is time invariant), X_t form a

Fourier-transform pair [258]:

$$P_X(f) = \int_{-\infty}^{\infty} C_X(t) e^{-i2\pi f t} dt \quad (4.2)$$

$$C_X(t) = \int_{-\infty}^{\infty} P_X(f) e^{i2\pi f t} df \quad (4.3)$$

These relations show that if either the autocorrelation function or power spectral density of a random process is known, the other can be found exactly.

Note that although the power spectrum is a theoretical quantity defined as an integral over continuous time and the periodogram is an estimate of this based on a finite amount of data, the terms (*power spectrum* and *periodogram*) are used interchangeably in this thesis (after Scargle [239]).

4.2.1 The Discrete Fourier Transform

Consider a physical variable X measured at a set of times t_j where the sampling is at equal times ($\Delta t = t_{j+1} - t_j = \text{constant}$) from a stochastic process. The resulting time series data, $\{X(t_j)\}$ ($i = 1, 2, \dots, N$), are assumed to be the sum of a signal X_s and random observational errors¹, R ;

$$X_j = X(t_j) = X_s(t_j) + R(t_j). \quad (4.4)$$

Furthermore, it is assumed that the signal is periodic, that the errors at different times are independent ($R(t_j) \neq f(R(t_k))$ for $j \neq k$) and that $R(t_j)$ is normally distributed with zero mean and constant variance, σ_o^2 .

The N -point Discrete Fourier transform (DFT) of this sequence is [122]

$$FT_X(\omega) = \sum_{j=0}^{N-1} X(t_j) e^{-i\omega t_j} \quad (4.5)$$

($\omega_n = 2\pi f_n$, $n = 1, 2, \dots, N$) and the power spectral density estimate is therefore given by the standard method [122] for calculating a periodogram:

$$P_X(\omega) = \frac{1}{N} \sum_{j=0}^{N-1} |X(t_j) e^{-i\omega t_j}|^2. \quad (4.6)$$

¹Due to the additive nature of the signal and the errors in measuring it, the errors are often referred to as noise.

4.2.2 Generalising the DFT - PSD estimation via the Lomb periodogram

Now consider arbitrary t_j 's or uneven sampling ($\Delta t = t_{j+1} - t_j \neq \text{constant}$) and a generalisation of the N -point DFT [239];

$$FT_X(\omega) = \left(\frac{N}{2}\right)^{\frac{1}{2}} \sum_{j=0}^{N-1} X(t_j)[A \cos(\omega t_j) - iB \sin(\omega t_j)], \quad (4.7)$$

where $i = \sqrt{-1}$, j is the summation index and A and B are as yet unspecified functions of the angular frequency ω . This angular frequency may depend on the vector of sample times, $\{t_j\}$, but not on the data, $\{X(t_j)\}$, nor on the summation index j . The corresponding (normalised) periodogram is then

$$P_X(\omega) = \left(\frac{1}{N}\right) |FT_X(\omega)|^2 = \frac{A^2}{2} \left[\sum_j X(t_j) \cos(\omega t_j) \right]^2 + \frac{B^2}{2} \left[\sum_j X(t_j) \sin(\omega t_j) \right]^2. \quad (4.8)$$

If $A = B = (\frac{2}{N})^{\frac{1}{2}}$, equations (4.7) and (4.8) reduce to the classical definitions (equations 4.5 and 4.6). For even sampling ($\Delta t = \text{constant}$) FT_X reduces to the DFT and in the limit $\Delta t \rightarrow 0, N \rightarrow \infty$, it is proportional to the Fourier transform. However, A and B are not unique: there are other choices for A and B which also reduce to the even sampling solution. We must therefore impose further conditions to determine A and B uniquely. Scargle [239] has shown that it is useful (in the context of statistical significance) that the Lomb periodogram has an exponential distribution, the same as in the even sampling case [239]. The following derivation (of Scargle's *modified* Lomb periodogram) demonstrates how this is possible by making simple choices for A and B .

Consider the case in which X is normally distributed noise, with zero mean and constant unit variance σ_o^2 . The quantity

$$G(\omega) = A \sum_j X(t_j) \cos(\omega t_j) \quad (4.9)$$

is then a linear combination of independent normal random variables, since the $A \cos(\omega t_j)$ are simply constant coefficients in this context. Noting that a linear combination of normally distributed random variables is also normal, the mean of G is $\langle G \rangle = 0$ and the variance of G is

$$\sigma_g^2 = \langle G^2(\omega) \rangle = A^2 \sum_{j=1}^N \sum_{k=1}^N \langle X(t_j) X(t_k) \rangle \cos(\omega t_j) \cos(\omega t_k) \quad (4.10)$$

where $\langle \rangle$ denotes the evaluation of the expectation. Since the cross terms ($j \neq k$) vanish due to the

assumed independence, this reduces to

$$\sigma_g^2 = A^2 N \sigma_o^2 \sum_j \cos^2(\omega t_j). \quad (4.11)$$

Similarly, define $H(\omega)$ to be equal to $B \sum_j X(t_j) \sin(\omega t_j)$, also a linear combination of independent normal random variables with zero mean and variance, σ_h^2 where

$$\sigma_h^2 = B^2 N \sigma_o^2 \sum_j \sin^2(\omega t_j). \quad (4.12)$$

Equation (4.8) can then be re-written so that P_X is the sum of the squares of two normally distributed, zero-mean random variables:

$$P_X(\omega) = \frac{1}{2} [G^2(\omega) + H^2(\omega)]. \quad (4.13)$$

To force such a sum to have an exponential probability distribution, the variances of the two normal variables must be equal [218]. The constraints for A and B which satisfy this latter criterion can be derived as follows:

Let U and V be two zero-mean random variables with variances σ_u and σ_v , respectively and let $Z^2 = U^2 + V^2$. Z is then distributed according to [218]

$$P_Z(z) = \frac{e^{-\frac{z}{2\sigma_u\sigma_v}}}{2\sigma_u\sigma_v} S \left[\frac{z}{4} \left(\frac{1}{\sigma_u^2} - \frac{1}{\sigma_v^2} \right) \right], \quad (\sigma_u \neq \sigma_v) \quad (4.14)$$

where

$$S(y) = e^{-y} I_o(y) \quad (4.15)$$

and I_o is the modified Bessel function of the first kind defined as [258]

$$I_o(y) = 1 - \frac{y^2}{2^2} + \frac{y^4}{2^2 4^2} - \frac{y^6}{2^2 4^2 6^2} + \dots \quad (4.16)$$

with $y = \frac{z}{4} \left(\frac{1}{\sigma_u^2} - \frac{1}{\sigma_v^2} \right)$. If $\sigma_u = \sigma_v = \sigma$, the distribution (equation (4.14)) reduces to

$$P_Z(z) = \left(\frac{1}{2\sigma^2} \right) e^{-\frac{z}{2\sigma^2}}, \quad (4.17)$$

the usual result for the sum of squares of two normal variables of equal variance (and mean), which is

exponential. Therefore setting $\sigma_g = \sigma_h = \sigma_o$ makes the distribution of the generalised periodogram exponential; the same as in the case of even sampling. From equations (4.11) and (4.12) it can be seen that the choices

$$A(\omega) = \frac{Q(\omega)}{\sqrt{N}} \left(\sum_j \cos^2(\omega t_j) \right)^{-\frac{1}{2}} \quad (4.18)$$

and

$$B(\omega) = \frac{Q(\omega)}{\sqrt{N}} \left(\sum_j \sin^2(\omega t_j) \right)^{-\frac{1}{2}} \quad (4.19)$$

give the necessary equality of the variances, $\sigma_g = \sigma_h = \sigma_o$, since the $N \sum_j \sin^2(\omega t_j)$ and $N \sum_j \cos^2(\omega t_j)$ terms cancel. In these equations $Q(\omega)$ is an arbitrary function of ω and its value, $Q(\omega) = 1$, is determined by the condition that P_X has the same mean value as in the evenly spaced case. The periodogram (equation (4.8)) is then given by:

$$P_X(\omega) = \frac{1}{2N} \left\{ \frac{[\sum_j X_j \cos(\omega t_j)]^2}{\sum_j \cos^2(\omega t_j)} + \frac{[\sum_j X_j \sin(\omega t_j)]^2}{\sum_j \sin^2(\omega t_j)} \right\}. \quad (4.20)$$

Note that for evenly spaced t_j , $A(\omega) = B(\omega) = (\frac{2}{N})^{\frac{1}{2}}$ whenever $\omega = \omega_n = \frac{2\pi n}{T}$ where n ranges over a set of well-known natural frequencies ($\{n = -\frac{N_0}{2}, \dots, +\frac{N_0}{2}\}$). This can be seen by equating (4.18) and (4.19), and using the trigonometrical identity $\sin^2(\omega t) = 1 - \cos^2(\omega t)$ to give $\cos(\omega t) = \frac{1}{\sqrt{2}}$, which is true for multiples of $\frac{2\pi}{N}$. Equations (4.7) and (4.8) then reduce to the classical definitions, equations (4.5) and (4.6).

The fundamental frequency, $\omega_1 = \frac{2\pi}{T}$, the lowest frequency about which there is information in the data, and corresponds to a sine wave of period equal to the whole interval T . The highest frequency about which there is information is the Nyquist frequency, $\omega_c = \frac{1}{2}(\frac{2\pi}{\Delta t}) = \frac{\pi N_0}{T}$, where the sampling interval is $\Delta t = \frac{T}{N_0}$. If the sampling is uneven, the fundamental frequency is unchanged in both meaning and value since the interval $T = \max(t_j) - \min(t_j)$ is still well defined. However, the meaning of the Nyquist frequency changes; the highest frequency about which there is information is $\frac{\pi}{\Delta t_{\min}}$ where $\Delta t_{\min} = \min(t_{j+1} - t_j)$ and a generalised Nyquist frequency is more commonly used [229]. This is calculated using Δt_{av} , the average value of Δt over all j 's and is therefore sometimes known as the average Nyquist frequency, $f'_c = 1/2\Delta t_{\text{av}}$.

Note that if the data is not zero-mean, unit variance then, defining the mean and variance in the usual

manner;

$$\bar{x} \equiv \frac{1}{N} \sum_0^{N-1} x_j, \quad \sigma^2 \equiv \frac{1}{N-1} \sum_0^{N-1} (x_j - \bar{x})^2, \quad (4.21)$$

we may replace $\left[\sum_j X_j\right]^2/N$ with $\left[\sum_j (x_j - \bar{x})\right]^2/\sigma^2$. The Lomb normalised periodogram then becomes

$$P_N(\omega) \equiv \frac{1}{2\sigma^2} \left\{ \frac{\left[\sum_j (x_j - \bar{x}) \cos(\omega t_j)\right]^2}{\sum_j \cos^2(\omega t_j)} + \frac{\left[\sum_j (x_j - \bar{x}) \sin(\omega t_j)\right]^2}{\sum_j \sin^2(\omega t_j)} \right\}. \quad (4.22)$$

If there is a shift of the time origin at every sample point ($t_j \rightarrow t_j + T_o, \forall j$), then the periodogram (equation (4.8)) is unchanged: there is simply a phase factor $e^{i\omega T_o}$, with unit modulus, introduced. The periodogram derived above (equation (4.22)) does not have this useful time translation-invariant property and it does not therefore measure the harmonic content of a signal independently of phase. Scargle [239] demonstrates how to restore this property by subtracting a delay τ from all of the time arguments in equation (4.22) such that

$$P_N(\omega) \equiv \frac{1}{2\sigma^2} \left\{ \frac{\left[\sum_j (x_j - \bar{x}) \cos(\omega(t_j - \tau))\right]^2}{\sum_j \cos^2(\omega(t_j - \tau))} + \frac{\left[\sum_j (x_j - \bar{x}) \sin(\omega(t_j - \tau))\right]^2}{\sum_j \sin^2(\omega(t_j - \tau))} \right\} \quad (4.23)$$

where $\tau \equiv \tan^{-1}\left(\frac{\sum_j \sin(2\omega t_j)}{2\omega \sum_j \cos(2\omega t_j)}\right)$. τ is an offset that makes $P_N(\omega)$ completely independent of shifting all the t_j 's by any constant. This choice of offset makes equation (4.23) exactly the solution that one would obtain if the harmonic content of a data set, at a given frequency ω , was estimated by linear least-squares fitting to the model $x(t) = A \cos(\omega t) + B \sin(\omega t)$ [176, 239, 229].

Thus, the Lomb periodogram, instead of weighting the data on a *per time interval* basis (where uneven sampling can introduce serious errors), weights the data on a *per point* basis and hence can give superior results to FFT based methods when estimating the spectrum of unevenly sampled time series. Appendix E illustrates the differences between these methods on a simple problem.

A note on spectral leakage and window carpentry

A finite length signal is rarely periodic at its boundaries. and as a result, the power in the periodogram will appear at other frequencies. Leakage to nearby frequencies due to the finite interval over which the data is sampled takes the form of side-lobes in the periodogram. This spectral leakage is classically minimised through windowing or other mathematically equivalent techniques.

In Harris' detailed paper on DFT windowing [108] he catalogued many of the most useful windowing

functions and their side-lobe structure. He showed that a Hamming window given by [35]

$$W(t_j) = 0.54 - 0.46 \cos[\omega t_j] \quad (j = 0, 1, 2, \dots, N - 1), \quad (4.24)$$

provides the optimal trade off between spectral leakage, side-lobes amplitude and width of the central peak (as well as a short computational time). This windowing function will therefore be applied to all data ($N=2048$) in a given window prior to PSD estimation using the FFT.

4.3 Practical considerations

The different HRV spectral estimation methods being considered in this chapter are;

- Welch's FFT of linear re-sampled data²,
- Welch's FFT of cubic spline re-sampled data, and
- the Lomb periodogram method.

In order to quantitatively compare these methods, metrics are required to measure the different PSD estimation techniques. When choosing such metrics, window sizes, the type of data and pre-processing techniques need to be considered.

4.3.1 Window size

In order to choose the necessary window size, we must balance the requirement of stationarity versus the time required to resolve the information present. The European and North American Task force on standards in HRV [184] suggested that the shortest time period over which HRV metrics should be assessed is 5 minutes. As a result, the lowest frequency that can be resolved is $\frac{1}{300} \approx 0.003Hz$ (just above the lower limit of the VLF region). Such short segments can therefore only be used to evaluate metrics involving the LF and HF metrics. The upper frequency limit of the highest band for HRV analysis is $0.4Hz$ [181]. Since the average time interval for N points over a time T is $\Delta t_{av} = \frac{T}{N}$ then the average Nyquist frequency [239] is $f'_c = \frac{1}{2\Delta t_{av}} = \frac{N}{2T}$. Thus, a 5-minute window ($T = 300$) leads to the constraint of $\frac{N}{2T} \geq 0.4$ on the number of points and hence to a lower limit on N of 240 beats (an average heart rate of 48 bpm if all beats in a 5-minute segment are used).

²A windowed version of equation 4.6 [279].

4.3.2 Sampling frequency

Most of the papers in the field of HRV report on the use of re-sampling rates between 2 and 4Hz (although 1Hz and 10Hz have also been used) [114, 181, 184] to produce an evenly sampled time series prior to the conventional FFT procedure. Since the human heart rate can sometimes exceed 3Hz (180 bpm), then a sample rate of at least 6Hz may be required to satisfy the Nyquist criterion. However, if one knows that the RR tachogram is unlikely to exceed 120 bpm then a re-sampling rate of 4Hz is sufficient. A choice of 7Hz for the up-sampling of the RR-tachogram satisfies the Nyquist criterion and gives a value of 2100 points in a 5-minute window. To compute a DFT the number of points in a time series should be a power of 2, thus the first 2048 points of each 7Hz re-sampled segment will be used in the sections that follow.

4.3.3 Pre-processing

Apart from windowing the data, the only pre-processing performed is the removal of the mean from the data. All other trends shall be considered as relevant information about the variability of the HR. In particular, no non-linear detrending will be performed.

4.3.4 Performance metrics

In general, in order to assess spectral leakage, the following parameters may be calculated:

- the amplitude of a particular side-lobe
- the sum of the amplitudes of the side-lobes from the first up to some specific frequency, such as the Nyquist frequency,
- the amplitude of the peak at the Nyquist frequency (this measures the aliasing) and
- the width of the main (highest amplitude) peak to measure the resolution.

However, since the sampling of an RR interval time-series is inherently uneven, only an *average* Nyquist frequency can be defined, and a meaningful comparison between the DFT and the Lomb method for computing spectral components near the Nyquist frequency cannot be made.

Therefore, the amplitude of the highest peaks and their widths at 3dBs below this peak are measured. To assess spectral leakage outside the main peak, the ratio of power inside a $\pm 0.01\text{Hz}$ band centred on each peak to the total power in each (LF and HF) band is calculated.

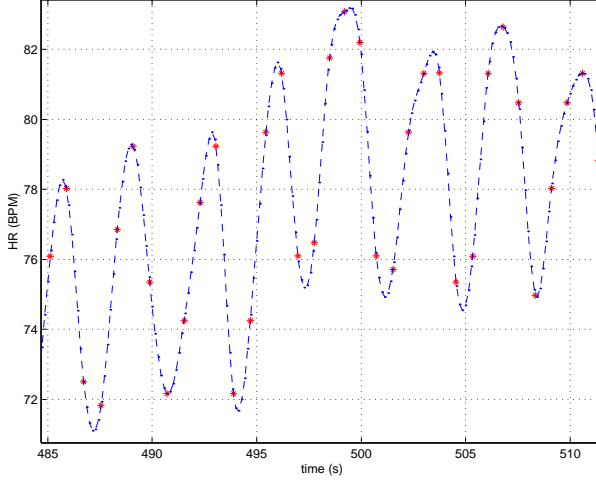


Figure 4.2: Real RR intervals (\diamond) with a (7Hz) cubic spline re-sampling overlaid.

4.4 Generating artificial data

4.4.1 A simple model

By its very nature, the RR tachogram is an unevenly sampled time series. In order to compare spectral estimation algorithms, it is important to know the underlying oscillations that produce the RR intervals. Since this cannot be done with real RR tachograms, an artificial signal is required. Recent attempts to create a realistic time series of RR intervals have included AR modelling [32] and extensions of DeBoer's model [281]. It is not clear however, how realistic the spectral characteristics of these models are. A new method of generating a continuous artificial RR tachogram time series is therefore introduced. This time series can then be evenly sampled at a high sample rate to produce an idealised discrete signal.

As discussed in section 1.6.4, it is well known that there are approximately two peaks in the PSD of a short-term (5 minute) RR tachogram: one at about 0.25 Hz (HF) and another at about 0.1Hz (LF). The relative heights of the LF and HF peaks can change significantly dependent on the autonomic tone of the patient [181], and hence the $\frac{\text{LF}}{\text{HF}}$ -ratio depends on the patient state.

An example of such a signal is given in figure 4.2 and the corresponding PSD (computed using the Lomb method) is shown in figure 4.3. Peaks at just under 0.1 Hz in the LF region and at around 0.275 Hz in the HF region are evident. Although the main body of literature in the field of HRV study presents frequency-domain data using linear scales for both the amplitude and frequency axes [184] the standard

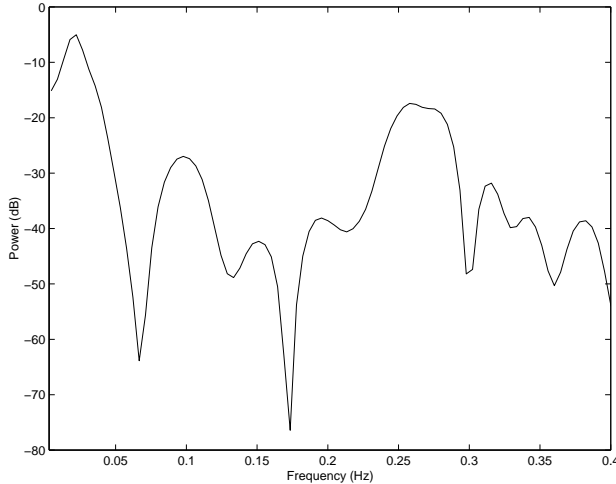


Figure 4.3: PSD of figure 4.2 - a real RR tachogram.

engineering practice of plotting the power axis on a logarithmic scale will be adopted³. An artificial RR tachogram can therefore be generated by mixing two sine waves with frequencies at these LF and HF peaks. Since the LF frequency boundaries are defined in the literature to be 0.04 and 0.15Hz [181], and the HF band lies between 0.15 and 0.4Hz, the centre frequencies of these bands, 0.095 and 0.275 Hz, are chosen as the LF and HF frequency components $\frac{\omega_l}{2\pi}$ and $\frac{\omega_h}{2\pi}$ for the synthetic signal. This corresponds well with the real data in figures 4.2 and 4.3 where the heart rate is about 76 bpm, with a variation of around ± 4.5 bpm once the very low-frequency component (below 0.04Hz) has been removed. The respiratory component (at 0.275Hz) is given an amplitude of 2.5 bpm and the LF component (at 0.095Hz) a 2 bpm amplitude. An expression for the HR can then be written as

$$\text{HR}(t) = \text{HR}_o + A_l \sin(\omega_l t) + A_h \sin(\omega_h t + \phi) \quad (4.25)$$

where, initially, $\text{HR}_o = 60$ bpm, $\omega_l = \frac{0.095}{2\pi}$, $\omega_h = \frac{0.275}{2\pi}$, $A_l = 2$ and $A_h = 2.5$, with no phase difference ($\phi = 0$) between ω_l and ω_h . The RR tachogram can then be formed by sampling $RR_t = \frac{60}{f_s}$ at the required frequency f_s , such that $t_n = \frac{n}{f_s}$ where ($n = 1, 2, \dots, N$).

Ideally one would like to make this sampling frequency as high as possible, but for a 300 second window, the computational time required to compute an FFT rapidly becomes prohibitive. As was pointed out in section 4.3.1, a reasonable choice for the 5 minute window is a sampling rate of 7Hz. There will then be 2048 points for the FFT computation in approximately 293 seconds of data.

³The frequency axis will be presented on a linear scale otherwise the LF region would dominate the plot.

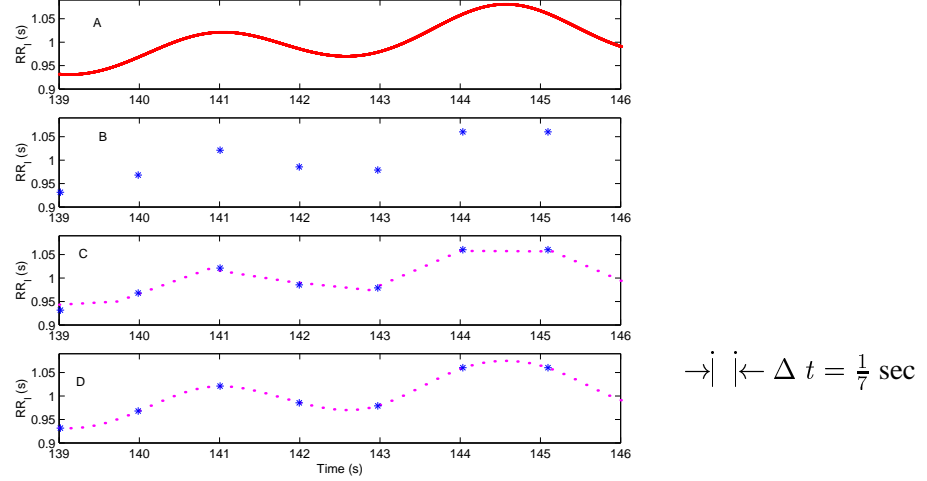


Figure 4.4: Artificial RR time series generated from equation 4.25 with a sampling rate of 1000 Hz (top figure, A). Figure B shows the physiologically plausible RR intervals extracted from the time series in figure A. Figure C shows these RR intervals with 7Hz linear re-sampling. Figure D shows the RR intervals with 7Hz cubic spline re-sampling.

However, it would be incorrect to generate a time series at 7Hz and *then* select physiologically plausible RR intervals. This would correspond to deriving RR intervals from an ECG that was sampled at only 7Hz. It has been demonstrated that the inaccuracies of R-peak location due to finite sampling times can significantly affect the RR tachogram and any metrics derived from it [181]. If a patient is suffering from low HRV (e.g. because they have recently undergone a heart transplant or are in a state of coma) then the sampling frequency of the ECG must be higher than normal. Abboud and Barnea [2] show that for such patients a sampling rate of at least 1000Hz is required. For normal patients however, a sampling rate of 128Hz has been found to be accurate enough to locate the R-peaks and hence compute HRV [184]. To minimise sampling errors, the artificial RR tachogram (equation 4.25) will be sampled at 1000Hz. Figure 4.4 (A) illustrates a short (7 second) segment produced from this procedure.

The time series only acquires ‘physiological plausibility’ when most of the points are removed, since the RR interval at each sample point RR_t must match the difference between the time stamp of this sample and the time of the previous sample (Δt) to duplicate what is observed for a real RR tachogram. The following algorithm can generate such a physiologically realistic time series from the original time series sampled at 1kHz (Figure 4.5A):

Record the first data point pair, (t_1, x_1) , as the first time stamp and RR interval pair (t'_1, RR_1) ,
Then proceed through each sample, t_i , until $x_n \geq t_i - t'_1$. This defines the second RR interval

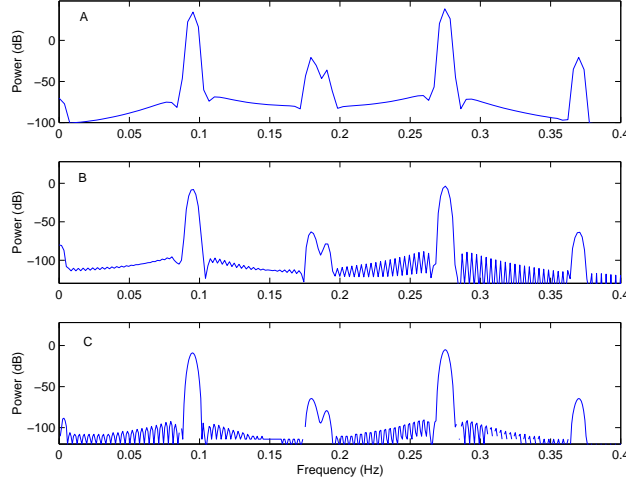


Figure 4.5: Periodograms of equation (4.25) for even sampling ($\text{HR}_o = 60$, $\frac{\omega_l}{2\pi} = 0.095$, $\frac{\omega_h}{2\pi} = 0.275$, $A_h = 2.5$, $\phi = 0$, $A_l = 2$, $t = 300$) computed using: A) FFT with $f = 1000\text{Hz}$, B) FFT with $f = 7\text{Hz}$ and C) Lomb periodogram with $f = 7\text{Hz}$.

($RR_2 = x_i, t'_2 = t_i$). This is generalised for all the $n = N$ RR intervals as $RR_n \geq t_i - t'_{n-1}$.

The result of applying this procedure to the short segment of the RR tachogram shown in figure 4.4A is plotted in figure 4.4B⁴. Figure 4.4C and 4.4D show the same physiologically realistic time series re-sampled at 7 Hz and using linear and cubic spline re-sampling respectively. Figures 4.4B to 4.4D are therefore the three different time series used as inputs to the three different PSD estimation methods being tested detailed in section 4.3.

4.4.2 Spectral estimation of artificial RR time series

Figure 4.5 compares the FFT method for power spectral estimation with the Lomb method on *evenly* sampled data. Figure 4.5A is an FFT derived estimate based on 2^{18} points sampled from the time series at 1kHz (approximately 262 seconds). This estimate represents our ‘gold standard’ reference. Figures 4.5B and 4.5C represent the spectral estimates derived from the FFT and the Lomb periodogram respectively, of the same (300 second) time series, generated at 7 Hz.

Although the expression for the Lomb periodogram reduces to the standard expression for the even sampling case, very small differences in the results between the FFT and the Lomb method are apparent since, in practice the \tan^{-1} function in the expression for τ in the Lomb periodogram (equation 4.23) has been approximated by a third order expansion for reasons of computational speed.

Now consider spectral estimates based on data from the *unevenly* sampled (physiologically realistic) data, as in figure 4.6. The sub-plots *a* to *c* correspond to the 5-minute time series for which a 5-second

⁴The artificial RR interval generator detailed in this section has been previously published by the author in [189] and [190]

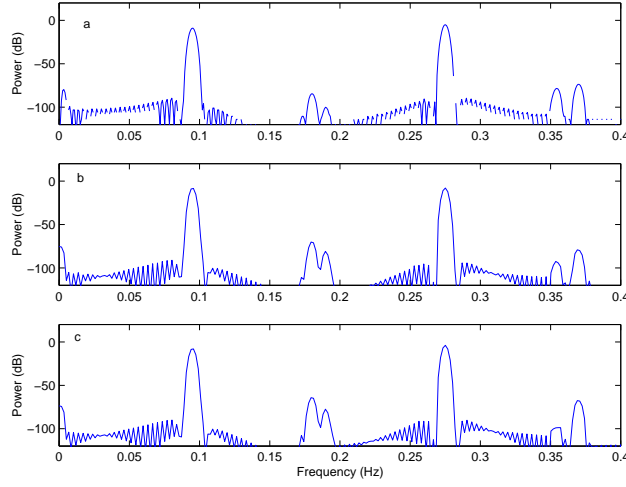


Figure 4.6: Periodograms of physiologically realistic data derived from equation (4.25). a) Lomb method of 300 individual beats in a 5 minute interval. b) 7 Hz linear re-sampling with FFT. c) 7 Hz cubic spline re-sampling with FFT.

segment is shown in figures 4.4 *B* to *D* respectively. Each calculation is based upon the physiologically realistic time series of 300 beats (in a 5 minute period) and the spectral estimate is computed using:

- a) The Lomb method applied to the 300 individual points in the 5 minute interval.
- b) 7Hz re-sampling using linear re-sampling and then Welch's FFT method.
- c) 7Hz re-sampling using cubic spline re-sampling and then Welch's FFT method.

Although there are small observable differences between each PSD estimate of the RR tachogram, the significance of these minor differences for HRV analysis is not clear.

However, before this issue is addressed, some modifications to the artificial RR tachogram are required. When real RR tachograms (as in figure 4.2) are studied, it becomes apparent that neither the relative amplitudes of the dominant LF and HF frequencies nor their values remain constant over time. The next two subsections deal with physiologically realistic methods for introducing such changes into the artificial RR tachogram.

4.4.3 Frequency variation

Figure 4.3 shows that there is a greater spread of frequencies in the real RR tachogram than in the artificially generated time series given by equation 4.25. A method for smearing out the frequencies is therefore introduced: the frequencies are gradually increased from one sample to the next to simulate slow changes in the frequency of the Meyer waves and RSA in the LF and HF regions (respectively) of the spectrum. Since the spread of frequency components is across the entire frequency band, with most

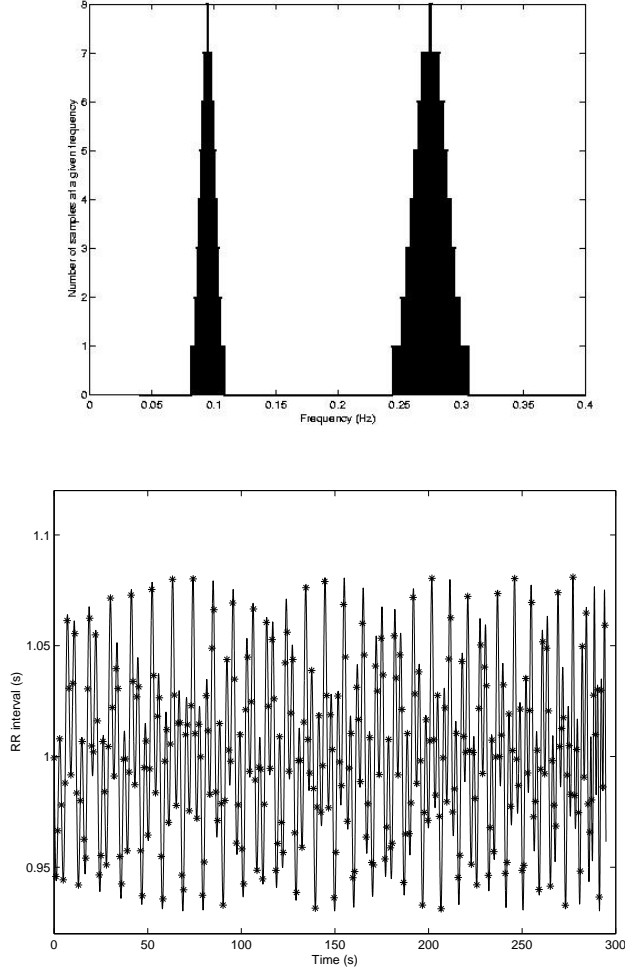


Figure 4.7: Sample-quantised frequency distribution with associated RR tachogram.

power concentrated at the central peaks of interest (0.095Hz and 0.275Hz), a logical choice of variation is a Gaussian spread of frequencies over each band. The number of samples in the LF and HF bands are (respectively) given by

$$\begin{aligned} S_l(j) &= \sum_{j=1}^N (\text{int}) \left| \frac{N}{\sqrt{(2\pi\sigma_l^2)}} e^{-\frac{1}{2}\left(\frac{\omega(j)-\omega_l}{\sigma_l}\right)^2} \right| \\ S_h(j) &= \sum_{j=1}^N (\text{int}) \left| \frac{N}{\sqrt{(2\pi\sigma_h^2)}} e^{-\frac{1}{2}\left(\frac{\omega(j)-\omega_h}{\sigma_h}\right)^2} \right| \end{aligned} \quad (4.26)$$

where $(\text{int}) ||$ indicates a standard rounding procedure to produce an integer number of samples, $\sigma_h = \frac{HF_h - HF_l}{\sigma}$, $\sigma_l = \frac{LF_h - LF_l}{\sigma}$, $HF_h = 0.4Hz$, $HF_l = 0.15Hz$, $LF_h = 0.15Hz$, $LF_l = 0.04Hz$, and $\sigma = 3$. The spread of frequencies given by such a procedure is shown in figure 4.7 (upper plot). The RR tachogram (lower plot in figure 4.7) is then formed as before (equation 4.25). Figure 4.8 shows the PSD

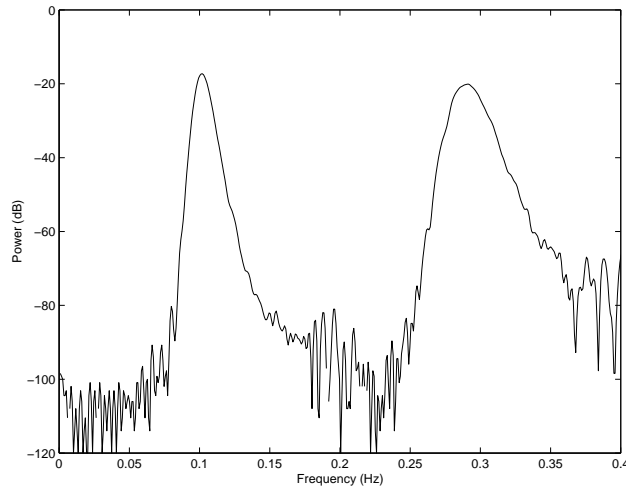


Figure 4.8: PSD of RR tachogram with a Gaussian ($\sigma = 3$) spread of frequencies generated by equations 4.26.

of such a time series computed using the FFT on a $t = 300$ second segment generated with sampling frequency, $f = 1000\text{Hz}$.

4.4.4 Frequency resolution

The choice of the number of samples to be used when estimating a periodogram and the frequency range over which the estimate is taken determines the frequency resolution. To determine the deterioration in the PSD estimation an artificial time series of 1300 beats is generated by the process detailed in section 4.4.3;

1. generate a 1kHz time series according to equation (4.25),
2. record the first sample as RR_1 with its time stamp, t_1 ,
3. proceed through each sample, t_i , consecutively, until $RR_n \geq t_i - t_{n-1}$,
4. record the RR_n and $t_n (= t_i)$ pair
5. repeat steps 3 & 4 until the end of the time series.

An estimate of the $\frac{\text{LF}}{\text{HF}}$ -ratio is then calculated using the Lomb method on the first N beats at the start of the 1300 beat artificial RR tachogram. This procedure is then repeated 1000 times, shifting the N beat window by one beat each time. A mean and variance is then calculated over these 1000 runs to assess the accuracy of the Lomb periodogram for that particular frequency resolution. The results of iterating the above procedure (in 10 bpm increments) for $HR = 50$ ($N = 250$) up to $HR = 120$ ($N = 600$) are

shown in table 4.1. Note that since the (average) Nyquist sampling frequency is $f'_c = \frac{1}{2\Delta t_{av}} = \frac{N}{2T}$, to resolve frequencies up to 0.4 Hz, Δt_{av} must be at least 1.25 seconds (an average HR of 48 bpm). For a heart rate of 50 bpm, a five minute segment contains $N = 250$ beats. Note that the estimate of the $\frac{\text{LF}}{\text{HF}}$ -ratio is highly consistent with low variances ($\sigma_{\frac{\text{LF}}{\text{HF}}}^2$) in the estimates. Below an average HR of 60 bpm, the variance begins to climb rapidly, however, even at 50 bpm, one standard deviation is only approximately 1% of the $\frac{\text{LF}}{\text{HF}}$ -ratio estimate. Therefore, the Lomb periodogram, $P(\omega_n)$ produces an accurate spectral estimate at the $n = N$ frequencies.

Heart Rate	50	60	70	80	90	100	110	120
Number of beats	250	300	350	400	450	500	550	600
$\frac{\text{LF}}{\text{HF}}$ -ratio	0.63	0.64	0.64	0.64	0.64	0.64	0.64	0.64
$\sigma_{\frac{\text{LF}}{\text{HF}}}^2 (\times 10^{-6})$	66	3.8	3.1	2.7	2.5	2.4	2.3	2.2

Table 4.1: Mean estimates of the $\frac{\text{LF}}{\text{HF}}$ -ratio and the variance $\sigma_{\frac{\text{LF}}{\text{HF}}}^2$ over 1000 runs using the Lomb method for differing mean heart rates.

4.5 Comparison of spectral estimation methods using artificial data

To summarise, the three techniques of PSD estimation for the RR tachogram that are being compared are:

1. Lomb periodogram of unevenly sampled data (with no re-sampling)
2. FFT-based PSD estimation using 7Hz cubic spline re-sampled signal
3. FFT-based PSD estimation using 7Hz linearly re-sampled signal

and the metrics used are:

- HF
- LF
- $\frac{\text{LF}}{\text{HF}}$ -ratio
- LF peak height
- HF peak height
- $\frac{\text{LF-peak-height}}{\text{HF-peak-height}}$
- Peak width at 3dB below each peak
- Fraction of power within $\pm 0.01\text{Hz}$ of each peak

In this section the above metrics are used to evaluate methods 1 to 3 above on a 5 minute segment of artificial data generated using equation 4.25. For the even sampling case, the sampling frequency is set to $f_s = 7\text{Hz}$ (and thus $N = 2100$). For the uneven sampling case, $f_s = 1000\text{Hz}$ and the physiologically realistic RR intervals are derived from this time series as described in section 4.4.1. Re-sampling is then performed with a 7Hz sampling rate using either linear or cubic splines between the original samples (see figures 4.4C and D) in order to allow a comparison with metrics evaluated on the original evenly sampled time series.

The comparisons performed are as follows:

- even and uneven sampling for a single sinusoid,
- even and uneven sampling with both LF and HF components and
- even and uneven sampling with frequency variation.

These experiments are designed to demonstrate how inaccuracies enter into the PSD estimation, and how they can be reduced.

4.5.1 Comparison of even and uneven sampling for a single sinusoid

Using equation 4.25 with the values $\text{HR}_o = 60$, $\frac{\omega_l}{2\pi} = 0.095\text{Hz}$, $\frac{\omega_h}{2\pi} = 0.275\text{Hz}$, $A_l = 0$, $A_h = 2.5$ and $\phi = 0$; the same values as previously except that no LF component is included ($A_l = 0$), an artificial RR tachogram is generated as described in section 4.4.1, with $f_s = 7\text{Hz}$ and $\Delta t = \text{constant}$. The PSDs

evaluated with the Welch FFT and Lomb methods on 2048 samples of this time series are presented in figure 4.9.

Table 4.2 presents a comparison of the relevant metrics introduced in section 4.4. As expected from theory, there is very close agreement between the two methods. In particular, they agree on the location of the peak frequency, f_{peak} , to approximately one part in two thousand. Note also the fraction of power ($\frac{P_p}{P_T}$) in the main lobe (within $\pm 0.01\text{Hz}$ of the 0.275Hz peak) is approximately 99.97% in both cases. This demonstrates that there is very little spectral leakage (using the Hamming window, equation 4.24) and agrees with the results of Harris [108]. Δf_{3dB} , $\frac{P_p}{P_T}$ and P_{sl} are the ‘gold standards’ with which the estimations on the unevenly sampled data will be compared.

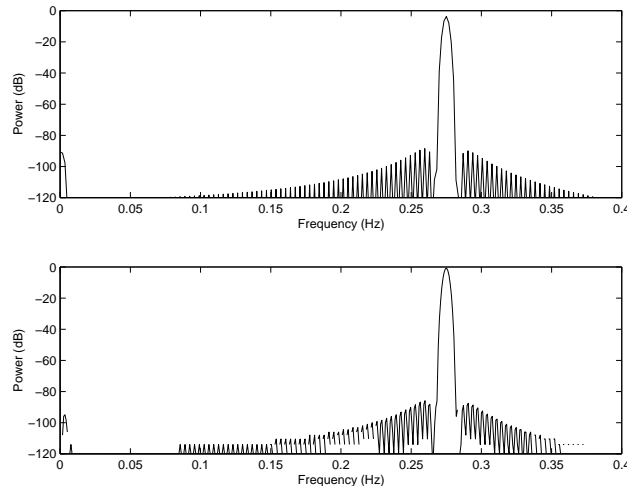


Figure 4.9: PSDs of evenly sampled (7Hz) artificial RR tachogram with a single component: $A_h \sin(2\pi(0.275)t)$, derived from the Welch FFT (upper) and Lomb (lower) methods.

Metric →	P_T	P_{peak}	f_{peak}	Δf_{3dB}	$\frac{P_p}{P_T}$	P_{sl}
DFT ↓	(dB)	(dB)	(Hz)	(Hz) $\times 10^{-3}$		(dB)
FFT	-50.33	-0.79	0.275	3.38	0.9997	-88
Lomb	-47.33	-4.23	0.275	3.42	0.9997	-86

Table 4.2: Total power (P_T), peak power (P_{peak}), frequency of peak (f_{peak}), 3dB bandwidth (Δf_{3dB}), fraction of power in a $\pm 0.01\text{Hz}$ band centred on the peak ($\frac{P_p}{P_T}$) and amplitude of the first side-lobe (P_{sl}) for figure 4.9; even sampling, single HF frequency. Note that Δf_{3dB} , $\frac{P_p}{P_T}$ and P_{sl} represent the ‘gold standard’ (see text).

Metric →	P_T (dB)	P_{peak} (dB)	f_{peak} (Hz)	Δf_{3dB} (Hz) $\times 10^{-3}$	$\frac{P_p}{P_T}$	P_{sl} (dB)
DFT ↓						
FFT_{lin}	-54.79	-0.73	0.275	3.42	0.9997	-93
FFT_{cub}	-50.75	-4.15	0.275	3.42	0.9997	-88
Lomb	-47.56	-8.17	0.275	2.51	0.9997	-86

Table 4.3: Total power (P_T), peak power (P_{peak}), frequency of peak (f_{peak}), 3dB bandwidth (Δf_{3dB}), fraction of power in a $\pm 0.01\text{Hz}$ band centred on the peak ($\frac{P_p}{P_T}$) and amplitude of the first side-lobe (P_{sl}) for figure 4.10; uneven sampling, single HF frequency.

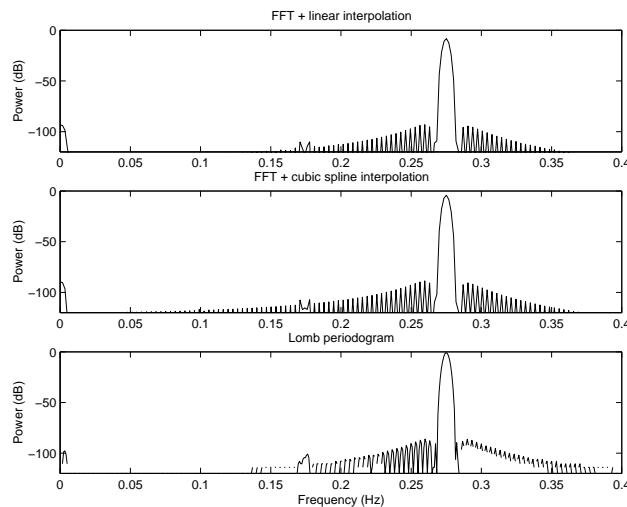


Figure 4.10: PSDs of unevenly sampled artificial RR tachogram with a single component: $A_h \sin(2\pi(0.275)t)$, derived from the FFT with linear re-sampling (upper), FFT with cubic spline re-sampling (middle) and Lomb (lower) methods.

Now consider the uneven sampling case (figure 4.10). From studying the FFT results in tables 4.2 and 4.3 it can be observed that for the even sampling case, the peak around 0.275 Hz is more narrowly defined and of higher amplitude than for linear and cubic spline re-sampling of the unevenly sampled data. Furthermore, by comparing the values of total power in the HF band, P_T , in tables 4.2 and 4.3 it can be seen that both re-sampling methods lead to an overestimation for the total power in the HF band (although the increase is marginal for the cubic spline method). This is consistent with what one would expect from such re-sampling methods. By referring back to figure 4.1 it can be seen that the cubic spline re-sampled data passes very close to each RR data point (*) and is a good approximation to the original

7Hz sinusoid, with only a small reduction in the high frequency content. However, linear re-sampling significantly reduces the high frequency content (within the 0.015Hz to 0.4Hz band of interest).

There are no significant differences between the even sampling and the uneven sampling cases for the Lomb method despite the reduction in the number of samples (from 2048 to 300, the number of actual RR intervals).

4.5.2 Comparison of even and uneven sampling for LF and HF components

Figure 4.11 shows the PSDs derived from the FFT and Lomb PSD estimation methods when the LF component is added in equation 4.25 ($A_l = 2$, $\frac{\omega_l}{2\pi} = 0.095\text{Hz}$) for the even sampling scenario. Table 4.4 records the results for the metrics presented in the previous section, for both the HF and the LF bands. As expected, the HF band is hardly affected by the addition of an extra frequency. The following sections therefore concentrate on experiments involving both frequency bands.

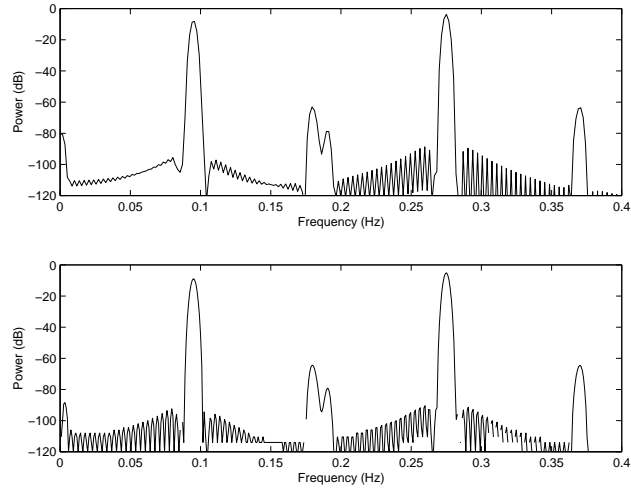


Figure 4.11: PSDs of evenly sampled artificial RR tachogram with a two sinusoidal components: $A_l \sin(2\pi(0.095)t) + A_h \sin(2\pi(0.275)t)$, derived from Welch's FFT (upper) and Lomb method (lower).

Metric →		P_T	P_{peak}	f_{peak}	Δf_{3dB}	$\frac{P_p}{P_T}$	P_{sl}
DFT ↓	Band ↓	(dB)	(dB)	(Hz)	(Hz) $\times 10^{-3}$		(dB)
FFT	HF	-50.28	-3.70	0.275	3.42	0.9973	-95.6
Lomb	HF	-51.62	-5.11	0.275	3.42	0.9973	-90.4
FFT	LF	-54.17	-8.13	0.095	3.42	0.9997	-88.9
Lomb	LF	-55.51	-8.92	0.095	2.57	0.9997	-92.4

Table 4.4: Total power (P_T), peak power (P_{peak}), frequency of peak (f_{peak}), 3dB bandwidth, (Δf_{3dB}) fraction of power in a $\pm 0.01Hz$ band centred on the peak ($\frac{P_p}{P_T}$) and amplitude of the first side-lobe (P_{sl}) for figure 4.11 (even sampling, LF and HF sinusoids).

Metric →	$\frac{A_L}{A_h}$ (exp)	LF (dB)	HF (dB)	$\frac{LF}{HF}$	LF	HF
DFT ↓						
FFT	0.60	-54.2	-50.3	0.64	0.39	0.61
Lomb	0.65	-55.5	-51.6	0.64	0.39	0.61

Table 4.5: Standard frequency metrics from the results presented in figure 4.11 (even sampling, LF and HF sinusoids). $\frac{A_L}{A_h}$ (exp) is the experimentally measured ratio of the two peak amplitudes in the low and high frequency regions.

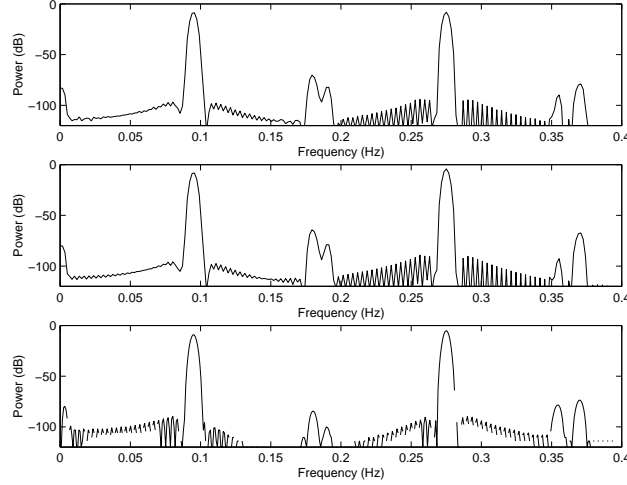


Figure 4.12: PSDs of unevenly sampled artificial RR tachogram (with two sinusoidal components: $A_l \sin(2\pi(0.095)t) + A_h \sin(2\pi(0.275)t)$) derived from the FFT with linear re-sampling (upper), FFT with cubic spline re-sampling (middle) and Lomb (lower) methods.

Metric →		P_T	P_{peak}	f_{peak}	Δf_{3dB}	$\frac{P_p}{P_T}$	P_{sl}
DFT ↓	Band ↓	(dB)	(dB)	(Hz)	(Hz) $\times 10^{-3}$		(dB)
Lomb	HF	-51.9	-5.03	0.275	2.51	0.9989	-89.6
FFT_{cub}	HF	-50.7	-4.64	0.275	3.38	0.9977	-92.0
FFT_{lin}	HF	-54.8	-8.17	0.275	3.42	0.9983	-91.3
Lomb	LF	-55.8	-9.00	0.095	3.34	0.9997	-89.5
FFT_{cub}	LF	-54.2	-7.65	0.095	3.38	0.9997	-92.0
FFT_{lin}	LF	-54.7	-8.67	0.095	3.42	0.9997	-91.2

Table 4.6: Total power (P_T), peak power (P_{peak}), frequency of peak (f_{peak}), 3dB bandwidth (Δf_{3dB}), fraction of power in a $\pm 0.01Hz$ band centred on the peak ($\frac{P_p}{P_T}$) and amplitude of the first side-lobe (P_{sl}) for figure 4.12.

Metric →	$\frac{A_l}{A_h}$ (exp)	LF	HF	$\frac{LF}{HF}$	LF	HF
DFT ↓		(dB)	(dB)			
Lomb	0.63	-55.8	-51.9	0.64	0.39	0.61
FFT_{cub}	0.71	-54.2	-50.7	0.67	0.40	0.60
FFT_{lin}	0.94	-54.7	-54.8	1.01	0.50	0.50

Table 4.7: Standard frequency metrics from the results presented in figure 4.12 (uneven sampling, LF and HF sinusoids).

It is important to note that the theoretical value of the $\frac{\text{LF}}{\text{HF}}$ -ratio is the ratio of the high to low frequency content is $(\frac{A_l}{A_h})^2 = (\frac{2}{2.5})^2 \approx 0.64$, the ratio of the square of the amplitudes of the two constituent sinusoids. For the evenly sampled case (table 4.5) the ratios of power between the LF and HF regions ($(\frac{\text{LF}}{\text{HF}})_{FFT} = 0.64$, $(\frac{\text{LF}}{\text{HF}})_{Lomb} = 0.64$) are the same as the theoretical value (to two decimal places). The results for the physiologically realistic (uneven sampling and in the case of the FFT, re-sampled) RR time series are presented in figure 4.12 and tables 4.6 and 4.7. The use of the Lomb method gives estimates of the $\frac{\text{LF}}{\text{HF}}$ -ratio and peak amplitude ratios closer to the theoretical value (0.6400) than either of the FFT methods. The FFT with linear re-sampling overestimates the ratios by about 50% and cubic spline re-sampling by only about 10%. It should also be noted that the FFT is performed on 2048 (evenly sampled) data points, whereas the Lomb method only has the 300 beats in the 5 minute window from which to compute the spectrum. The Lomb method is still able to achieve more accurate results because re-sampling always introduces errors which confound rather than help the PSD estimate.

An important observation to make is that the effect of linear re-sampling is an under-estimation of the power in the HF band because of heavy smoothing of the sinusoidal peaks in the RR time series. Although the periodograms produced by each method appear similar on visual inspection, slight variations in the PSD can lead to significantly different values in some of the HRV metrics.

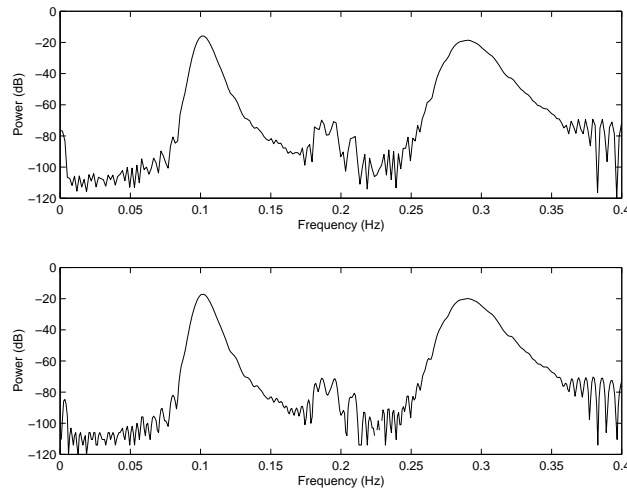


Figure 4.13: PSDs of a Gaussian ($\sigma = 3$) frequency modulated evenly sampled artificial RR tachogram (with two sinusoidal components: $A_l \sin(2\pi f_l t) + A_h \sin(2\pi f_h t)$) derived from the FFT (upper) and Lomb (lower) methods.

Metric → DFT ↓	Band ↓	P_T (dB)	P_{peak} (dB)	f_{peak} (Hz)	Δf_{3dB} (Hz) × 10 ⁻²	$\frac{P_p}{P_T}$
FFT	HF	-50.3	-18.6	0.291	1.71	0.244
Lomb	HF	-51.6	-19.9	0.291	1.62	0.265
FFT	LF	-54.2	-15.9	0.101	0.68	0.712
Lomb	LF	-55.5	-17.2	0.101	0.77	0.687

Table 4.8: Total power (P_T), peak power (P_{peak}), frequency of peak (f_{peak}), 3dB bandwidth, (Δf_{3dB}) and the fraction of power in a ±0.01Hz band centred on the peak ($\frac{P_p}{P_T}$) for figure 4.13.

Metric → DFT ↓	$\frac{A_l}{A_h}$ (exp)	LF (dB)	HF (dB)	$\frac{LF}{HF}$	LF	HF
FFT	1.36	-54.2	-50.3	0.64	0.39	0.61
Lomb	1.38	-55.5	-51.6	0.64	0.39	0.61

Table 4.9: Standard frequency metrics from the results presented in figure 4.13 (even sampling, LF and HF sinusoids).

4.5.3 Comparison of even and uneven sampling with frequency variation

This section now presents results obtained for the different spectral estimation methods on a more physiologically realistic RR tachogram as described in section 4.4.3 (3 σ Gaussian distributions for the HF and LF frequency components). Figure 4.13 represents the PSDs of a 7Hz evenly sampled RR tachogram (generated with the same parameters as in the previous section) derived from the FFT and Lomb methods. The performances of the chosen metrics on a 5 minute (7Hz evenly sampled) generated by this method are presented in tables 4.8 and 4.9.

Note that comparing this data to the idealised (no frequency variation) even sampling case (table 4.4) highlights how the frequency shifting has caused a significant drop in the LF and HF peak heights, as expected. Furthermore, there are significant drops in the 3dB bandwidths (Δf_{3dB}) and percentage of

Metric → DFT ↓	Band ↓	P_T (dB)	P_{peak} (dB)	f_{peak} (Hz)	Δf_{3dB} (Hz) × 10 ⁻²	$\frac{P_p}{P_T}$
Lomb	HF	-51.8	-20.2	0.290	1.70	0.247
FFT_{cub}	HF	-50.9	-19.2	0.291	1.71	0.247
FFT_{lin}	HF	-55.4	-23.6	0.291	1.71	0.257
Lomb	LF	-55.6	-17.3	0.102	0.76	0.682
FFT_{cub}	LF	-54.2	-16.0	0.103	0.68	0.710
FFT_{lin}	LF	-54.8	-16.6	0.101	0.68	0.713

Table 4.10: Total power (P_T), peak power (P_{peak}), frequency of peak (f_{peak}), 3dB bandwidth (Δf_{3dB}) and fraction of power in a ±0.01Hz section centred on the peak ($\frac{P_p}{P_T}$).

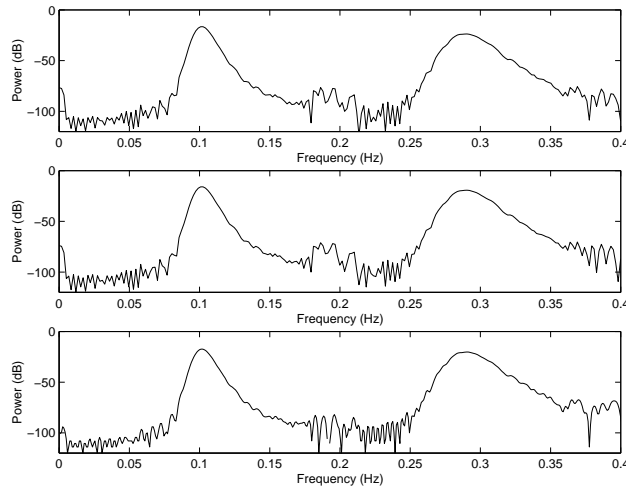


Figure 4.14: PSDs of a $\sigma = 3$ frequency modulated unevenly sampled artificial RR tachogram (with two sinusoidal components: $A_l \sin(2\pi f_l t) + A_h \sin(2\pi f_h t)$) derived from the FFT with linear re-sampling (upper), FFT with cubic spline re-sampling (middle) and Lomb (lower) methods.

Metric → DFT ↓	$\frac{A_l}{A_h}$ (exp)	LF (dB)	HF (dB)	$\frac{\text{LF}}{\text{HF}}$	LF	HF
Lomb	1.39	-55.6	-51.8	0.64	0.39	0.61
FFT_{cub}	1.45	-54.2	-50.9	0.70	0.41	0.59
FFT_{lin}	2.25	-54.8	-55.4	1.07	0.52	0.48

Table 4.11: Standard frequency metrics from the results presented in figure 4.14 (uneven sampling, LF and HF sinusoids).

powers in a $\pm 0.01\text{Hz}$ band centred on the peaks ($\frac{P_p}{P_T}$). A slight shift in the peak frequencies to higher values is also observed. However, the total power (P_T) in each band is similar to the idealised case (table 4.4). Comparing the metrics derived from the PSDs in figure 4.13 (table 4.9) and those from the idealised case (table 4.5) it becomes clear that although the ratio of the peak heights ($\frac{A_l}{A_h}$) changes considerably, the $\frac{\text{LF}}{\text{HF}}$ -ratio does not change (from the theoretical value of 0.64) for either the Lomb or the FFT methods. The slow change in frequency over the 5 minute window does not significantly affect the HRV metrics being considered.

However, departures from this idealised value are again apparent when the realistic (unevenly sampled) RR tachogram is used. Figure 4.14 illustrates that there is very little difference in the appearance of the PSDs derived from each of the 3 estimation methods. Furthermore, comparing the parameters derived from these PSDs (table 4.10) with those in the previous example (table 4.4) demonstrates that there appears to be only a very small numerical differences in the spectral estimates. However, on analysing HRV metrics (comparing tables 4.5 and 4.11), it is evident that small errors occur when using cubic spline re-sampling and gross errors when using linear re-sampling in the PSD estimation process.

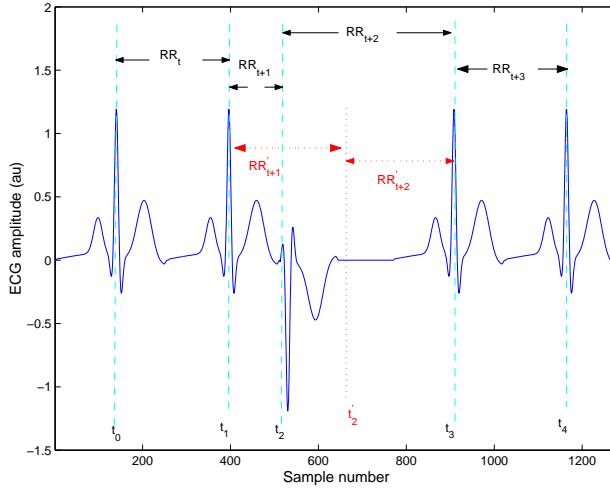


Figure 4.15: Sinus beats occurring at times t_0 , t_1 , t_3 and t_4 , and an ectopic beat occurring at t_2 . The ectopic beat occurs earlier than would be expected for a sinus rhythm beat and shortens the first associated RR interval (RR_{t+1}) and lengthens the second (RR_{t+2}). To avoid introducing high frequency components at this point, a phantom beat can be placed at t'_2 half way between t_1 and t_3 so that RR_{t+1} and RR_{t+2} become RR'_{t+1} and RR'_{t+2} , both equal to $\frac{t_3-t_1}{2}$.

4.6 Performance of algorithms on artificial data when coping with ectopy

In chapter 3 it was pointed out that ectopic beats (abnormal beats that usually occur early with an unusual timing) are removed from the RR tachogram prior to HRV analysis for two main reasons. Firstly it is thought that an ectopic beat is not generated by the mechanism that is responsible for the variability in the RR intervals. Secondly, ectopic beats occur substantially earlier than one would expect a normal beat to occur and are followed by a prolonged pause. These unusually short RR intervals create higher than normal frequency components and lead to a significant rise in the estimation of the high frequency components that may distort the true measure of an HRV metric. Ectopic beats can occur either instead of a sinus beat or in addition to the sinus rhythm. In the latter case, it would be appropriate to remove the beat altogether and calculate the RR interval as being the interval between the two normal beats either side of the ectopic beat. However, in the case where the beat occurs instead of a sinus beat, it is more appropriate to replace the beat with a ‘phantom’ beat, which is usually taken to be half way between the two sinus beats either side of the ectopic beat (see figures 4.15 and 4.16). Both these methods of ectopic removal and replacement (interpolation) are explored, together with the linear and cubic spline resampling methods. How the pre-processing using removal or replacement affect frequency domain HRV metric estimation are investigated in detail, and compared to the performance of the Lomb periodogram,

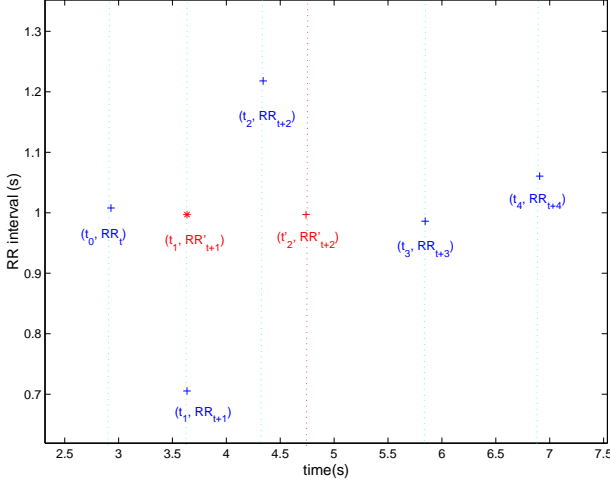


Figure 4.16: RR intervals from data in figure 4.15. Sinus beats occurring at times t_0 , t_1 , t_3 and t_4 , and an ectopic beat occurring at t_2 . The ectopic beat occurs earlier than would be expected for a sinus rhythm beat and shortens the first associated RR interval (RR_{t+1}) and lengthens the second (RR_{t+2}). To avoid introducing high frequency components at this point, a phantom beat placed at t'_2 , half way between t_1 and t_3 changes RR_{t+1} and RR_{t+2} to RR'_{t+1} (indicated by a red *) and RR'_{t+2} (indicated by a red +). Both these new intervals have the same value.

which requires neither beat replacement nor re-sampling.

4.6.1 Previous Work

Albrecht and Cohen [10] compared FFT-based estimates of RR tachograms in which either linear interpolation or an autocorrelation method was used for replacing timings of ectopic or missing beats. They showed that, for typical RR tachograms, linear interpolation to create phantom beats in an RR tachogram produced a more accurate PSD estimate than using an autocorrelation method to approximate the location (in time) of the phantom beat. This was only tested for low numbers of beat removal (a typical procedure for occasional ectopy). Birkett *et al.* [33] compared two methods of computing HRV spectra for congestive heart failure patients. In the first method, linear or cubic spline interpolation was used to replace ectopic beats. In the second method, segments with ectopy were discarded. They found that HF calculations were unaffected, but LF power was significantly higher in the case of interpolation. In both methods the same FFT-based algorithm was used. In 1994 Lippman *et al.* [172] compared ectopy section removal with linear, cubic and nonlinear predictive interpolation as well as the null case (no ectopic removal). They concluded that ectopy correction is necessary for HRV analysis but that section removal performs as well as more complicated interpolation techniques. Their results indicated that linear or

cubic interpolation of removed sections of the RR tachogram led to significant errors in some frequency and time domain HRV metrics.

4.6.2 Artificial ectopy

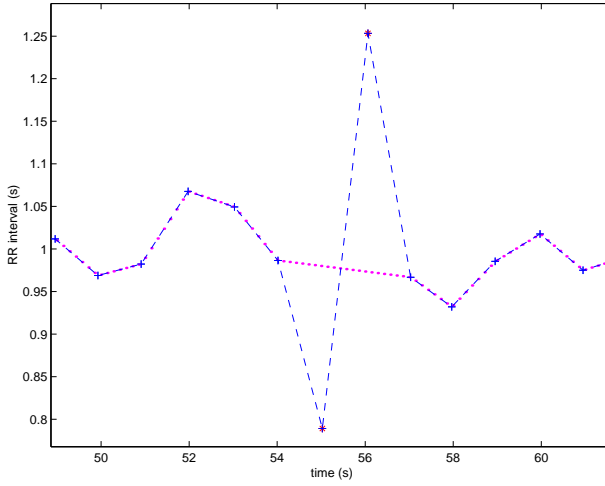


Figure 4.17: *Realistic* RR tachogram (+) evenly re-sampled with linear interpolation (— · —). An ectopic beat is chosen to occur at about 55 seconds. Application of equation 4.28 moves the corresponding RR interval downwards and to the left. The following RR interval occurs at the same time as before, but has a much larger magnitude since the previous RR intervals occurred prematurely and thus its location in time has moved. Note that the line of magenta dots which forms a straight line through this segment (54 to 57 seconds) corresponds to the 7Hz re-sampled (linearly interpolated) RR tachogram after these two points are removed (see section 4.6.4).

In the previous section an artificial RR tachogram was constructed that reflects many of the properties of real data. Ectopic beats can be added to this time series using a simple procedure. As stated in section 3.4, Kamath and Fallen [138] define ectopic beats (in terms of timing) as those which have intervals less than or equal to 80% of a sinus cycle length. For the artificial data we are considering (with a mean HR of 60 bpm), this corresponds to an average RR interval of 0.8s. Each datum in the RR tachogram represents an interval between two beats and the insertion of an ectopic beat therefore corresponds to the replacement of 2 data points as follows. The n^{th} and $(n + 1)^{th}$ beats (chosen randomly) are replaced (respectively) by RR'_n and RR'_{n+1}

$$RR'_n = \gamma RR_{n-1}, \quad (4.27)$$

$$RR'_{n+1} = RR_{n+1} + RR_n - RR'_n \quad (4.28)$$

where the ectopic beat's timing is the fraction, γ , of the previous RR interval (initially 0.8). Figure 4.17

shows an artificial RR tachogram (generated as in the last section) with the effects of the ectopic beat added (a sharp dip and then an increase in the following RR interval because of the prematurity of the ectopic beat). The two points affected are marked by asterisks (*).

Metric → DFT ↓	$\frac{LF}{HF}$	LF	HF	γ
Lomb	0.60	0.38	0.62	0.8
FFT_{cub}	0.63	0.40	0.61	0.8
FFT_{lin}	1.00	0.50	0.50	0.8
Lomb	0.34	0.26	0.74	0.7
FFT_{cub}	0.40	0.29	0.71	0.7
FFT_{lin}	0.98	0.49	0.51	0.7
Lomb	0.32	0.25	0.76	0.6
FFT_{cub}	0.34	0.25	0.75	0.6
FFT_{lin}	0.53	0.35	0.65	0.6

Table 4.12: Standard frequency metrics for differing magnitudes of ectopy (γ).

Metric → DFT ↓	$\frac{LF}{HF}$	LF	HF
Lomb	0.47	0.32	0.68
FFT_{cub}	0.50	0.33	0.67
FFT_{lin}	0.77	0.43	0.57

Table 4.13: Standard frequency metrics for $\gamma = 0.8$ and two ectopic beats.

Table 4.12 details the results of the three most used frequency-domain HRV metrics for differing strengths of ectopy (γ) for a single beat in a 5-minute section of unevenly sampled RR data (300 beats). The interpolation (in the case of FFT derived results) is performed at 7Hz , as before. Note that for decreasing values of γ , corresponding to increasingly earlier arrival times of the ectopic beat, both the values of the $\frac{LF}{HF}$ -ratio and LF decrease while the HF increases. Table 4.11 (in section 4.5.3) gives the values that these metrics have in the no ectopy case. In particular the $\frac{LF}{HF}$ -ratio drops from 1.07, 0.70 and 0.64 for the FFT_{lin} , FFT_{cub} and Lomb methods respectively to approximately 50% of these values in the case of $\gamma = 0.6$ (a relatively common occurrence in normal humans [181]).

For more than one ectopic in a five minute section of data (not occurring sequentially), the same trend is observed. Table 4.13 presents results for HRV metric estimation with two ectopies and $\gamma = 0.8$. Again, the power in the LF region is under-estimated and over-estimated in the HF region resulting in a value for the $\frac{LF}{HF}$ -ratio of approximately 50% of the no-ectopy case.

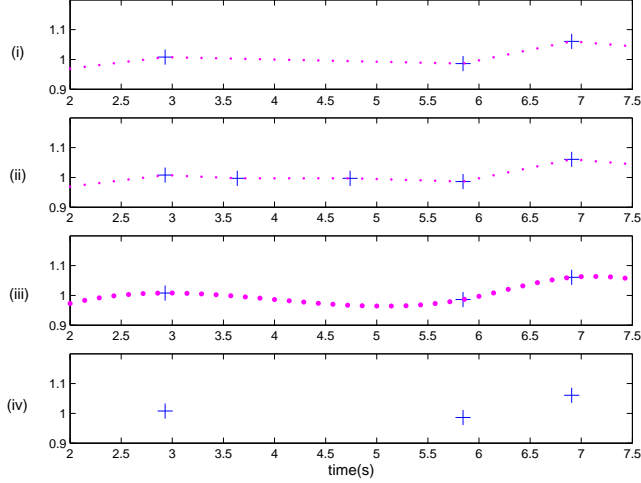


Figure 4.18: Re-sampled data (magenta dots) from original RR intervals (+) using the four methods detailed in the text; (i) Ectopic RR interval removal followed by 7Hz linear resampling; (ii) Ectopic beat replacement followed by 7Hz linear re-sampling; (iii) Ectopic RR interval removal followed by 7Hz cubic spline re-sampling; (iv) Ectopic RR interval removal with no re-sampling.

4.6.3 Beat replacement and removal: a comparison

In order to evaluate the effect of beat replacement or removal on the spectral estimation methods being tested in this chapter, the following four $\frac{\text{LF}}{\text{HF}}$ -ratio estimation techniques are compared for varying levels of ectopy:

- (i). FFT with ectopic beat removal, 7Hz linear re-sampling
- (ii). FFT with ectopic beat removal and insertion of phantom beat, 7Hz linear re-sampling
- (iii). FFT with ectopic beat removal, 7Hz cubic spline re-sampling
- (iv). Lomb method with ectopic beat removal, no re-sampling

Figure 4.18 illustrates the data after phantom beat insertion (if applicable) and re-sampling, prior to spectral estimation using the FFT or Lomb periodogram for each of these four methods for the data in figure 4.15. Each segment is five minutes long and for methods (i), (ii) and (iii), a Hamming window is applied to the re-sampled data.

4.6.4 Metric performance when removing or replacing ectopic beats

Figure 4.19 presents results on $\frac{\text{LF}}{\text{HF}}$ -ratio estimates from the four methods being tested (detailed in the previous section). For each method, 1000 five-minute artificial RR tachograms each with an $\frac{\text{LF}}{\text{HF}}$ -ratio

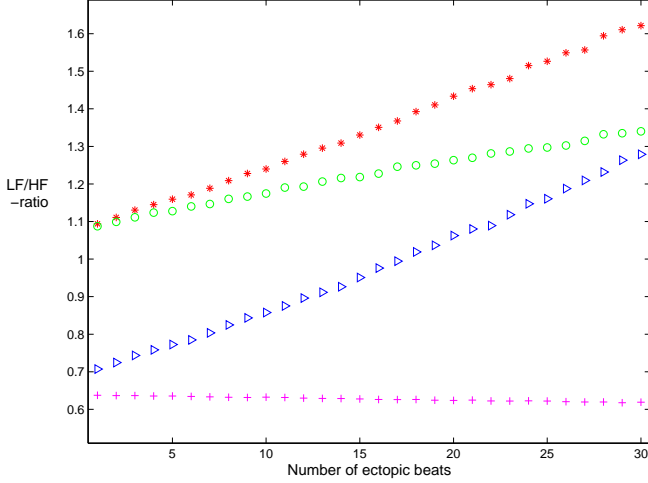


Figure 4.19: $\frac{\text{LF}}{\text{HF}}$ -ratio LF/HF-ratio estimates for methods i (*), ii (o), iii (\triangleright) and iv (+) when dealing with differing numbers of ectopic beats in a five-minute RR tachogram with an actual $\frac{\text{LF}}{\text{HF}}$ -ratio of 0.64. Each point is an average of 1000 randomly seeded runs.

of 0.64, are generated and an ectopic beat is introduced at random within the central 50% of the five minute window. For method (ii), the ectopic beat is then replaced by a phantom beat, half way between the two adjacent beats. For methods (i), (iii) and (iv), the two (abnormal) RR intervals associated with the ectopic beat are removed. The appropriate re-sampling method is then employed, noting that no re-sampling is performed for method (iv). The mean and variance of these 1000 runs is then calculated. This is then repeated, gradually increasing the number of ectopic beats introduced within the window, up to the average Nyquist limit⁵, where $\Delta\text{RR}_{av} \geq 0.8$, giving an upper limit of 60 (out of 300) RR intervals (from 30 ectopic beats) being removed at most.

4.6.5 Discussion

Beat replacement using linear interpolation for ectopic beats (method (ii)) results in a similar performance to method (i), where no beat replacement is performed, because there is only a small difference in the value of the relevant RR intervals (see figure 4.15). However, as the incidence of ectopic beats increases, it becomes noticeable that the increase in over-estimation of the $\frac{\text{LF}}{\text{HF}}$ -ratio using method (i) is twice that of method (ii). This is as expected; twice the number of RR intervals are changed using linear re-sampling in method (i), since the ectopic beat is not replaced, but removed (see figure 4.16(i) and 4.16(ii)). A similar trend can be observed in method (iii), but since cubic spline re-sampling produces a

⁵see section 4.3.1

more accurate representation of the underlying signal than linear re-sampling (see figure 2.1(iii)), cubic spline re-sampling produces only a small over-estimate of the $\frac{LF}{HF}$ -ratio with a low incidence of ectopy. Interpolation of ectopic beats with re-sampling prior to FFT analysis (method (ii)) therefore produces an estimate with accuracy between methods (i) and (iii); no beat replacement and re-sampling with linear and cubic spline interpolation respectively.

Method (iv) produces an accurate estimate of the $\frac{LF}{HF}$ -ratio to within 1% of the theoretical value of 0.64, with a standard deviation of less than 1%. At the limit of 30 ectopic beats, method (iv) continues to result in an accurate estimate (to within 3% of the theoretical value and a standard deviation of less than 2.8%, an order of magnitude lower than for methods (i), (ii) and (iii)).

It is clear that the interpolation techniques used to replace ectopic beats adds low frequency components and reduces the high-frequency content. HF is therefore under-estimated whilst LF and the $\frac{LF}{HF}$ -ratio are over-estimated with even re-sampling PSD methods.

Birkett *et al.* [33] showed that linear interpolation over segments of ectopy significantly changed calculations of LF (but not HF), whereas Lippman *et al.* [172] showed that linear or cubic interpolation methods over-estimated measures of LF and under-estimated measures of HF. The results presented in this chapter are in agreement with these observations, noting that the LF over-estimation dominates the calculation of the $\frac{LF}{HF}$ -ratio.

4.7 Conclusions

In conclusion, it can be seen that the Lomb technique for evaluating frequency domain HRV metrics is better than the best methods currently employed (an FFT of cubic spline interpolated data) when ectopy is absent from the data. It has also been demonstrated that ectopic beats must be removed from the RR tachogram prior to frequency domain HRV metric calculation. Furthermore, the calculation of such metrics after the removal of ectopic beats using the Lomb technique is stable as expected (from earlier results in the chapter) whereas the error in the PSD estimate using interpolation prior to an FFT grows linearly with the number of ectopics removed.

It should be noted that an optimal adaptive threshold timing for removing abnormal beats, prior to the use of the Lomb periodogram, is now appropriate. Since the number of missing beats does not significantly affect the Lomb estimate of the $\frac{LF}{HF}$ -ratio, (as long as the average Nyquist criterion is satisfied) the timing threshold, λ , to exclude abnormal beats from the RR tachogram can be reduced (see section

3.4.1). In order to resolve frequencies as high as 0.4 Hz (the upper limit of the HF frequency band), at least 240 beats are needed in a 300 second window (see section 4.3.1). If, after removal of ectopic beat candidates there are still more than 240 beats in a particular window, the threshold for rejecting ectopic beats can be made more stringent. Since the number of beats will change from one five minute section to another, this threshold can be adaptive, being systematically reduced until the lower information limit is reached. Figure 3.16 shows that reducing the beat rejection threshold, λ , to 6% will on average, preserve 80% of the sinus beats in a five minute window (240, if the heart rate is 60bpm). However, the number of ectopics excluded changes very little below $\lambda = 10\%$. Therefore, a more sensible choice of timing filtering is to use $\lambda = 10\%$ as the lower threshold and increment it only when the Nyquist criterion cannot be adhered to. If a value of $\lambda > 20\%$ is required, then the RR time series segment should be rejected as a candidate for spectral analysis because the potential for including ectopic beats, which significantly distort the PSD estimate, is then high.

In the next chapter, the performance of the Lomb and FFT methods are further compared on real data to ascertain if the errors introduced by re-sampling are large enough to obscure inter- and intra-patient HRV changes.

Chapter 5

HRV analysis during sleep

5.1 Introduction

In the review of the current HRV literature in chapter 1 it was noted that one of the most significant factors that affects HRV metrics is the patient's mental activity. Therefore in attempting to assess patient welfare or improvement through HRV analysis it is important that some indicator is used to quantify the subject's level of mental activity.

Although there is no general consensus on how to measure levels of mental activity while a subject is awake because of extraneous factors [118, 209], there is a generally agreed classification of mental activity for subjects during sleep [166, 231] (see section 5.4.1). During sleep, the influence of extraneous factors is reduced. Recent reports have shown that significant differences in HRV metrics exist between some sleep states and in particular, the $\frac{LF}{HF}$ -ratio has been shown to vary significantly between deep and light sleep [184, 275].

This chapter describes an investigation into the value of the the $\frac{LF}{HF}$ -ratio during sleep states for both normal and abnormal patients in an attempt to see if differences can be observed between differing populations for particular sleep states. Before this is presented, however, a brief overview of the physiological mechanisms that lead to HRV variations during sleep are described in order to demonstrate the relevance of the $\frac{LF}{HF}$ -ratio in this context.

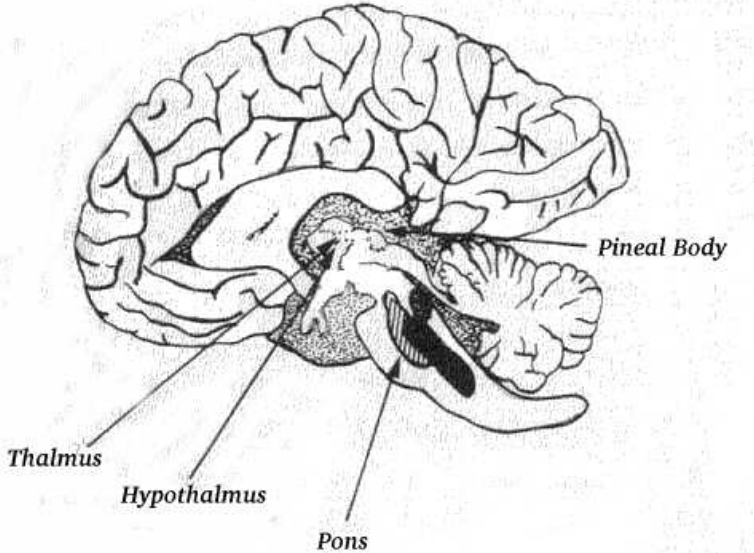


Figure 5.1: The regions of the brain that control rapid eye movement (REM) sleep (dotted), non-REM sleep (striated), wakefulness (black) and the respiratory-cardiovascular system (nuclei in the hypothalamus). See sections 5.2.1 and 5.4.1 for details. Adapted from [165].

5.2 Physiological control and variation

5.2.1 The autonomic nervous system

The autonomic nervous system is controlled by neurons found in the nuclei of the hypothalamus, located just above the pituitary gland at the central base of the brain (see figure 5.1). Hypothalamic nuclei regulate heart rate, blood pressure, respiration, gastrointestinal motility and temperature (amongst other functions) mainly through the sympathetic and parasympathetic systems (see § 1.5.1). The hypothalamus also regulates the release of hormones from the pituitary gland, which in turn releases hormones that affect distant cells, tissue and glands. Control of the endocrine system¹, and hence the release of the hormone cortisol, is another critical regulatory role of the hypothalamus. High levels of cortisol are released during stressful situations and increase appetite and (stored) energy delivery to the muscles. However, continual cortisol release in response to prolonged emotional or physically stressful situations has been linked to high blood pressure, gastric ulcers, impotence, reduced immune system response and loss of neurons in the brain [70]. Although much is known about how the autonomic nervous system regulates the body's critical cardiovascular function (autoregulation), the question of how the hypothalamus functions is still open.

¹The system of glands that release their secretions (hormones) directly into the circulatory system.

5.2.2 Circadian rhythms

It is also known that regions within the hypothalamus are involved in regulating the transition between wakefulness and sleep [165]. The hypothalamus is connected by neural paths to the *reticular* formation, which retards the activity of the arousal centre within the brain and causes a transition from wakefulness to sleep. The exact cause of this change of consciousness is not known, but the moment of change appears to be strongly correlated with a subject's circadian rhythms.

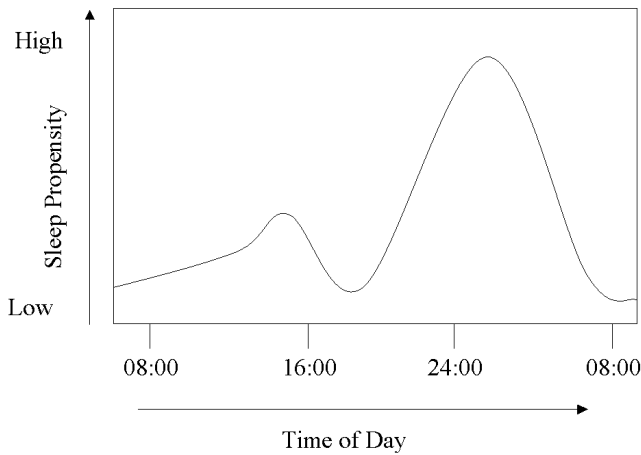


Figure 5.2: The propensity for a normal subject to fall asleep over the 24 hour clock (adapted from [165]).

Figure 5.2 shows the propensity for a subject to fall asleep over a typical day. Note that the easiest times to fall asleep are 3p.m. (the traditional 'siesta' time) and 3a.m.. Lavie [165] refers to these maxima as the *opening of the sleep gate*. This cycle is strongly inversely correlated with the 24 hour variations in core body temperature; a drop in temperature to near the minimum is observed leading up to the onset of sleep (see chapter 1). This is also true of both blood pressure and heart rate, although there are phase differences between each of the physiological parameters. In the absence of light (which resets biological cycles every 24 hours), these phase differences grow to significant levels [165] with temperature having a natural period of around 23 hours and consciousness between 25 and 27 hours. The human body's main clock is located in a nucleus found in the hypothalamus and receives direct input from the retina. This is the pathway through which light resets the circadian (24 hour) clock via the production of melatonin, a hormone secreted by the pineal gland in the brain (which is in turn linked to genital function, skin pigmentation and possibly the control of brain activity). Melatonin itself is a

neurotransmitter derived from serotonin and affects melanin in the skin. As melatonin is only produced in the hours of darkness, melatonin levels in the blood reflect the number of daylight and night-time hours being experienced. During the short summer nights melatonin levels are comparatively low. Conversely, during long winter nights melatonin levels in the blood are high and genital development is repressed. Once the hours of daylight begin to lengthen in the spring melatonin levels decrease, and conditions are conducive for breeding in most animals. These fluctuations also occur on a day-to-day basis, and exposure to bright light suppresses melatonin production. Such exposure during the evening hours can delay the daily body temperature nadir (which occurs during the early hours of the morning) and delay sleep time. Exposure to bright light in the early morning advances the sleep-wake cycle and the daily low point of the body temperature rhythm. It has been suggested [165] that melatonin is therefore linked to the control of the human sleep-wakefulness rhythm; both light and melatonin therapy have been used to correct maladjusted body clocks and a strong correlation between the rise in melatonin and the onset of sleep has been observed in many people [165]. Furthermore, Kunz *et al.* [159] have proposed that melatonin plays a key role in sleep and actually acts to reinforce dream sleep by enhancing inhibition of motor activity present during this phase of sleep. Lavie *et al.* [165] have shown that reduced melatonin secretion exists in elderly insomniac patients (often to barely detectable melatonin levels), particularly in those who are institutionalised.

To summarise, the human body is affected by a set of differing but interrelated cycles with periods of around 24 hours. They are entrained by the action of light and are controlled by the hypothalamus. Although there is a strong correlation between cardiovascular changes and levels of awareness, the mechanism that links these changes together is not clear. Furthermore, awareness has proved difficult to define and label [118, 209], thereby complicating any investigation into these links.

5.3 Changes in HRV with activity

Activity	$\frac{\text{LF}}{\text{HF}}$ -ratio
Spontaneous Breathing	1.39 ± 0.28
Controlled Breathing (15 breaths per min)	0.69 ± 0.37
Controlled Breathing (18 breaths per min)	1.09 ± 0.36
Silent reading	1.52 ± 0.26
reading aloud	1.59 ± 0.21
free talking	3.58 ± 0.45
performing mentally stressful tasks silently (such as mental arithmetic)	3.05 ± 0.39
performing mentally stressful tasks aloud	2.89 ± 0.31

Table 5.1: Activity dependent changes of the $\frac{\text{LF}}{\text{HF}}$ -ratio for conscious normal patients (with ± 1 standard deviation). Taken from results of [31].

Bernardi *et al.* [31] recently demonstrated that HRV (as measured by the $\frac{\text{LF}}{\text{HF}}$ -ratio) in conscious patients changes markedly depending on the subject's particular activity. Their analysis involved measuring the ECG, respiration and blood pressure of 12 healthy subjects aged 29 ± 1 years during a series of simple physical (verbal) and mental activities (see table 5.1). Each activity was approximately five minutes long and the subjects remained in a supine position for 20 to 30 minutes prior to the experiment (for rest and familiarisation) and throughout the activity itself. Table 5.1 presents their results (means of the 12 subjects with standard deviations). It is important to note that although the range of values for conscious subjects is not highly variable for a particular task, the day-time $\frac{\text{LF}}{\text{HF}}$ -ratio changes significantly depending upon the mental and physical activity a subject is engaged in. It may be argued that the changes in these values are simply an effect of changing breathing patterns (that modify the HF component). However, significant changes in both the LF band and blood pressure readings were also observed, indicating that the feedback loop to the CNS was definitely affected and the resultant change in HRV is more than just a respiratory phenomenon.

Differences in activity should therefore be minimised when comparing HRV metrics on an inter- or intra-patient basis. Since it is very difficult for a researcher to be sure whether or not even a willing subject is controlling their thought processes for a few minutes (the shortest time window for HRV metrics [184]), this would imply that HRV is best monitored while the subject is asleep during which the level of mental activity can be more easily assessed.

5.4 HRV and sleep

5.4.1 The physiology and classification of sleep

Although the physiological state of sleep is substantially different to that of being awake (consciousness), it is generally accepted that sleep is also distinct from unconsciousness. While transitions to sleep and unconsciousness can both be identified by changes in the power spectral density of the electroencephalogram² (EEG) [231, 118], subtle differences in cardiovascular and electro-physiology do exist between these states. Unconscious subjects (such as those under anaesthetic or in a coma) are totally unresponsive to external stimuli. However, a sleeping subject may react to external events, depending on how deeply he or she is sleeping. Sleep is defined (mainly from the energy content of the EEG) as consisting of 5 stages [231]; stage 1 being the lightest (and therefore the closest to being awake) and stage 4 being the deepest. There is however, one further stage of sleep that is termed *paradoxical* sleep since the subject does not appear to be conscious, despite the fact that the EEG resembles that of a fully conscious subject. This stage, known as dream sleep, is often termed rapid eye movement (REM) sleep, since the eyes move around under closed eye-lids in a manner unique to such sleep. Stages 1-4 are therefore known as non-REM (NREM) sleep. The set of heuristics which categorise sleep according to these 5 stages are known as the *R & K rules* after the authors of the original paper, Rechtschaffen and Kales [231]. The graphical representation of a subject's sleep staging is known as the hypnogram (see figure 5.3). The horizontal axis is time into the study and the vertical axis represents depth of sleep. The higher the number of the sleep stage, the more deeply asleep the subject is considered to be. Note that the deeper stages of sleep are lower than the lighter stages (and therefore the vertical axis should be described as *lightness of sleep*). Note also that REM sleep (R) is plotted between Wakefulness (W) and the lightest sleep stage (1) because of the similarity of brain (EEG) activity in stages W and R. Note also that the label 'drowsy' is used to represent stage 1 sleep and the deeper stages (3 and 4) have been merged and labelled Slow Wave Sleep (SWS).

Just before loss of consciousness, respiration becomes less erratic and shallow, and sustained deep periodic breathing can be observed [196]. The brain stem takes over the respiratory regulatory mechanism at this point [165]. The onset of sleep is usually defined by either the loss of muscle tone (often by observing the subject drop an object they have been clutching) [165] or by rolling eye movements on the electro-oculogram (EOG) [231]. The subject initially falls into light sleep but quickly progresses into a

²A recording of the micro-volt potential difference fluctuations between electrodes attached to the scalp.

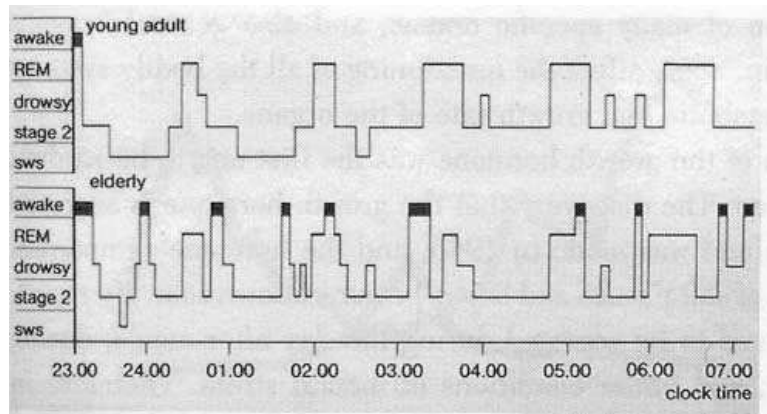


Figure 5.3: A typical sleep-wake plot (taken from [165]) showing the stages of sleep for a healthy young adult (top). Note that stage 1 is labelled ‘drowsy’ and stages 3 and 4 have been merged and labelled SWS (slow wave sleep). Within about 45 minutes of the young adult falling asleep, a deep phase of sleep occurs. This is interrupted after about an hour by a less deep phase of sleep leading to REM sleep. As the night progresses, the periods of deep sleep become progressively shorter and more shallow, whereas REM sleep becomes more prominent. The lower graph demonstrates how elderly patients tend to suffer from a significantly more fragmented sleep pattern than young healthy adults.

deep sleep. After about 90 minutes, a healthy young human adult will move rapidly through light sleep into the REM stage lasting around 20 minutes. Then the cycle is repeated (usually another 3 or 4 times) with a period of around 90 minutes, although the length of the dream sleep periods tends to increase (and that of deep sleep periods to shorten) as the night progresses.

The cardiovascular changes that occur during these cycles tend to follow the changes in depth of sleep; as the sleep state deepens, blood pressure and heart rate drop, while respiration becomes less erratic, deeper and slower. As a human subject moves back into lighter sleep these changes reverse and notably, the cardiovascular physiology during REM sleep resembles that just before loss of consciousness; breathing is erratic and shallow, heart rate and blood pressure are significantly higher and the EEG is indistinguishable from consciousness.

The lower plot in figure 5.3 illustrates how elderly patients tend to have a more fragmented sleep pattern than healthy young adults, waking many more times during the night and experiencing less frequent and shorter periods of deep sleep. It is not clear whether, for otherwise healthy elderly subjects, this pattern is independent of the lower level of cardiac health compared to younger more healthy subjects.

5.4.2 HRV changes with sleep state

On falling asleep, parasympathetic activity increases and begins to dominate over the falling levels of sympathetic activity. The metabolic rate declines to a relatively constant lower level during stages 1 to 4 NREM sleep causing a general relaxation of the cardiovascular system, a drop in BP, HR, stroke volume, cardiac output, and systemic vascular resistance [169]. As a result of the reduction in autonomic activity, myocardial workload is reduced. The baroreflex sensitivity is increased during NREM sleep in comparison to wakefulness.

Although NREM sleep is characterised by relative stability of the respiratory, cardiovascular and autonomic systems, intermittent arousals are common. These arousals are associated with abrupt increases in chemosensitivity and the momentary restoration of the wakefulness-type breathing, and hence augmented ventilation. HR and BP increases from NREM to relaxed wakefulness involve augmented sympathetic nerve activity, but not parasympathetic withdrawal. This indicates that arousal is a distinct transient state of heightened respiratory and cardiovascular activity [169]. On entering REM sleep, sympathetic activity begins to dominate and the EEG and respiratory-cardiovascular behaviour resemble those in a conscious state [165].

Loss of consciousness is accompanied by a change in autoregulation. Not only does the voluntary motor system relinquish any effect it had over parts of the involuntary motor system (such as respiration - when a subject begins to ‘doze off’, their breathing becomes deeper and more regular), but the parasympathetic nervous system begins to dominate. It is therefore unsurprising that changes in HRV occur at this transition. However, the more significant changes in HRV occur *during* sleep.

In particular, short term HRV tends to be higher the deeper the sleep is (HF increases and the $\frac{LF}{HF}$ -ratio falls) [155, 186, 213, 275]. Figure 5.4 shows that the PSDs calculated from 5 minutes of RR interval data during wakefulness and REM sleep have similar spectral components and $\frac{LF}{HF}$ -ratios. However, stage 2 sleep and SWS sleep exhibit a shift towards an increase in percentage contributions from the HF components (above 0.15 Hz).

In 1995 Vanoli *et al.* [275] conducted a detailed investigation into HRV changes during the various sleep stages of healthy subjects and post-myocardial infarction (MI) patients. They explained the PSD changes in normal subjects (detailed above) by noting that parasympathetic (vagal) activity tends to dominate during sleep. Since the increased vagal levels are the dominant contributor to increased short term variability of the heart rate then the HF power will increase. Furthermore, they found that MI results

in a raised overall nocturnal $\frac{\text{LF}}{\text{HF}}$ -ratio. In terms of spectral components, normalised HF is lower and LF higher at night in post-MI patients. Hence they showed that the $\frac{\text{LF}}{\text{HF}}$ -ratio was sufficient to separate post-MI from normal (healthy) subjects. However, no results on long-term outcome differences for the post-MI population were presented.

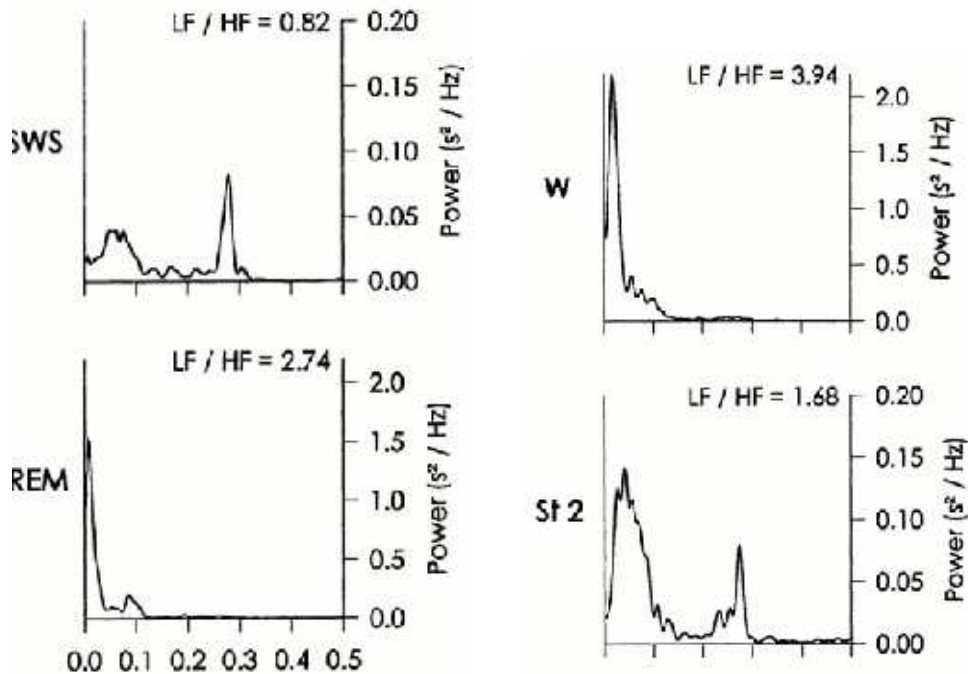


Figure 5.4: 5 minute PSDs of RR intervals, according to sleep states: awake (W), stage 2 (St2), slow-wave sleep (SWS), and rapid eye movement sleep (REM). $\frac{\text{LF}}{\text{HF}}$ -ratio is also indicated for each physiological state. Taken from Otzenberger *et al.* [213].

Condition → Activity ↓	Norm [213]	Norm [184]	Norm [275]	CNS † Problem [166]	Post-MI [275]
Awake	N/A	3.9	4.0 ± 1.4	N/A	2.4 ± 0.7
REM Sleep	$2 \rightarrow 2.5$	2.7	3.1 ± 0.7	$3.5 \rightarrow 5.5$	8.9 ± 1.6
NREM Sleep	$0.5 \rightarrow 1$	1.7	1.2 ± 0.4	$2 \rightarrow 3.5$	5.1 ± 1.4

Table 5.2: $\frac{\text{LF}}{\text{HF}}$ -ratios during Wakefulness, NREM and REM sleep. N/A = not available, Norm = normal, Post-MI = a few days after myocardial infarction, † indicates a non-cardiac related problem. Taken from [213, 184, 275, 166].

In 1998 Lavie *et al.* [166] obtained for a patient suffering from a psychosomatic disorder only, an $\frac{LF}{HF}$ -ratio between 0.5 and 1 in NREM sleep and between 2 and 2.5 for REM sleep. In patients suffering from a simple CNS but non-cardiac related problem³ Lavie *et al.* [166] found NREM $\frac{LF}{HF}$ -ratio values of between 2 and 3.5 and between 3.5 and 5.5 for REM sleep.

Table 5.2 presents a summary of activity dependent $\frac{LF}{HF}$ -ratios described in the literature. Comparing the values for normal and post-MI patients during sleep, it can be seen that the values of the $\frac{LF}{HF}$ -ratio during REM and NREM sleep are significantly higher than those for normals. It is interesting to note however, that the lower bound of the $\frac{LF}{HF}$ -ratio in NREM sleep for post-MI patients is similar to that of normal patients in REM sleep. Values for all subjects during wakefulness (2.4 to 4.0) lie well within the range of values during sleep (0.5 to 8.9).

5.4.3 Sleep disruption; pain, drugs and noise

Unfortunately, patients who may benefit from HRV analysis often suffer from severe disruption of their normal sleep cycles. ITU patients are subject to noise and external disruption that may adversely affect their rate of recovery. Patients under the influence of pain and/or pain killers experience serious sleep disruption [58] and may not experience a recognisable or true sleep cycle. Effects of the administered drugs (ACE inhibitors, β -blockers, aspirin, nitrate and calcium channel blockers) may ‘mask’ the effects we are attempting to observe [49].

Rosenberg-Adamsen *et al.* [235] analysed sleep states of patients after general anaesthesia with and without the postoperative administration of opioids. They found no significant disturbance in sleep patterns from normal activity only when opioids were not administered. Comparisons of these results with previous studies on slow wave sleep (SWS) and REM sleep disturbances after open laparotomy suggest that the depth of surgery or the administration of opioids, or both, may be important factors in the development of postoperative sleep disturbances.

5.5 Summary

A patient’s physical and mental activity (eating, exercise, respiration, wakefulness and diurnal variations) affects the HRV to such an extent that inter- and intra-patient comparisons cannot be made without taking such factors into consideration. Without reference to the patient’s physiological (and mental)

³Organic Erectile Dysfunction.

state, a measure of HRV is not useful for assessing the patient's ANS response and/or vagal tone.

The variation in $\frac{LF}{HF}$ -ratio with respect to the mean value is least during a sleep state and artefact in the ECG is significantly reduced (because there is less physical movement by the subject). Since sleep stages usually last more than five minutes they provide excellent segments of ECG data for HRV analysis with minimal data corruption and departures from stationarity.

During sleep stages, the values of HRV metrics are closely related to the depth of sleep, and it has been suggested that HRV could be used to differentiate between sleep states [213]. The key paper [169] reviewed in the previous section postulates that the changes in HRV observed between REM and NREM sleep are due to the changes in respiratory and cardiac regulatory control between these states. Current literature [213] indicates that HRV changes in SWS rather than NREM sleep should be studied, as light NREM sleep produces HRV values similar to that of REM sleep. In the following sections the variations of the $\frac{LF}{HF}$ -ratio during the sleep REM, NREM and SWS categories in both a normal healthy population and a non-normal population are investigated and $\frac{LF}{HF}$ -ratio estimates are compared with those of table 5.2.

5.6 Methods for analysing HRV during sleep

The data for the healthy group is taken from the OBS polysomnographic database⁴ 02 and consists of records from 6 males between the ages of 21 and 42 (mean age 32), weighing between 65kg and 88kg with no known cardiac or sleeping disorders. Subjects 01 to 06 slept for 6.5, 7.0, 3.3, 7.7, 7.5, and 7.4 hours respectively. Subject 3 awoke early because of a non-health related incident. Subject 05's ECG was of too low quality to be included in the study.

The unhealthy group consists of 16 males, aged 32 to 56 (mean age 43), with weights ranging from 89 to 152 kg (mean weight 119 kg), recorded at Boston's Beth Israel Deaconess Medical Center and freely available as the MIT polysomnographic database [194].

5.6.1 The MIT polysomnographic database

The 16 patients in this database suffer from a condition known as sleep apnoea, in which they are repeatedly awoken during the night due to their breathing being interrupted. If this is caused by a blockage in the respiratory pathways then it is known as obstructive sleep apnoea (OSA). If the cessation of breathing

⁴The author gratefully acknowledges the assistance of Oxford BioSignals Ltd for providing access to this data.

label	meaning
W	subject is awake
1	sleep stage 1
2	sleep stage 2
3	sleep stage 3
4	sleep stage 4
R	REM sleep
H	Hypopnoea
HA	Hypopnoea with arousal
OA	Obstructive apnoea
X	Obstructive apnoea with arousal
CA	Central apnoea
CAA	Central apnoea with arousal
L	Leg movements
LA	Leg movements with arousal
A	Unspecified arousal
MT	Movement time

Table 5.3: The labelling scheme for the polysomnographic database. Each sleep stage or apnoea annotation applies to a thirty-second segment.

is due to a neurally mediated problem then it is known as central sleep apnoea (CSA) which is known to be more closely linked with advanced cardiac problems than OSA [169].

Each record in the database includes sleep stage and apnoea annotations as well as ECG beat annotations. Each sleep stage annotation (and apnoea annotation if relevant) is assigned to a particular thirty-second segment. Table 5.3 details the labelling scheme; a more detailed description of the database is given by Moody *et al.* [194].

5.6.2 Preprocessing and artefact rejection

The RR interval data available in the MIT databases has been scored according to the ANSI standards [1] and therefore the clinical markers for each beat are accurate to only $\pm 150\text{ms}$. For RR interval calculations this has been shown to introduce significant errors in frequency-domain HRV calculations (see [2]). The RR interval times are therefore extracted using the method described in chapter 2, section 2.3.1. However, the beat classification labels can still be used to remove ‘beat-to-beat’ intervals involving artefacts and ectopic beats, by associating the label which occurs within ± 0.15 seconds (or $0.15 \times 256\text{Hz} \approx 39$ samples) of each detected beat.

To further enhance the robustness of the ectopic removal (to allow for beat-misclassification by the experts), a timing threshold of $\lambda = 10\%$ is also used. It should be noted that the Lomb periodogram PSD estimate is robust to lower values of λ than 10% (which lead to a reduction in the number of sinus beats as well as abnormal beats in a given section of an RR tachogram). However, $\lambda = 10\%$ is chosen so

that the large volume of data reduction data that a low value of λ would cause, does not lead to a severe distortion of the interpolated RR tachogram used for the FFT spectral estimates.

The changes in the ECG (and hence HRV) due to sleep apnoea are complex [47] and therefore sections free from apnoeas are selected to ensure that the analysis is not complicated by the apnoeic episodes. During such events a patient has difficulty breathing and moves rapidly through different levels of consciousness. The RR interval data during such episodes is therefore dominated by respiratory effects and often the data is corrupted by movement. In fact, there is frequent corruption of the ECG data from movement artefact in the MIT polysomnographic database. If more than 20 beats are corrupted and thus removed from the analysis, then the FFT estimation techniques will overestimate the $\frac{LF}{HF}$ -ratio by over 30% (see section 4.6.4). Therefore only relatively low-noise ECG sections, free from apnoeic events are considered (see table 5.4).

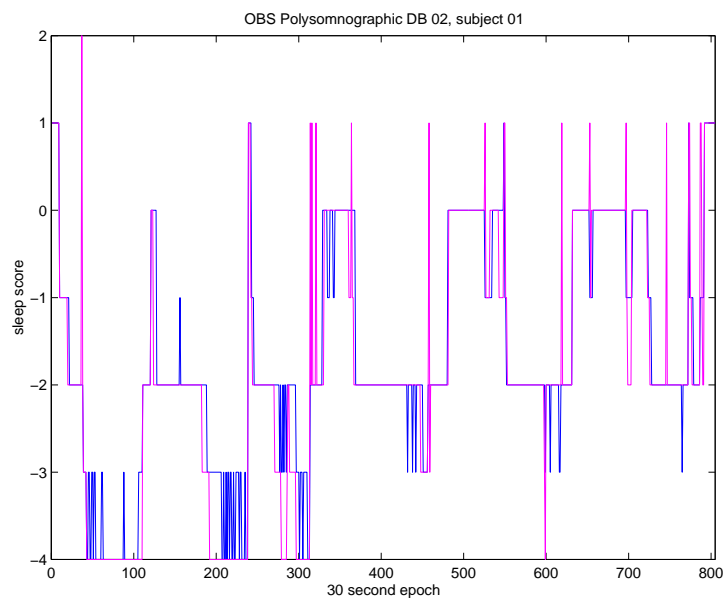


Figure 5.5: Two different expert sleep scores are plotted in blue and magenta for patient 02-01 from the OBS polysomnographic database. The horizontal time axis is in 30 second epochs. 1 represents wakefulness, 0 REM sleep and -1, -2, -3 and -4 indicate sleep states 1 to 4 respectively. Movement artefact is assigned a value of 2. Note the close correspondence between expert scores (86% agreement.)

Record name	start index	end index	length (mins)
slp03	2748292	3472103	48
slp04	3832987	4393917	37
slp41	3498887	4559463	71
slp48	2756692	3595661	56

Table 5.4: Patients and sections chosen from the MIT polysomnographic database with little or no noise and apnoeic episodes.

The selected data segments are longer than 30 minutes and contain little or no artefact. This allows a reasonable length of continuous analysis, providing sufficient data to investigate if there is a correlation between HRV and depth of sleep, since usually two or three sleep states are observed in a 30-minute segment of data. Furthermore, a check is performed to ensure that the average heart rate in a segment is at least 48 bpm. This satisfies the Nyquist criterion for the Lomb method (see section 4.3.1). In an attempt to remove outliers that could bias any mean calculations or significance tests, values of the $\frac{LF}{HF}$ -ratio above 20 are not considered, as the literature indicates that valid values are rarely above 15 [184].

5.7 Mathematical analysis of HRV during sleep

5.7.1 Mathematical analysis

The $\frac{LF}{HF}$ -ratio is computed over a 300 second window every 30 seconds, using a sliding window with a 270 second overlap (see figure 5.6). This produces the same number of data points as the sleep scores (which are allocated to 30 second segments). However, the differing window sizes for the sleep score and the $\frac{LF}{HF}$ -ratio means that a direct one-to-one comparison of these values cannot be made. Furthermore, experts do not always agree on the sleep score for a particular 30 second period. (Figure 5.5 illustrates the difference between two expert scorers for a single night's data. This patient is typical in as much as the experts differ on 114 out of the 805 labels; 14% of the time).

A consensus labelling method is therefore used, and a sleep score is allocated to a particular $\frac{LF}{HF}$ -ratio if and only if:

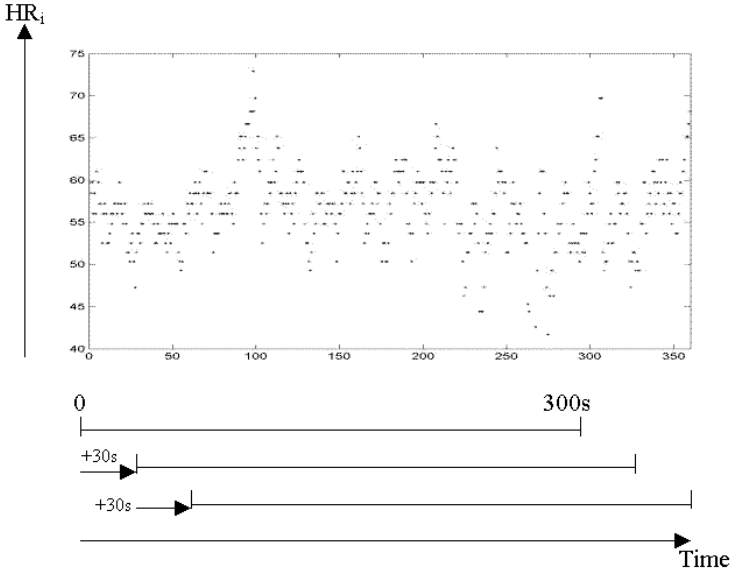


Figure 5.6: 6 minutes of HR_i data with a 5 minutes sliding window marked along the time axis. PSD calculations are made on each of these windows, which overlap by 270 seconds.

1. both experts agree on the score *and*
2. when in a 5-minute window (i.e. ten 30-s epochs), there is a majority of epochs (i.e. at least 5) with the same consensus score *and*
3. the $\frac{LF}{HF}$ -ratio < 20 .

Calculations of the mean and variance of all the $\frac{LF}{HF}$ -ratios in each of these three categories of sleep (SWS, REM and NREM sleep) are performed for consensus labelled periods. In addition, statistical significance differences between the mean $\frac{LF}{HF}$ -ratios for each of these sleep states is calculated for each spectral estimation method using the F-test, the Kolmogorov-Smirnov (K-S) test, and Student's t-test for unequal variances [229, 71]. The F-test evaluates the probability that the variances in each distribution are significantly different (and hence one variance is significantly *less* than another). The K-S statistic is used for calculating the significance level of two data sets being drawn from different distributions functions. It is therefore useful for testing whether the distributions of $\frac{LF}{HF}$ -ratios in different sleep categories are significantly different. In particular, the K-S test is a robust method of finding shifts (rather than spreads) in a probability distribution (especially changes in the median value). Spreading of the distribution affects the tails of the probability distribution and may leave the median value unchanged. The K-S statistic is therefore insensitive to outliers and changes in the distribution's tails. Student's t-test (for

unequal variances) is applied to calculate the probability that the mean $\frac{LF}{HF}$ -ratio in a particular sleep state is significantly different from the mean in another sleep state. The assumptions of these statistical tests are that the samples are drawn from normal distributions and the variances of each data set are homogeneous [71]. Current research indicates that these criteria are fulfilled for the $\frac{LF}{HF}$ -ratio during sleep [275].

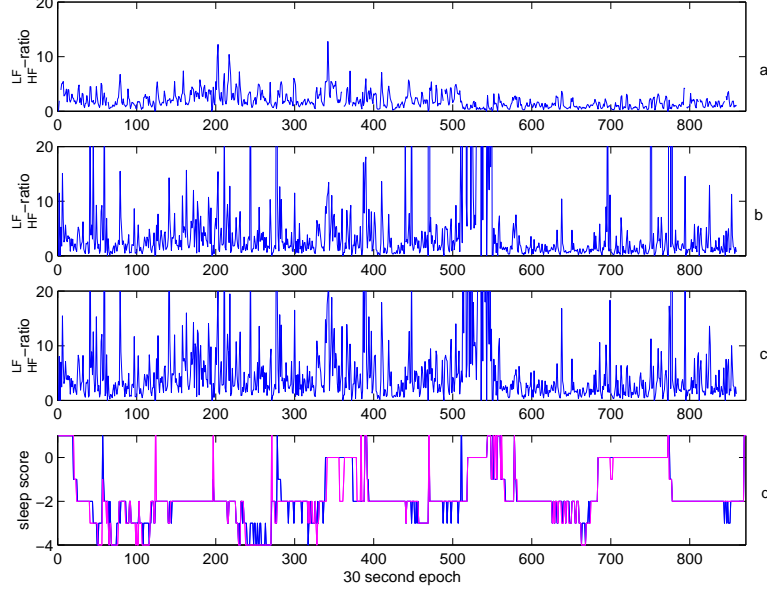


Figure 5.7: $\frac{LF}{HF}$ -ratio estimates (a-c) and sleep scores (d) during 7.2 hours of sleep for a normal healthy human male (subject OBS-02-02). $\frac{LF}{HF}$ -ratio is estimated using the three methods; (a) Lomb periodogram, (b) FFT after cubic spline interpolation and (c) FFT after linear interpolation. Note the FFT methods produce estimates with a higher variance. The lower graph (the corresponding hypnogram) is plotted for two expert scorers (one in blue and one in magenta). Note the high degree of agreement between scorers.

5.7.2 Results on normal subjects

The upper three plots in figure 5.7 illustrate typical fluctuations in the $\frac{LF}{HF}$ -ratio over an entire night's sleep (7.2 hours) for a normal healthy human male (subject 02 from the OBS polysomnographic database 02). The $\frac{LF}{HF}$ -ratio is estimated using the three methods; Lomb periodogram (a), the FFT after cubic spline interpolation (b) and FFT after linear interpolation (c). Note that the Lomb spectral estimation method produces values with a lower overall variance, and that the two FFT methods produce more frequent artefactual estimates (where no value is plotted, or the $\frac{LF}{HF}$ -ratio is larger than 20). Note the high values of the $\frac{LF}{HF}$ -ratio as calculated by the two FFT methods at about 500-550 epochs. This is due to high amounts of movement artefact leading to the removal of a large number of RR intervals during this period. The FFT methods therefore greatly over-estimate the $\frac{LF}{HF}$ -ratio (see section 4.6.4), whereas the

Lomb method does not. The lower graph shows the corresponding expert-scored hypnograms. Note the high degree of correspondence between the two expert's labels (768 out of 871 labels, or 88%) which is typical for normal data.

Table 5.5 presents results for the within-sleep state (SWS, REM or NREM) mean $\frac{LF}{HF}$ -ratio (\bar{x}) and standard deviation (σ) for each of the three PSD estimation methods; the Lomb periodogram (Lomb), FFT with cubic spline interpolation (FFT_{cub}) and FFT with linear interpolation (FFT_{lin}). Note that in general the mean $\frac{LF}{HF}$ -ratio is significantly⁵ higher in REM sleep than in NREM sleep, which in turn has significantly higher means than those found in SWS (for all three PSD techniques). Furthermore the variance (and hence σ) in NREM and REM sleep is comparable, whereas that in SWS is significantly lower. Although this trend is true for all three $\frac{LF}{HF}$ -ratio estimation methods, the σ in each of the three sleep categories is generally significantly lower for the Lomb method than for the FFT methods.

Tables 5.6 and 5.7 presents results of testing the significance in the differing variances and means derived from the values given in table 5.5. Where the F-test gives a low probability, ($P < 0.05$), this indicates that the variance (and hence σ) of the $\frac{LF}{HF}$ -ratio in one particular sleep state is significantly different from another sleep state. Where the K-S test results in a low probability, the distributions of the $\frac{LF}{HF}$ -ratio can be said to be different in each sleep state. Finally, if the t-test (for different variances) results in a low probability, then there exists a significant difference in the mean $\frac{LF}{HF}$ -ratio calculated in each sleep state.

The results in table 5.6 show that in general, only the Lomb method gives significantly different variances in NREM and REM sleep. Furthermore, although there is a high probability that the $\frac{LF}{HF}$ values in REM sleep have a different distribution to those in NREM sleep for each spectral estimation technique, only the Lomb periodogram gives significantly different mean $\frac{LF}{HF}$ -ratios for all subjects.

Table 5.7 indicates that in general, all three spectral estimation methods give significantly different σ , means and distributions for estimations of the $\frac{LF}{HF}$ -ratio in SWS and REM sleep. Although the σ in SWS is significantly lower for subject 02, no significant differences in the mean $\frac{LF}{HF}$ -ratio values calculated by each of the three PSD methods exists. However, in the case of the Lomb periodogram only, the K-S test indicates that the distribution of $\frac{LF}{HF}$ -ratio values for subject 02 is also significantly different between SWS and REM sleep.

⁵Using the F-test, K-S test and unequal t-test; see tables 5.6 and 5.7.

Subject	Sleep Stage →	REM		NREM		SWS	
	PSD method ↓	\bar{x}	σ	\bar{x}	σ	\bar{x}	σ
01	Lomb	3.02	1.79	1.50	1.21	0.62	0.77
	FFT_{cub}	6.46	3.84	3.14	3.57	0.83	1.30
	FFT_{lin}	6.67	3.50	3.61	3.48	1.10	1.25
02	Lomb	1.59	1.71	2.07	1.51	1.92	1.12
	FFT_{cub}	2.89	3.12	2.76	2.84	2.27	1.87
	FFT_{lin}	4.42	4.59	3.80	3.36	3.46	2.93
03	Lomb	4.63	1.96	3.10	2.12	1.18	0.52
	FFT_{cub}	7.94	4.98	4.10	4.19	1.30	0.74
	FFT_{lin}	9.44	5.21	5.09	4.39	1.94	1.14
04	Lomb	2.44	1.35	1.82	1.60	0.95	0.40
	FFT_{cub}	3.57	3.28	2.60	3.39	1.07	0.68
	FFT_{lin}	4.66	4.15	3.08	3.42	1.48	0.96
06	Lomb	5.88	3.60	4.39	2.91	2.39	1.31
	FFT_{cub}	6.79	4.57	5.01	4.19	2.53	1.76
	FFT_{lin}	8.59	5.13	6.19	4.48	3.65	2.50

Table 5.5: Mean $\frac{LF}{HF}$ -ratio (\bar{x}) and S.D. (σ) for each of the three PSD estimation methods for normal subjects in REM sleep, NREM sleep and SWS.

	Lomb	F-test FFT_{cub}	FFT_{lin}		Lomb	K-S test FFT_{cub}	FFT_{lin}		Lomb	t-test FFT_{cub}	FFT_{lin}
01	*	NS	NS		*	*	*		*	*	*
02	< 0.05	NS	*		*	< 0.05	NS		< 0.01	NS	NS
03	NS	NS	NS		*	*	*		*	*	*
04	< 0.05	NS	NS		*	*	*		*	< 0.01	*
06	< 0.0005	NS	NS		*	*	*		*	*	*

Table 5.6: Results of significance of F-test, K-S test and unequal t-test between $\frac{LF}{HF}$ -ratio variances, distribution and means in REM and NREM sleep for normal subjects. Significance is denoted with an asterisk (*) for $P < 10^{-4}$, or as $P < 0.0005$, $P < 0.005$, $P < 0.01$, $P < 0.05$. NS denotes not significant. Note that in general, only the Lomb method gives significantly different variances in NREM and REM sleep. Although there is a high probability that the $\frac{LF}{HF}$ values in REM sleep have a different distribution to those in NREM sleep for each spectral estimation technique, only the Lomb periodogram gives significantly different mean $\frac{LF}{HF}$ -ratios for all subjects.

		Lomb	F-test FFT_{cub}	FFT_{lin}		Lomb	K-S test FFT_{cub}	FFT_{lin}		Lomb	t-test FFT_{cub}	FFT_{lin}
01		*	*	*		*	*	*		*	*	*
02		< 0.005	*	< 0.005		*	NS	NS		NS	NS	NS
03		*	*	*		*	*	*		*	*	*
04		*	*	*		*	*	*		*	*	*
06		*	*	*		*	*	*		*	*	*

Table 5.7: Results of significance of F-test, K-S test and unequal t-test between $\frac{LF}{HF}$ -ratio variances, distribution and means in SWS and REM sleep for normal subjects. Significance is denoted with an asterisk (*) for $P < 10^{-4}$, or as $P < 0.0005$, $P < 0.005$, $P < 0.01$, $P < 0.05$. NS denotes not significant. Note that in general, all three spectral estimation methods gives significantly different variances, means and distributions between SWS and REM sleep. Although the variance in SWS is significantly lower for subject 02, no significant differences in the mean $\frac{LF}{HF}$ -ratio values calculated by each of the three PSD methods exists. However, in the case of the Lomb periodogram only, the K-S test indicates that the distribution of $\frac{LF}{HF}$ -ratio values is significantly different between SWS and REM sleep.

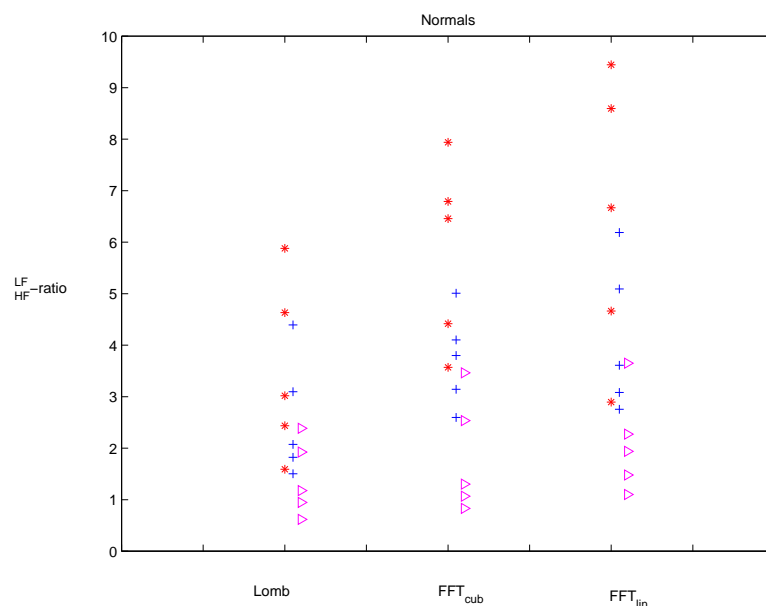


Figure 5.8: $\frac{LF}{HF}$ -ratio estimates for normal healthy humans (OBS Polysomnographic database 02). Each patient's average $\frac{LF}{HF}$ -ratio is given for REM sleep (*), NREM sleep (+) and SWS sleep (▷) for each of the three spectral estimation methods (see text for details).

Figure 5.8 presents calculations of the mean values of the $\frac{LF}{HF}$ -ratio in REM sleep (*), NREM sleep (+) and SWS sleep (>) for the three spectral estimation methods: the Lomb periodogram, the FFT after cubic spline interpolation (FFT_{cub}) and the FFT after linear interpolation (FFT_{lin}), as detailed in table 5.5.

Note that the largest separation of $\frac{LF}{HF}$ -ratio estimates occurs between SWS and REM sleep. FFT methods also appear to allow a greater separation between REM and deep sleep (SWS) than the Lomb periodogram. However, the standard deviations in the calculation of the sleep stage-specific means are large ($5.2 \geq \sigma \geq 3.1$ for REM sleep and $3.6 \geq \sigma \geq 0.83$ for SWS - see table 5.5). In contrast to this, the standard deviations in the Lomb estimates are significantly smaller. For both the FFT methods, the standard deviations are $3.6 \geq \sigma \geq 1.4$ for REM sleep and $2.4 \geq \sigma \geq 0.6$ for SWS - see tables 5.5, 5.6 and 5.7.

5.7.3 Results on sleep apnoeic subjects

Figures 5.9, 5.10, 5.11, and 5.12, show expert sleep scoring (lower plots) and the corresponding $\frac{LF}{HF}$ -ratios (upper plots) for segments of noise- and apnoea-free data for the four patients from the MIT polysomnographic database being considered. Note the visual correspondence between a change in sleep state and a change in the $\frac{LF}{HF}$ value for all three estimation methods. Movements into and out of REM sleep cause particularly noticeable changes in the $\frac{LF}{HF}$ -ratio. Note also that the FFT methods (green and red lines) produce a more variable estimate of the $\frac{LF}{HF}$ -ratio within a particular sleep state.

Figure 5.9 illustrates the fact that movements into deeper sleep do not always result in an increase in $\frac{LF}{HF}$ -ratio; at around epoch 240, the subject moves from stage 2 to stage 3, but the $\frac{LF}{HF}$ -ratio rises. Note also that the $\frac{LF}{HF}$ -ratio decreases to the same level it was in stage 2, just before sharply rising at the end as the subject enters REM sleep (a sleep score of 0). It is interesting to note that the awakening (around epoch 310) precedes a significant rise in the $\frac{LF}{HF}$ -ratio. This is not always the case however (see figure 5.11, where the brief drop in the $\frac{LF}{HF}$ -ratio as the subject moves from REM to NREM sleep is uninterrupted despite an awakening after epoch 565).

Figure 5.11 also demonstrates how changes between light and deeper (a shift from stage 2 to stage 3 at around epoch 500 - sleep scores -2 and -3) do not always produce significant changes in the $\frac{LF}{HF}$ -ratio. Furthermore, figure 5.11 illustrates how a single sleep state can have a range of HRV values associated with it, which can be significantly different over time.

Table 5.8 presents the mean $\frac{LF}{HF}$ -ratios for each of the four sleep apnoeic subjects in each of the three sleep categories (REM, NREM and SWS). N/A (not applicable) indicates that for the segment of data analysed the subject did not experience that particular stage of sleep. Figure 5.13 is a plot of the mean values from this table. REM sleep averages are marked with an asterisk (*), NREM sleep means are marked with a cross (+) and SWS mean values are marked with triangles (\blacktriangleright). Note that some values are so close together, there appears to be fewer values plotted than are present in table 5.8. Note also that some subjects did not experience all three sleep states and therefore there are fewer than 4 of each type of data point per PSD method.

Table 5.9 presents results of significance testing using the F-test, K-S test and unequal t-test between $\frac{LF}{HF}$ -ratio variances, distribution and means in NREM and REM sleep for the sleep apnoeic subjects who experienced all three sleep categories (SWS, NREM and REM). Note that in general, only the Lomb method gives significantly different variances between NREM and REM sleep. Although there is a high probability that the $\frac{LF}{HF}$ values in REM sleep have a different distribution to those in NREM sleep for each spectral estimation technique, all PSD estimation methods lead to the conclusion that no significant difference exists between the mean $\frac{LF}{HF}$ -ratios calculated in NREM and REM sleep.

Table 5.10 presents results of the same significance testing between means in SWS and REM sleep. Note that there exist significantly different variances, distributions and means of the $\frac{LF}{HF}$ -ratio between SWS and REM sleep. Only mean $\frac{LF}{HF}$ -ratios measured in REM and SWS are significantly different for this non-normal patient population, due to the low variance of the $\frac{LF}{HF}$ -ratio in SWS. Although the results (plotted in figure 5.13) appear to indicate that mean $\frac{LF}{HF}$ -ratios measured in REM and NREM sleep are greatly separated, the variances of the distributions of the $\frac{LF}{HF}$ -ratios are large and calculations using Student's t-test reveal that there is not a significant difference between mean $\frac{LF}{HF}$ -ratios calculated in REM and NREM sleep.

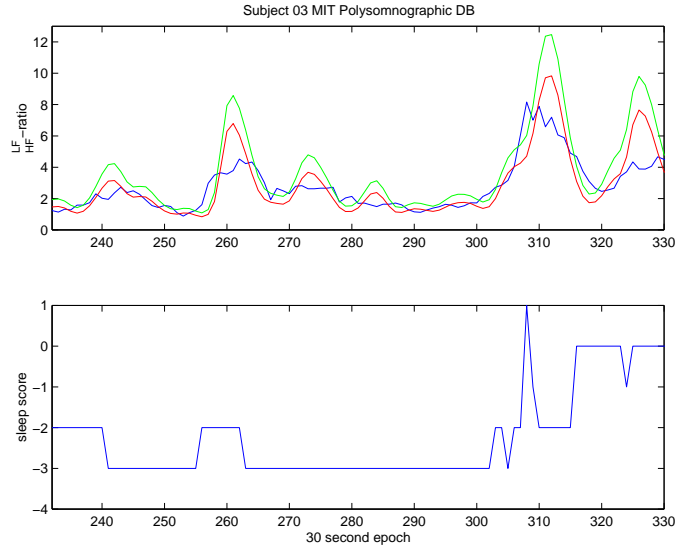


Figure 5.9: Expert scored hypnogram (lower trace) and $\frac{LF}{HF}$ -ratio estimates (upper plots) for a non-apnoeic and non-noisy section of data for patient 03 of the MIT polysomnographic database using the three methods; Lomb periodogram (blue), FFT after cubic spline interpolation (green) and FFT after linear interpolation (red).

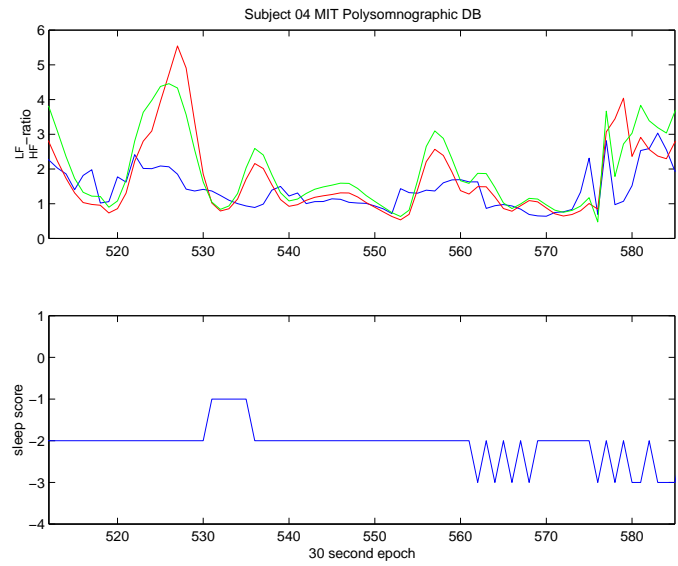


Figure 5.10: Expert scored hypnogram (lower trace) and $\frac{LF}{HF}$ -ratio estimates (upper plots) for a non-apnoeic and non-noisy section of data for patient 04 of the MIT polysomnographic database using the three methods; Lomb periodogram (blue), FFT after cubic spline interpolation (green) and FFT after linear interpolation (red).

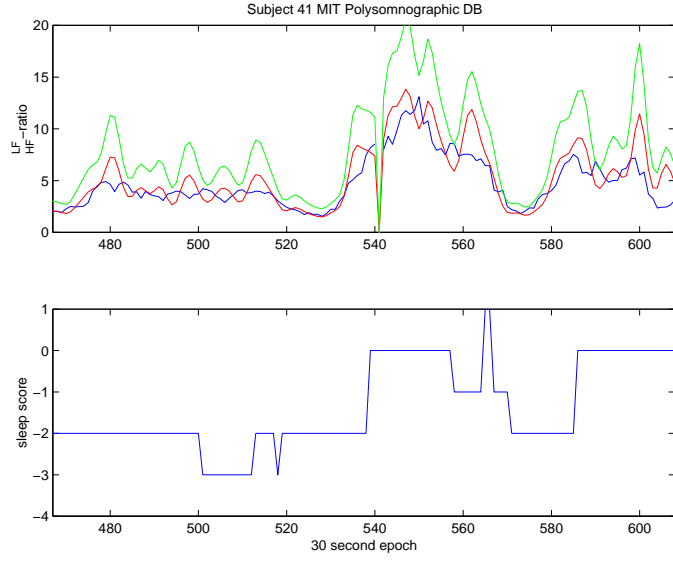


Figure 5.11: Expert scored hypnogram (lower trace) and $\frac{LF}{HF}$ -ratio estimates (upper plots) for a non-apnoeic and non-noisy section of data for patient 41 of the MIT polysomnographic database using the three methods; Lomb periodogram (blue), FFT after cubic spline interpolation (green) and FFT after linear interpolation (red).

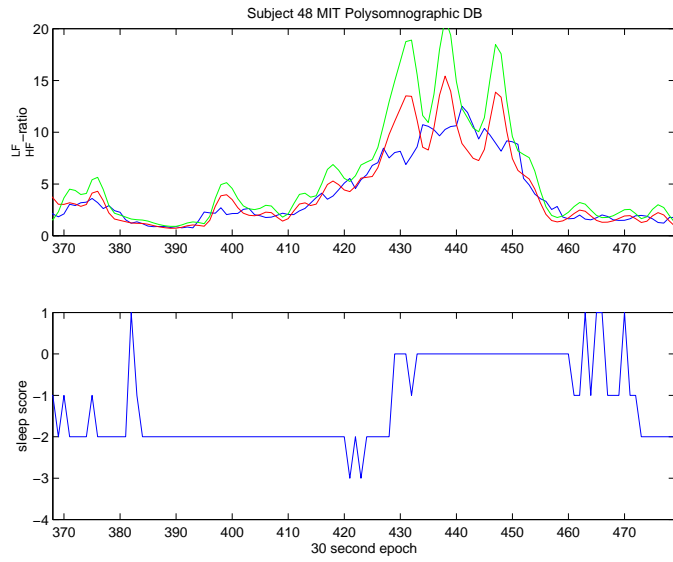


Figure 5.12: Expert scored hypnogram (lower trace) and $\frac{LF}{HF}$ -ratio estimates (upper plots) for a non-apnoeic and non-noisy section of data for patient 48 of the MIT polysomnographic database using the three methods; Lomb periodogram (blue), FFT after cubic spline interpolation (green) and FFT after linear interpolation (red).

Subject	Sleep Category → PSD method ↓	REM		NREM		SWS	
		\bar{x}	σ	\bar{x}	σ	\bar{x}	σ
03	Lomb	6.20	1.49	2.03	1.42	2.31	0.85
	FFT_{cub}	6.22	2.59	2.01	1.50	2.27	1.30
	FFT_{lin}	8.10	3.25	2.59	1.91	2.92	1.66
04	Lomb	N/A	N/A	1.52	0.48	N/A	N/A
	FFT_{cub}	N/A	N/A	1.77	1.11	N/A	N/A
	FFT_{lin}	N/A	N/A	1.96	1.02	N/A	N/A
41	Lomb	7.22	2.43	3.87	1.72	3.77	0.41
	FFT_{cub}	8.39	2.69	4.31	2.33	3.63	0.86
	FFT_{lin}	12.21	3.86	6.38	3.21	5.79	1.40
48	Lomb	7.97	2.16	2.05	1.17	N/A	N/A
	FFT_{cub}	8.66	3.16	2.20	1.30	N/A	N/A
	FFT_{lin}	11.53	4.14	2.68	1.66	N/A	N/A

Table 5.8: Mean $\frac{LF}{HF}$ -ratio (\bar{x}) and variance for each of the three PSD estimation methods in REM sleep, NREM sleep and SWS for sleep apnoeic subjects. N/A indicates not applicable; in the segment of data analysed the subject did not experience this category of sleep.

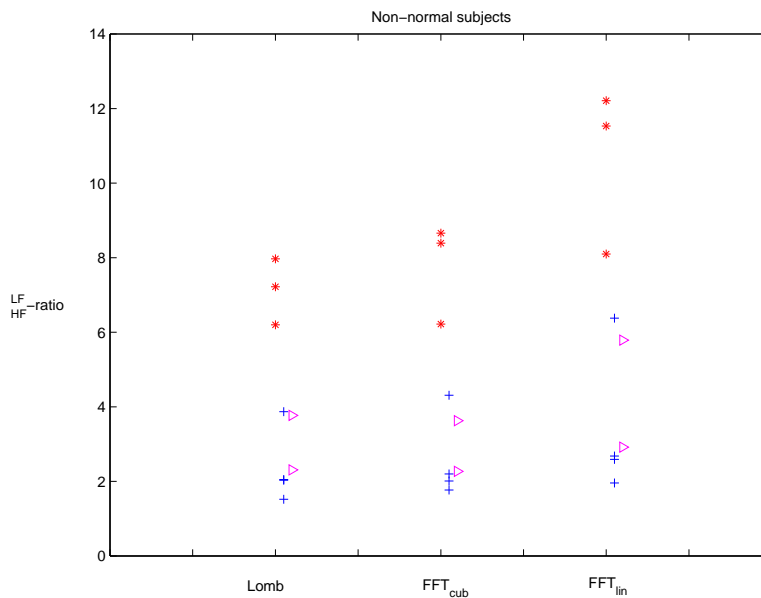


Figure 5.13: $\frac{LF}{HF}$ -ratio estimates for sleep apnoeic subjects (MIT Polysomnographic database). Each patient's average $\frac{LF}{HF}$ -ratio is given for REM sleep (*), NREM sleep (+) and SWS sleep (>) for each of the three spectral estimation methods (see text for details).

	Lomb	F-test FFT_{cub}	FFT_{lin}		Lomb	K-S test FFT_{cub}	FFT_{lin}		Lomb	t-test FFT_{cub}	FFT_{lin}
03	*	NS	NS		*	< 0.01	< 0.01		NS	NS	NS
41	*	< 0.005	< 0.01		*	*	< 0.01		NS	NS	NS

Table 5.9: Results of significance of F-test, K-S test and unequal t-test between $\frac{LF}{HF}$ -ratio variances, distribution and means in NREM and REM sleep for sleep apnoeic subjects who experienced all three sleep categories (REM, NREM and SWS). Significance is denoted with an asterisk (*) for $P < 10^{-4}$, or as $P < 0.005$, $P < 0.01$, $P < 0.05$. NS denotes not significant. Note that in general, only the Lomb method gives more significantly different variances between NREM and REM sleep. Although there is a high probability that the $\frac{LF}{HF}$ values in REM sleep have a different distribution to those in NREM sleep for each spectral estimation technique, all PSD estimation methods lead to the conclusion that no significant difference exists between the mean $\frac{LF}{HF}$ -ratios calculated in NREM and REM sleep.

	Lomb	F-test FFT_{cub}	FFT_{lin}		Lomb	K-S test FFT_{cub}	FFT_{lin}		Lomb	t-test FFT_{cub}	FFT_{lin}
03	< 0.005	< 0.001	< 0.001		*	< 0.01	< 0.01		*	*	*
41	*	< 0.001	< 0.005		*	*	*		*	*	*

Table 5.10: Results of significance of F-test, K-S test and unequal t-test between $\frac{LF}{HF}$ -ratio variances, distribution and means in SWS and REM sleep for sleep apnoeic subjects who experienced all three sleep categories (REM, NREM and SWS). Significance is denoted with an asterisk (*) for $P < 10^{-4}$, or as $P < 0.005$, $P < 0.01$, $P < 0.05$. Note that there exist significantly different variances, distributions and means of the $\frac{LF}{HF}$ -ratio between SWS and REM sleep.

5.7.4 Comparison of PSD estimations methods for separating patients groups using REM and SWS

The results from the $\frac{LF}{HF}$ -ratio estimates for sleep apnoea sufferers and normal healthy humans are compared on a per-sleep category in figures 5.14, 5.15 and 5.16. Figure 5.14 contrasts the range of $\frac{LF}{HF}$ values for the three spectral estimation methods;

1. the Lomb periodogram,
2. cubic spline interpolation then FFT,
3. linear interpolation then FFT.

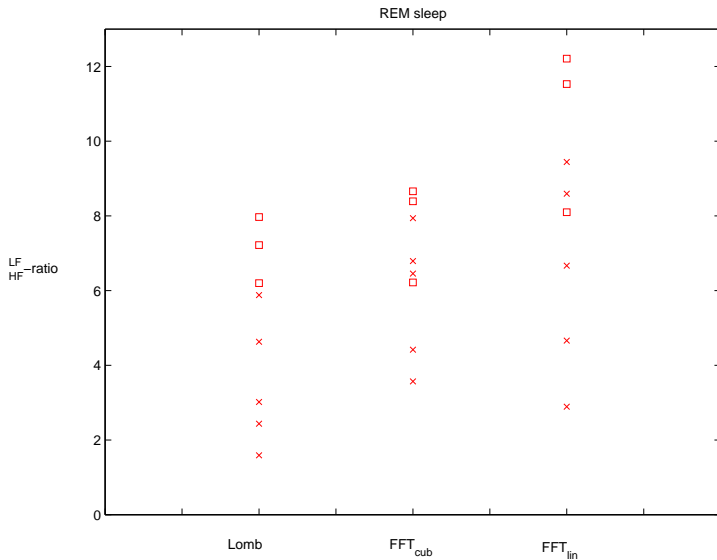


Figure 5.14: $\frac{\text{LF}}{\text{HF}}$ -ratio estimates for normal subjects (\times) and patients suffering from sleep apnoea (\square) in REM sleep for each of the three spectral estimation methods being tested; the Lomb periodogram, the FFT after cubic spline interpolation (FFT_{cub}) and FFT after linear interpolation (FFT_{lin}). Note that better patient group separation is achieved by $\frac{\text{LF}}{\text{HF}}$ -ratio estimates using the Lomb periodogram.

Normal subjects' values are represented by crosses (\times) and sleep apnoeic patients' values are labelled by boxes (\square). Variances quoted earlier are not plotted (for reasons of clarity). Note that the Lomb method results in a higher degree of separation of $\frac{\text{LF}}{\text{HF}}$ values for both NREM and deep sleep (SWS).

5.8 Conclusions

Deep sleep (SWS) and REM sleep produce the largest contrasting mean values of $\frac{\text{LF}}{\text{HF}}$ -ratio. Calculations of these values using the Lomb method produces a more consistent estimate (lower variances) than with either of the two FFT methods. Thus, the Lomb method may allow a categorisation of the state of the autonomic control system for patients using an HRV metric alone, provided that it is measured in SWS or REM sleep. Results from this study are consistent with those in the current literature (see table 5.11). SWS and REM sleep provide good candidates for inter-patient HRV comparisons. SWS is a particularly good candidate for segmenting epochs of RR interval data for HRV studies because of the low variance in $\frac{\text{LF}}{\text{HF}}$ -ratio values in deep sleep, and should be the preferred sleep category to compare $\frac{\text{LF}}{\text{HF}}$ -ratios between patients. However, certain conditions (such as sleep apnoea) severely reduce the amount of SWS sleep a subject experiences and so it may be necessary to compare mean $\frac{\text{LF}}{\text{HF}}$ -ratios from REM sleep periods.

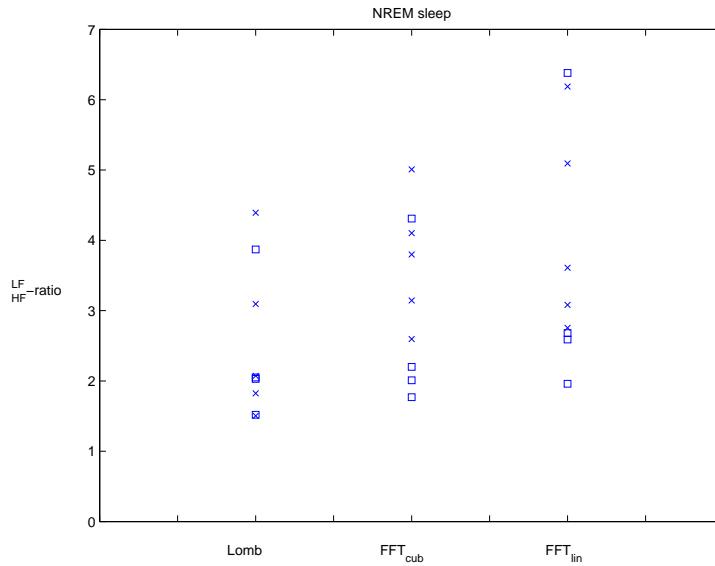


Figure 5.15: $\frac{LF}{HF}$ -ratio estimates for normal subjects (\times) and patients suffering from sleep apnoea ($[]$) in NREM sleep for each of the three spectral estimation methods being tested; the Lomb periodogram, the FFT after cubic spline interpolation (FFT_{cub}) and FFT after linear interpolation (FFT_{lin}). Note that no spectral estimation method gives better separation between patient groups in NREM sleep.

Subject → Sleep State ↓	Normal [213](‡)	Normal [275]	Normal (*)	Apnœic (**)	Post-MI [252]
REM	2.7	3.1 ± 0.7	3.6 ± 1.7	7.1 ± 0.8	8.9 ± 1.6
NREM	N/A	1.2 ± 0.4	2.6 ± 1.2	2.4 ± 1.0	5.1 ± 1.4
SWS	0.8	N/A	1.4 ± 0.7	3.0 ± 1.0	N/A

Table 5.11: Average $\frac{LF}{HF}$ -ratio estimates for subjects tested in the OBS polysomnographic normal database 02 (*), normals in the current literature ([213, 275]), the MIT polysomnographic (sleep apnoeic) database (**) and a post-MI population (taken from [252]). N/A indicates the results are not available from current literature. $\frac{LF}{HF}$ -ratios quoted from this study are means over all subjects in the group using Lomb periodogram-derived estimates. ‡ indicates that no variance calculations were given in the paper

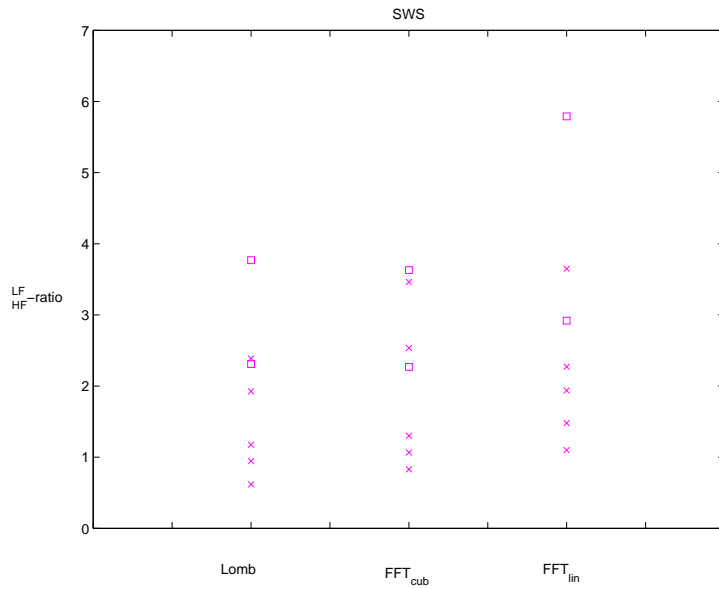


Figure 5.16: $\frac{LF}{HF}$ -ratio estimates for normal subjects (\times) and patients suffering from sleep apnoea (\square) in deep sleep (SWS) for each of the three spectral estimation methods being tested; the Lomb periodogram, the FFT after cubic spline interpolation (FFT_{cub}) and FFT after linear interpolation (FFT_{lin}). Note that better patient group separation is achieved by $\frac{LF}{HF}$ -ratio estimates using the Lomb periodogram.

Chapter 6

HRV: Applicability in controlled studies - Head-up tilts

6.1 Introduction

Since the evaluation of HRV in conscious patients is highly dependent upon the mental and physical activity the subject is experiencing (see section 5.3), investigations linking the HRV of conscious patients to the monitoring of their condition can only take place in the context of controlled studies. This requires that the experimental conditions are such as to allow inter-experiment comparisons. In this chapter, a preliminary analysis of a controlled experimental procedure is undertaken, utilising the robust HRV analysis methods developed in this thesis. The study method in question is known as a ‘Head-up Tilt’ (HUT) and is designed to assess the response of the cardiovascular system to a rapid postural change. In general, this involves recording blood pressure and heart rate for a period of about 10 to 40 minutes before and after a subject is tilted from a supine position to approximately 20 degrees from vertical [150].

The data analysed in this chapter is recorded from patients attending the *Falls Clinic*¹ at the Radcliffe Infirmary in Oxford. The purpose of the HUT test is to analyse the patient’s susceptibility to *syncope* (see section 6.2) following which an appropriate treatment will be prescribed. Before the analysis of the data is presented, however, a brief description of the physiological mechanisms that may be involved in syncope is given with particular reference to the sympathovagal balance, leading to an overview of HRV in the context of syncope.

¹It is known as a ‘falls’ clinic because the referred patient has usually experienced a fall after a loss of consciousness.

6.2 Syncope: Classification

Syncope is the sudden loss of consciousness resulting from a temporary impairment of cerebral blood flow. Although recovery is often rapid, a syncopal attack is also always accompanied by the loss of muscle tone, and hence presents a serious health risk; syncopal events account for up to 3% of casualty room visits and 6% of hospital admissions [188]. Patients with recurrent syncope endure a quality of life comparable to sufferers of rheumatoid arthritis or chronic lower back pain.

There is some confusion in the literature as to the causes of syncope as it is a symptom rather than a discrete pathological entity which has many distinct origins. There is broad agreement that the causes of syncope-like symptoms can be divided into three main classes [99]:

1. Cardiovascular causes (25-30% of patients; usually the most dangerous)
2. Non-cardiovascular causes (20-40%)
3. Unknown causes (30-50%; often more benign)

Strictly speaking, true syncope is cardiovascular in origin and therefore, only patients in the first category above, ought to be classified as suffering from syncope. In many studies of syncope patients, the above percentages vary considerably, owing to the diversity of criteria applied to select patients. However, the percentage attributed to ‘unknown’ causes is gradually reducing, as diagnostic methods improve. In particular, tilt testing and carotid sinus massage² (CSM) have proved to be two important means of reducing the percentage of syncope-like symptoms being classified as of ‘unknown cause’.

More specific classification schemes subdivide syncope into further sub-groups. For example, the recent Task Force Report Guidelines on management (diagnosis and treatment) of syncope [9] considers five types of syncope:

1. neurally mediated reflex syncopal syndromes,
2. orthostatic hypotension,
3. cardiac arrhythmias as primary cause,
4. structural cardiac or cardiopulmonary disease and
5. cerebrovascular.

²firmly massaging the carotid artery on the right-hand side of the patient’s neck for 5-10 seconds

There exists a consensus that the origin of syncope lies in transient cerebral hypoperfusion (a reduction in the volume of bloodflow in the cerebrum; the portion of the brain (frontal lobes) where thought and higher function reside). It has been shown that syncope is associated with 6 to 8 seconds of cessation of cerebral blood flow [233], or a systolic blood pressure fall of over 60 mmHg [248]. However, there is still uncertainty regarding the exact mechanisms which give rise to cerebral hypoperfusion. The following sections (6.2.1 to 6.2.5) present a brief overview of the suspected causes of the most common types of syncope.

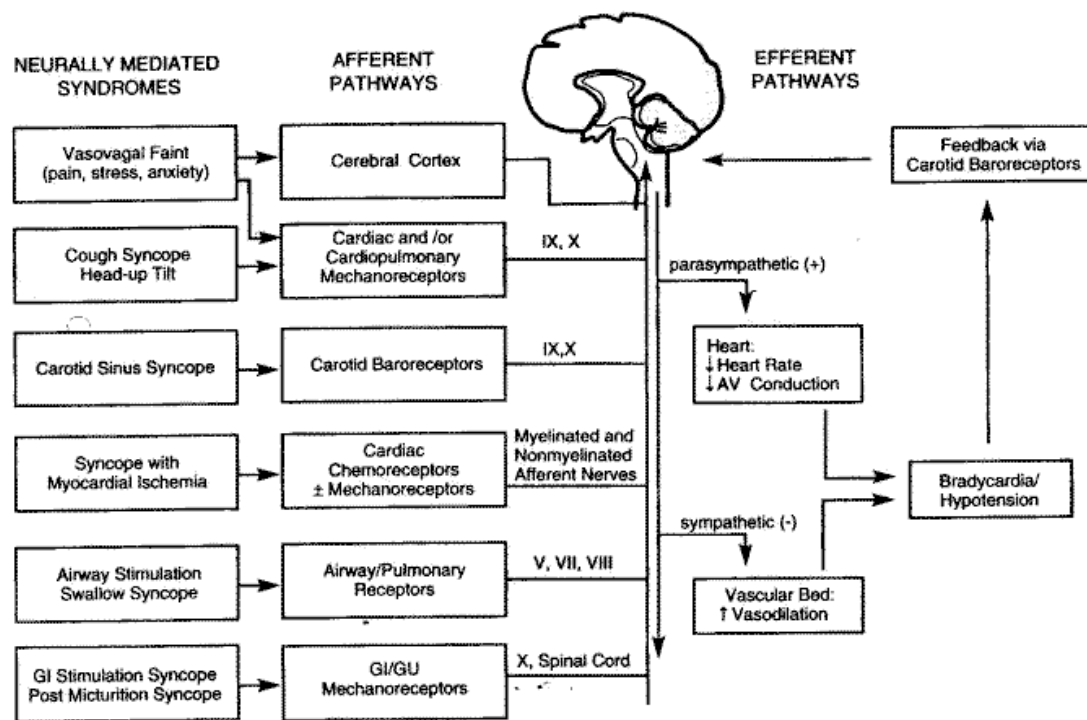


Figure 6.1: Proposed mechanisms for various types of neurally mediated syncope. Taken from [28].

6.2.1 Neurally mediated syncope

Proposed mechanisms for various types of neurally mediated syncope are illustrated in figure 6.1 and include [28];

- Vasovagal Syncope,
- HUT (or Cough) Syncope,

- Carotid Sinus Syncope,
- Syncope with Myocardial Ischemia,
- Airway Stimulation/Swallow Syncope and
- Gastrointestinal (GI) Stimulation Syncope.

The first two categories under ‘Neurally mediated syndromes’ in figure 6.1 demonstrate the difficulty of categorising syncope, since syncope can be mediated by multiple neural pathways. Both vasovagal fainting and ‘Head-up Tilt’ syncope can be caused by hypersensitive cardiac mechanoreceptors and therefore the latter syncope is often thought by some authors to be a form of vasovagal syncope, the most common form of neurally mediated syncope. Vasovagal syncope manifests itself as follows:

1. Subject stands or is passively tilted upright.
2. Roughly a quarter of the blood is redistributed in response to this orthostatic stress. Venous pooling occurs in the legs.
3. Decreased venous return is an obvious result.
4. Tachycardia, vasoconstriction, and increased inotropy³ attempt to compensate - as they should in healthy subjects. Everything up to this point represents a more or less normal compensatory reaction to orthostatic stress.
5. However, in vasovagal patients, the forceful ventricular contractions activate hypersensitive cardiac mechanoreceptors, triggering an afferent (vagal) nerve pathway. This problem is known as the Bezold-Jarisch reflex.
6. This reflex ultimately reduces sympathetic tone and increases parasympathetic tone which results in vasodilation and/or bradycardia, with subsequent hypotension.
7. When cerebral perfusion decreases sufficiently, syncope results.

Some experiments, including those performed with atropine to suppress vagal tone [103], challenge this theory, but at present it remains popular in the syncope field.

³strength of contraction of the muscles

6.2.2 Orthostatic Hypotension

While neurally mediated syncope is probably caused by an oversensitive autonomic nervous system, orthostatic hypotension often results from the patient's current medication regime and impairment to the Central Nervous System (often due to drugs and/or ageing). Orthostatic hypotension can be caused by the body's failure to react fully during step 4 above. (For example, the heart rate does not increase significantly, or more commonly, vasoconstriction is too weak.) This causes a distinct transition to step 7 above and the subject loses postural tone.

Recurrent syncope in the elderly is therefore most likely to be of the orthostatic type. Elderly patients often suffer from less responsive autonomic nervous systems: for example, reduced baroreflex sensitivity and ability to maintain cerebral autoregulation. Furthermore, elderly patients are usually on medication, and many of these drugs have the side effect of exacerbating orthostatic hypotension. (For instance, anti-hypertension drugs can directly oppose the vasoconstriction mechanism in step 4 above.)

6.2.3 Cardiac arrhythmia/structural heart disease

Syncope caused primarily by cardiac problems is commonly the result of more than one pathology. These pathologies include arrhythmia, valvular lesions, impaired left ventricular function, and the inadequacy of neurally mediated vascular compensation mechanisms.

Five of the most common cardiac causes of syncope are [99]:

- Atrio-Ventricular (AV) conduction system disease / block (see chapter 1).
- Sinus pauses / bradycardia (see chapter 1).
- Aortic stenosis; progressive narrowing of the aortic valve resulting in the obstructed passage of blood from the left ventricle into the aorta. Chronic stenosis can lead to left ventricular enlargement and congestive heart failure.
- Hypertrophic cardiomyopathy; enlargement of the ventricular septum can result in ventricular outflow obstruction (subaortic stenosis) and eventual cardiomyopathy (disease of the cardiac muscle mass).
- Atrial myxoma; a very rare primary cardiac tumour, composed of connective tissue, located in the left or right atrium, leading to intermittent, abrupt, obstruction of blood flow.

6.2.4 Cerebrovascular (steal syndromes)

In steal syndromes, blood is diverted from its expected path. Steal syndromes occur when the arterial circulation to the arm is occluded, thereby shunting blood through a parallel system, which then necessarily assumes the responsibility of supplying the arm, causing insufficient cerebral perfusion. The most common affliction is subclavian steal, which occurs especially during upper arm exercise. A proposed mechanism is the following:

1. Low pressure exists in the subclavian artery.
2. Retrograde flow occurs in the ipsilateral vertebral artery.
3. Cerebral blood flow is decreased.
4. Syncope occurs.

6.2.5 Controversial classifications

It has become doubtful that vertebro-basilar or carotid TIAs (transient ischaemic attacks) are responsible for true syncope [9], but many authors include them as a source [99, 111, 143]. Basilar migraines, metabolic problems (such as hypoglycaemia or hyperventilation), intoxication, cataplexy, and psychogenic syncope all have non-cardiac origins [9, 99, 143]. Today, few believe that drop attacks⁴ or epileptic seizures should be classified as syncopal, although differentiating them from syncope is one of the difficult tasks facing physicians.

6.3 Syncope: Tests and Diagnosis

6.3.1 Head Upright Tilt Table Testing

Head Upright Tilt (HUT) Table Testing has excellent specificity and sensitivity when performed correctly. A general outline of a test is:

- A passive, supine phase of 20 to 45 minutes
- A tilt to 60° or 70° degrees (occasionally as high as 80°), for about 40 minutes

⁴sudden spontaneous falls while standing or walking, with complete recovery in seconds or minutes. There is usually no recognised loss of consciousness, and the event is remembered. It should be noted that it is a symptom, not a diagnosis.

- The test ends earlier if syncope occurs; patient should then be immediately returned to supine position to recover.

Two well-known protocols are the Westminster protocol [81] and, more recently, the Newcastle protocol [150]. In general, the Newcastle protocol appears to be in good agreement with the other tilt procedures and in the case of a tilt with no administration of intravenous drug injections, lasts for 40 minutes in the supine position at an angle of 70° (after a 20 minute supine period at the start of the test). For the Newcastle Protocol, tilt is terminated if ‘*symptom reproduction with concomitant hypotension/bradycardia or an adverse event develops*’ [150].

6.4 HRV in the context of HUT and syncope

Given that the sympathetic and parasympathetic branches of the nervous system are greatly affected by the changes that occur during HUT for syncopal patients, (see section 6.2.1) it is not surprising that HRV has been considered as an investigatory tool in this field since the late 1980’s.

It is generally accepted that in healthy individuals, HRV increases upon orthostatic stress (e.g. head-up tilt testing), whereas autonomic neuropathy (for example from ageing or diabetes) reduces this HRV increase and in fact can lead to a decrease in HRV during HUT [45, 145, 156]. The $\frac{LF}{HF}$ -ratio usually increases on tilt for normals because sympathetic stimulation manifests as an increased LF component. For patients with autonomic neuropathy, HUT leads to an increase in parasympathetic stimulation which often leads to an increase in the HF component. A parallel reduction in sympathetic drive, meanwhile, causes a drop in the LF component, leading to an overall drop in the $\frac{LF}{HF}$ -ratio. However, autonomic neuropathy is merely one of the many possible causes of syncope [9], and the multifactorial nature of syncope may be responsible for some of the controversy amongst HRV analysis in the context of HUT’s.

Guzman *et al.* [103] focused their investigations on vasovagal syncope, which they further divided into cardioinhibitory, vasodepressive, or mixed (both cardioinhibitory and vasodepressive) vasovagal syncope. Their study revealed that simple classifications based on a rise or fall in a HRV metric are too naive. Within their study population, it was shown that those with cardioinhibitory or mixed vasovagal syncope experience an initial rise in the $\frac{LF}{HF}$ -ratio during HUT, whereas vasodepressive vasovagal syncope patients experience a drop. This HRV comparison may be used to support the suspicion that cardioinhibitory syncope is due to the Bezold-Jarisch reflex (involving hypersensitive cardiac mechanoreceptors) whereas peripheral vasoconstriction is suspected to be the major component in vasodepressive syncope.

Although they recorded intra-subject oscillations in the $\frac{LF}{HF}$ -ratio between values of $\frac{LF}{HF}=3$ and $\frac{LF}{HF}=10$, over five minutes before and after HUT, the range of these changes over the entire patient group was found to be between 50% and 100% of the actual values. This high degree of inter-patient variability means that it is unlikely that, for vasovagal syncope at least, averaged absolute values of the $\frac{LF}{HF}$ -ratio can be used to discriminate between the different types of syncope.

Ruiz *et al.* [236] found that age is the major determinant of autonomic behaviour during head-up tilting and so consideration of the patient's age *may* assist prognosis: Lipsitz *et al.* [173] found that amongst young people, HUT-positive patients (diagnosed with syncope) experience a greater increase in HRV than HUT-negative patients (diagnosed as not suffering from syncope). However, Ruiz *et al.* [236] found no significant change in HRV to differentiate HUT positives from HUT negatives in either the young (aged 15 to 35) or elderly (aged 60+).

Results using frequency domain metrics for evaluating HRV on suspected sufferers of syncope are often reported because of the link between these measurements and the sympathovagal balance. However, the methods used to calculate the frequency domain metrics differ from paper to paper. Badilini *et al.* [18] compared a limited number of autoregressive and FFT techniques for calculating frequency domain HRV metrics on young healthy adults⁵ during tilt testing. They obtained different baseline values of the HRV metrics when using autoregressive and FFT methods, but both methods were equally effective for assessing the changes during tilt. For young (aged 29 ± 5 years) healthy female volunteers, after upright tilting to 90° , they recorded a significant⁶ rise in the $\frac{LF}{HF}$ -ratio from 1.15 ± 0.68 to 6.56 ± 5.45 , (calculated using the FFT of 5 minute RR segments after interpolation with an unspecified method) over the subsequent fifteen minutes. However, for the same segments, AR modelling led to a change in the $\frac{LF}{HF}$ -ratio from 1.16 ± 1.26 to 12.07 ± 8.99 . It should be noted that the variance around these mean values was of the order of the $\frac{LF}{HF}$ -ratio itself, demonstrating the high variability of the metrics over a short time frame.

It is difficult to compare the results and conclusions for different studies since there is often insufficient detail in the papers to determine how the PSD estimates are computed. No current method refers to unevenly sampled spectral analysis, yet details of interpolation methods are usually not given. Other problems include the comparability of populations in terms of age, pathology, medication and test protocol as well as the small sample sizes involved.

⁵8 females, 10 males with mean ages of 29 ± 5 years.

⁶tested using a paired Wilcoxon test

In summary there is a need for interpreting HRV changes during the course a HUT test in the context of the patient's age and medical history, which together may narrow down the suspected causes of syncope. Furthermore, an agreed robust measure of frequency-domain metric calculation is needed to allow between-study comparisons.

6.5 HUT data analysis

6.5.1 Methodology

In this chapter, a preliminary investigation into HRV changes during head-up tilt for a limited population sample is presented. Six subjects are analysed, two young healthy males, two elderly females with no known cardiac-related problems and two elderly females diagnosed with the same type of syncope, vasovagal syndrome. The effect of HUT on their HRV is explored in terms of both the $\frac{LF}{HF}$ -ratio and the standard deviation of a five-minute window, denoted by σ_5 . Both quantities are calculated over the entire procedure using a sliding window with a 240 second overlap.

Although gender can contribute towards significant differences in HRV response to HUT, the large difference in age is a much more significant factor [236]. Given the review of existing knowledge of the sympathovagal balance and HRV during HUT, it is expected that, after tilting through 70° , the young healthy subjects (group A), will experience an $\frac{LF}{HF}$ -ratio increase and an overall increase in HRV (as measured by the standard deviation over five minutes, σ_5). The elderly healthy adults (group B) are expected to have little or no change in both the $\frac{LF}{HF}$ -ratio and σ_5 . However, the elderly subjects with vasovagal syndrome (group C) are expected to experience an initial drop in both the $\frac{LF}{HF}$ -ratio and σ_5 unless part of their problem is cardioinhibitory in origin. The changes over the course of the tilt are analysed and the differences between each patient group is highlighted.

6.5.2 Clinical protocol

The data analysed in this chapter is from the Radcliffe Infirmary (RI) Falls Clinic. The protocol that they have adopted is as follows:

- The patient is asked to lie on the tilt table in the supine position, while the procedure is explained to them.
- The cardiorespiratory equipment is attached, including 3 leads of ECG, one channel of respiration

(electrical impedance measured across two of the ECG leads [272]), a pulse oximeter, a continuous blood pressure (BP) device (the Finapres [149]) and a self-inflating brachial cuff for intermittent BP readings.

- The patient remains supine for 10 minutes.
- The patient is then told that the tilt is about to occur and the staff tilt the table through 70 degrees.
- The patient is then made comfortable so that they may remain (patiently) in the ‘head-up’ position for the next 40 minutes.
- About 30 minutes into the test Carotid Sinus Massage is performed on the left and right sides of the neck.
- 40 minutes after the tilt, the patient is returned to the supine position.
- The data recording is then stopped.

Drugs are not administered *during* the test, although the patients are often on medication related to other medical conditions such as hypertension.

6.5.3 Description of patients

The subjects chosen for analysis in this chapter are separated into 3 groups, denoted by letters A, B or C. The following number (1 or 2) represents the first or second patient in the group. The groups are as follows:

- Group A - Normal healthy young male adults (aged 23 and 31) with no history of cardiac problems or other serious health issues.
- Group B - Elderly female patients, referred to the Falls Clinic with suspicion of a syncope-related illness, but later diagnosed without such a problem. No history of cardiac problems.
- Group C - Elderly female patients, referred to the Falls Clinic with suspicion of a syncope-related illness, later diagnosed as being vasovagal syndrome.

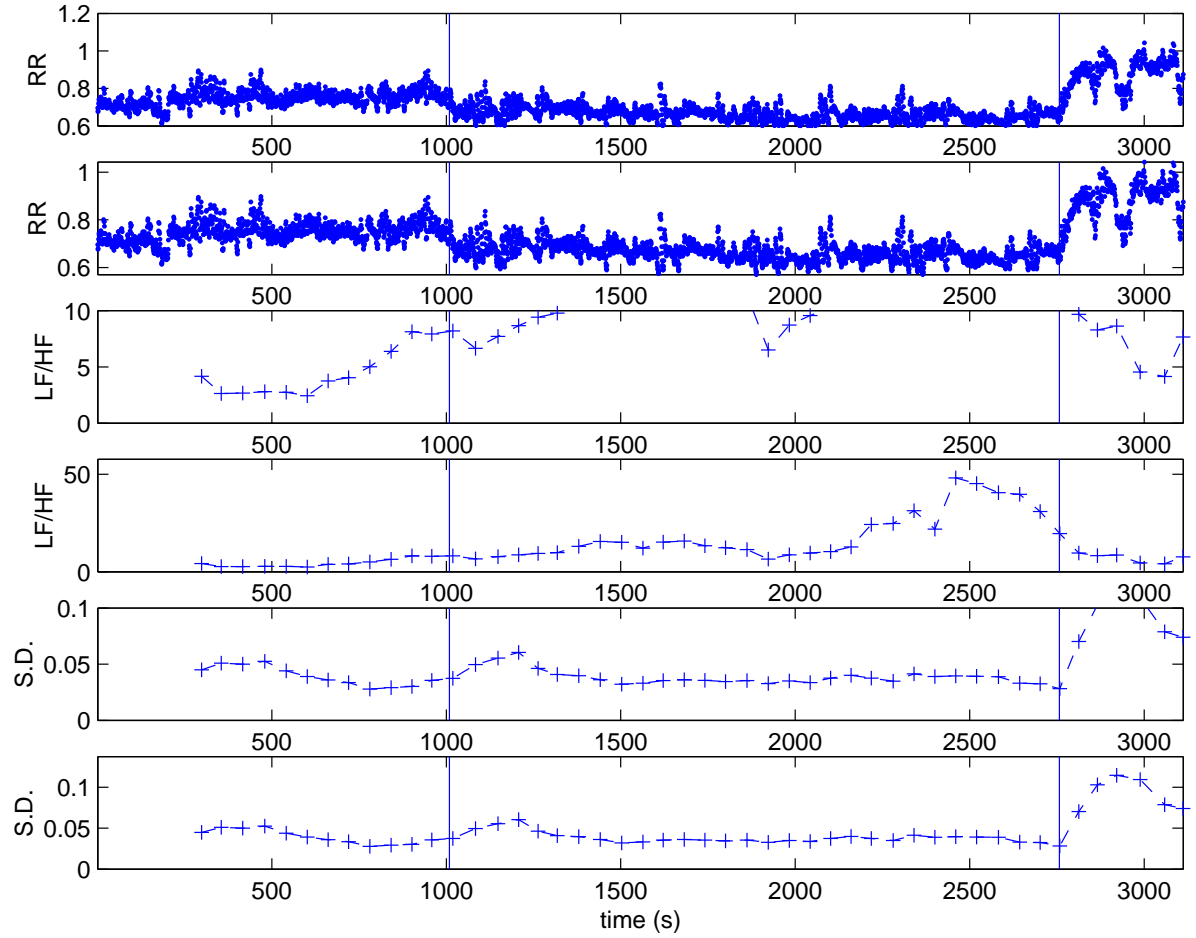


Figure 6.2: RR and HRV data for subject A1 during HUT. From top to bottom; beat-to-beat RR interval, $\frac{LF}{HF}$ -ratio over 5 minute windows with 240 second overlap, standard deviation of the same windows. The time marker represents the front of the 5 minute window. Note also that each plot appears in pairs, one with an optimal scaling to observe the changes, and one with the same scaling as each of the other patient plots. The left vertical line represents the time of the initial tilt to 70° and the right line represents the return to the supine position.

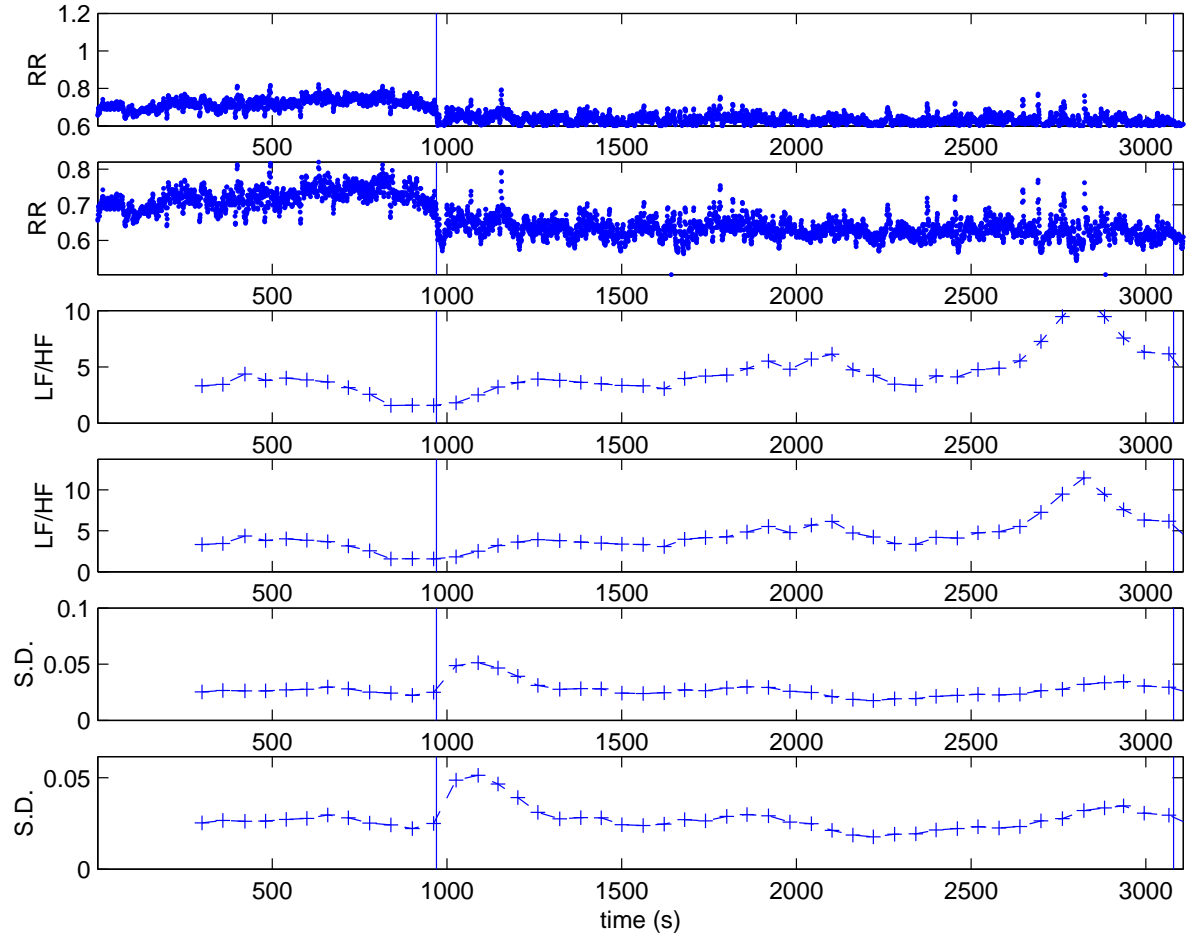


Figure 6.3: RR and HRV data for subject A2 during HUT. From top to bottom; beat-to-beat RR interval, $\frac{LF}{HF}$ -ratio over 5 minute windows with 240 second overlap, standard deviation of the same windows. The time marker represents the front of the 5 minute window. Note also that each plot appears in pairs, one with an optimal scaling to observe the changes, and one with the same scaling as each of the other patient plots. The left vertical line represents the time of the initial tilt to 70° and the right line represents the return to the supine position.

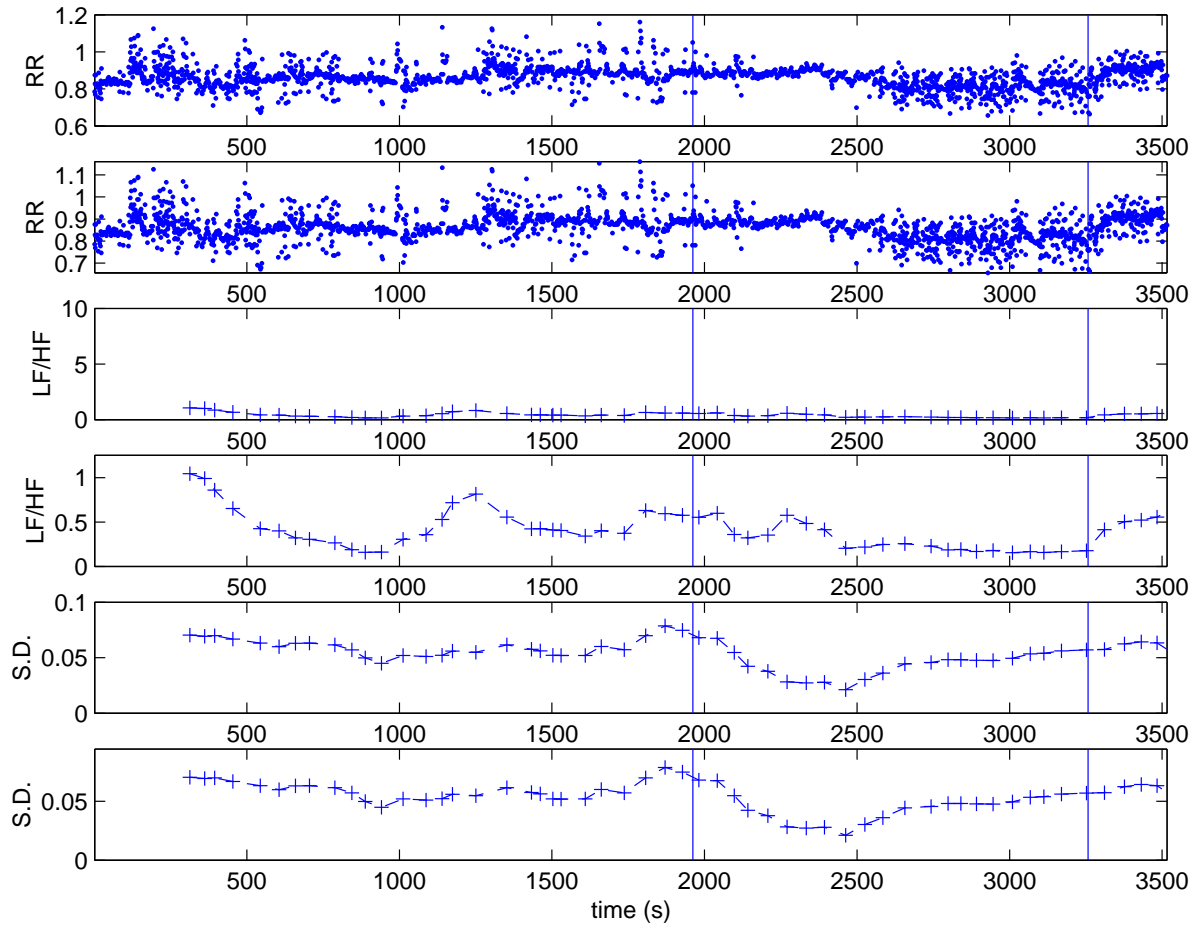


Figure 6.4: RR and HRV data for subject B1 during HUT. From top to bottom; beat-to-beat RR interval, $\frac{LF}{HF}$ -ratio over 5 minute windows with 240 second overlap, standard deviation of the same windows. The time marker represents the front of the 5 minute window. Note also that each plot appears in pairs, one with an optimal scaling to observe the changes, and one with the same scaling as each of the other patient plots. The left vertical line represents the time of the initial tilt to 70° and the right line represents the return to the supine position.

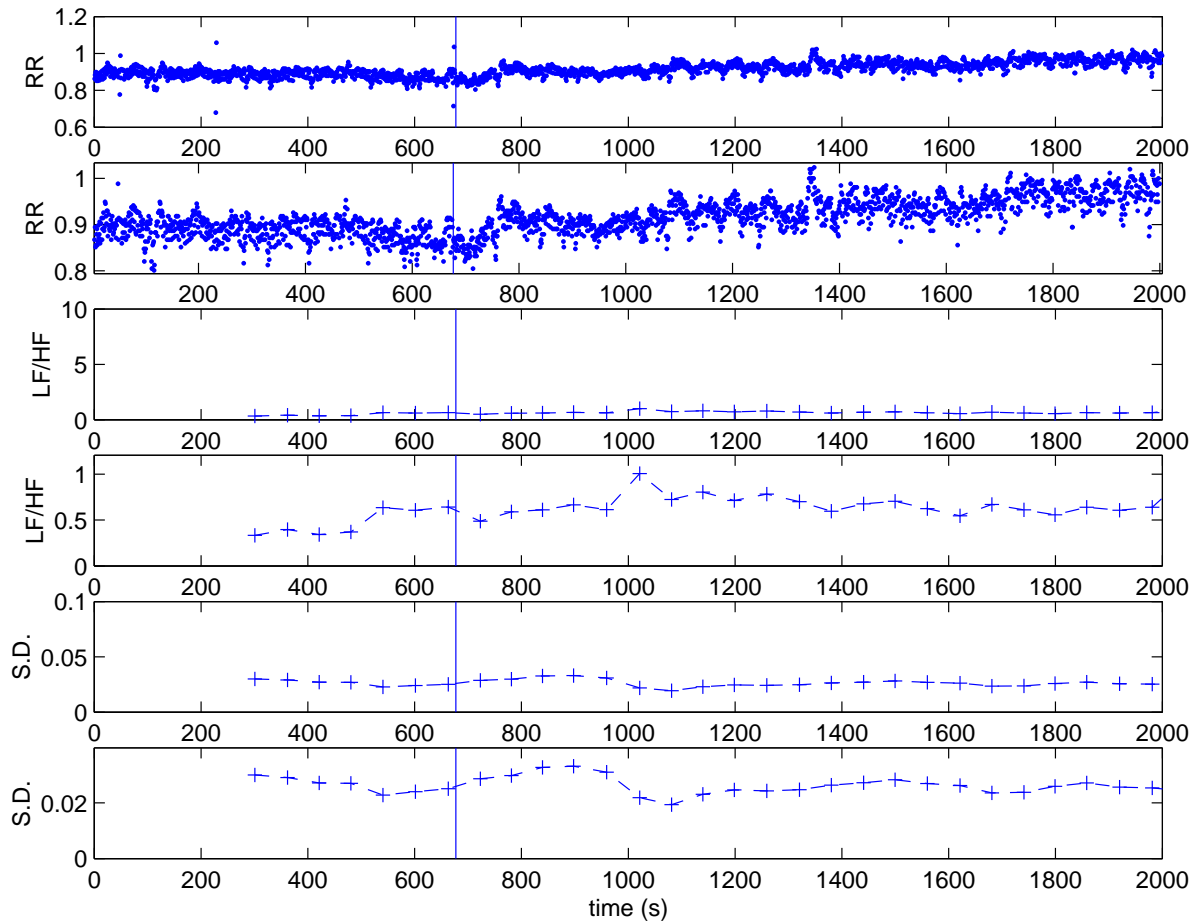


Figure 6.5: RR and HRV data for subject B2 during HUT. From top to bottom; beat-to-beat RR interval, $\frac{LF}{HF}$ -ratio over 5 minute windows with 240 second overlap, standard deviation of the same windows. The time marker represents the front of the 5 minute window. Note also that each plot appears in pairs, one with an optimal scaling to observe the changes, and one with the same scaling as each of the other patient plots. The left vertical line represents the time of the initial tilt to 70° . Note that the recording was terminated before the return to supine position.

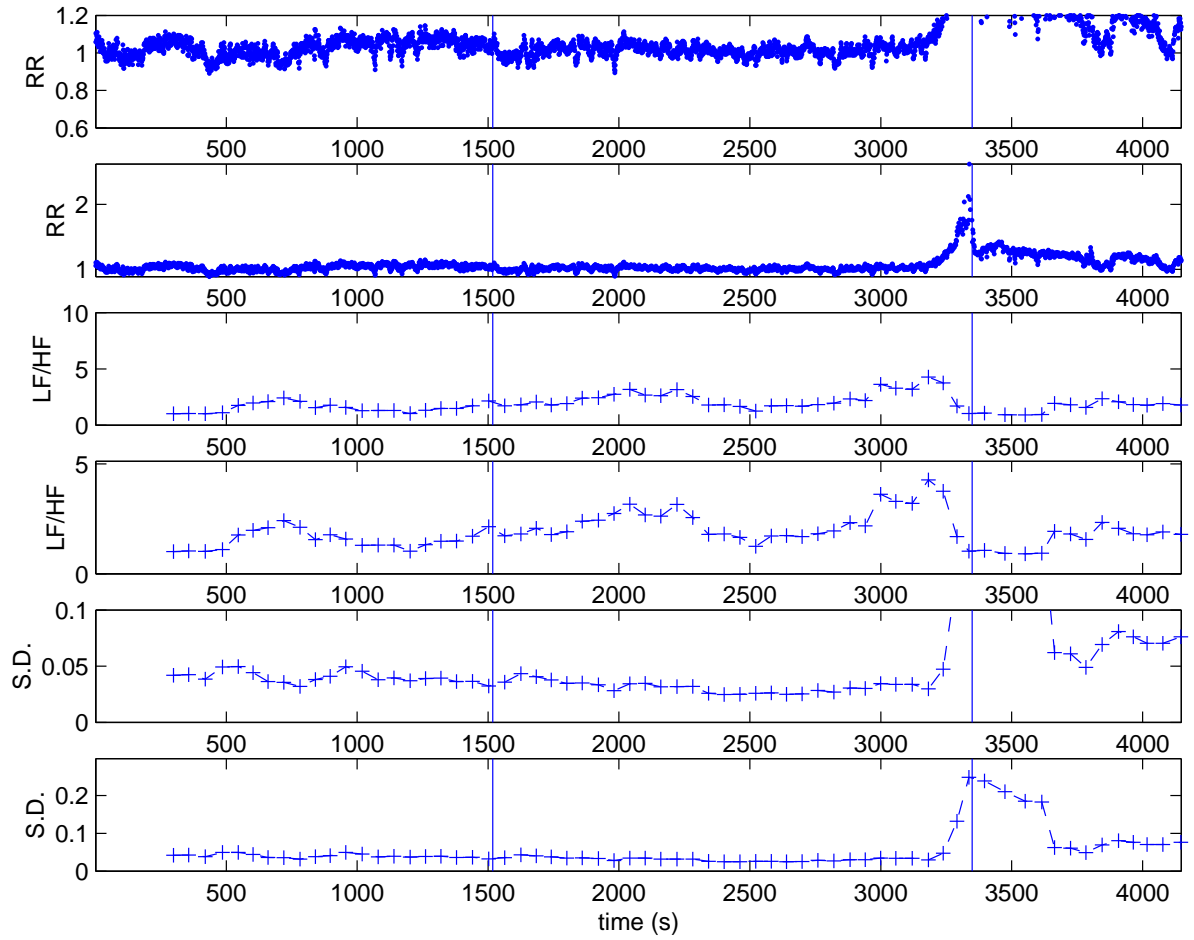


Figure 6.6: RR and HRV data for subject C1 during HUT. From top to bottom; beat-to-beat RR interval, $\frac{LF}{HF}$ -ratio over 5 minute windows with 240 second overlap, standard deviation of the same windows. The time marker represents the front of the 5 minute window. Note also that each plot appears in pairs, one with an optimal scaling to observe the changes, and one with the same scaling as each of the other patient plots. The left vertical line represents the time of the initial tilt to 70° and the right line represents the return to the supine position.

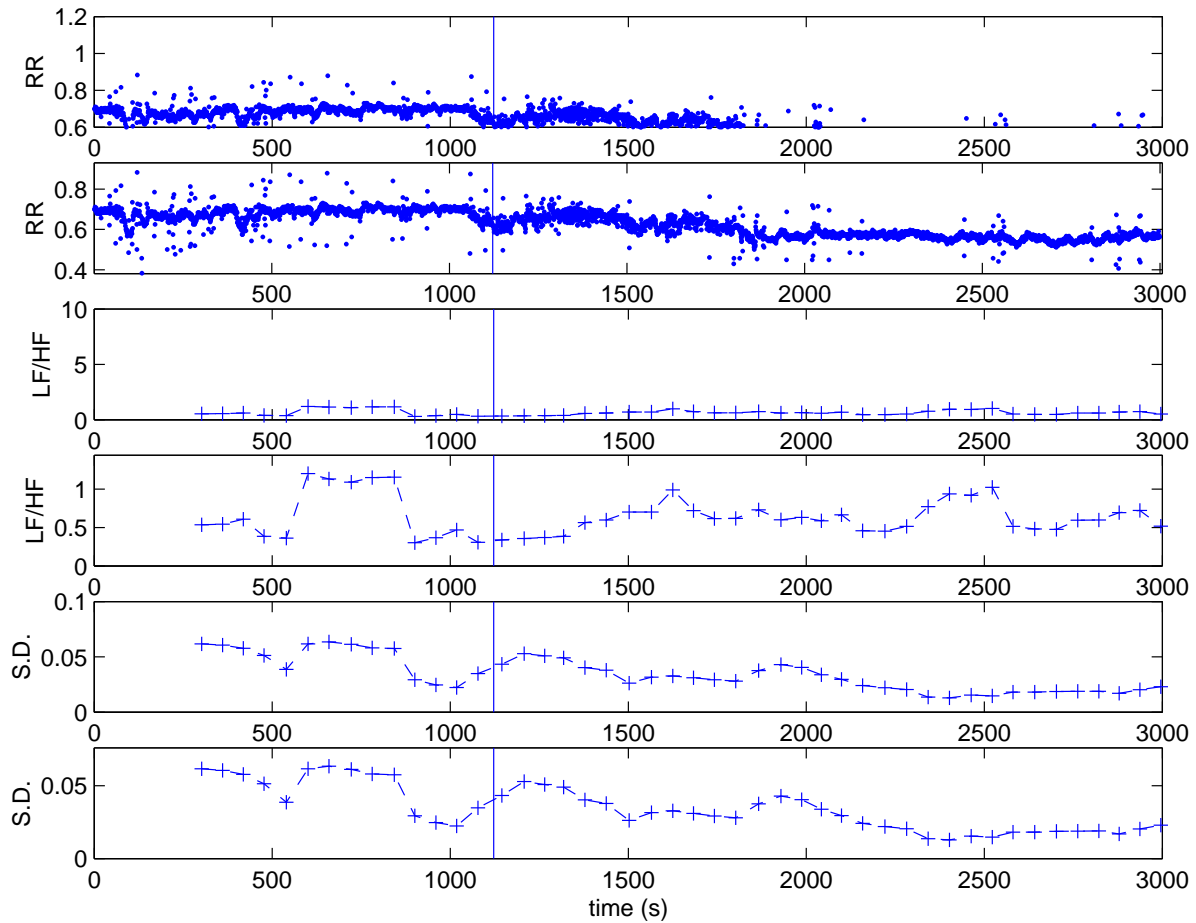


Figure 6.7: RR and HRV data for subject C2 during HUT. From top to bottom; beat-to-beat RR interval, $\frac{LF}{HF}$ -ratio over 5 minute windows with 240 second overlap, standard deviation of the same windows. The time marker represents the front of the 5 minute window. Note also that each plot appears in pairs, one with an optimal scaling to observe the changes, and one with the same scaling as each of the other patient plots. The left vertical line represents the time of the initial tilt to 70° . Note that the recording was terminated before the return to supine position.

6.5.4 Signal Analysis

Figures 6.2 to 6.7 show comparisons of HRV changes during HUT for the three patient groups (A, B and C) detailed above. For each subject the beat-to-beat RR interval, the $\frac{LF}{HF}$ -ratio over 5 minute windows with 240 second overlap and the standard deviation (SD) of the same 5 minute windows are plotted. Vertical markers are also plotted to locate the actual times of the 70° HUT (left marker) and the return to the supine (right marker). The time stamp for each HRV estimate (indicated by '+') represents the time of the last heart beat in each 5 minute window. Note also that each parameter is plotted twice with different scaling. The first, third and fifth plots on each of the figures all have the same scaling to facilitate inter-patient comparisons. The second, fourth and sixth plots are scaled individually (between the individual's maximum and minimum values) to highlight the intra-patient changes.

Short-term changes after HUT

In the five minutes following HUT, subjects A1 and A2 (figures 6.2 and 6.3) exhibit the typical changes that one would expect from normal subjects; an increase in mean heart-rate (i.e. decrease in RR interval) accompanied by sympathetic stimulation which manifests as an $\frac{LF}{HF}$ -ratio rise followed by oscillations between values of about 3 and 10 [103] (see section 6.4). The elderly but otherwise healthy subjects B1 and B2 exhibit low $\frac{LF}{HF}$ -ratio values and very small oscillations in the $\frac{LF}{HF}$ -ratio rise following a tilt. Upon tilt, subject B2 exhibits an increase in the mean RR interval and subject B1 experiences almost no change. Both these trends are consistent with reported $\frac{LF}{HF}$ -ratio changes in current literature for healthy elderly subjects [45, 145, 156].

The behaviour of the $\frac{LF}{HF}$ -ratio of the two elderly vasovagal syndrome patients (C1 and C2) differs slightly and initially it appears that only subject C2's response is consistent with their diagnosis of profound carotid sinus hypersensitivity. That is, upon tilt they experience a small rise in the $\frac{LF}{HF}$ -ratio with little change in the mean RR interval. Carotid sinus hypersensitivity is associated with a cardioinhibitory response on tilt; sympathetic activation leading to a rise in the $\frac{LF}{HF}$ -ratio. In contrast, subject C1, who is diagnosed as having **no** cardioinhibitory component to their vasovagal syndrome, would be expected to experience a drop in the initial value of the $\frac{LF}{HF}$ -ratio and a drop in overall variability (as measured by the standard deviation). This is not the case however, and a significant initial rise in the $\frac{LF}{HF}$ -ratio rise is observed instead.

Although there is a significant change in the mean RR interval between each five minute section

of the RR tachogram either side of the tilt ($P < 0.05$ using Student's t-test) for all subjects, there is no significant change in the variance between these periods ($P < 0.05$ using the *F-test* on the same segments). This illustrates that the relatively large increases in the standard deviation around the time of tilt is an artefact of the steep change in mean RR interval at this time. Subject A1 (figure 6.2) illustrates this effect particularly well, with large increases in the measured standard deviation for windows that include data over the time of the tilt, despite there being little or no change in the actual variance, a minute after the tilt.

Longer-term changes after HUT

After approximately 30 minutes into the tilt, a large increase in the $\frac{LF}{HF}$ -ratio is observed in subjects A1 and A2 and to a lesser extent, in subjects C1 and C2. This is, as yet, unreported in the current literature on HUT studies and could possibly be attributed to the subjects' natural intolerance to such a lengthy experiment. It should be recalled from chapter 5, table 5.1, that even subtle changes in a conscious patient's mental activity may lead to an order of magnitude change in the $\frac{LF}{HF}$ -ratio. The elderly 'healthy' group (B) exhibit very little change however, since their autonomic nervous system response is suppressed in the normal manner expected for this age group.

Significant long term changes, measured over entire pre- and post-tilt sections of the RR tachogram, are observed in both the variance and mean RR interval ($P < 0.01$ using the *F-test* and $P < 0.01$ using Student's t-test, respectively) for the elderly patient groups (B and C) irrespective of the actual condition. No significant changes in the variance or mean RR interval for the young healthy group (A) after tilt and before the return to supine can be detected.

One particularly significant change can be observed in figure 6.6 for subject C1. Approximately 25 minutes into the tilt ($t = 3100$ seconds), the $\frac{LF}{HF}$ -ratio begins to rise to a peak value of over 4 at approximately $t = 3200$ seconds. However, the $\frac{LF}{HF}$ -ratio then rapidly drops to a value of approximately 1. For an elderly subject, this represents a large change in the $\frac{LF}{HF}$ -ratio. It should be noted that during this period there was no significant change in the standard deviation of the RR intervals over this period and the subject was becoming severely bradycardic (a plummeting heart rate). The onset of bradycardia was accompanied by a large drop in systolic blood pressure to under 60mmHg (not shown) and finally, a complete cessation of the heart for over 4 seconds (at $t = 3300$ seconds), whereupon the clinical team was forced to return the subject to the supine to aid recovery. The clinical expectation of either dramatic

vasodilation or deceleration in HR directly causing the observed (severe) BP drop is consistent with the observed changes in the $\frac{LF}{HF}$ -ratio. Either of these cardiovascular changes would lead to sympathetic outflow (and a consequent rise in the LF component) and/or a parasympathetic withdrawal (leading to a consequent drop in the HF component). The resultant steady rise in the $\frac{LF}{HF}$ -ratio before the asystole is therefore explicable. A parasympathetic outflow accompanied by a sympathetic withdrawal, leading to the observed drop in the $\frac{LF}{HF}$ -ratio at the time of the asystole is consistent with the Bezold-Jarisch reflex reflex in vasovagal syncope (see section 6.2.1). The possibility of the Bezold-Jarisch reflex being involved suggests that subject C1 has some cardioinhibitory component to their syncope and therefore may explain the initial $\frac{LF}{HF}$ -ratio rise observed immediately after tilt (see section 6.4).

6.6 Conclusions

Although generalisations about HRV changes during HUT experiments have been made in the literature, this preliminary study shows that these are not valid unless more data is available to the clinician (such as age). Results in this chapter indicate that HRV measures based upon variance are relatively insensitive to real cardiovascular changes and may be heavily influenced by baseline shifts in the RR tachogram. However, the $\frac{LF}{HF}$ -ratio appears to be a sensitive measure of the autonomic nervous system's response to a sudden change in cardiovascular control, although the exact manner in which this response manifests can be complicated by factors such as age and the multiple effects associated with some medical conditions. Furthermore, it is also possible that results obtained from performing head-up tilts can be affected by the background changes caused by varying mental activity.

Chapter 7

Summary, conclusions and future work

7.1 Summary and key conclusions

Although there are generally accepted standards for the calculation of HRV metrics and some agreement concerning the clinical application of these metrics [184], the field of HRV analysis contains many contradictory studies and there exists no clear consensus on the clinical value of HRV metrics. This thesis has endeavoured to develop HRV analysis within a principled framework, based on the development of appropriate signal processing techniques and pilot studies in two fields of potential application.

Chapter 2 identified frequency-domain techniques as the most promising methods for analysing HRV. Since the RR tachogram is inherently an unevenly sampled time series, re-sampling has been used to generate an evenly sampled time series which is then amenable to spectral analysis using traditional methods such as the FFT. By introducing a method for generating a realistic artificial RR tachogram, for which the spectral components are completely known *a priori*, it was shown in chapter 4 that linear re-sampling introduces significant errors in the computation of frequency-domain metrics (the LF, HF and $\frac{\text{LF}}{\text{HF}}$ -ratio) when they are computed using the FFT (FFT_{lin}). In the case of no missing data, the FFT of cubic spline re-sampled RR tachograms (FFT_{cubic}) was shown to produce an accurate estimation of the spectral components of the artificial data, and also of the spectral HRV metrics being considered. A spectral estimation technique for unevenly sampled data known as the Lomb periodogram, initially developed for analysis of astrophysical data, was introduced. The performance of the Lomb periodogram for estimating frequency-domain HRV metrics (without re-sampling) was shown to be at least as good as the FFT_{cubic} method when no ectopic beats or artefacts are present in the ECG waveform.

The presence of just a single ectopic beat in a five minute RR tachogram was shown to give rise to

significant corruption of frequency-domain HRV measures. Robust techniques for the removal of ectopic beats were therefore presented in chapter 3. A novel method for characterising normality was described, based upon the morphological characteristics of sinus beats. A training set of normal beats was presented to a neural network, trained to learn normality for a particular subject. The neural network, an auto-associative multilayer perceptron (MLP), was trained to reconstruct its input as a normal ECG waveform with its R-peak at the centre of the window. A new stopping criterion for the training process was proposed, based on the ratio of the variance in the training set and the variance in the set of reconstructed output vectors. Once the network is trained, the potential sinus-beat candidates are identified by a conventional beat detector and presented to the MLP. The output is then compared to the input and the mean square error (MSE) is calculated. The reciprocal of this quantity (the RMSE) was shown to provide a highly sensitive measure for identifying sinus beats.

A further method for classifying beats based upon their timing was introduced, and the analysis of the beat-to-beat intervals of sinus beats, non-sinus beats and artefacts on a scored database of 24-hours RR tachograms of 19 normal subjects was presented. Classification error rates demonstrated that thresholds can be selected depending on the application's tolerance to these errors.

In chapter 4, experiments on artificial 5-minute RR tachograms showed that the removal of RR intervals from the tachogram to simulate the presence of ectopy, led to an over estimation of the $\frac{LF}{HF}$ -ratio by approximately 1.5% per beat removed for the even-sampling PSD estimation techniques. However, the Lomb periodogram was shown to produce a consistently accurate estimate of the frequency components used to generate the artificial RR tachogram, even when as many as 60 of the 300 beats were removed in a 5 minute RR tachogram (for an average HR of 60 bpm). This analysis demonstrated for the first time, the superiority of the Lomb periodogram over FFT methods for analysing RR tachograms. Furthermore, recent research by Teich *et al.* [268] and Heneghan *et al.* [112] have demonstrated the explicit relationship between Fourier PSD estimation techniques and other non-stationary PSD estimation techniques (such as wavelet and detrended fluctuation analysis). The results in chapter 4 on the effects of re-sampling on spectral HRV measures are therefore also applicable to these non-stationary techniques.

A survey in chapter 5 of HRV analysis in the literature highlighted the activity dependence of HRV metrics. Thus even controlled studies may be confounded by mental activity changes over the course of the study. However, these confounding effects are reduced during sleep. A new method of segmenting the RR tachogram into sections based upon sleep staging was proposed in chapter 5 and this allowed the separation of normal and abnormal (sleep apnoeic) subjects by comparing the $\frac{LF}{HF}$ -ratio averaged during

periods of deep sleep. The variance of $\frac{\text{LF}}{\text{HF}}$ -ratio estimates during each sleep stage was also shown to be lower using the Lomb method.

Finally, the methods developed in this thesis were applied to controlled studies (head-up tilt tests) on conscious subjects suspected of suffering from syncope, an autonomic nervous system problem that can lead to a sudden loss of consciousness. The results on a small database of subjects showed that changes in the $\frac{\text{LF}}{\text{HF}}$ -ratio during the course of the tilt test provide a method for differentiating between sub-classes of syncope.

7.2 Future work

7.2.1 Signal processing

There exists a growing body of evidence that useful information concerning the variability of the heart rate can be gained from using nonlinear and nonstationary mathematical techniques [29, 212, 245, 250, 251, 274]. Although the methods developed in this thesis do not address the problem of nonlinearity or nonstationarity, stationarity is implicitly assumed through the segmenting of the RR tachogram into sections according to sleep stages and assuming that the data within each section is stationary. Furthermore, the Lomb technique is only able to assess the linear power in a system.

A method for locating significant changes in the RR tachogram based upon statistical tests of shifts in mean values over varying windows [29] may provide the basis for segmenting windows into stationary sections for spectral analysis, without the need for other information (such as sleep state). However, this does not address the problem of comparing HRV estimates between patients experiencing similar activity states. Recent work by Moody [199] for segmenting the RR tachogram into periods of similar *activity* states may provide a solution to this problem. A more robust method for allowing inter- and intra-patient HRV assessment of conscious patients by comparing HRV metric estimates within the same activity state (in the same manner as was performed with the sleep stages in chapter 5) could therefore be developed.

A recent technique for spectral estimation of unevenly sampled nonstationary data by Qi *et al.* [226] may present a useful technique for assessing HRV if the assumption that the variability in the RR tachogram is due to a small number of influences holds true. Qi *et al.*'s technique uses a Kalman filter formulation to estimate the Fourier coefficients over local (short) windows. This has the advantage of allowing for nonstationarity in a signal (by treating it as a set of near-stationary windows and averaging) without the need for re-sampling. Furthermore, prior information about the noise and signal structure of

the data being analysed can be included in the estimation. It may also be possible to use the *Extended* Kalman Filter formulation [23] to quantify the nonlinear components of an RR tachogram. These new (unevenly sampled) techniques could be compared to the linear stationary techniques explored in this thesis to assess whether quantification of nonlinear and/or nonstationary information in the RR tachogram leads to more effective HRV metrics.

7.2.2 Clinical studies

Although medium-term changes in HRV (over the several day post-operative period in hospital) have been linked with long-term (6 months+) survival rates for cardiac patients, it is not clear whether this is simply a reflection of the amount of sleep a patient is experiencing. Chapter 5 showed that HRV during sleep and waking hours is substantially different. A relatively high average $\frac{LF}{HF}$ -ratio may be indicative of a patient experiencing little sleep. However, if the patient is sleeping as expected, then a high $\frac{LF}{HF}$ -ratio (for a particular age range and gender) would indicate that the patient has some type of cardiovascular or circulatory problem.

Furthermore, current literature [58] indicates that the single largest contributor to patient recovery in ITU is the amount of sleep experienced by the patient. It is therefore unclear whether, studies that link HRV to long-term outcome are simply measuring quality of sleep through HRV metrics. Since environmental disturbances that affect sleep on ITU are different from location to location and throughout the year (and even on a day-to-day basis) [58], sleep disturbances differ between patients, in a manner that may be unrelated to their condition. A study that simultaneously measures cardiac parameters (such as ECG) and EEG analysis for sleep staging should help to disentangle the sleep related and cardiac related causes that affect patient recovery. Furthermore, a comparative analysis of cardiovascular activity between patient groups who are experiencing a similar level of CNS activity (quantised by sleep state) can then be performed.

HRV is currently not one of the parameters used in syncope diagnosis. However, interest in HRV during HUT remains, in part because it does appear to give information about the sympathovagal changes that are affected by syncope. It would therefore be logical to attempt to provide a measure of the extraneous variables during experiments such as HUT and correlate these with the estimated HRV values. The problem of allowing for variations in mental activity is certainly not trivial (since there is no accepted measure of it in conscious subjects [118, 209]) but power spectral analysis of EEG may provide some

clues. This is not without precedent, although recent experiments where EEG was recorded during HUT were directed towards finding events in the EEG which could allow the identification of the early stages of a syncopal incident before its completion [249]. Furthermore, a method for characterising the changes in HRV over the course of an HUT-test may provide a more robust method for identifying the sub-classes of syncope.

Appendix A

The MIT-BIH database

A.1 Appendix: The Annotation Definitions

NORMAL	N	Normal beat
LBBB	L	Left bundle branch block beat
RBBB	R	Right bundle branch block beat
BBB	B	Bundle branch block beat (unspecified)
APC	A	Atrial premature beat
ABERR	a	Aberrated atrial premature beat
NPC	J	Nodal (junctional) premature beat
SVPB	S	Supraventricular premature or ectopic beat (atrial or nodal)
PVC	V	Premature ventricular contraction
RONT	r	R-on-T premature ventricular contraction
FUSION	F	Fusion of ventricular and normal beat
AESC	e	Atrial escape beat
NESC	j	Nodal (junctional) escape beat
SVESC	n	Supraventricular escape beat (atrial or nodal)
VESC	E	Ventricular escape beat
PACE	P	Paced beat
PFUS	f	Fusion of paced and normal beat
UNKNOWN	Q	Unclassifiable beat
LEARN	?	Beat not classified during learning

Table A.1: Beat annotation codes.

VFON	[Start of ventricular flutter/fibrillation
FLWAV	!	Ventricular flutter wave
VFOFF]	End of ventricular flutter/fibrillation
NAPC	x	Non-conducted P-wave (blocked APC)
WFON	(Waveform onset
WFOFF)	Waveform end
PWAVE	p	Peak of P-wave
TWAVE	t	Peak of T-wave
UWAVE	u	Peak of U-wave
PQ	'	PQ junction
JPT	,	J-point
PACESP	^	(Non-captured) pacemaker artifact
ARFCT	—	Isolated QRS-like artifact
NOISE	~	Change in signal quality
RHYTHM	+	Rhythm change
STCH	s	ST segment change
TCH	T	T-wave change
SYSTOLE	*	Systole
DIASTOLE	D	Diastole
MEASURE	=	Measurement annotation
NOTE	"	Comment annotation
LINK	@	Link to external data

Table A.2: Non-beat annotation codes.

Appendix B

Mathematical derivations

B.1 Appendix: Derivation of error back-propagation

The error E is given over all input patterns p by:

$$E = \frac{1}{2} \sum_p \sum_k (y_k^p - t_k^p)^2 \quad (\text{B.1})$$

Which may be written as:

$$E = \frac{1}{2} \sum_p \sum_k (f_\sigma(\sum_j w_{jk} f_\sigma(\sum_i y_i w_{ij})) - t_k^p)^2 \quad (\text{B.2})$$

To calculate the update rules the gradient of the error with respect to the weights w_{ij} and w_{jk} must be calculated. The update equations (B.3) (B.4) are given below, η is the learning rate.

$$w_{jk}^{(\tau+1)} = w_{jk}^{(\tau)} - \eta \frac{\partial E}{\partial w_{jk}} \quad (\text{B.3})$$

$$w_{ij}^{(\tau+1)} = w_{ij}^{(\tau)} - \eta \frac{\partial E}{\partial w_{ij}} \quad (\text{B.4})$$

The calculation of the gradients is performed using simple chain rule partial differentiation.

$$\frac{\partial E}{\partial w_{jk}} = \frac{\partial E}{\partial y_k} \cdot \frac{\partial y_k}{\partial a_k} \cdot \frac{\partial a_k}{\partial w_{jk}} \quad (\text{B.5})$$

The input to the output units a_k is given by

$$a_k = \sum_j y_j w_{jk} \quad (\text{B.6})$$

From (B.1) and (B.6) we may write

$$\frac{\partial E}{\partial y_k} = (y_k - t_k) \quad (\text{B.7})$$

$$\frac{\partial a_k}{\partial w_{jk}} = y_j \quad (\text{B.8})$$

Since y_k is defined as

$$y_k = f_\sigma(a_k) = \frac{1}{1 + e^{-a_k}} \quad (\text{B.9})$$

We may write

$$\frac{\partial y_k}{\partial a_k} = \frac{\partial}{\partial a_k} \left(\frac{1}{1 + e^{-a_k}} \right) = \frac{e^{-a_k}}{(1 + e^{-a_k})^2} = y_k(1 - y_k) \quad (\text{B.10})$$

Hence

$$\frac{\partial E}{\partial w_{jk}} = (y_k - t_k)y_k(1 - y_k)y_j \quad (\text{B.11})$$

Therefore we may write the w_{jk} update as

$$w_{jk}^{(\tau+1)} = w_{jk}^{(\tau)} - \eta \delta_k y_j \quad (\text{B.12})$$

Where

$$\delta_k = \frac{\partial E}{\partial y_k} \cdot \frac{\partial y_k}{\partial a_k} = \frac{\partial E}{\partial a_k} = (y_k - t_k)y_k(1 - y_k) \quad (\text{B.13})$$

In order to calculate the w_{ij} update equation the chain rule is applied several times, hence

$$\frac{\partial E}{\partial w_{ij}} = \frac{\partial E}{\partial a_j} \cdot \frac{\partial a_j}{\partial w_{ij}} \quad (\text{B.14})$$

$$\frac{\partial E}{\partial w_{ij}} = \frac{\partial E}{\partial a_k} \cdot \sum_k \left(\frac{\partial a_k}{\partial y_j} \right) \cdot \frac{\partial y_j}{\partial a_j} \cdot \frac{\partial a_j}{\partial w_{ij}} \quad (\text{B.15})$$

From (B.6)

$$\frac{\partial a_k}{\partial y_j} = \sum_k w_{jk} \quad (\text{B.16})$$

The input to the hidden units is given by

$$a_j = \sum_i y_i w_{ij} \quad (\text{B.17})$$

Hence

$$\frac{\partial a_j}{\partial w_{ij}} = y_i \quad (\text{B.18})$$

By symmetry from (B.10) we have

$$\frac{\partial y_j}{\partial a_j} = y_j(1 - y_j) \quad (\text{B.19})$$

Therefore from (B.13),(B.16),(B.18) and (B.19) the update equation for the w_{ij} weights is given by

$$w_{ij}^{(\tau+1)} = w_{ij}^{(\tau)} - \eta \delta_j y_i \quad (\text{B.20})$$

Where

$$\delta_j = \frac{\partial E}{\partial a_j} = \sum_k \delta_k w_{jk} y_j (1 - y_j) \quad (\text{B.21})$$

B.2 Appendix: Karhunen-Loéve Transformation

The Karhunen-Loéve transformation maps vectors \mathbf{x}^n in a d -dimensional space (x_1, \dots, x_d) onto vectors \mathbf{z}^n in an M -dimensional space (z_1, \dots, z_M) , where $M < d$.

The vector \mathbf{x}^n can be represented as a linear combination of a set of d orthonormal vectors \mathbf{u}_i

$$\mathbf{x} = \sum_{i=1}^d z_i \mathbf{u}_i \quad (\text{B.22})$$

Where the vectors \mathbf{u}_i satisfy the orthonormality relation

$$\mathbf{u}_i \mathbf{u}_j = \delta_{ij} \quad (\text{B.23})$$

in which δ_{ij} is the Kronecker delta symbol.

This transformation can be regarded as a simple rotation of the coordinate system from the original \mathbf{x} 's to a new set of coordinates represented by the \mathbf{z} 's. The z_i are given by

$$z_i = \mathbf{u}_i^T \mathbf{x} \quad (\text{B.24})$$

Suppose that only a subset of $M < d$ basis vectors \mathbf{u}_i are retained so that we use only M coefficients of z_i . The remaining coefficients will be replaced by constants b_i so that each vector \mathbf{x} is approximated by the expression

$$\tilde{\mathbf{x}} = \sum_{i=1}^M z_i \mathbf{u}_i + \sum_{i=M+1}^d b_i \mathbf{u}_i \quad (\text{B.25})$$

The error in the vector \mathbf{x}^n introduced by the dimensionality reduction is given by

$$\mathbf{x}^n - \tilde{\mathbf{x}}^n = \sum_{i=M+1}^d (z_i - b_i) \mathbf{u}_i \quad (\text{B.26})$$

We can then define the best approximation to be that which minimises the sum of the squares of the errors over the whole data set. Thus we minimise

$$E_M = \frac{1}{2} \sum_{n=1}^N \sum_{i=M+1}^d (z_i - b_i)^2 \quad (\text{B.27})$$

If we set the derivative of E_M with respect to b_i to zero we find

$$b_i = \frac{1}{N} \sum_{n=1}^N z_i^n = \mathbf{u}_i^T \bar{\mathbf{x}} \quad (\text{B.28})$$

Where we have defined the vector $\bar{\mathbf{x}}$ to be

$$\bar{\mathbf{x}} = \frac{1}{N} \sum_{n=1}^N \mathbf{x}^n \quad (\text{B.29})$$

We can now write the sum-of-squares-error as

$$E_M = \frac{1}{2} \sum_{n=1}^N \sum_{i=M+1}^d (\mathbf{u}_i^T (\mathbf{x}^n - \bar{\mathbf{x}}))^2$$

$$= \frac{1}{2} \sum_{n=1}^N \mathbf{u}_i^T \Sigma \mathbf{u}_i \quad (\text{B.30})$$

Where Σ is the covariance matrix of the set of vectors \mathbf{x}^n and is given by

$$\Sigma = \sum_n (\mathbf{x}^n - \bar{\mathbf{x}})(\mathbf{x}^n - \bar{\mathbf{x}})^T \quad (\text{B.31})$$

It can be shown [34] that the minimum occurs when the basis vectors satisfy

$$\Sigma \mathbf{u}_i = \lambda_i \mathbf{u}_i \quad (\text{B.32})$$

so that they are eigen vectors of the covariance matrix. Substituting (B.32) into (B.30) and making use of the orthonormality relation of (B.23), the error criterion at the minimum is given by

$$E_M = \frac{1}{2} \sum_{i=M+1}^d \lambda_i \quad (\text{B.33})$$

Thus the minimum error is obtained by choosing the $d-M$ smallest eigenvalues, and their corresponding eigenvectors, as the ones to discard.

Appendix C

Normal Values of Standard Measures of HRV

HRV metric	units	mean 24-hour value (± 1 S.D.)
SDNN	ms	141 ± 39
SDANN	ms	127 ± 35
RMSSD	ms	27 ± 12
HRV triangular index		37 ± 15
TP	ms^2	3466 ± 1018
LF	ms^2	1170 ± 416
HF	ms^2	975 ± 203
LF	nu	54 ± 4
HF	nu	29 ± 3
$\frac{\text{LF}}{\text{HF}}$ -ratio		1.75 ± 0.35

Table C.1: Nominal 24-hour HRV metric values for normal subjects (mean values \pm one standard deviation). Taken from [184]).

Appendix D

Cubic Spline Interpolation

It is well known that interpolation using high-order polynomials often produces ill-behaved results [157]. There are numerous approaches to eliminating the poor behaviour of polynomial fitting, and cubic splines have often been used instead of linear interpolation. In the case of cubic splines, cubic polynomials are used to approximate the curve between each of the N abscissae. Since an infinite number of cubic polynomials can be used to approximate a curve between two points, additional constraints are placed on the cubic polynomials to make the result unique. By constraining the first and second derivatives of each cubic polynomial to match at the abscissae, all internal cubic polynomials are well defined, with the slope and curvature of the approximating polynomials continuous across the abscissae.

Since the n^{th} cubic polynomial ($n = 1, 2, \dots, N$) is given by

$$s_n(x) = a_n(x - x_n)^3 + b_n(x - x_n)^2 + c_n(x - x_n) + d_n, \quad (x_n \leq x \leq x_{n+1}),$$

the first and second derivatives of $s_n(x)$ over the same segment are therefore

$$\begin{aligned} \frac{ds_n(x)}{dx} &= 3a_n(x - x_n)^2 + 2b_n(x - x_n) + c_n \quad \text{and} \\ \frac{ds_n^2(x)}{dx^2} &= 6a_n(x - x_n) + 2b_n. \end{aligned} \tag{D.1}$$

Equating the right hand side of the above two equations gives a quadratic in $(x - x_n)$ which therefore defines the conditions for an optimal cubic polynomial fit to the data. However, since the first and last polynomials do not have adjoining cubic polynomials additional constraints must be introduced for these two. The most common approach is to adopt a *not-a-knot* condition. This condition forces the third

derivative of the first and second cubic polynomials to be identical, and likewise for the last and second to last cubic polynomials. The computation of the derivative of a function described by splines is then straightforward.

Appendix E

A Simple Illustration of the Lomb Periodogram

Consider a 1 second $N = 128$ point, zero mean and unit variance ($\bar{x} = 0$, $\sigma^2 = 1$) signal $x(t) = \cos(2\omega t)$ sampled at 128Hz (see figure E.1a). The 128-point DFT is performed (for each required frequency) by multiplying $x(t)$ by $\exp(-\frac{i2\pi ft}{N})$ (figure E.1b) and summing over all $t = 1, 2, \dots, N$ points.

Writing this calculation explicitly for each of the n ($n = 1, 2, \dots, 128$) points of the DFT;

$$\begin{aligned} F(n) &= \sum_{k=0}^{k=127} X(t_j) e^{-\frac{i2\pi}{128} nk}, \\ &= x(1)e^0 + x(2)e^{-\frac{i2\pi}{128}n} + \dots + x(127)e^{-\frac{i2\pi}{128}126n} + x(128)e^{-\frac{i2\pi}{128}127n}, \end{aligned} \quad (\text{E.1})$$

where $x(n) = \cos(2\omega \frac{n}{2\pi N}) = 1.9844, 1.9748, \dots, 1.9462, 1.9748$ (see figure E.1a). This results in 128 (complex) Fourier coefficients ($F(n)$) which represent the contributions at the frequencies $\pm \frac{f_c}{2}$, where f_c is the Nyquist frequency (64Hz in this example). The periodogram is then calculated (up to the Nyquist frequency, 64Hz) using equation (4.6) to give $P_X(f = 2) \approx 126$ and $P_X(f \neq 2) = 0$ (see figure E.1c).

Now consider the same signal, unevenly sampled (figure E.1d) with only 16 of the 128 original points remaining ($x(1, 8, 17, 24, 33, 39, 48, 58, 62, 71, 82, 86, 97, 102, 112, 124)$). These can now be taken as the x_j ($j = 1, \dots, 16$) in equation (4.22), the Lomb periodogram. Explicitly calculating this periodogram $P_N(f)$ at each frequency gives $P(0) = 0.0367$, $P(1) = 0.0062$, $P(2) = 7.4994$, $P(3) = 0.0577$, $P(4) = 0.1943$, $P(5) = 0.0396$, $P(6) = 0.4063$ and $P(7) = 0.2050$ (shown in figure E.1e). Note that the average separation of the 16 points in time is $\Delta t_{\text{av}} \approx 0.064$ and so the the calculation is only performed

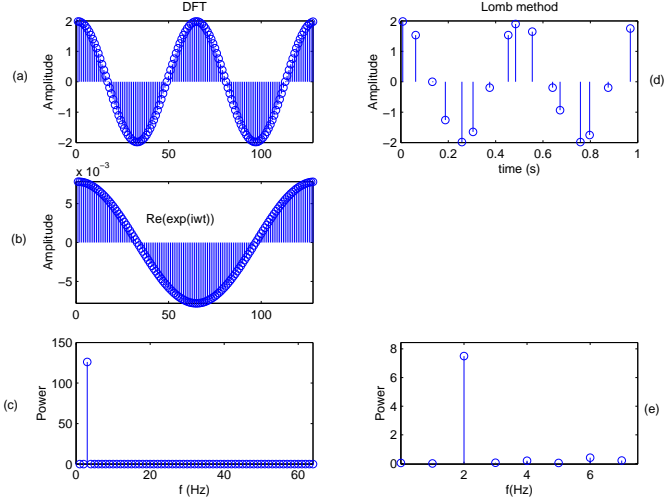


Figure E.1: Comparison of calculating the periodogram from the DFT of evenly sampled data (left) and using the Lomb periodogram on unevenly sampled data (right). See text for explanation.

for frequencies up to the average Nyquist frequency, $f'_c = \frac{1}{2\Delta t_{av}} \approx 7.8$ Hz.

It can be seen that despite the Lomb periodogram having 16 times fewer points from which to estimate the power spectrum, it provides a similar estimate to the DFT.

Bibliography

- [1] AAMI ECAR — 1987. *Recommended Practice for Testing and Reporting Performance Results of Ventricular Arrhythmia Detection Algorithms*, Association for the Advancement of Medical Instrumentation. April 1987.
- [2] Abboud S., Barnea O.: *Errors due to sampling frequency of electrocardiogram in spectral analysis of heart rate signals with low variability*, Computers in Cardiology, pp 461-463, 1995.
- [3] ACC Position Statement, *Heart rate variability for risk stratification of life-threatening arrhythmias*, J. Am. Coll. Cardiol; 948-950, 1993.
- [4] Acar B., Irina S., Hemingway H., Malik M.: *Automatic ectopic beat elimination in short-term heart rate variability measurements*, Comp. Meth. and Prog. in Biomed. 63: 123-131, 2000.
- [5] Ahlstrom M. L., Tompkins W. J.: *Automated high speed analysis of holter tapes with microcomputers*, IEEE Trans. Biomed. Eng., vol. BME-30, pp. 651-657, Oct 1983.
- [6] Akselrod S., Gordon D., Ubel F.A., Shannon D.C., Barger A.C., Cohen R.J.: *Power spectrum analysis of heart rate fluctuation: a quantitative probe of beat to beat cardiovascular control*, Science, 213:220-222, 1981.
- [7] Akselrod S.: *Components of Heart Rate Variability*, In: Malik M., Camm A.J. (eds.): *Heart Rate Variability*, Armonk, N.Y. Futura Pub. Co. Inc., pp 147-163, 1995.
- [8] Al-Aweel I.C., Krishnamurthy K.B., Hausdorff J.M., Mietus J.E., Ives J.R., Blum A.S., Schomer D.L., Goldberger A.L., *Post-Ictal Heart Rate Oscillations in Partial Epilepsy*, eurology 53(7):1590-1592, 1999.
- [9] Alboni P., Benditt D., Bergfeldt L., Blanc J.J., Bloch Thomsen P.E., van Dijk J.G., Fitzpatrick A., Hohnlose S., Janousek J., Kapoor W., Kenny R.A., Kulakowski P., Moya A., Raviele A., Sutton G., Theodorakis G., Wieling W.: *Task Force Report: Guidelines on management (diagnosis and treatment) of syncope* European Heart Journal 22, 1256-1306, 2001.
- [10] Albrecht P., Cohen R.J.: *Estimation of heart rate power spectrum bands from real-world data: dealing with ectopic beats and noisy data*, Harvard-MIT Div. of Health Sci. & Technol., Cambridge, MA, USA Proc. Computers in Cardiology (Cat. No.88CH2733-4) 1988. IEEE Comput. Soc. Press, Washington, DC, USA; xx+594 pp. p.311-14, 1988
- [11] Anderson S. T.: *Advanced Electrocardiography* Spacelabs Medical Biophysical Measurement, SpaceLabs Medical Inc., Washington USA, 1995.
- [12] Anderson K.P., Bigger J.T., Freedman R.A.: *Electrocardiographic predictors in the ESVEM trial: unsustained ventricular tachycardia, heart period variability, and the signal-averaged electrocardiogram*, Prog. Cardiovasc. Dis. 38(6): 463-88, 1996.

- [13] ANSI/AAMI-EC38—1994 *Ambulatory electrocardiographs*, American National Standard Institute, August 1994.
- [14] Arrowood J.A., Minisi A.J., Goudreau E., Davis A.B., King A.L.: *Absence of Parasympathetic Control of Heart Rate After Human Orthotopic Cardiac Transplantation*, Circulation 96: 3492-3498, 1997.
- [15] Ashkenazy Y., M. Lewkowicz, J. Levitan, S. Havlin, K. Saermark, H. Moelgaard, P. E. Bloch Thomsen: *Discrimination between healthy and sick cardiac autonomic nervous system by detrended heart rate variability analysis*, Fractals 7,85, 1999.
- [16] Ashkenazy Y., Lewkowicz M., Levitan J., Havlin S., Saermark K., Moelgaard H., Bloch Thomsen .P. E., Moller M., Hintzel U., and Huikuri H.: *Scale specific and scale independent measures of heart rate variability as risk indicators* Europhys. Lett. , (in press) (2001)
- [17] Ashkenazy Y., Ivanov P. Ch., Havlin S., Peng C.-K., Goldberger A. L., and Stanley H. E.: *Magnitude and sign correlations in heartbeat fluctuations*, Phys. Rev. Lett. 86, 1900, 2001
- [18] Badilini F., Maison-Blanche P., Coumel P.: *HRV in passive tilt test: comparative evaluation of AR and FFT spectral analyses* Pacing-Clin-Electrophysiol. May; 21(5): 1122-32, 1998 .
- [19] Balda R.A.: *The HP ECG analysis program*, Trends in Computer-Processed Electrocardiograms, J.H. vanBemmel & J.L. Willems, Eds. North Holland, pp. 197-205, 1977.
- [20] Bardonova, J., Provaznik, I., Novakova, M., Novakova, Z.: *Hidden Markov model in wavelet analysis of myocardial ischemia in rabbit*, Computers in Cardiology, pp 419-421, 2000.
- [21] Barrett-Connor E., Khaw K.: *Family history of heart attack as an independent predictor of death due to cardiovascular disease*, Circulation, Vol 69, 1065-1069, 1984.
- [22] Barros A.K., Mansour A., Ohnishi N.: *Removing artifacts from electrocardiographic signals using independent components analysis*, Neurocomputing, Volume 22, Issues 1-3, pp 173-186, 20 November 1998.
- [23] Bar-Shalom Y., Li X.: *Estimation and tracking: principles, techniques and software*, Artech House Inc., Norwood, MA 02062, 1993.
- [24] Baselli G., Cerutti S., Civardi S.: *Cardiovascular variability signals: toward the identification of a closed-loop model of the neural control mechanisms*, IEEE Trans. Biomed. Eng., 35:1033-1046, 1998.
- [25] Basseville M., Nikiforov I.V.: *Detection of Abrupt Changes - Theory and Application*, Prentice-Hall, Inc., Englewood Cliffs, N.J., ISBN 0-13-126780-9, 1993.
- [26] Batzel J., Kappel F.: *Survey of Research in Modeling the Human Respiratory and Cardiovascular Systems*, In Press, University of Graz, Austria, 2002.
- [27] Bauer T. Ewig S. Schafer H. Jelen E. Omran H. Luderitz B.: *Heart rate variability in patients with sleep-related breathing disorders*, Cardiology. 87(6):492-6, 1996.
- [28] Benditt D.G.: *Neurally mediated syncopal syndromes: pathophysiological concepts and clinical evaluation* PACE 1997; 20(2) Part II:
- [29] Bernaola-Galvan P., Ivanov P. Ch., Amaral L.A.N., and Stanley H. E.: *Scale Invariance in the Nonstationarity of Human Heart Rate*, Phys. Rev. Lett. 87.168105, 2001

- [30] Bernardi L., Bianchini B., Spadacini G., Leuzzi S., Valle F., Marchesi E., Passino C., Calciati A., Vigano M., Rinaldi M.: *Demonstrable cardiac reinnervation after human heart transplantation by carotid baroreflex modulation of RR interval*, Circulation, 92:2895-2903; 1995
- [31] Bernardi L., Wdowczyk-Szulc J., Valenti C., Castoldi S., Passino C., Spadacini G., Sleight P.: *Effects of controlled breathing, mental activity and mental stress with or without verbalization on heart rate variability*, Journal of the American College of Cardiology, Volume 35, Issue 6, pp 1462-1469, May 2000.
- [32] Bianchi A.M., Mainardi L.T., Pagani M., Cerutti S.: *Robust Time-Variant Spectral Identification for On-Line Frequency Analysis of HRV Signal*, Eng. in Med. and Biol., 18th Annual Int. Conf. IEEE, Vol, pp. 1602-1603, 1997
- [33] Birkett C.L., Kienzle M.G., Myers G.A.: *Interpolation over ectopic beats increases low frequency power in heart rate variability*, Computers in Cardiology, Proceedings. Page(s): 257 -259 1991.
- [34] Bishop C.M.: *Neural Networks for Pattern Recognition*, Clarendon Press, 1995.
- [35] Blackman R.B., Tuckey J.W.: *The Measurement of Power Spectra*, appendix B.5, pp.95-100, New York, 1958.
- [36] Blanchet T., Kember G.C., Fenton G.A.: *KLT based quality controlled compression of single lead ECG*, IEEE Transactions in Biomedical Engineering, 45(7), 942-945, 1998.
- [37] Bourlard, H. and Kamp, Y.: *Auto-Association by Multilayer Perceptrons and Singular Value Decomposition*, Biol. Cybern. 59, 291-294, 1988.
- [38] Bunde A., Havlin S., Kantelhardt J.W., Penzel T., Hermann P., Voigt K.: *Correlated and Uncorrelated Regions in Heart-Rate Fluctuations during Sleep*, Phys. Rev. Lett. Vol 85, no.17, October 2000
- [39] Bunch, J.R. and Nielsen, C.P.: *Updating the Singular Value Decomposition*, Numer. Math. 31, 111-129, 1978.
- [40] Camm A.J., Fei L.: *Risk Stratification Following Myocardial Infarction: Heart Rate Variability and Other Risk Factors*, In: Malik M., Camm A.J. (eds.): *Heart Rate Variability*, Armonk, N.Y. Futura Pub. Co. Inc., pp 347-361, 1995.
- [41] Cao L., Mees A.: *Deterministic Structure in Multi-channel Physiological Data*, Int. J. Bif. Chaos, in press, 2000.
- [42] Cardoso J.F.: *Multidimensional independent component analysis*, Proc. ICASSP '98. Seattle, 1998, pp 1941-1944.
- [43] Castiglioni P., Di Rienzo M.: *On the evaluation of heart rate spectra*, the Lomb Periodogram Computers in Cardiology, pp. 505-508, IEEE Computer Society Press, 1996.
- [44] Cavalcanti S.: *Arterial baroreflex influence on heart rate variability: a mathematical model-based analysis*, Med. Biol. Eng. Comput., 38(2): 189-97. Mar 2000.
- [45] Cencetti S., Lagi A., Cipriani M., Fattorini L., Bandinelli G., Bernardi L.: *Autonomic control of the cerebral circulation during normal and impaired peripheral circulatory control*, Heart. 1999 Sep; 82(3): 365-72

- [46] Cerutti S., Bianchi A.M., Mainardi L.T.: *Spectral Analysis of Heart Rate Variability Signal*, In: Malik M., Camm A.J. (eds.): *Heart Rate Variability*, Armonk, N.Y. Futura Pub. Co. Inc., pp 63-74, 1995.
- [47] Chazal P., Heneghan C., Sheridan E., Reilly R., Nolan P., O'Malley M.: *Automatic Classification of Sleep Apnea Epochs using the Electrocardiogram*, Computers in Cardiology, 2001.
- [48] Chazal P., Heneghan C., Reilly R.: *Automatic Sleep Apnoea Detection using Measures of Amplitude and Heart Rate Variability from the Electrocardiogram*, IEEE Int. Conf. on Patt. Recognition, Quebec City, Aug 2002.
- [49] Chowdhary S., Vaile J.C., Fletcher J., Ross H.F., Coote J.H., Townend J.N.: *Nitric Oxide and Cardiac Autonomic Control in Humans*, Hypertension, 36:264, 2000.
- [50] Clayton R.H., Campbell R.W.F., Murray A.: Time-frequency analysis of human polymorphic ventricular tachycardia, Computers in Cardiology '97, pp 97 -100, 1997.
- [51] Clayton R.H., Lord S.W., McComb J.M., Murray A.: *Comparison of autoregressive and Fourier transform based techniques for estimating RR interval spectra*, Computers in Cardiology, Page(s): 379 -382, 1997
- [52] Clayton R.H., Yu D.J., Small M., Biktashev V.N., Harrison R.G., Holden, A.V.: *Linear and non-linear characteristics of ECG signals produced by simulations of ventricular tachyarrhythmias*, Computers in Cardiology '99, pp 479-482, 1999 .
- [53] Clayton R.H., Bailey A., Biktashev V.N., Holden, A.V.: *Re-entrant arrhythmias in simulations of the long-QT syndrome*, Computers in Cardiology '99, pp 121-124, 1999.
- [54] Clifford, G., Tarassenko, L., Townsend, N.: Fusing Conventional ECG QRS Detection Algorithms with an Auto-associative Neural Network for the Detection of Ectopic Beats, Proceedings of 5th International Conference on Signal Processing, 16th IFIP World Computer Congress, Beijing, Vol.III, 1623-1628, 2000.
- [55] Clifford, G., Tarassenko, L., Townsend, N.: One-pass training of optimal architecture auto-associative neural network for detecting ectopic beats, Electronic Letters, Vol.37, No.18, pp 1126-1127, Aug. 2001.
- [56] Clifford G.D., McSharry P.E., Tarassenko L.: *Characterizing Artefact in the Normal Human 24-Hour RR Time Series to Aid Identification and Artificial Replication of Circadian Variations in Human Beat to Beat Heart Rate Using a Simple Threshold*, Computers in Cardiology, September 2002.
- [57] Cooper A. B., Thornley K. S., Young G. B., Slutsky A. S., Stewart T. E., Hanly P. J.: *Sleep in Critically Ill Patients Requiring Mechanical Ventilation*, Chest 117: 809-818, 2000
- [58] Cronin A.J., Keifer J.C., Davies M.F., King T.S., Bixler E.O.: *Postoperative sleep disturbance: Influences of opioids and pain in humans*, Autonomic Neuroscience, Vol24, Issue 1, pp 39-44, Feb 2001.
- [59] Coumel P., Maison-Blanche P., Catuli D.: *Heart Rate and Heart Rate Variability*, In: Malik M., Camm A.J. (eds.): *Heart Rate Variability*, Armonk, N.Y. Futura Pub. Co. Inc., pp 207-221, 1995.
- [60] Courtemanche M.S., Talajic M., Kaplan D.T.: Multi-parameter Quantification of 24-Hour Heart Rate Variability, Computers in Cardiology, IEEE Computer Society Press, pp.299-302 1992

- [61] Dark, G. (Ed.): *On-Line Medical Dictionary*, (The CancerWEB Project) Published at the Dept. of Medical Oncology, University of Newcastle upon Tyne, 2002.
- [62] Davey, P.: *A new physiological method for heart rate correction of the QT interval*, Heart, Vol.82, pp. 183-186, 1999.
- [63] D'Addio G., Acanfora D., Pinna G.D., Maestri R., Furgi G., Picone C., Rengo F.: *Reproducibility of Short and Long-Term Poincarè Plot Parameters Compared with Frequency-Domain HRV Indexes in Congestive Heart Failure*, IEEE, Computers in Cardiology, 25:381-384, 1998.
- [64] DeBoer RW, Karemaker JM, Strackee J.: *Hemodynamic fluctuations and baroreflex sensitivity in humans: a beat-to-beat model*, Am J Physiol., 253:H680-H689, 1987.
- [65] De Boor: *A Practical Guide to Splines*, Applied Math. Sciences Vol. 27, xxiv+392p. Springer V. 1978.
- [66] Dekker J.M., Crow R.S., Folsom A.R., Hannan P.J., Liao D., Swenne C.A., Evert G.S.: *Low Heart Rate Variability in a 2-Minute Rhythm Strip Predicts Risk of Coronary Heart Disease and Mortality From Several Causes - The ARIC Study*, Circulation 102:1239-1244, 2000.
- [67] Deeming T.J.: *erratum* Applied Space Science, 36 137, 1975; *erratum* Ap. Space Sci., 42 257
- [68] Diggle P.J.: *Time Series: A Biostatistical Introduction* Clarendon Press, Oxford, 2000.
- [69] Doughty R.N., Sharpe N.: *Beta-adrenergic blocking agents in the treatment of congestive heart failure: Mechanisms and Clinical Results* Annu. Rev. Med. 48:103-114, 1997.
- [70] Dowling J.E.: *Creating Mind (How The Brain Works)*, W.W. Norton & Co. New York 1998,
- [71] Downie N.M., Heath R.W.: *Basic Statistical Methods*, Harper & Brothers, New York, 1959
- [72] Ebrahim H.M., Feldman J., Bar-Kana I., *Robust Sensor Fusion Improves Heart Rate Estimation: ClinicalEvaluation*, Journal of Clinical Monitoring, 13:379-384,1997.
- [73] Ebrahim H.M., Feldman J., Bar-Kana I., *A Robust Sensor Fusion Method for Heart Rate Estimation*, Journal of Clinical Monitoring, 13:385-393,1997.
- [74] Eckberg D.L.: *Sympathovagal Balance*, Circulation, 96:3224-3232, 1997.
- [75] Elghazzawi Z., Geheb F. *A knowledge-based system for arrhythmia detection*, Computers in Cardiology. 1997, 24:299-302.
- [76] Engelse W.A.H., Zeelenberg C.: *A single scan algorithm for QRS-detection and feature extraction*, IEEE Comput. Card., Long Beach: IEEE Computer Society, pp. 37-42 1979.
- [77] Fallen E.L., Kamath M.V., Ghista D.N., Fitchett D.: *Spectral analysis of heart rate variability following human heart transplantation: evidence for functional reinnervation*, J Auton Nerv Syst. 1988;23:199-206.
- [78] Fallen E.L., Kamath M.V.: *Circadian Rhythms of Heart Rate Variability*, In: Malik M., Camm A.J. (eds.): *Heart Rate Variability*, Armonk, N.Y. Futura Pub. Co. Inc., pp 293-310, 1995.
- [79] Luigi Ferini-Strambi, Anna Bianchi, Marco Zucconi, Alessandro Oldani, Vincenza Castronovo and Salvatore Smirne: *The impact of cyclic alternating pattern on heart rate variability during sleep in healthy young adults*, Clinical Neurophysiology, Volume 111, Issue 1, pp 99-101, 1 January 2000.

- [80] Ferri R., Parrino L., Smerieri A., Terzano M.G., Elia M., Musumeci S.A., Pettinato S.: *Cyclic alternating pattern and spectral analysis of heart rate variability during normal sleep*, J. Sleep Res. 9, 13-18, 2000.
- [81] Fitzpatrick A.P., Theodorakis G., Vardas P., Sutton R.: *Methodology of head-up tilt testing in patients with unexplained syncope* J Am Coll Cardiol 1991; 17: 125-30
- [82] Fraden J., Neuman. M.R.: *QRS wave detection*, Med. Biol. Eng. Comp., vol. 18, pp. 125-132, 1980.
- [83] Frederiks J., Swenne C.A., Kors J.A., van Herpen G., Mann A.C., Levert J.V., Schalij M.J., Bruschke A.V.G.: *Within-subject electrocardiographic differences at equal heart rates: role of the autonomic nervous system* Euporean Journal of Physiology, December 2000.
- [84] Freitas J., Azevedo E., Teixeira J., Carvalho M. J., Costa O. Falcão de Freitas A.: *Heart rate variability as an assessment of brain death*, Transplantation Proceedings, Volume 32, Issue 8, pp 2584-2585, December 2000.
- [85] Friesen G.M., Jannett T.C., Jadallah M.A., Yates S.L., Quint S.R., Nagle H.T.: *A Comparison of the Noise Sensitivity of Nine QRS Detection Algorithms*, IEEE Transactions on Biomedical Engineering, vol. 37 NO. 1. 1990.
- [86] Funck-Bretano C., Jaillon P.: *Rate-corrected QT interval: techniques and limitations*, American Journal of Cardiology, 72:17B-22B, 1993.
- [87] Furlan R., Piazza S, Dell'Orto S., Barbic F., Bianchi A., Mainardi L., Cerutti S., Pagani M., Malliani A.: *Cardiac Autonomic Patterns Preceding Occasional Vasovagal Reactions in Healthy Humans*, Circulation, 98:1756-1761, 1998.
- [88] Furlan R., Piazza S, Barbic F., Tinelli M., Seghizzi P., Malliani A.: *Modifications of Cardiac Autonomic Profile Associated With a Shift Schedule of Work*, Circulation, 2000:1756-1761, 1998.
- [89] Furlan R.: *Autonomic Neuroscience; Basic and Clinical* 90:83-88, 2001.
- [90] Furnival C.M., Linden R.J., Snow H.M.: *Chronotropic and inotropic effects on the dog heart of stimulating the efferent cardiac sympathetic nerves*, J. Physiol., 230:137-153, 1973
- [91] Gajraj R.J., M. Doi, H. Mantzaridis, G.N. Kenny: *Comparison of bispectral EEG analysis and auditory evoked potentials for monitoring depth of anaesthesia during propofol anaesthesia*, Br. J. Anaesth. 82: 672-678, 1999.
- [92] Goldberger J.J.: *Sympathovagal balance: how should we measure it?* Am. J. Physiol. 276: 1273-1280, 1999.
- [93] Golub, G.H.: *Least squares, singular values and matrix approximations*, Applikace Matematiky, 13,44-51, 1968.
- [94] Golub, G.H., and Van Loan, C.F.: *Matrix Computations*, 2nd ed. Johns Hopkins Univ. Press, Baltimore 1989.
- [95] Gonzalez R., Woods R. *Digital Image Processing*, Addison-Wesley Pub. Co. 1993.
- [96] Greene H.L., Richardson D.W., Barker A.H., Roden D.M., Capone R.J., Echt D.S., Friedman L.M. Gillespie M.J. Hallstrom A.P., Verter J.: *Classification of deaths after myocardial infarction as arrhythmic or nonarrhythmic (the Cardiac Arrhythmia Pilot Study)*, Am-J-Cardiol. 63(1): 1-6 0002-9149; Jan 1 1989.

- [97] Grewal M.S., Andrews A.P.: *Kalman Filtering: Theory and Practice Using MATLAB*, 2nd Ed., John Wiley and Sons, Inc. 2001.
- [98] Griffin M.P., Moorman J.R.: *Toward the Early Diagnosis of Neonatal Sepsis and Sepsis-like Illness Using Novel Heart Rate Analysis*, Pediatrics, Vol. 107, No. 1, 2001.
- [99] Grubb B., Olshansky B.: *Syncope: Mechanisms and Management*, Armonk, NY, Futura Publishing 1997.
- [100] Guegan D.: *Some Remarks on the Statistical Modelling of Chaotic Systems*, In: Mees A. (ed.): *Nonlinear Dynamics and Statistics*, Univ. West. Aust. Press, Ch 5, 2000.
- [101] Guevara, M.: *Scale Invariance in the Cardiovascular System*, Presented at the Workshop on Cardiovascular-Respiratory Control Modeling, Graz, Austria, June 2001. (<http://bedvgm.kfunigraz.ac.at:8001/jerry/conference.html>).
- [102] Gustafson D.: *Automated VCG interpretation studies using signal analysis techniques*, R-1044 Charles Stark Draper Lab., Cambridge, MA, 1977.
- [103] Guzman C.E., Sanchez G.M., Marquez M.F., Hermosillo A.G., Cardenas M.: *Differences in HRV between cardioinhibitory and vasodepressive responses to head-up tilting* Arch-Med-Res. 1999 May-Jun; 30(3): 203-11
- [104] Haaksma J., Dijk W.A., Brouwer J., van den Berg M.P., Dassen W.R.M., Mulder B., Crijns H.J.G.M.: *The Influence of Recording Length on Time and Frequency Domain Analysis of Heart Rate Variability*, IEEE, Computers in Cardiology, 25:377-380, 1998.
- [105] Hainsworth R.: *The Control and Physiological Importance of Heart Rate*, In: Malik M., Camm A.J. (eds.): *Heart Rate Variability*, Armonk, N.Y. Futura Pub. Co. Inc., pp 3-19, 1995.
- [106] Hamilton J.D.: *Time Series Analysis: Modeling Time Series with Changes in Regime*, Princeton University Press, pp 677-703, 1994.
- [107] Hamilton P., Tompkins W.: *Quantitative Investigation of QRS Detection Rules Using the MIT/BIH Arrhythmia Database*, IEEE Transactions on Biomedical Engineering, vol. BME-33, NO. 12. 1986.
- [108] Harris F.J.: *On the Use of Windows for Harmonic Analysis with the Discrete Fourier Transform*, Proc. IEEE, Vol. 66, No. 1, Jan 1978.
- [109] Havard C.W.H. (Ed): *Black's Medical Dictionary*, 35th Edition, A & C Black Ltd., London 1987
- [110] He T., Clifford G.D., Tarassenko L.: *Application of ICA in Removing Artefacts from the ECG*, Neural Computing Applications 2003 (in press).
- [111] Heaven D.J., Sutton R.: *Syncope*, Crit Care Med 2000 Vol. 28, No. 10 (Suppl.): N116-N120
- [112] Heneghan C., McDarby G.: *Establishing the relation between detrended fluctuation analysis and power spectral density analysis for stochastic processes*, Physical Review E, Vol. 62, 5; Nov 2000.
- [113] Henneveld H., Hutter P., Bink-Boelkens M., Sreeram N.: *Junctional ectopic tachycardia evolving into complete heart block*, Heart 1998;80:627-628.
- [114] Hilton M.F., Bates R.A., Godfrey K.R., Cayton R.M.: *A New Application For Heart Rate Variability: Diagnosing the Sleep Apnoea Syndrome*, IEEE, Computers in Cardiology, 25:1-4, 1998.

- [115] Hirsch J.A., Bishop B.: *Respiratory sinus arrhythmia in humans: how breathing pattern modulates the heart rate*, Am. J. Physiol., 241:11620-11629, 1981.
- [116] Hirsch J.A., Bishop B.: *Respiratory sinus arrhythmia in humans: how breathing pattern modulates the heart rate*, Am. J. Physiol., 241:11620-11629, 1981.
- [117] Holsinger W. P.: *A QRS preprocessor based on digital differentiation*, IEEE Trans. Biomed. Eng., vol. BME-18, pp.212-217, 1971.
- [118] Holt M.: *The Use of Neural Networks in the Analysis of the Anaesthetic Electroencephalogram* DPhil. Thesis, Department of Engineering Science, University of Oxford, 1997.
- [119] Hon E.H., Lee S.T.: *Electronic evaluation of the fetal heart rate patterns preceding fetal death*, Am. J. Obstet. Gynecol., 87:814-826, 1965.
- [120] Horne, J.: *Why We Sleep: The functions of sleep in humans and other mammals*, Oxford University Press, 1988.
- [121] Houghton A., Gray D.: *Making Sense of the ECG*, OUP, 1997.
- [122] Howatson A.M., Lund P.G., Todd J.D.: *Engineering Tables and Data*, 2nd ed., Chapman & Hall, London 1991.
- [123] Hoyer D., Frasch M.G., Eiselt M., Hoyer O., Zwiener U.: *Validating phase relations between cardiac and breathing cycles during sleep*, IEEE Eng. Med. Biol, March/April 2001.
- [124] Hoyle R.H.: *Statistical strategies for small sample research*, SAGE Publications Ltd., 2455 Teller Rd., Thousand Oaks, California, USA, 1999.
- [125] Hu Y.H., Tompkins W.J., Urrusti J. L., Afonso V X. *Applications of Artificial Neural Networks for ECG Signal Detection and Classification*, Journal of Electrocardiology Vol. 26 Supplement 1995.
- [126] Hughson RL, Quintin L, Annat G, Yamamoto Y, Gharib C.: *Spontaneous baroreflex by sequence and power spectral methods in humans*, Clin Physiol., 13:663-676, 1993.
- [127] Huikuri H.V., Makikallio T.H., Airaksinen K.E.J., Seppanen T., Puukka P., Raiha I.J., Sourander L.B.: *Power-Law Relationship of Heart Rate Variability as a Predictor of Mortality in the Elderly*, Circulation. 97:2031-2036, 1998.
- [128] Ichimaru Y, Clark KP, Ringler J, Weiss WJ.: *Effect of sleep stage on the relationship between respiration and heart rate variability*, Computers in Cardiology 17:657-660, 1990.
- [129] Ichimaru Y., Moody G.B.: *Development of the polysomnographic database on CD-ROM*, Psychiatry and Clinical Neurosciences 53(2):175-177 (April 1999).
- [130] Ivanov P.Ch., Rosenblum M.G., Peng C-K., Mietus J., Havlin S., Stanley H.E., Goldberger A. L.: *Scaling Behaviour of Heartbeat Intervals Obtained by Wavelet-Based Time-Series Analysis*, Nature 383, 323, 1996.
- [131] Ivanov P.Ch., Bunde A., Amaral A.N., Havlin S., Fritsch-Yelle J., Baevsky R.M., Stanley H.E., Goldberger A.L.: *Sleep Wake Differences in scaling behavior of the human heartbeat: Analysis of terrestrial and long-term space flight data*, Europhys. Lett., 48 (5), pp.594-600, 1999.
- [132] Jabri M., S. Pickard, P. Leong, Z. Chi, B. Flower, Y. Xie *ANN Based Classification for Heart Defibrillators*, Sydney University Electrical Engineering Dept., 1993.

- [133] Jaladdine S., Hutchens C.: *Ambulatory ECG wave detection for automated analysis: a review*, ISA Transactions, 26(4):33-43, 1987.
- [134] Jager F., Moody G.B., Mark R.G.: *Characterization of Transient Ischemic and Non-ischemic ST Segment Changes*, Computers in Cardiology 95, pp.721-724, IEEE Computer Society, 1995.
- [135] Jung T-P., Makeig S., Westerfield W., Townsend J., Courchesne E., and Sejnowski T.J.: *Removal of eye activity artifacts from visual event-related potentials in normal and clinical subjects*, Clinical Neurophysiology, 111:10, 1745-58, 2000.
- [136] Kalman, R. E.: *A New Approach to Linear Filtering and Prediction Problems*, Transactions of the ASME-Journal of Basic Engineering, 82: Series D; 35-45, 1960.
- [137] Kamath M.V., Fallen E.L.: *Power spectral analysis of HRV: a noninvasive signature of cardiac autonomic functions*, Crit. Rev. Biomed. Eng. 21(3):245-311, 1993.
- [138] Kamath M.V., Fallen E.L.: *Correction of the Heart Rate Variability Signal for Ectopics and Missing Beats*, In: Malik M., Camm A.J. (eds.): *Heart Rate Variability*, Armonk, N.Y. Futura Pub. Co. Inc., pp 75-85, 1995.
- [139] Kantz H., Schreiber T.: *Human ECG: nonlinear deterministic versus stochastic aspects*, IEE Proc. Science, Measurement and Technology (chao-dyn/9807002) 1998.
- [140] Kaplan D.T., Cohen R.J. *Refractory period dynamics and cardiac stability: results from a computer model*, Computers in Cardiology, pp. 403 -406, 1988.
- [141] Kaplan D.T.: *Simultaneous QRS Detection and Feature Extraction Using Simple Matched Filter Basis Functions*, Computers in Cardiology, IEEE Computer Society Press, pp.503-506, 1990.
- [142] Kaplan D.T.: *The analysis of variability*, J Cardiovasc Electrophysiol., 5:16-19, 1994.
- [143] Kapoor W.N.: *Review: Syncpe* The New England Journal of Medicine 2000 December 21: 1856-62
- [144] Kautzner J.: *Reproducibility of Heart Rate Variability Measurement*, In: Malik M., Camm A.J. (eds.): *Heart Rate Variability*, Armonk, N.Y. Futura Pub. Co. Inc., pp 165-171, 1995.
- [145] Kawaguchi T., Uyama O., Konishi M., Nishiyama T., Iida T.: *Orthostatic hypotension in elderly persons during passive standing: a comparison with young persons*, J-Gerontol-A-Biol-Sci-Med-Sci. 2001 May; 56(5): M273-80
- [146] Keating M.T.: *Genetic Approaches to Cardiovascular Disease Supravalvular Aortic Stenosis, Williams Syndrome, and Long-QT syndrome*, Circulation, 92:142-147, 1995.
- [147] Kennedy H.L., Whitlock J.A., Sprague M.K., Kennedy L.J., Buckingham T.A., Goldberg R.J.: *Long-term follow-up of asymptomatic healthy subjects with frequent and complex ventricular ectopy*, N Engl. J. Med. 312(4):193-7, 1985.
- [148] Kennedy H.L.: *Heart Rate Variability Instruments from Commercial Manufacturers*, In: Malik M., Camm A.J. (eds.): *Heart Rate Variability*, Armonk, N.Y. Futura Pub. Co. Inc., pp 127-134, 1995.
- [149] Kenner,T., *Indirect measurement of blood pressure without a cuff*, Zitschrift fur Kardiologie, 1996, 85(S3):45-50.

- [150] Kenny R.A., O'Shea D., Parry S.W.: *The Newcastle protocols for Head-Up Tilting in the diagnosis of vasovagal syncope, carotid sinus hypersensitivity and related disorders*, Heart 2000;83:564-569.
- [151] Keselbrener L., Akselrod S.: *Selective Discrete Fourier Transform Algorithm for Time- Frequency Analysis: Method and Application on Simulated and Cardiovascular Signals*, IEEE Transactions on Biomedical Engineering, vol. 43 NO. 8, 1996.
- [152] Keyl, C., Lemberger, P. *Heart rate variability in patients with daytime sleepiness suspected of having sleep apnoea syndrome: a receiver-operating characteristic analysis*, Clinical Science 92: 335 - 343, 1997.
- [153] Kim S.Y., Euler D.E.: *Baroreflex sensitivity assessed by complex demodulation of cardiovascular variability*, Hypertension, 29:1119-1125, 1997.
- [154] Kleiger R.E., Stein P.K., Bosner M.S., Rottman J.N.: *Time Domain Measurements of Heart Rate Variability*, In: Malik M., Camm A.J. (eds.): *Heart Rate Variability*, Armonk, N.Y. Futura Pub. Co. Inc., pp 33-45, 1995.
- [155] Korpelainen JT, Sotaniemi KA, Huikuri HV, Myllyla VV *Circadian rhythm of heart rate variability is reversibly abolished in ischemic stroke*, Stroke, 28(11):2150-4, 1997.
- [156] Kouakam C. Lacroix D., Zghal N., Logier R., Klug D., Le Franc P., Jarwe M., Kacet S.: *Inadequate sympathovagal balance in response to orthostatism in patients with unexplained syncope and a HUT Heart*. 1999 Sep; 82(3): 312-8
- [157] Kreyzig E.: *Advanced Engineering Mathematics*, Wiley, New York, 7th ed. 1993.
- [158] Kropyvnytskyy I., Sounders F., Schierek P., Pols M.: *A computer system for continuous long-term recording, processing, and analysis of physiological data of brain injured patients in ICU settings*, Brain-Inj, 17(7): 577-83, July 2001.
- [159] Kunz D., Bes F.: *Melatonin Effects in a Patient with Severe REM Sleep Behavior Disorder: Case Report and Theoretical Considerations*, Neuropsychobiology; 36:211-214, 1997.
- [160] Kwan C.P.: *Neural Networks for Data Compression*, Department of Engineering Science, University of Oxford, 1998.
- [161] La Rovere M.T., Mortara, A., Pinna G.D., Bernardi L.: *Baroreflex Sensitivity and Heart Rate Variability in the Assessment of the Autonomic Status*, In: Malik M., Camm A.J. (eds.): *Heart Rate Variability*, Armonk, N.Y. Futura Pub. Co. Inc
- [162] Laguna P, Moody GB, Mark RG: *Power spectral density of unevenly sampled data by least-square analysis: performance and application to heart rate signals*, IEEE Trans. Biomed. Eng., BME-45, 698-715, 1998.
- [163] Laitinen T., Hartikainen J., Niskanen L., Ghilaine G., Lansimies E.: *Sympathovagal balance is a major determinant of short-term blood pressure variability in healthy subjects*, Am. Physiol. Soc. 0363-6135, 1999.
- [164] La Rovere MT, Bigger JT, Jr., Marcus FI, Mortara A, Schwartz PJ. *Baroreflex sensitivity and heart-rate variability in prediction of total cardiac mortality after myocardial infarction. The results of ATRAMI (Autonomic Tone and Reflexes After Myocardial Infarction)*, Lancet. 351:478-484 1998.
- [165] Lavie P.: *The enchanted world of sleep*, Yale Uninversity Press, New Haven, 1996.

- [166] Lavie P., Shlitner A., Nave R.: *Cardiac autonomic function during sleep in psychogenic and organic erectile dysfunction*, J. Sleep Res. 8, 135-142, 1999.
- [167] Lavery C.E., Murray A., Mittleman M Mylan C., Cohen M., Muller J.E., Verrier R.L.: *Nonuniform Nighttime Distribution of Acute Cardiac Events: A Possible Effect of Sleep States*, Circulation, 96:3321-3327, 1997.
- [168] Leong, K. S., Mann, P., Wallymahmed, M., MacFarlane, I. A., Wilding, J. P. H.: *Abnormal Heart Rate Variability in Adults with Growth Hormone Deficiency*, J Clin Endocrinol Metab 85: 628-633, 2000.
- [169] Leung S.T., Bradley D.T.: *Sleep Apnea and Cardiovascular Disease*, Am J Respir Care Med Vol 164. pp 2147-2165, 2001.
- [170] Levy M.N., Martin P.J.: *Neural control of the heart*, In: Berne R.M. (ed.): *Handbook of Physiology*, Section 2, Vol. 1, Bethesda, Md: Am. Physiol. Soc., 581-620, 1979.
- [171] Ligtenberg A., Kunt M.: *A Robust Digital QRS detection algorithm for arrhythmia monitoring*, Computers & Biomedical Research, 16(3):273-286, June 1983.
- [172] Lippman N., Stein K.M., Lerman B.B.: *Comparison of methods for removal of ectopy in measurement of heart rate variability*, Am. J. Physiol. 267 (Heart Circ. Physiol. 36): H411-H418, 1994.
- [173] Lipsitz L.A., Mietus J., Moody G.B., Golberger A.L.: *Spectral characteristics of HRV before and during postural tilt. Relation to aging and risk of syncope* Circulation. 1990; 81:1803
- [174] Loadsman J. A., Wilcox I.: *Is obstructive sleep apnoea a rapid eye movement-predominant phenomenon?* Br. J. Anaesth. 85: 354-358, 2000.
- [175] Loadsman, J. A., Hillman, D. R.: *Anaesthesia and sleep apnoea*, Br. J. Anaesth. 86: 254-266, 2001.
- [176] Lomb N.R: *Least-squares frequency analysis of unequally spaced data*, Astrophysical and Spcae Science, vol 39, pp. 447-462, 1976.
- [177] Luria M.H., Debanne S.M., Osman M.I.: *Long-term follow-up after recovery from acute myocardial infarction. Observations on survival*, Arch. Intern. Med. 145(9): 1592-5, 1985.
- [178] Lydic R.: *Pain: A bridge linkin anesthesiology and sleep research*, Sleep Vol 24, Issue 1, pp 10-12, Feb 2001.
- [179] Maglaveras N., Stamkopoulos T., Pappas C., Strinzis M.G.: *An Adaptive Backpropagation Neural Network for Real-Time Ischemia Epsiodes detection: Development and Performance Analysis Using the European ST-T Database*, IEEE Transactions on Biomedical Engineering, Vol 45, No.7, July 1998.
- [180] Malik M., Farrell T., Camm A.J.: *Circadian rhythm of heart rate variability after acute myocardial infarction and its influence on the prognostic value of heart rate variability*, Am J Cardiol. 66:1049-1054, 1990.
- [181] Malik M., Camm A.J. (eds.): *Heart Rate Variability*, Armonk, N.Y. Futura Pub. Co. Inc., 1995.
- [182] Malik M.: *Geometric Methods for Heart Rate Variability Assessment*, In: Malik M., Camm A.J. (eds.): *Heart Rate Variability*, Armonk, N.Y. Futura Pub. Co. Inc., pp

- [183] Malik M.: *Effect of Electrocardiogram Recognition Artifact on Time-Domain Measurement of Heart Rate Variability*, In: Malik M., Camm A.J. (eds.): *Heart Rate Variability*, Armonk, N.Y. Futura Pub. Co. Inc., pp 99-118, 1995.
- [184] Malik M. (Chairman of Writing Committee of Task Force of the European Society of Cardiology and the North American Society of Pacing Electrophysiology): *Heart Rate Variability: Standards of Measurement, Physiological Interpretation, and Clinical Use*, Circulation, 93:1043-1065, 1996.
- [185] Malliani A. Pagani M. Furlan R., Guzzetti S., Lucini D., Montano N., Cerutti S., Mela G.S.: *Individual recognition by heart rate variability of two different autonomic profiles related to posture*, Circulation, 96:4143-4145, 1997.
- [186] Mathias C.J., Alam M.: *Circadian Changes of the Cardiovascular System and the Autonomic Nervous System*, In: Malik M., Camm A.J. (eds.): *Heart Rate Variability*, Armonk, N.Y. Futura Pub. Co. Inc., pp 21-30, 1995.
- [187] McClements BM Adgey AA Value of signal-averaged electrocardiography, radionuclide ventriculography, Holter monitoring and clinical variables for prediction of arrhythmic events in survivors of acute myocardial infarction in the thrombolytic era. J.Am.Coll.Cardiol. 12(6): 1419-27, 1993.
- [188] McGavigan A.D., Hood S.: *The influence of sex and age on response to head-up tilt in patients with recurrent syncope*, Age and Ageing; 30:295-8, 2001.
- [189] McSharry P.E., Clifford G.D., Tarassenko L., Smith L.: Method for generating an artificial RR tachogram of a typical healthy human over 24-hours, Computers in Cardiology, September 2002.
- [190] McSharry P.E., Clifford G., Tarassenko L., Smith L.: A dynamical model for generating synthetic electrocardiogram signals, IEEE Transactions On Biomedical Engineering, 50(3), 289-294, March 2003.
- [191] Mees A.: *Nonlinear Dynamics and Statistics*, Univ. West. Aust. Press, 2000.
- [192] Mehta R.H., Bossone E.. Eagle K.A., *Current concepts in secondary prevention after acute myocardial infarction*, Herz. 25(1): 47-60, 2000.
- [193] Menrad A.: *Dual microprocessor system for cardiovascular data acquisition, processing and recording*, Proc 1981 IEEE Int. Conf. Industrial Elect. Contr. Instrument., pp 64-69, 1981.
- [194] Moody, G.B. : *Harvard-Massachusetts Institute of Technology Division of Health Science and Technology's MIT-BIH arrhythmia database*, Room E25-506A, Cambridge, MA 02139 USA, Updated 16 October 1999.
- [195] Molgaard H.: *Evaluation of the Reynolds Pathfinder II system for 24h heart rate variability analysis*, Eur. Heart J., 12:153-1162, 1991.
- [196] Monk T.H.: *Sleep, sleepiness and performance*, John Wiley and Sons Ltd., 1991.
- [197] Moody G.B, Mark R.G.: *QRS morphology representation and noise estimation using the Karhunen-Loeve transform*, Computers in Cardiology, 269-272, 1989.
- [198] Moody, G.B.: *Spectral Analysis of Heart Rate Without Resampling*, Computers in Cardiology, pp. 715-718, IEEE Comp. Soc. Press 1993.
- [199] Moody G.B.: *ECG-based indices of physical activity*, Computers in Cardiology 19:403-406, 1992.

- [200] Mahoudeaux P.M.: *Simple microprocessor-based system for on-line ECG analysis*, Med. Biol. Eng. Comput., vol 19, pp. 497–500, 1981.
- [201] Mortara A., Sleight P., Pinna G.S., Maestri R., Pipa A., La Rovere M.T., Cobelli F., Tavazzi L.: *Abnormal Awake Respiratory Patterns Are Common in Chronic Heart Failure and May Prevent Evaluation of Autonomic Tone by Measures of Heart Rate Variability*, Circulation 96:246-252, 1997.
- [202] Munakata M, Imai Y, Takagi H, Nakao M, Yamamoto M, Abe K.: *Altered frequency-dependent characteristics of the cardiac baroreflex in essential hypertension*, J Auton Nerv Syst., 49:33-45, 1994.
- [203] Murray, A., Whittam, A.M., Clayton, R.H., Lord, S.W., McComb, J.M. Computer simulation of heart rate and blood pressure changes, and comparison with clinical data, Simulation in Medicine (Ref. No. 1998/256), IEE Colloquium on , 1998 Page(s): 8/1 -8/3
- [204] Murray J., Bradley H., Craigie W., Onions C.T., Burchfield R., Weiner E., Simpson J. (Eds.): *Oxford English Dictionary*, 2nd Edition, Oxford University Press, Oxford 2001.
- [205] Myers G., Workman M., Birkett C.: *Problems in measuring heart rate variability of patients with congestive heart failure*, J. Electrocardiol., 25(suppl):214-219, 1992.
- [206] Nitzan M., Babchenko A., Khanokh B.: *Very low frequency variability in arterial blood pressure and blood volume pulse*, Medical & Biological Engineering & Computing, 1999, 37,54-58.
- [207] Nolan J., Batin P.D., Andrews R., Lindsay S.J., Brooksby P., Mullen M., Baig W., Flapan A.D., Cowley A., Prescott R.J., Neilson J.M.M., Fox K.A.A.: *Clinical Investigation and Reports: Prospective Study of Heart Rate Variability and Mortality in Chronic Heart Failure - Results of the United Kingdom Heart Failure Evaluation and Assessment of Risk Trial (UK-Heart)*, Circulation, 98:1510-1516, 1998.
- [208] Odemuyiwa O., Malik M., Farrell T., Bashir Y., Poloniecki J., Camm J.: *Comparison of the predictive characteristics of heart rate variability index and left ventricular ejection fraction for all-cause mortality, arrhythmic events and sudden death after acute myocardial infarction*, Am J Cardiol. 1991;68:434-439
- [209] Ogilvie R.D., Wilkinson R.T., Allison S.: *The detection of sleep onset: behavioural, physiological and subjective convergence*, Sleep, 12: 458–474, 1989.
- [210] Ohayon, M.M., Guilleminault, C., Paiva, T., Priest, R.G., Rapoport, D., Sagales, T., Smirne, S., Zulley, J.: *An International Study on Sleep Disorders in the general Population: Methodological Aspects*, Sleep 20(12): 1086-1092, 1997.
- [211] Okada M.: *A digital filter for the QRS complex detection*, IEEE Trans. Biomed. Eng., vol. BME-26, pp. 700-703, Dec 1979.
- [212] Ortega G.J., Golombok D.A.: *Detection of Nonlinear Coupling and its Application to Cardiorespiratory Interaction*, arXiv:nlin.CD/0001044 20 Jan 2000.
- [213] Otzenberger, H., Gronfier, C., Simon, C., Charloux, A., Ehrhart, J., Piquard, F., Brandenberger, G.: *Dynamic heart rate variability: a tool for exploring sympathovagal balance continuously during sleep in men*, Am. J. Physiol. 275: 946H-950, 1998.
- [214] Pahlm O., Sornmo L. *Software QRS detection in ambulatory monitoring - a review*, Medical & Biological Engineering & Computing, 22(4):289-297, July 1984.

- [215] Pan J., Tompkins W.: *A real-time QRS detection algorithm*, IEEE Transactions on Biomedical Engineering, vol. BME-32 NO. 3. 1985.
- [216] Parker P., Celler B.G., Potter E.K.: *Vagal stimulation for cardiac slowing*, J Auton Nerv Syst, 11:226-231, 1984.
- [217] Paolillo V., Marra S., Rendine S., Baduini G., Altieri A., De-Berardinis A., Riva L., Spadaccini F.: *The prognostic significance of clinical history, exercise testing and ambulatory electrocardiography in patients with uncomplicated myocardial infarction*, G. Ital. Cardiol., 15(5): 465-71, 1985.
- [218] Papoulis A.: *Probability, Random Variables and Stochastic Processes*, New York, McGraw-Hill, 1965
- [219] Peng C-K, Havlin S, Stanley HE, Goldberger AL.: *Quantification of scaling exponents and crossover phenomena in nonstationary heartbeat time series*, CHAOS, 5:82-87, 1995
- [220] Pikkujamsa S.M., Makikallio T.H., Airaksinen K.E.J., Huikuri H.V.: *Determinants and interindividual variation of R-R interval dynamics in healthy middle-aged subjects*, Am. J. Physiol. Heart. Circ. Physiol. 280:H1400-H1406, 2000.
- [221] Pikkujamsa S.M., Makikallio T.H., Sourander L.B., Raiha I.J., Puukka P., Skytta J., Peng C-K., Goldberger A.L., Huikuri H.V.: *Cardiac Interbeat Interval Dynamics From Childhood to Senescence*, Circulation, 100:393-399, 1999
- [222] Pilgram B., Kaplan D.T.: *A comparison of estimators for $\frac{1}{f}$ noise*, Physica D; 114, 108-122, 1998.
- [223] Pitzalis M.V., Mastropasqua F., Massari F., Passantino A., Colombo R., Mannarini A., Foreleo C., Rizzon P.: *Effect of respiratory rate on the relationship between RR interval and systolic blood pressure fluctuations: a frequency- dependent phenomenon*, Cardiovascular Research 38: 332-339, 1998
- [224] Pomerleau D.A.: *Input Reconstruction Reliability Estimation*, Carnegie Mellon University. 1993.
- [225] Ramset M.W., Stewart W.R., Jones C.J.H., *Real Time measurement of pulse wave velocity from arterial pressure waveforms*, Medical & Biological Engineering & Computing, September 1995, 33(5):636-642.
- [226] Qi Y., Minka T.P., Picard R.W.: *Bayesian Spectrum Estimation of Unevenly sampled nonstationary data* Int. Conf. on Acoustics, Speech and Signal Processing (ICASSP), Orlando, Fl. May 13-17 2002.
- [227] Quattrochi J.J., Shapiro J., Verrier R.L., Hobson A.: *Transient cardiorespiratory events during NREM sleep: A feline model for human microarousals*, J. Sleep Res. 9, 185-191, 2000.
- [228] Rapaport E., Remedios P., The high risk patient after recovery from myocardial infarction: recognition and management. J. Am. Coll. Cardiol., 1(2 Pt 1): 39-400, 1983.
- [229] Press W.H., Teukolsky S.A., Vetterlin W.T., Flannery B.P.: *Numerical Recipes in C: The art of scientific computing*, 2nd Ed., Camb. Univ. Press, 1992.
- [230] Parks, McClellan. *Algorithm 5.1*. IEEE. Programs for Digital Signal Processing. IEEE Press. New York: John Wiley & Sons, 1979.
- [231] Rechtschaffen A., Kales A.: *A Manual of Standardized Terminology, Techniques and Scoring System for Sleep Stages of Human Subjects*, Public Health Service, U.S. Government Printing Office, Washington D.C., 1968.

- [232] Ripley, B.D.: *Pattern Recognition and Neural Networks*, Camb. Univ. Press, 1996.
- [233] Rosen R.: *Acute arrest of cerebral circulation in man* Arch. Neurol. Psychiatr. 1943; 50: 510-28
- [234] Rosenberg J., G Wildschiodtz, MH Pedersen, F von Jessen and H Kehlet: *Late postoperative nocturnal episodic hypoxaemia and associated sleep pattern*, British Journal of Anaesthesia, Vol 72, Issue 2 145-150, OUP 1994.
- [235] Rosenberg-Adamsen S., Skarbye M., Wildschiodtz G., H Kehlet H., Rosenberg J.: *Sleep after laparoscopic cholecystectomy* British Journal of Anaesthesia, Vol 77, Issue 5 572-575, OUP, 1996.
- [236] Ruiz G.A., Madoery C., Arnaldo F., Menendez C., Tentori M.C.: *Frequency-domain analysis of HRV during positive and negative head-up tilt: importance of age* Pacing-Clin-Electrophysiol. 2000 Mar; 23(3): 325-332
- [237] Sato N., Kawamoto M., Yuge O., Suyama H., Sanuki M., Matsumoto C., Inoue K.: *Effects of pneumoperitoneum on cardiac autonomic nervous activity evaluated by heart rate variability analysis during sevoflurane, isoflurane, or propofol anesthesia*, Surgical Endoscopy, Volume 14, Issue 4, Pages 362-366, 2000.
- [238] Saul J.P., Berger R.D., Albrecht P.: *Transfer function analysis of the circulation: unique insights into cardiovascular regulation*, Am. J. Physiol. (Heart Circ. Physiol. 30), 261:H153-H161, 1991.
- [239] Scargle J.D.: *Studies in astronomical time series analysis. II. Statistical aspects of spectral analysis of unevenly spaced data*, Astrophysical Journal, vol 263, pp. 835-853, 1982.
- [240] Scargle J.D.: *Studies in astronomical time series analysis. III - Fourier transforms, autocorrelation functions and cross-correlation functions of unevenly spaced data*, Astrophysical Journal, vol 343, pp. 874-887, 1989.
- [241] Schmidt G., Malik M., Barthel P., Schneider R., Ulm K., Rolnitzky L., Camm A.J., Bigger Jr. J.T., Schomig A.: *Heart-rate turbulence after ventricular premature beats as a predictor of mortality after acute myocardial infarction*, Lancet, Vol. 353, No. 9162, pp. 1390-1396, 1999.
- [242] Schreiber T., Kaplan D.T.: *Nonlinear noise reduction for electrocardiograms*, CHAOS 6; 87-92, 1996.
- [243] Schreiber T., Schmitz A.: *Improved surrogate data for nonlinearity tests*, Phys. Rev. Lett. 77, 635 (chao-dyn/9909041) 1996.
- [244] Schreiber T.: *Detecting and analysing nonstationarity in a time series using nonlinear cross predictions*, Phys. Rev. Lett. 78:843 (chao-dyn/9909044) 1997.
- [245] Schreiber T., Schmitz A.: *Classification of Time Series Data with Nonlinear Similarity Measures*, Phys. Rev. Lett. 79:8, 1997.
- [246] Schmitz A., Schreiber T.: *Testing for nonlinearity in unevenly sampled time series*, Phys. Rev. E 59, 4044 (chao-dyn/9804042) 1999.
- [247] Serrador J.M., Finlayson H.C., Hughson R.L.: *Physical activity is a major contributor to the ultra low frequency components of heart rate variability*, Heart, 82:e9, 1999.
- [248] Sheldon R., Killam S.: *Methodology of isoproterenol-tilt table testing in patients with syncope* J Am Coll Cardiol 1992; 19:773-9

- [249] Sheldon R.S., Koshman M-L., Murphy W.F.: *Electroencephalographic findings during presyncope and syncope induced by tilt table testing*, Can. J. Cardiol. Vol 14, No. 6, June 1998.
- [250] Signorini M.G., Guzzetti S., Manzoni C., Milani S., Cerutti S.: *Multiparametric Analysis of HRV Signal by Linear and Nonlinear Methods in Heart Failure Patient Population*, Proc of 20th Int. Conf. IEEE Eng. Med. Biol. Soc., Vol 20, No. 1, 1998.
- [251] Silipo R., Deco G., Vergassola R.: *Nonlinear models and Heart Rate Variability Hidden Dynamic*, IEEE, Computers in Cardiology, 25:337-340, 1998.
- [252] Singh N., Mironov D./ Armstrong P.W., Ross A.M., Langer A.,: *Heart Rate Variability Assessment Early After Acute Myocardial Infarction: Pathophysiological and Prognostic Correlates - for the GUSTO ECG Substudy*, Circulation, Vol 93, 1388-1395, 1996.
- [253] Sinnreich R., Kark J.D., Friedlander Y., Sapoznikov D., Luria M.H.: *Five Minute Recordings of Heart Rate Variability for Population Studies: Repeatability and age-sex characteristics*, Heart, 80:156-162, 1998.
- [254] Sinnreich R., Kark J.D., Friedlander Y., Sapoznikov D., Luria M.H.: *Five minute recordings of heart rate variability for population studies: repeatability and age-sex characteristics*, Heart, 80:156-162, 1998.
- [255] Sleight P., Casadei B.: *Relationships between Heart Rate, Respiration and Blood Pressure*, In: Malik M., Camm A.J. (eds.): *Heart Rate Variability*, Armonk, N.Y. Futura Pub. Co. Inc., pp 311-330, 1995.
- [256] Small, M., Yu, D.J., Clayton, R.H., Simonotto, J., Harrison, R.G: Evolution of ventricular fibrillation revealed by first return plots Computers in Cardiology 2000 , 2000 Page(s): 525 -528
- [257] Smith ML, Ellenbogen KA, Eckberg DL, Szentpetery S, Thames MD.: *Subnormal heart period variability in heart failure: effect of cardiac transplantation*, J Am Coll Cardiol. 14:106-111, 1989.
- [258] Spiegel M.R.: *Schaum's Outline Series - Theory and Problems of Advanced Mathematics for Engineers and Scientists*, New York, McGraw-Hill 1971.
- [259] Stefanovska, A.: *The cardiovascular system as a system of coupled oscillators*, Presentation at the Workshop on Cardiovascular-Respiratory Control Modeling, Graz, Austria, June 2001.
- [260] Sun W., Combs W., Panken E., Fotuhi P., Stangl K., Baumann G., Theres H.: *Automatic and efficient R wave discrimination in the right atrium using a two-state hidden Markov model*, Journal of Cardiovascular Electrophysiology, Volume 10, Issue 3, pp 343-350, 1999.
- [261] Sweeney MO, Moss AJ, Eberly S.: Instantaneous cardiac death in the posthospital period after acute myocardial infarction, Am J Cardiol, 70(18): 1375-9, 1992.
- [262] Tarassenko, L.T.: *Lecture Notes for Neural Networks*, Engineering Department, Oxford University, October, 1998.
- [263] Tarassenko L.T.: *A Guide to Neural Computing Applications*, OUP. 1998.
- [264] Tarassenko, L., Townsend, N., Clifford, G., Mason, L., Burton J., Price, J.: Neural Networks and Data Fusion for the Next Generation of Patient Monitors, Neural Computing Applications Forum, Oxford, July 2001.

- [265] Tarassenko, L., Clifford, G., Townsend, N.: Detection of ectopic beats in the electrocardiogram using an auto-associative neural network, *Neural Proc. Letts.*, vol.14, no.1; p.15-25; Aug. 2001.
- [266] Tarassenko, L., Townsend, N., Clifford, G., Mason, L., Burton J., Price, J.: Medical Signal Processing Using The Software Monitor, DERA/IEE Workshop Intelligent Sensor Processing (Ref.No.01/050). IEE, London, UK; 2001; 140 pp. p.3/1-4.
- [267] Taylor J.A., Carr D.L., Myers C.W., Eckberg D.L. : *Mechanisms Underlying Very-Low-Frequency RR-Interval Oscillations in Humans*, *Circulation* 98: 547-555, 1998.
- [268] Teich M.C., Lowen S.B., Jost B.M., Vibe-Rheymer K., Heneghan C.: *Heart Rate Variability: Measures and Models*, arXiv:physics/0008016, 7 Aug 2000, and in Nonlinear Biomedical Signal Processing Vol. II: Dynamic Analysis and Modeling, edited by M. Akay, IEEE Press, Piscataway, NJ, 2000.
- [269] Thakor N.V., Zhu Y., Pan K.: *Ventricular Tachycardia and Fibrillation detection by a sequential Hypothesis Testing Algorithm*, *IEEE Transactions on Biomedical Engineering*, vol. 37 NO. 9. 1990.
- [270] Tompkins W.J., Webster J.G., *Design of Microcomputer-Based Medical Instrumentation*, Prentice Hall, USA, 1981.
- [271] Tulppo M.P., Hughson R.L., Makikallio T.H., Airaksinen K.E.J., Seppanen T., Huikuri H.V.: *Effects of exercise and passive head-up tilt on fractal and complexity properties of heart rate dynamics*, *Am. J. Physiol. Heart. Circ. Physiol.* 280:H1081-H1087, 2001.
- [272] Valentinuzzi M.E., Geddes L.A. Baker L.E.: *The Law of impedance pneumography* *Med. Biol. Eng.* 9: 157-163, 1971.
- [273] Valkama J.O., Huikuri H.V., Airaksinen K.E., Linnaluoto M.L., Takkunen J.T.: *Determinants of frequency domain measures of heart rate variability in the acute and convalescent phases of myocardial infarction*, *Cardiovasc-Res.* 28(8): 1273-6, Aug 1994.
- [274] Vallverdú M., Àlvarez C., Baranowski R., Chojnowska L., Caminal P. : *Nonlinear Dynamics Analysis of Heart Rate Variability Signal Based on Entropies in Hypertrophic Cardiomyopathy Patients*, IEEE, Computers in Cardiology
- [275] Vanoli V., Adamson P.B., Ba-Lin, Pinna G.D., Lazzara R., Orr W.C.: *Heart Rate Variability During Specific Sleep Stages*, *Circulation*, 91:1918-1922, 1995.
- [276] Vetter R., Celka P., Vesin J.M., Scherrer U.: *Sub-signal extraction of RR time series using independent component analysis*, Proc of 20th Int. Conf. IEEE Eng. Med. Biol. Soc., Vol 20, No. 1, 1998.
- [277] Vikman S., Timo H. Mäkikallio, Sinikka Yli-Mäyry, Sirkku Pikkujämsä, Anna-Maija Koivisto, Pekka Reinikainen, K. E. Juhani Airaksinen, Heikki V. Huikuri, *Altered Complexity and Correlation Properties of R-R Interval Dynamics Before the Spontaneous Onset of Paroxysmal Atrial Fibrillation*, *Circulation*. 100:2079-2084, 1999
- [278] Wang Z.S., Cheung J.Y. Chen J.D.Z., *Blind separation of multichannel electrogastrograms using independent component analysis based on a neural network*, *Medical & Biological Engineering & Computing*, 1999, 37:80-86.
- [279] Welch, P.D.: *The Use of Fast Fourier Transform for the Estimation of Power Spectra: A Method Based on Time Averaging Over Short, Modified Periodograms*, *IEEE Trans. Audio Electroacoust.* Vol. AU-15, Pgs. 70-73, June 1967.

- [280] Whincup PH Wannamethee G Macfarlane PW Walker M Shaper AG, *Resting electrocardiogram and risk of coronary heart disease in middle-aged British men*, J. Cardiovasc. Risk, 2(6): 533-43, 1995
- [281] Whittam, A.M., Clayton R.H., Lord S.W., McComb J.M., Murray A.: *Computer modelling of heart rate and blood pressure* Computers in Cardiology, Page(s): 149 -152, 1998.
- [282] Wilson A.C., Kostis J.B.: *The prognostic significance of very low frequency ventricular ectopic activity in survivors of acute myocardial infarction. BHAT Study Group*, Chest. Sep '92; 102(3): 732-6 (0012-3692), 1992.
- [283] Wisbeck J.O., Barros A.K., Ojeda R.: *Application of ICA in the Separation of Breathing artefacts in ECG Signals*, International Conference on Neural Information Processing, (ICONIP '98), Kyushu, Japan, 1998.
- [284] Wolf M.M., Varigos, G.A., Hunt D., Sloman J.G.: *Sinus arrhythmia in acute myocardial infarction*, Med. J. Aust., 2:52-53, 1978.
- [285] Zemaityte D., Varonekas G., Sokolov E.: Heart rhythm control during sleep, *Psychophysiology* 21:279-289, 1984.
- [286] Zulley, J., Cronlein, T., Hell, W., Langwieder, K.: *Fatal Highway Accidents mainly caused by falling asleep*, Sleep Research 24 A: 555. 1995.